

# **Synthesis and Characterization of Fluorescent Hydroxyapatite Nanoparticles and Their Applications in Bioimaging and Plasmid Delivery**

**THESIS**

Submitted in partial fulfillment  
of the requirements for the degree of  
**DOCTOR OF PHILOSOPHY**

by

**KETAKI R DESHMUKH**

Under the Supervision of

**Prof. Meenal Kowshik**

and

Co-Supervision of

**Prof. Sutapa Roy Ramanan**



**BITS Pilani**  
K K Birla Goa Campus

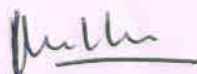
**BIRLA INSTITUTE OF TECHNOLOGY AND SCIENCE, PILANI**

**2016**

**BIRLA INSTITUTE OF TECHNOLOGY AND SCIENCE, PILANI**

**CERTIFICATE**

This is to certify that the thesis entitled “**Synthesis and Characterization of Fluorescent Hydroxyapatite Nanoparticles and Their Applications in Bioimaging and Plasmid Delivery**” and submitted by **Ketaki R Deshmukh**, ID No. 2010PH29011G for award of Ph.D. of the Institute embodies original work done by him under my supervision.



Signature of the Supervisor :

Name in capital letters: PROF. MEENAL KOWSHIK

Designation: Associate Professor



Signature of Co-supervisor

PROF. SUTAPA ROY RAMANAN

Professor

Date: 14/12/16

**Acknowledgements**

First and foremost, I would like to express my sincere gratitude towards my supervisor, Prof. Meenal Kowshik for her continuous support, motivation and encouragement throughout the duration of my research work. I am deeply indebted to her for her thoughtful guidance, patience, expertise and valuable suggestions. I am grateful to my co-supervisor Prof. Sutapa Roy Ramanan for her valuable guidance and support.

I would like to thank Prof. Souvik Bhattacharya, current Vice-Chancellor, and Prof. Bijendra Nath Jain, former Vice-Chancellor BITS, Pilani; Prof. Raghurama, Director, BITS, Pilani - K. K. Birla Goa Campus, Prof. Sasikumar Punnekkat, Late Prof. Sanjeev K Aggrawal and Prof K. E Raman Ex-directors; Prof. P.K.Das, Associate Dean, Academic Research division; and Prof. S. D Manjare, former-in-charge, RCED for all their support and help.

I am sincerely thankful to my Doctoral Advisory Committee members Dr. Raviprasad Aduri and Dr. Jegatha Nambi Krishnan for their valuable advice and scientific critiques that have helped me in refining my work. I extend my sincere thanks to present and past Doctoral Research Committee (DRC) Head and members for their guidance and support.

I am extremely grateful to the faculty members of Department of Biological Sciences, Prof. Judith Braganca, Prof. Dibakar Chakrabarty, Prof. Utpal Roy, Prof. Srikanth Mutnuri, Prof. Vijayashree Nayak, Prof. Angshuman Sarkar, Dr. Indrani Talukdar, Dr. Anasuya Ganguly, Dr. Sumit Biswas, Dr. Malabika Biswas, Dr. Kundan Kumar, Dr. Sukanto Mandal and Dr. Arnab Banerjee for their timely help throughout this work.

I am grateful to Sophisticated Analytical Instruments Facility (SAIF) at IIT Bombay for their assistance in TEM and SEM-EDS analysis. I would like to thank Dr. Teny T. John and Ms. P. R Chithira, Department of Physics, for their kind

## ***Acknowledgements***

help with photoluminescence studies. I extend my thanks to Prof. Amrita Chatterjee, for the spectrofluorometric studies and Prof. N. N. Ghosh for the DLS analysis. I also thank Dr. E. S. Kannan for help with the interpretation of **data analysis**.

I thank Mr. Pratap (ARD), Mrs. Kamana Upadhyay, Mr. Mahadeo Shetkar, Mr. Mahaling Lamani and all others who make the graduate student's life easier.

I would like to express my gratitude towards all the research scholars of the department. This work would have not been possible without support of my friends and most importantly 'nano' group.

I am grateful to my family members for believing in me and giving me the opportunity to pursue my dreams. This work is complete because of their continuous support.

**Ketaki R Deshmukh**



**ABSTRACT**

Nanoparticles provide exciting opportunities in the field of bioimaging and molecular biology. Bio-imaging has drastically transformed the field of medicine, and made the process of diagnosis easy and fast. Visualization of complete organ to complex biological processes has now become possible. Amongst the various imaging processes, fluorescence imaging using non-toxic fluorescent nanomaterials is advantageous for several beneficial features including high sensitivity, minimal invasiveness and safe detection limit. In the present work, we have synthesized rod shaped hydroxyapatite nanoparticles (HAp NPs) of different aspect ratios (diameter: length) at room temperature using modified sol gel method. HAp NPs with thin rod (aspect ratio 1:10), short rod (aspect ratio: 1:5), microrods (aspect ratio: 1:5) and rod (aspect ratio: 1:4) shaped morphology were obtained by changing the stabilizing agents (triethyl amine and acetyl acetone) and/or solvents (water and dimethyl sulfoxide). X-ray diffraction (XRD), Fourier transform infrared (FTIR), Raman spectroscopy, transmission electron microscopy (TEM), energy dispersive analysis of X-ray (EDAX), photoluminescence spectroscopy and electron spin resonance (ESR) were used to characterize these NPs. The experimental results showed that all the HAp samples exhibited excellent fluorescence with broad emission spectrum ranging from 350-750nm and maximum at 502nm. The emission spectra of all HAPs synthesized were similar, but with significant changes in the intensity of fluorescence signal, which was in the order of: thin rod > short rod > rod > microrods. Fluorescence intensity of all HAPs decreased with decreasing aspect ratio. Fluorescent property of synthesized NPs was attributed to the electronic transition in the asymmetric structure of HAp NPs as confirmed by ESR spectroscopy and absence of fluorescence in symmetric HAp NPs. In addition to self activated fluorescence behavior, these NPs were found to be non-toxic in

nature as confirmed using 3-(4,5-dimethylthiazol-2-yl)-2,5-diphenyltetrazolium bromide (MTT), lactate dehydrogenase (LDH), reactive oxygen species (ROS) and hemocompatibility assays. These self-activated fluorescent HAp NPs (fHAp) exhibited excellent cellular internalization in both prokaryotic and eukaryotic systems such as *Escherichia coli* (*E. coli*), *Staphylococcus aureus* (*S. aureus*), *Candida albicans* (*C. albicans*), bone osteosarcoma (MG63), human cervical cancer (HeLa) and keratinocyte (HaCaT) cells. These non-toxic fHAp provide a safe and a potential alternative to the current fluorescent materials for bio-labelling and bio-imaging applications.

Further, a novel one step transformation method using fHAp for both Gram-positive and Gram-negative bacteria was developed. To achieve transformation, binding of plasmid DNA (pDNA) to fHAp is necessary; therefore, the binding affinity of pDNA to thin rod, short rod and rod shaped fHAp was determined. The obtained binding efficiency was in the order of: thin rod>short rods>rods. The thin rod HAp NPs exhibited highest pDNA binding efficiency (50%) compared to short rods (27%) and rods (15%), and were selected for further modifications. HAp NPs were functionalized with positively charged amino acids, histidine, lysine, and arginine, respectively, to increase the positive surface charge of the NPs for effective binding to pDNA. Arginine-fHAp (R-G-fHAp) exhibited the highest binding efficiency (90%), and were further functionalized with glucose to enhance the transformation efficiency (T.E). R-G-fHAp-pDNA complexes were stable at a wide range of temperatures (37-90°C), pH (6-11) and sonication-induced stress. R-G-fHAp served as carriers to deliver pDNA into intact cells of *E. coli* and *S. aureus* at room temperature, without the need for preparation of competent cells. The T.E was high in minimal medium as compared to that in complex Luria-Bertani medium. This could be attributed to the abundance of bio-micromolecules (electrolytes, proteins, lipids, etc) in the

complex medium in comparison to minimal media, which are easily adsorbed on to the NPs enhancing the inter-particle interaction, resulting in aggregation and reduction in T.E. High T.E in *E. coli* ( $10^9$  cfu/ $\mu$ g of pDNA) and *S. aureus* ( $10^7$  cfu/ $\mu$ g of pDNA) was achieved using R-G-fHAPs as compared to R-fHAPs, chemical ( $\text{CaCl}_2$ ) and electroporation methods. These NPs were also non-toxic towards both Gram-positive and Gram-negative bacteria.

R-G-fHAPs were further modified with polyethylene glycol (modified-fHAPs) to use it as a pDNA vehicle for *C. albicans* transformation. PEG functionalization helped pDNA to bind on the surface of yeast cells and enhanced the T.E of *C. albicans*. Modified-HAP NPs exhibited an enhanced pDNA binding efficiency of 93.5% as compared to R-G-fHAPs, which may be attributed to the increase in the positive charge on the surface due to PEG functionalization. These modified fHAPs-pDNA complexes were also stable in a wide range of temperatures (37-90°C), pH (6-11) and sonication-induced stress. High transformation efficiency in *C. albicans* ( $10^6$  cfu/ $\mu$ g of pDNA) was achieved using modified-fHAPs as compared to R-G-fHAPs, fHAPs, and electroporation methods. These NPs were also non-toxic towards *C. albicans* cells. We propose that, this nanoparticle based approach is safe and potential process to achieve high transformation efficiencies in yeast cells, Gram-positive and Gram-negative bacterial cells.

This is the first study to report the self-activated fluorescent properties of fHAPs that may be exploited for *in-situ* bio-imaging and bio-labeling applications. At the same time, the functionalized fHAPs were used to successfully develop a novel, single step transformation protocol for both the prokaryotic and the eukaryotic systems.

**Table of contents**

|  | <b>PAGE</b> |
|--|-------------|
| <b>Thesis title page (Annexure I)</b>            |             |
| <b>Certificate from Supervisor (Annexure II)</b> |             |
| <b>Acknowledgements</b>                          |             |
| <b>Abstract</b>                                  | <b>i</b>    |
| <b>Table of contents</b>                         | <b>iv</b>   |
| <b>List of tables</b>                            | <b>x</b>    |
| <b>List of figures</b>                           | <b>xii</b>  |
| <b>List of abbreviations and symbols</b>         | <b>xxi</b>  |

**Chapter 1: Introduction and Review of Literature**

|         |   |    |
|---------|---|----|
| 1.1     | Introduction  | 1  |
| 1.1.1   | Nanotechnology in ancient era                                     | 2  |
| 1.2     | Nanomaterials   | 2  |
| 1.2.1   | Naturally produced nanomaterials                                  | 3  |
| 1.3     | Nanostructures engineered by human and its biomedical application | 4  |
| 1.3.1   | Liposomes   | 7  |
| 1.3.2   | Gold NPs  | 7  |
| 1.3.3   | Quantum dots  | 8  |
| 1.3.4   | Carbon nanotubes  | 8  |
| 1.3.5   | Upconversion nanoparticles  | 8  |
| 1.4     | Hydroxyapatite nanoparticles                                      | 9  |
| 1.5     | Synthesis of hydroxyapatite nanoparticles                         | 11 |
| 1.5.1   | Solid state   | 12 |
| 1.5.1.1 | Solid-state reaction  | 12 |
| 1.5.1.2 | Mechanochemical process   | 12 |
| 1.5.2   | Wet state methods   | 13 |
| 1.5.2.1 | Precipitation method  | 13 |
| 1.5.2.2 | Emulsion method   | 13 |

## ***Table of contents***

|         |  |    |
|---------|--|----|
| 1.5.2.3 | Hydrothermal method                                    | 14 |
| 1.5.2.4 | Sol-gel synthesis                                      | 14 |
| 1.6     | Applications of HAp NPs                                | 15 |
| 1.6.1   | Bioimaging   | 15 |
| 1.6.1.1 | Doping of HAp NPs with organic dye                     | 17 |
| 1.6.1.2 | Lanthanides doped HAp NPs                              | 17 |
| 1.6.1.3 | Fluorescence property in HAp NPs caused due to defects | 25 |
| 1.6.2   | HAp for gene delivery                                  | 25 |
| 1.6.3   | Drug delivery using HAp                                | 29 |
| 1.6.4   | HAp NPs coating for orthopedic implants                | 31 |
| 1.7     | Biocompatibility and non-toxicity                      | 33 |
| 1.8     | Gaps in Existing Research                              | 34 |
| 1.9     | Aims and objectives of the research work               | 35 |

## **Chapter 2: Room Temperature Synthesis and Characterization of Self Activated Fluorescent Hydroxyapatite by Modified Sol-gel Technique**

|         |   |    |
|---------|---|----|
| 2.1     | Introduction                                | 36 |
| 2.2     | Materials and Methods                       | 38 |
| 2.2.1   | Synthesis of HAp NPs                        | 38 |
| 2.2.2   | Characterization of the HAp NPs             | 40 |
| 2.2.2.1 | X-ray diffraction                           | 41 |
| 2.2.2.2 | Fourier transform infrared spectroscopy     | 42 |
| 2.2.2.3 | Raman spectroscopy                          | 42 |
| 2.2.2.4 | Transmission electron microscope            | 43 |
| 2.2.2.5 | Energy dispersive analysis of X-ray         | 43 |
| 2.2.2.6 | Dynamic light scattering and zeta potential | 43 |
| 2.2.2.7 | Photoluminescence spectroscopy              | 44 |
| 2.2.2.8 | Electron Spin Resonance                     | 44 |
| 2.3     | Results and Discussion                      | 45 |

|         |  |    |
|---------|--|----|
| 2.3.1   | Synthesis and characterization of HAp NPs        | 45 |
| 2.3.1.1 | XRD analysis                                     | 45 |
| 2.3.1.2 | FTIR analysis                                    | 46 |
| 2.3.1.3 | Raman spectra analysis                           | 48 |
| 2.3.1.4 | EDAX analysis                                    | 48 |
| 2.3.1.5 | TEM analysis                                     | 51 |
| 2.3.1.6 | Zeta potential measurement                       | 54 |
| 2.3.1.7 | Self-activated fluorescent properties of HAp NPs | 55 |
| 2.4     | Conclusion                                       | 61 |

### **Chapter 3: Self Activated Fluorescent Hydroxyapatite Nanoparticles: A Promising Alternative for Bioimaging and Biolabeling**

|         |   |    |
|---------|---|----|
| 3.1     | Introduction  | 62 |
| 3.2     | Materials and Methods   | 63 |
| 3.2.1   | Biocompatibility studies  | 63 |
| 3.2.1.1 | 3-(4,5-dimethylthiazol-2-yl)-2,5-diphenyltetrazolium Bromide MTT) assay | 63 |
| 3.2.1.2 | Lactate dehydrogenase assay   | 64 |
| 3.2.1.3 | Reactive oxygen species generation assay                                | 64 |
| 3.2.1.4 | Hemolytic assay   | 65 |
| 3.2.2   | Fluorescence stability  | 66 |
| 3.2.3   | Uptake of HAp NPs by eukaryotic and prokaryotic cells                   | 66 |
| 3.2.4   | Time dependent uptake studies of thin rods                              | 67 |
| 3.2.5   | Statistical analysis  | 68 |
| 3.3     | Results and Discussion  | 68 |
| 3.3.1   | Biocompatibility  | 69 |
| 3.3.1.1 | MTT assay   | 69 |
| 3.3.1.2 | LDH assay   | 70 |
| 3.3.1.3 | ROS generation assay  | 70 |
| 3.3.1.4 | Hemolytic assay   | 71 |

|       |   |    |
|-------|---|----|
| 3.3.2 | Fluorescence stability                              | 75 |
| 3.3.3 | Uptake of fHApS by eukaryotic and prokaryotic cells | 76 |
| 3.3.4 | Time dependent uptake studies of thin rods          | 87 |
| 3.4   | Conclusion  | 88 |

## **Chapter 4: Novel One Step Transformation Method for *Escherichia coli* and *Staphylococcus aureus* Using Arginine-glucose Functionalized Fluorescent Hydroxyapatite Nanoparticles**

|          |   |     |
|----------|---|-----|
| 4.1      | Introduction  | 89  |
| 4.2      | Materials and Methods   | 90  |
| 4.2.1    | Synthesis of hydroxyapatite nanoparticles                           | 90  |
| 4.2.2    | Functionalization of thin rod fHApS with amino acids and glucose    | 91  |
| 4.2.3    | Characterization  | 91  |
| 4.2.4    | Aggregation studies of R-G-fHApS using dynamic light scattering     | 92  |
| 4.2.5    | Plasmid isolation   | 92  |
| 4.2.6    | Plasmid DNA binding efficiency to NPs                               | 92  |
| 4.2.7    | Stability of R-G-fHApS-pDNA complex                                 | 93  |
| 4.2.8    | Effect of physical shear force R-G-fHApS-pDNA complex               | 94  |
| 4.2.9    | Transformation of non-competent <i>E. coli</i> and <i>S. aureus</i> | 94  |
| 4.2.10   | Transformation using chemical and electroporation methods           | 95  |
| 4.2.10.1 | Chemical method   | 95  |
| 4.2.10.2 | Electroporation method  | 96  |
| 4.2.11   | Cell toxicity and growth kinetics studies                           | 96  |
| 4.2.12   | Statistical analysis  | 97  |
| 4.3      | Results and Discussion  | 97  |
| 4.3.1    | Functionalization of fHApS  | 99  |
| 4.3.2    | Characterization of fHApS   | 100 |

|       |  |     |
|-------|--|-----|
| 4.3.3 | Binding of pDNA to functionalized fHApS                                | 103 |
| 4.3.4 | Stability of R-G-fHApS-pDNA complex                                    | 105 |
| 4.3.5 | Transformation of non-competent bacteria cells                         | 106 |
| 4.3.6 | Plasmid isolation from transformed <i>E. coli</i> and <i>S. aureus</i> | 109 |
| 4.3.7 | Cell viability and growth kinetics                                     | 109 |
| 4.4   | Conclusion   | 112 |

## **Chapter 5: One Step Transformation Method for *C. albicans* Using Modified- fluorescent Hydroxyapatite Nanoparticles**

|        |  |     |
|--------|--|-----|
| 5.1    | Introduction   | 113 |
| 5.2    | Materials and Methods                                      | 114 |
| 5.2.1  | Synthesis of functionalized modified-fHApS                 | 114 |
| 5.2.2  | Characterization   | 115 |
| 5.2.3  | Modified fHApS-DNA complex                                 | 115 |
| 5.2.4  | Stability of modified-fHApS-pDNA complex                   | 116 |
| 5.2.5  | Effect of physical shear force modified-fHApS-pDNA complex | 117 |
| 5.2.6  | Transformation of non-competent <i>C. albicans</i> cells   | 117 |
| 5.2.7  | Electroporation method                                     | 118 |
| 5.2.8  | Plasmid isolation from <i>C. albicans</i>                  | 118 |
| 5.2.9  | Cell viability and growth kinetics                         | 119 |
| 5.2.10 | Statistical analysis                                       | 120 |
| 5.3    | Results and Discussion                                     | 120 |
| 5.3.1  | Synthesis and characterization                             | 120 |
| 5.3.2  | Binding efficiency or DNA binding to modified-fHApS        | 123 |
| 5.3.3  | Stability of modified-fHApS-pDNA complex                   | 124 |
| 5.3.4  | Yeast Transformation                                       | 125 |
| 5.3.5  | Plasmid isolation from transformed <i>C. albicans</i>      | 128 |
| 5.3.6  | Cell toxicity and Growth kinetics                          | 128 |
| 5.4    | Conclusion   | 130 |



*Table of contents*

|  |            |
|--|------------|
| <b>Summary of Results and conclusion</b>                   | <b>131</b> |
| <b>Future Scope of Work</b>                                | <b>136</b> |
| <b>References</b>  | <b>137</b> |
| <b>Appendix I</b>  |            |
| <b>List of Publications and Presentations -Appendix II</b> |            |
| <b>Brief Biography of the Candidate – Appendix III</b>     |            |
| <b>Brief Biography of the Supervisor – Appendix IV</b>     |            |

## List of Tables

| Table            | Table heading  | Page |
|------------------|--|------|
| <b>Chapter 1</b> |  |      |
| <b>Table 1.1</b> | Commercially available NPs for various biomedical applications.  | 6    |
| <b>Table 1.2</b> | Phases of calcium phosphate present in bone  | 9    |
| <b>Table 1.3</b> | Methods for synthesis of hydroxyapatite nanoparticles  | 12   |
| <b>Table 1.4</b> | Europium doped hydroxyapatite nanoparticles for use in bioimaging and biolabelling   | 21   |
| <b>Table 1.5</b> | Lanthanides doped hydroxiapatite nanoparticles for use in bioimaging and biolabelling.   | 23   |
| <b>Table 1.6</b> | Lanthanide doped hydroxyapatite nanomaterials for multimodal imaging.  | 24   |
| <b>Chapter 2</b> |  |      |
| <b>Table 2.1</b> | Crystallite size, crystallinity and unit cell parameters of fabricated cells.  | 48   |
| <b>Table 2.2</b> | Different morphologies of HAp NPs synthesized using various solvent/stabilizing agent combinations.  | 54   |
| <b>Chapter 3</b> |  |      |
| <b>Table 3.1</b> | Optimized concentrations of thin rod, short rod and rods for which highest cell fluorescence intensities were achieved for HeLa, MG63, <i>C. albicans</i> , <i>S. aureus</i> and <i>E. coli</i> cells. | 78   |

---

| Chapter 4        |  |     |
|------------------|--|-----|
| <b>Table 4.1</b> | Transformation efficiencies of <i>E. coli</i> and <i>S. aureus</i> obtained using nanoparticles mediated (fHAp, R-fHAp, R-G-fHAp), calcium chloride and electroporation methods. | 108 |
| <b>Table 4.2</b> | Growth kinetics parameters of <i>E. coli</i> and <i>S. aureus</i> at different concentrations of R-G-fHAp.   | 110 |

---

| Chapter 5        |  |     |
|------------------|--|-----|
| <b>Table 5.1</b> | Transformation efficiencies of <i>C. albicans</i> obtained using modified-fHAp of various NP:pDNA ratio.   | 127 |
| <b>Table 5.2</b> | Transformation efficiencies of <i>C. albicans</i> obtained using nanoparticles mediated (modified-fHAp fHAp, R-G-fHAp), and electroporation methods. | 128 |
| <b>Table 5.3</b> | Growth kinetics parameters of <i>C. albicans</i> at different concentrations of modified-fHAp.   | 129 |

---

## LIST OF FIGURES

| Figure            | Figure Legend   | Page      |
|-------------------|---|-----------|
| <b>Chapter 1</b>  |   |           |
| <b>Figure 1.1</b> | Nanotechnology used in ancient era a) Lycurgus cup<br>b) Damascus steel sword.  | <b>2</b>  |
| <b>Figure 1.2</b> | Naturally occurring nanosystems (a) Nacre; (b) Butterfly wings; (c) Feet of geckos; (d) Lotus leaves  | <b>4</b>  |
| <b>Figure 1.3</b> | Schematic representation of Top-Down and Bottom-Up approaches for the fabrication of nanoparticles  | <b>5</b>  |
| <b>Figure 1.4</b> | a) Various applications of HAp NPs b) Hexagonal crystalline structure of HAp NPs green dots: OH <sup>-</sup> molecules, red dots: PO <sub>4</sub> and blue dots: Ca <sup>2+</sup> .   | <b>11</b> |
| <b>Figure 1.5</b> | Confocal laser scanning microscopy images of A549 cells incubated with fluoridated Eu <sup>3+</sup> -HAP/iron oxide nanocomposites at 37 °C for 2 h without magnetic field (Row 1) and under a magnetic field of 1.3T (Row 2). (A) The blue channel with excitation at 340 nm. (B) The red channel with excitation at 405 nm. (C) The combined red and blue channels. | <b>20</b> |
| <b>Figure 1.6</b> | Schematics of pDNA-Calcium phosphate gene delivery. Once the pDNA-CaP complex is formed by the co-precipitation process, the complex enters the cell through endocytosis. Through the endocytic pathway, pDNA translocates into the nucleus, and subsequently become translated and transcribed, expressing therapeutic proteins of interest                          | <b>27</b> |
| <b>Chapter 2</b>  |   |           |
| <b>Figure 2.1</b> | Schematic illustration of synthesis of HAp NPs by using DMSO (a) and water (b) as solvent while TEA/ACA as reducing agents  | <b>40</b> |

---

|                   |  |           |
|-------------------|--|-----------|
| <b>Figure 2.2</b> | XRD spectra of HAp samples obtained using various stabilizing agents (TEA and ACA) and solvents (water and DMSO) a) Sigma-control b) ACA and water c) no stabilizing agent and in water d) TEA and water e) TEA and DMSO f) ACA and DMSO.  | <b>47</b> |
| <b>Figure 2.3</b> | a) FTIR b) Raman spectra of HAp samples obtained using various stabilizing agents (TEA and ACA) and solvents (water and DMSO) i) commercially purchased control from Sigma ii) ACA and water iii) no stabilizing agent and in water iv) TEA and water v) TEA and DMSO vi) ACA and DMSO   | <b>49</b> |
| <b>Figure 2.4</b> | EDAX spectra of HAp samples obtained using various stabilizing agents (TEA and ACA) and solvents (water and DMSO) a) ACA and water b) no stabilizing agent and in water c) TEA and water d) TEA and DMSO e) ACA and DMSO.  | <b>50</b> |
| <b>Figure 2.5</b> | TEM micrographs of HAp NPs with different morphologies obtained using varied stabilizing agents (TEA and ACA) and solvents (water and DMSO) a) rods with average length 92.8nm and average diameter 23.2nm were obtained when water was used as a solvent and TEA as a stabilizing agent b) short-rods with average length 35nm and average diameter 7nm were obtained when DMSO was used as a solvent and TEA as a stabilizing agent c) thin-rods with average length 62.5nm and average diameter 6.2nm were obtained when DMSO was used as a solvent and ACA as a stabilizing agent d) mixed morphology nanostructures were obtained when water was used as a solvent and ACA as a stabilizing agent e) microrods with average length of | <b>53</b> |

---

---

|                   |   |           |
|-------------------|---|-----------|
|                   | 1.42 $\mu$ m and average diameter of 0.29 $\mu$ m without using any stabilizing agent while maintaining Ca/P ratio 1.67 f) spherical sigma control  |           |
| <b>Figure 2.6</b> | Epi-fluorescence microscope images of fHAp NPs using FITC (green) and TRITC (red) filters a) thin-rods b) short-rods c) rods, synthesized at room temperature by modified sol-gel method. d) microrods synthesized without stabilizing agents. All the fHAp exhibit both green and red fluorescence. Commercially obtained spherical HAp NPs (symmetric in shape) that do not show any fluorescence are shown for comparison in (d).  | <b>56</b> |
| <b>Figure 2.7</b> | Fluorescence spectra of fHAp at an excitation of 325nm. fHAp exhibit a broad emission spectrum ranging from 350-750nm with maximum at 502nm and additional peaks at 528nm, 567nm and 609nm. The fluorescence spectrum of commercially obtained spherical HAp NPs (red) is shown for comparison. Although, the emission spectra of fHAp were similar, significant changes in the intensity of fluorescence signal of the order of thin-rods (black line) > short-rods (blue) > rods (magenta) > microrods (green) were observed. | <b>57</b> |
| <b>Figure 2.8</b> | Fluorescence spectra of a) thin rod b) short rods c) rods d) microrods fHAp at different temperatures ranging from 300 to 15K. The emission signals across the spectra are shown with a connected line for clarity. Only an increase in the intensity of the emitted fluorescence signal, without any additional peaks was observed at low temperatures.  | <b>59</b> |
| <b>Figure 2.9</b> | ESR spectra of a) thin-rods b) short rods c) rods d)  | <b>60</b> |

---

---

microrods fHAp with three hyperfine splittings and “g” values (2.0082, 2.0069 and 2.0046) indicating the presence of free electrons owing to the asymmetric nature of these NPs. For comparison, the ESR spectrum of the commercially obtained spherical HAp NPs, which are symmetric, is shown in (e). Notice the absence of hyperfine splitting in the case of spherical HAp NPs.

---



---

### Chapter 3

---

|                   |  |           |
|-------------------|--|-----------|
| <b>Figure 3.1</b> | a) MTT and b) LDH c) ROS generation data showing non-toxicity, no oxidative stress on HeLa cell lines after 24 h d) hemolytic rate of thin rods, short rods and rods fHAp NPs various concentrations ranging from 10-1000 µg/ml.   | <b>73</b> |
| <b>Figure 3.2</b> | a) MTT and b) LDH c) ROS generation data showing non-toxicity, no oxidative stress on HaCaT cell lines after 24 h.   | <b>74</b> |
| <b>Figure 3.3</b> | Fluorescence spectra of a) thin rod b) short rod c) rod fHAp in biological media DMEM (red) and PBS (pH 7) (black). No change in fluorescence spectra in both the conditions indicating that fluorescence of fHAp is not dependent on the surrounding environment, and is rather an intrinsic property of the nanoparticles. | <b>75</b> |
| <b>Figure 3.4</b> | Relative fluorescence intensities of a) thin rods b) short rods c) rods, obtained in PBS, DMEM, DMEM plus FBS, LB and SB media for different time intervals (0-12h).   | <b>77</b> |
| <b>Figure 3.5</b> | Average fluorescence intensities of a) HeLa b) MG63  | <b>80</b> |

---

---

|                    |  |           |
|--------------------|--|-----------|
|                    | c) HaCaT d) <i>C. albicans</i> e) <i>E. coli</i> f) <i>S. aureus</i> under<br>i) TRITC and ii) FITC filters using thin rods (black<br>line), short rods(red) and rods(blue).   |           |
| <b>Figure 3.6</b>  | Bright intracellular fluorescence with green and red<br>emissions was observed inside the cells under epi-<br>fluorescence microscope, using bright field (i), TRITC<br>(ii) and FITC (iii) filter indicating that a) thin rods b)<br>short rods c) rod HAp NPs were internalized by HeLa<br>cells.                      | <b>81</b> |
| <b>Figure 3.7</b>  | Bright intracellular fluorescence with green and red<br>emissions was observed inside the cells under epi-<br>fluorescence microscope, using bright field (i), TRITC<br>(ii) and FITC (iii) filter indicating that a) thin rods b)<br>short rods c) rod HAp NPs were internalized by<br>MG63 cells.                      | <b>82</b> |
| <b>Figure 3.8</b>  | Bright intracellular fluorescence with green and red<br>emissions was observed inside the cells under epi-<br>fluorescence microscope, using bright field (i), TRITC<br>(ii) and FITC (iii) filter indicating that a) thin rods b)<br>short rods c) rod HAp NPs were internalized by<br>HaCaT cells.                     | <b>83</b> |
| <b>Figure 3.9</b>  | Bright intracellular fluorescence with green and red<br>emissions was observed inside the cells under epi-<br>fluorescence microscope, using bright field (i), TRITC<br>(ii) and FITC (iii) filter indicating that a) thin rods b)<br>short rods c) rod HAp NPs were internalized by <i>C.</i><br><i>albicans</i> cells. | <b>84</b> |
| <b>Figure 3.10</b> | Bright intracellular fluorescence with green and red<br>emissions was observed inside the cells under epi-<br>fluorescence microscope, using bright field (i), TRITC<br>(ii) and FITC (iii) filter indicating that a) thin rods b)   | <b>85</b> |

---



|                    |   |            |
|--------------------|---|------------|
|                    | short rods c) rod HAp NPs were internalized by <i>E. coli</i> cells.  |            |
| <b>Figure 3.11</b> | Bright intracellular fluorescence with green and red emissions was observed inside the cells under epifluorescence microscope, using bright field ( i), TRITC (ii) and FITC (iii) filter indicating that a) thin rods b) short rods c) rod HAp NPs were internalized by <i>S. aureus</i> cells.   | <b>86</b>  |
| <b>Figure 3.12</b> | Time dependent internalization of thin rods in HeLa (black colour line), <i>E.coli</i> (red colour line), <i>S. aureus</i> (blue colour line) and <i>C. albicans</i> (magenta colour line) observed under a) TRITC and b) FITC filter.  | <b>87</b>  |
| <b>Chapter 4</b>   |   |            |
| <b>Figure 4.1</b>  | Binding efficiencies of NPs:pDNA with various ratios a) Thin rod (black line), short rod(red line) and rod(blue line) shaped fHAp. The order of B.E is Thin rod>short rod >rod shaped fHAp b) Image of agarose gel electrophoresis confirming binding of pDNA to rod fHAp(lane i), short rod fHAp(lane ii) and thin rod fHAp (lane iii) at NPs:pDNA ratio of 130:1, lane iv is control. | <b>99</b>  |
| <b>Figure 4.2</b>  | a) XRD pattern b) FTIR spectra and c) TEM micrographs of fHAp, H-fHAp, K-fHAp, R-fHAp and R-G-fHAp. Characteristic XRD peaks of fHAp were observed in all the samples. FTIR spectra showed characteristic bands of HAp, amide I, amide II, NH <sub>2</sub> and glucose. TEM morphology observed was similar for all the samples.  | <b>102</b> |
| <b>Figure 4.3</b>  | Binding efficiencies of NPs:pDNA with various ratios  | <b>104</b> |

- 
- a) fHAp-pDNA(dash), H-fHAp-pDNA(dash dot dot), K-fHAp-pDNA (short dots), R-fHAp-pDNA(dots) and R-G-HAp NPs-pDNA (straight line). The order of B.E is R-fHAp > K-fHAp > H-fHAp > fHAp b) Image of agarose gel electrophoresis confirming binding of pDNA to H-fHAp(lane i), K-fHAp(lane ii) and R-fHAp (lane iii) at NPs:pDNA ratio of 70:1, lane iv is control. c) Image of agarose gel electrophoresis confirming binding of pDNA to R-G-HAp NPs. Lane i-v shows R-G-fHAp-pDNA complex when weight ratios of R-G-fHAp:pDNA were 10:1, 30:1, 50:1, 70:1 and 100:1 respectively. Lane vi is control (0:1).
- Figure 4.4** Image of agarose gel electrophoresis, demonstrating stability of R-G-fHAp-pDNA complex a) in the temperature of 37(lane i), 60 (lane ii), 80 (lane iii), 90 (lane iv) and room temperature(lane v) b) at room temperature for 30 days (lane i- control R-G-fHAp-pDNA complex, ii- complex after 30 days) c) in buffer of pH 4 (lane v), 6 (lane i), 7 (lane ii), 9 (lane iii) and 11 (lane iv) d) in sonication-induced stress for 0 (lane i), 2 (lane ii), 5 (lane iii), 10 (lane iv) and 30s (lane v). **105**
- Figure 4.5** Transformed bacterial colonies of a) *E. coli* (b) *S. aureus* on kanamycin containing LB agar plates. Both the strains were transformed using R-G-fHAp without preparation of competent cells. **108**
- Figure 4.6** a) MTT and b) Resazurin data showing non-toxic nature of R-G-fHAp on i) *E. coli* and ii) *S. aureus* after 6, 12 and 18h of growth in presence of various concentrations ranging from 10-1000 µg/mL. c) Growth curve showing no change of growth pattern in presence of R-G-fHAp at various concentrations. **109**
-

|                   |  |            |
|-------------------|--|------------|
| <b>Figure 4.7</b> | Agarose gel image of pDNA i) isolated from <i>E.coli</i> ii) <i>S. aureus</i> transformed using R-G-fHAp ii) control pDNA.   | <b>111</b> |
| <b>Chapter 5</b>  |  |            |
| <b>Figure 5.1</b> | a) XRD pattern b) FTIR spectra and c) TEM micrographs of HAp and modified-fHAp. Characteristic XRD peaks of HAp were observed in all the samples. FTIR spectra showed characteristic bands of HAp, amide I, amide II, NH <sub>2</sub> glucose and PEG. TEM morphology observed was same for modified-fHAp with average length and diameter of 67.27nm and 6.9nm.   | <b>122</b> |
| <b>Figure 5.2</b> | a) Binding efficiencies of modified-fHAp:pDNA of various ratios b) Image of agarose gel electrophoresis confirming binding of pDNA to modified-HAp NPs. Lane i-v shows modified-HAp NPs-pDNA complex when weight ratios of modified-fHAp:pDNA were 10:1, 30:1, 50:1, 70:1 and 100:1 respectively.  | <b>124</b> |
| <b>Figure 5.3</b> | Image of agarose gel electrophoresis, demonstrating stability of modified-fHAp-pDNA complex a) in the temperature of 37(lane i), 60 (lane ii), 80 (lane iii), 90°C (lane iv) and room temperature(lane v) b) at room temperature for 30 days (lane i- control modified-fHAp-pDNA complex, ii- complex after 30 days) c) in buffer of pH 4 (lane v), 6 (lane i), 7 (lane ii), 9 (lane iii) and 11 (lane iv) d) in sonication-induced stress for 0 (lane i), 2 (lane ii), 5 (lane iii), 10 (lane iv) and 30s (lane v). | <b>125</b> |
| <b>Figure 5.4</b> | Transformed <i>C. albicans</i> on kanamycin and gentamicin   | <b>127</b> |

---

|                   |  |            |
|-------------------|--|------------|
|                   | containing SB agar plates. It was transformed using modified-fHAp without preparation of competent cells.  |            |
| <b>Figure 5.5</b> | Agarose gel image of pDNA i) isolated from <i>C. albicans</i> transformed using modified-fHAp ii) control pDNA.  | <b>128</b> |
| <b>Figure 5.6</b> | a) MTT and b) Resazurin data showing non-toxic nature of modified-fHAp on <i>C. albicans</i> after 12, 24 and 36h of growth in presence of various concentrations ranging from 10-1000µg/mL. c) Growth curve showing no change of growth profile in presence of modified-fHAp at various concentrations. | <b>130</b> |

---

**List of Abbreviations and Symbols**

ACA - acetyl acetone

Ag- silver

B.E - Binding efficiency

Ca<sup>2+</sup>- Calcium

CaP - calcium phosphate

CNTs - Carbon nanotubes

CO<sup>2</sup> - carbon dioxide

Cu - copper

CT - computed tomography

DNA - Deoxyribonucleic acid

DCPD - dicalcium phosphate dehydrate

DCFH - 2', 7'- dichlorofluorescein diacetate

DMSO - dimethyl sulfoxide

DMEM - Dulbecco's modified Eagle's medium

DLS - Dynamic light scattering

DI - de-ionized water

EDAX - energy dispersive analysis of X-ray

EDTA - ethylenediamine tetraacetic acid

EGFP - enhanced green fluorescent protein plasmid

ESR - Electron spin resonance

Eu<sup>3+</sup>- Europium

F<sup>-</sup> - fluorine

Fe<sup>3+</sup>- Iron

FTIR - Fourier transform infrared

Gd<sup>3+</sup>- gadolinium

## **List of abbreviations and symbols**

GFP - green fluorescent protein

H - histidine

HAp - Hydroxyapatite

H<sub>2</sub>O<sub>2</sub> - Hydrogen peroxide

ICG - indocyanine green

K - lysine

La - lanthanum

LB - Luria Bertani

LDH - lactate dehydrogenase

Ln - lanthanides

Lu - lutetium

LiAc - lithium acetate

MCPH - Monohydrate calcium phosphate

MCP - Monocalcium phosphate

MRI - magnetic resonance imaging

MTT - 3-(4,5-dimethylthiazol-2-yl)-2,5-diphenyltetrazolium bromide

Nd<sup>3+</sup> - neodymium

NPs - Nanoparticles-

NIR - near infra red

O - oxygen

OCP - Octacalcium phosphate

OD - optical density

OH<sup>-</sup> - Hydroxyl

P- Phosphorous

PBS - phosphate buffer saline

pDNA - plasmid DNA

PO<sub>4</sub><sup>3-</sup> - Phosphate

PEG - polyethylene glycol

## **List of abbreviations and symbols**

PL - Photoluminescence  
Pr<sup>3+</sup>- praseodymium  
QDs - quantum dots  
R - arginine  
ROS - reactive oxygen species  
SB - Sabouraud dextrose media  
SDS - sodium dodecyl sulfate  
Sr<sup>3+</sup>- Strontium  
Tb<sup>3+</sup> - Terbium  
TCP - Tricalcium phosphate  
TEA - triethyl amine  
TEM - Transmission electron microscope  
T.E - Transformation efficiency  
TRITC - Tetramethylrhodamine  
UcNPs - upconversion NPs  
UV- Ultraviolet  
XRD - X-ray diffraction  
Yb<sup>3+</sup> - ytterbium  
Zn- zinc  
 $\Delta\nu$  - Stokes' shift  
 $\lambda_{\text{ex}}$  - excitation maximum  
 $\lambda_{\text{em}}$  - emission maximum

## CHAPTER 1

### Introduction and Review of Literature

#### 1.1 Introduction

Nanotechnology is defined as design and production of structures, devices and systems by controlled manipulation of sizes and shapes at atomic, molecular and macromolecular scale where properties differ significantly from those of bulk materials. According to National Nanotechnology Initiative (NNI), nanotechnology is: “The understanding and control of matter at dimensions of roughly 1 to 100nm, where unique phenomena enable novel applications.”

The concept of “*nanoscience/nanotechnology*” was introduced by the Nobel laureate Richard Feynman in 1959, in his visionary talk entitled “*There is plenty of room at the bottom*” at the American Physical Society meeting. Though he did not explicitly mention the term “*nanotechnology*”, he suggested the eventual possibility of manipulating atoms and molecules precisely in a desired fashion to create molecular-machines. According to him, the advent of this technology could facilitate the writing of the entire 24 volumes of the Encyclopedia Britannica on the head of a pin (Feynman 1960). In 1974, the term “nanotechnology” was used for the first time by Professor Norio Taniguchi to describe the processes of creating semiconductor with nanometer dimension. The term was used again in 1981 when Eric Drexler, inspired by Richard Feynman’s talk, developed and popularized the concept of nanotechnology (Feynman 1960). He published the famous book “Engines of creation: the coming era of nanotechnology” in which he used the word nanotechnology to describe engineering on the billionth of a meter scale. Invention of scanning tunneling microscope and the atomic force microscope has offered opportunities for scientists to the “nanoworld” by providing them the tools not only to image surfaces with atomic resolution, but also to move individual atoms as previously predicted by Richard Feynman.



### 1.1.1 Nanotechnology in ancient era

Long before the beginning of “nanoera”, ancient people used various nanoparticles (NPs) and processes related to it. Some classic examples are the Lycurgus cup: a cup made up of glass containing gold-silver alloyed NPs which changes colour from greenish-yellow to red when light is shone on it (Figure 1.1); Maya blue: a corrosion resistant blue pigment which consists of indigo molecules incorporated into needle-shaped palygorskite crystallites; Damascus steel sword: an unbreakable and exceptionally sharp sword built using steel blades containing oriented nanowires and nanotube like structure (Figure. 1.1). However, most of these antiques were developed accidentally without any understanding of process or nature of the object. They were aware of the fact that the properties of small particles are different from those of large; however, the reason behind it was not known. In many instances, technology was just delivered from one generation to another (Schaming and Remita 2015).

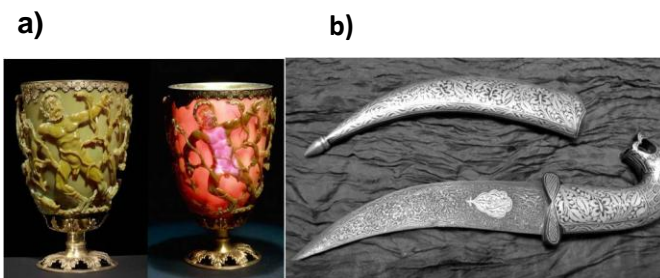


**Figure 1.1** Nanotechnology used in ancient era a) Lycurgus cup ([https://en.wikipedia.org/wiki/Lycurgus\\_Cup](https://en.wikipedia.org/wiki/Lycurgus_Cup)) b) Damascus steel sword ([https://en.wikipedia.org/wiki/Damascus\\_steel](https://en.wikipedia.org/wiki/Damascus_steel))

## 1.2 Nanomaterials

Nanomaterials possess physical and chemical properties that are different than their bulk counterparts. This difference arises due to the decrease in size, large surface area to volume ratio, large surface energy, spatial confinement of electrons and reduced imperfections. In fact, structural properties are intermediary to bulk materials and atoms. As size decreases from bulk to nano dimension, the properties become size dependent instead of being composition dependent due to alteration in electron structure from continuous energy level

(electronic state) to discrete energy level (Burda et al. 2005). The large surface area to volume ratio is responsible for novel surface dependent properties such as unique optical and magnetic behavior, electrical resistivity etc. (Gleiter 2000). Nanomaterials/particles/devices/systems are of two types: (i) naturally occurring and (ii) artificially synthesized as discussed in the following sections.

### **1.2.1 Naturally produced nanomaterials**

Naturally occurring NPs are dispersed uniformly, complex in shape, highly organized and mostly formed in hydrous environments. Few examples of naturally occurring nanosystems include nacre, colours in the wings of butterflies, feet of geckos and lotus leaves (Figure 1.2). Nacre (Figure 1.2a), the nanocomposites found inside mollusk shells, is composed of mineral platelets of calcium carbonate which is highly organized and provides strength, stiffness, impact resistance and toughness to the structure. The multilayered nanostructures on the wings of butterflies' (Figure 1.2b) act as diffraction gratings to induce interferences which results in myriad colours and patterns. Geckos (Figure 1.2c) possess nanostructured hairs on their feet that increase surface area leading to strong surface adhesion even on slippery, wet or dirty surfaces. The microscale mounds and nanoscaled hair like structures present on the lotus (Figure 1.2d) leaves are responsible for self-cleaning properties of the leaves. Biological processes in animals also involve lot of nanomachinery. These naturally found nanomaterials have inspired many scientists to design new materials mimicking nature with advanced properties (Wagner et al. 2014; Waychunas 2009).

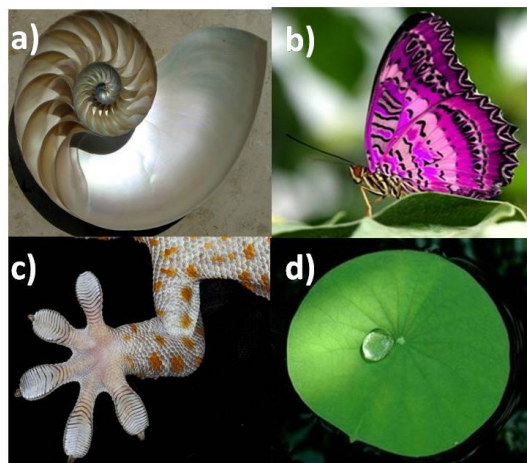


**Figure 1.2** Naturally found nanosystems (a) Nacre ( <https://en.wikipedia.org/wiki/Nacre>); (b) Butterfly wings (<https://en.wikipedia.org/wiki/Butterfly>); (c) Feet of geckos; ([https://en.wikipedia.org/wiki/Gecko\\_feet](https://en.wikipedia.org/wiki/Gecko_feet)) (d) Lotus leaves ([https://en.wikipedia.org/wiki/Lotus\\_effect](https://en.wikipedia.org/wiki/Lotus_effect)).

### 1.3 Nanostructures engineered by human and its biomedical application

Scientists have engineered many organic and inorganic nanoparticles for applications in the fields of biomedicine, electronics, automobiles, textiles, etc. Nanofabrication results in materials with unique physicochemical, electronic, magnetic, mechanical, optical and biological properties. Over the last three decades many techniques have been devised for the fabrication of nanomaterials. These techniques broadly include physical, chemical or bio-inspired/biogenic methods. These methodologies mostly depend on two traditional approaches (Figure 1.3): (i) top down- where the bulk particles are broken down to nanoscale; (ii) bottom up- where the elemental constituents are assembled into nanostructures. Some techniques also use both top-down and bottom up approaches for the fabrication of desired nanosystems (Wagner et al. 2014).

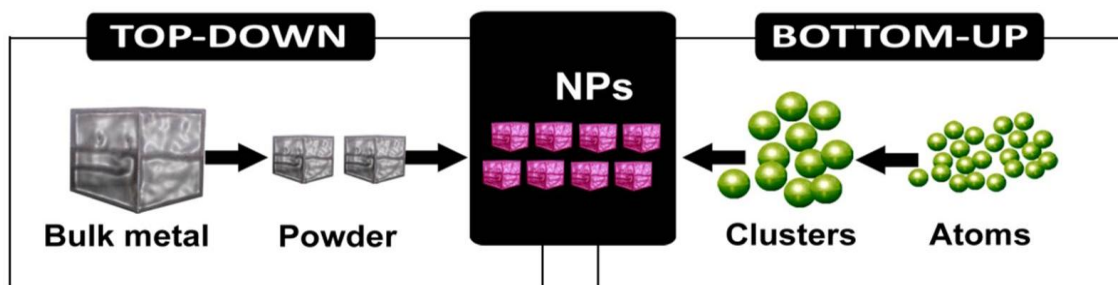


**Figure 1.3:** Schematic representation of Top-Down and Bottom-Up approaches for the fabrication of nanoparticles (NPs) (<http://www.epmagazine.org>).

In recent years, nanotechnology has emerged as a multidisciplinary area of research involving various disciplines such as materials science, chemistry, physics and biology. Since sizes of these NPs are comparable to that of large biological molecules such as enzymes, receptors, and antibodies, they can interact with biomolecules both on the surface as well as inside the cells. These particles can also be easily modified by altering their surface chemistry or by attaching specific ligands (Salata 2004; Sanvicens and Marco 2008). Moreover, the sizes and shapes of the NPs are easily manipulated by using various synthesis processes (Chen et al. 2000; Sun and Xia 2002). These exceptional properties of NPs give rise to their vast potential application in the field of biology. This rapidly growing field provides opportunities to develop multifunctional nano-devices which could target, diagnose and treat intractable diseases like cancer. Various NPs like liposomes, gold NPs, upconversion NPs (UcNPs), quantum dots (QDs), calcium phosphate/hydroxyapatite NPs, etc. are under investigation for diverse biomedical applications (Salata 2004; Thanh and Green 2010). Commercially available NPs for biological applications are listed in table 1.1

**Table 1.1** Commercially available NPs for various biomedical applications.

| <b>Technology</b>  | <b>Applications</b>                        | <b>Company name</b>          |
|--|--|------------------------------|
| Polymeric NPs engineered to transmit anti-tumor drug through blood brain barrier                           | Drug delivery                              | Advectus life sciences, Inc. |
| Hydroxyapatite NPs used to improve dental surface  | Toothpaste ingredients                     | BSF                          |
| Nanomagnetic/carbon composites shield the medial devices from radio frequency field.                       | MRI shielding                              | Biophan technologies, Inc.   |
| Silica coated gold NPs as fluorescent probe  | Bioimaging agents                          | Nanohybrids                  |
| Gold nanoconjugates for TEM and fluorescence marker  | Biolabelling agents                        | Nanoprobes Inc.              |
| Antimicrobial activity of silver nanocrystals  | Bandages                                   | Smith & Nephew               |
| Semiconductor quantum dots modified with amine or carboxyl groups, emission from 350-2500nm                | Luminescent biomarkers                     | Evident technologies         |
| Ceramic nanoporous materials for orthopedic and dental implant as well as for DNA and protein purification | Implant technology and membrane filtration | Argonide                     |
| Micellar NPs for encapsulation of drugs, DNA, proteins   | Drug/ DNA/ protein delivery                | NanoCarrier co. ltd.         |

### 1.3.1 Liposomes

Liposomes are one of the first NPs used for gene and drug delivery. They are spherical vesicles composed of phospholipid bilayer and cholesterol (Torchilin 2005). They acquire numerous advantageous characteristics such as non-immunogenicity, biocompatibility, biodegradability and the ability to carry and protect many types of biomolecules/drugs (Felgner and Ringold 1989; Torchilin 2005). These properties led to the wide use of liposomes as transfection agents of genetic material into cells (lipofection) for biological research (Felgner et al. 1987). Another major application of liposomes is as therapeutic carriers by entrapping hydrophilic compounds within the core and hydrophobic drugs in the lipid bilayer itself (Bangham 1993). It can also be functionalized with targeting ligands for targeted drug delivery. Today, there are twelve clinically approved liposome-based therapeutic drugs. However, the cost of production is high which limits their application (Akbarzadeh et al. 2013; Wang and Wang 2014).

### 1.3.2 Gold NPs

Gold NPs are extensively studied for wide biological applications. It has distinctive characteristics such as biocompatibility, exceptional size-shape dependent optical and chemical properties and facile surface modification (Daniel and Astruc 2004). These properties facilitated the use of gold NPs in various applications such as drug/protein/gene delivery, bio-imaging, biochemical sensing and detection, etc. Gold NP probes are used as marker for cancer and heart disease (Liu et al. 2008; Peng et al. 2009). They also have the potential in phototherapy due to their property of converting absorbed light into heat. Although gold nanoparticles are being used for a variety of applications, they have less solubility, low colloidal stability and toxicity at high concentration (Dykman and Khlebtsov 2011; Wang and Wang 2014).

### 1.3.3 Quantum dots

Quantum dots (QDs) such as zinc sulfide-capped cadmium selenide, indium phosphide, indium arsenide, etc possess a narrow, tunable and symmetric emission spectrum. Moreover, they are also resistant to metabolic degradation, thereby opening up new possibilities for bioimaging and diagnostics, in ultrasensitive biological detection such as deep tissue imaging, *in vitro* detection assays, etc. (Parak et al. 2005). Despite their potential and success in biological applications, there exist several limitations associated with their use. A common problem in QDs is optical blinking and photochemical oxidation, which causes difficulty in quantitative assays (Hardman 2006; True and Gao 2007). It is also found to be cytotoxic to the cells due to the presence of core metallic ions (Alivisatos 1996; Hardman 2006; Shiao 2008).

### 1.3.4 Carbon nanotubes

Carbon nanotubes (CNTs) are cylindrical shaped with nanoscale diameter and length in several millimeters. They have notable structural, electronic and mechanical properties such as high electrical and thermal conductivity and strong mechanical potency (Baughman et al. 2002). They are being majorly studied for drug/gene delivery, tissue regeneration and biosensor application. However, they are toxic and their surface modification is relatively difficult (He et al. 2013).

### 1.3.5 Upconversion nanoparticles

Upconversion nanoparticles (UcNPs) have gained much interest due to their unique characteristics of excitation at low energy and emission at higher energy (Wang et al. 2010a). They generally absorb light in the near infra red (NIR) region and emit at shorter wavelength (NIR/visible/UV). Lanthanide doped UcNPs are promising bioimaging agents of new generation due to high resistance to photobleaching, narrow emission bandwidth, large anti-Stokes' shift

and no autofluorescence (Chen et al. 2014). However, these NPs are not biocompatible and cannot be easily used for bio-applications.

All the above mentioned NPs are being extensively studied for many biological applications. However, uses of these nanomaterials for biological applications are limited due to their physicochemical properties, biocompatibility, bioactivity and toxicity (Kherlopian et al. 2008). Amongst all of these NPs, calcium phosphate/hydroxyapatite, a natural biomaterial, possesses desirable properties such as biodegradability, bioactivity, biocompatibility, etc. (Uskoković and Uskoković 2011) and hence could be used as a multifunctional nanomaterial.

#### 1.4 Hydroxyapatite nanoparticles

Calcium phosphates are primary constituents of bone and have been used as bone grafts in tissue engineering. It was first proposed as a material for fracture treatment in 1920, and the first study on bone defect repair using calcium phosphates was reported in 1950. In the following decades, extensive studies on these materials for biomedical applications were reported (Jarcho 1981; LeGeros et al. 2003). Hausen et al in the 19<sup>th</sup> century described the concept of different crystal phases of calcium phosphates (Dorozhkin 2007) as described in table 1.2.

**Table 1.2** Phases of calcium phosphate present in bone

| Phases of calcium phosphates         | Ca/P ratio | Molecular formula  |
|--------------------------------------|------------|--|
| Monohydrate calcium phosphate(MCPH)  | 0.50       | $\text{Ca}(\text{H}_2\text{PO}_4)_2 \cdot \text{H}_2\text{O}$  |
| Monocalcium phosphate(MCP)           | 0.50       | $\text{Ca}(\text{H}_2\text{PO}_4)_2$                           |
| Dicalcium phosphate dihydrate (DCPD) | 1.00       | $\text{Ca}(\text{HPO}_4) \cdot 2\text{H}_2\text{O}$            |
| Tricalcium phosphate(TCP)            | 1.50       | $\alpha$ and $\beta$ - $\text{Ca}_3(\text{PO}_4)_2$            |
| Octacalcium phosphate(OCP)           | 1.33       | $\text{Ca}_4\text{H}(\text{PO}_4)_3 \cdot 2\text{H}_2\text{O}$ |
| Hydroxyapatite(HAp)                  | 1.67       | $\text{Ca}_{10}(\text{PO}_4)_6(\text{OH})_2$                   |



Amongst all the phases of calcium phosphate, hydroxyapatite (HAp) is the most extensively studied phase, due to its stability in the physiological environment. It is the mineral from the family of apatite which consists of fluorapatite, chlorapatite and hydroxyapatite. The term apatite was first coined by Werner in 1788 and its composition first studied by Porust. HAp represented as  $\text{Ca}_5(\text{PO}_4)_3\text{OH}$  is the molecular formula whereas  $\text{Ca}_{10}(\text{PO}_4)_6(\text{OH})_2$  is the formula of the unit cell, in which the OH group can be easily replaced by fluorine/chlorine to form fluorapatite/chlorapatite (Baddiel and Berry 1966; Prener 1967). HAp exhibits hexagonal crystalline lattice with a stoichiometric Ca:P ratio of 1.67 (Figure 1.4b). The unit cell of HAp can also be represented with the formula:  $\text{M1}_4\text{M2}_6(\text{PO}_4)_6(\text{OH})_2$ , where M1 and M2 are two different crystallographic positions for 10 calcium atoms. M1 position is occupied by four Ca atoms in the unit cell and is surrounded by nine oxygen atoms of  $\text{PO}_4$  tetrahedra. The other six Ca atoms occupy M2 site where they are coordinated by six O atoms of the  $\text{PO}_4$  tetrahedra and one of the two  $\text{OH}^-$  groups. The unit cell dimensions of pure hexagonal HAp are: a = b axis= 0.937nm, c axis= 0.688nm (Figure 1.4b). Mainly covalent and ionic bonds are found in HAp (Kay et al. 1964; Uskoković and Uskoković 2011).

HAp is known to be brittle like other ceramics and degrades at pH >4.0. It is an interesting biomaterial with similar morphology and chemical composition to the human hard tissue such as bone and teeth. Bones or dentins consist of 70 weight% apatite, 20 weight% collagen, and 10 weight% water (Monroe et al. 1971; Penel et al. 2005). It possesses several characteristic features of an ideal biomaterial such as biodegradability, bioactivity, biocompatibility, osteointegration, osteoconductivity and osteoinductivity (Uskoković and Uskoković 2011; Woodard et al. 2007). It is being extensively studied as bone fillers, bioactive coatings, drug/protein/gene delivery system, bioimaging agents, etc. Size, morphology and chemical composition of HAp plays a vital role to determine its properties and applications. HAp NPs could significantly enhance bioactivity and restorability due to large surface area and hence could be efficient

candidates for bioimaging, targeted protein/drug/gene delivery, diagnosis and treatment (Figure 1.4a). Moreover, it is an ideal host for various doping agents such as metal ions, organic dyes, proteins, drugs and other substrates (Uskoković and Uskoković 2011), and exploited in the field of chemistry, biology and medicine.

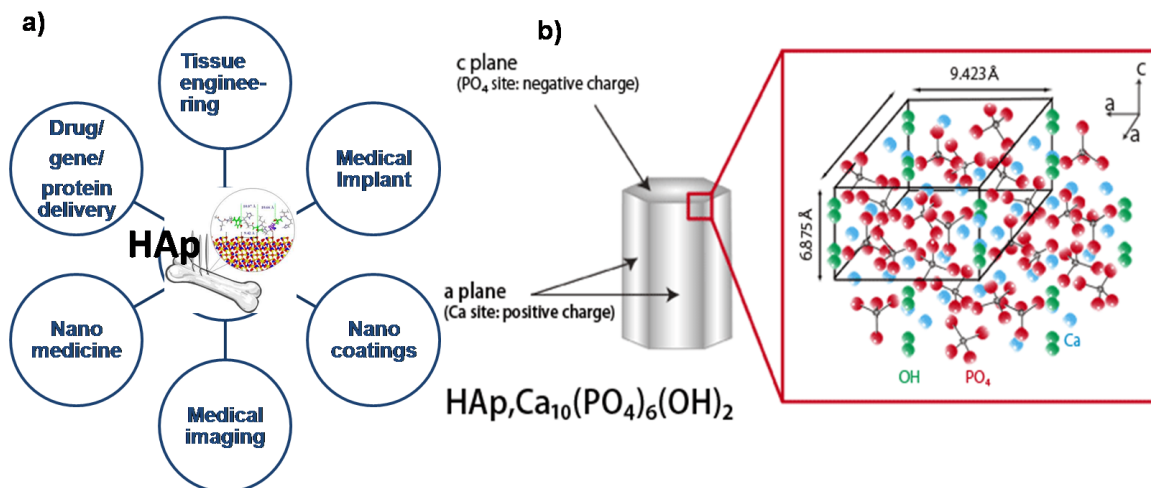


**Figure 1.4:** a) Various applications of HAp NPs b) Hexagonal crystalline structure of HAp NPs green dots: OH<sup>-</sup> molecules, red dots: PO<sub>4</sub> and blue dots: Ca<sup>2+</sup> (Selvig 1972).

### 1.5 Synthesis of hydroxyapatite nanoparticles

Hydroxyapatite nanoparticles (HAp NPs) can be synthesized using various methods which are categorized into solid state and wet chemical methods (table 1.3). These methods have been modified to develop controlled morphology. All these methods can synthesize different morphologies of HAp NPs depending on reaction parameters.

**Table 1.3:** Methods for synthesis of hydroxyapatite nanoparticles

|             |                           |
|-------------|---------------------------|
| Solid state | Solid state reaction      |
|             | Mechanochemical           |
| Wet state   | chemical precipitation    |
|             | Homogeneous precipitation |
|             | Emulsion                  |
|             | Hydrothermal              |
|             | Sol-gel                   |

### 1.5.1 Solid state

Solid state methods involve addition of powdered calcium and phosphate precursor in the Ca:P ratio of 1.67. Commonly used solid state methods to obtain HAp NPs are as follows:

#### 1.5.1.1 Solid-state reaction

In solid-state reaction powdered calcium and phosphate precursors are stimulated by thermal treatment to obtain well crystallized HAp particles. This process is simple, economic and suitable for large scale production of HAp (Fowler 1974; Okada and Matsumoto 2015; Rao et al. 1997). However, relatively long treatment times and high temperatures (mostly exceeding 700°C) make this process cumbersome.

#### 1.5.1.2 Mechanochemical process

Mechanochemical process includes mixing of calcium and phosphate precursors using mechanical force where techniques like milling or grinding break down the particles into nanoparticulate form (Briak - BenAbdeslam et al. 2003; Koutsopoulos 2002; Okada and Matsumoto 2015). Although, used instead of solid-state reactions, mechanochemical methods are time and energy intensive with low yield of product.

## **1.5.2 Wet state methods**

In wet state methods, for synthesis of HAp NPs, aqueous solutions of various calcium (calcium chloride, calcium oxide, etc.) and phosphate (orthophosphate, phosphorous pentoxide, etc.) precursors are added together while maintaining Ca:P ratio at 1.67. These methods are most popular for the synthesis of controlled morphologies of HAp NPs at relatively low temperature and are described below:

### **1.5.2.1 Precipitation method**

This method is the simplest route for synthesis of nano-HAp which is carried out by dissolving calcium and phosphate solution above pH 7 for precipitation. The typical procedure involves the dropwise addition of one reagent into another under continuous stirring while maintaining the stoichiometric ratio of Ca:P at 1.67. The resulting suspension is aged under atmospheric pressure, washed, filtered, dried and crushed into powder (Koutsopoulos 2002; Monmaturapoj 2008; Okada and Matsumoto 2015). Although this method is simple and relatively less expensive, the NPs obtained through this method tend to agglomerate faster/easily.

### **1.5.2.2 Emulsion method**

In the emulsion method, similar to precipitation technique, aqueous solutions of calcium and phosphate are dissolved. The resulting suspension is added dropwise in an emulsion system to produce small aqueous droplets (Furuzono et al. 2001; Lim et al. 1996; Okada and Matsumoto 2015). The emulsion is prepared by adding an appropriate amount of surfactant in oil-water phase. The surfactant reduces agglomeration of NPs by acting as capping/stabilizing agent. This method provides an easier way to control particle size, morphology and agglomeration; however, they are time consuming and produce low yields.

### 1.5.2.3 Hydrothermal method

The hydrothermal method entails the dissolution of aqueous calcium precursor into phosphate precursor with thorough mixing. The obtained solution is heated at high temperature (150–400°C) under high pressure (120Psi) (Koutsopoulos 2002; Okada and Matsumoto 2015; Yang et al. 2014). Microwave irradiation can also be used instead of the conventional method of autoclaving (Katsuki et al. 1999; Loo et al. 2008). Although HAp formed using this method is highly crystalline without any contamination with secondary phases like calcium oxide,  $\alpha$ -TCP,  $\beta$ -TCP, this method is time consuming and requires expensive instrumentation.

### 1.5.2.4 Sol-gel synthesis

The sol-gel synthesis involves the formation of colloidal suspension (sol) in a liquid medium that acts as the precursor to form an integrated network (gel) of colloid and liquid. HAp NPs synthesis using this method is obtained by dropwise addition of the aqueous calcium precursor into aqueous phosphate precursor under stirring conditions. The resulting suspension is aged, washed, dried and calcined. HAp NPs of varying shapes and sizes can be fabricated using this method.

The sol-gel process has been modified by varying parameters/ingredients like precursors, solvent system, calcination temperatures, pH, etc. to achieve HAp NPs of various sizes, shapes and crystallinity. For example, Liu et al reported sol-gel synthesis of porous nanocrystalline HAp by dissolving triethyl phosphite and calcium nitrate, subsequently, ageing the resultant suspension for 16 h at room temperature and further calcining at 300 to 800°C (Liu et al. 2002b). Fathi et al obtained crystalline HAp NPs (10-15nm) using phosphorous pentoxide and calcium nitrate tetrahydrate as precursors and calcination of the resultant gel at 600-700°C (Fathi and Hanifi 2007). Similarly, Padmanabhan et al have obtained hexagonal crystalline HAp nanorods using a calcination temperature of 300-

400°C, pH of 9.0 and phosphorous pentoxide and calcium nitrate tetrahydrate as calcium and phosphate precursors were obtained (Padmanabhan et al. 2009).

In recent years, sol-gel process for synthesis of HAp NPs has gained much interest due to low temperature and easy synthesis. This method has improved chemical homogeneity by mixing calcium and phosphate precursors at molecular level compared to conventional methods such as solid state reactions, wet precipitation, and hydrothermal syntheses. HAp NPs obtained using sol-gel method are pure, homogeneous, analogous to biological apatite as compared to HAp obtained through other methods.

## **1.6 Applications of HAp NPs**

HAp NPs have used for various biological applications such as bioimaging, and targeted drug/protein/gene delivery and are described below.

### **1.6.1 Bioimaging**

Bioimaging is the technique of acquiring images of biological processes such as changes in receptor kinetics, cellular signaling, the movement of molecules through membranes, etc. using various imaging techniques and equipments. This technique can be used for both diagnostic as well as therapeutic purposes (theranostics). For example effectiveness of particular therapy can be assessed by tagging the molecule (drugs, proteins, enzymes) and observing cellular changes (Dong and Roman 2007). In the past two decades, there has been tremendous development of new imaging techniques. Various techniques such as magnetic resonance imaging (MRI), computed tomography (CT), fluorescence imaging, radio imaging, etc., enable visualization of multi-dimensional and multi-parameter data (Kherlopian et al. 2008; Prasad 2003). Compared to other techniques, fluorescence imaging is advantageous as it is highly sensitive, selective, minimally-invasive, safe and a widely used technique (Ntziachristos 2006; Wang et al. 2005).

Fluorescence imaging is the visualization of fluorescent probe labeled processes or structures with the help of various fluorescence imaging techniques such as time-lapse microscopy, confocal microscopy, fluorescence microscopy, etc. In recent years, fluorescence imaging has received much attention, especially in the field of biology and medicine due to the increasing availability of fluorescent dyes, proteins, and probes which provide ease to the non-invasive study of many biological processes (Ettinger and Wittmann 2014). Fluorescent labeling using usual organic dyes, fluorescent proteins and lanthanide chelates is the preferred method due to its low cost, ease of availability and use. However, they possess some inherent drawbacks such as poor photochemical stability, short Stokes' shift (difference between wavelengths of excitation and emission maxima), susceptibility to photo-bleaching (permanent loss of fluorophore to fluoresce), decomposition under repeated excitation and low quantum yields (efficiency of the energy transferred from incident light to emitted fluorescence) (Wang et al. 2005). In view of the existing limitations, more efficient fluorescent nanomaterials have been developed as alternative bioimaging agents. Fluorescent nanomaterials including quantum dots(QDs), carbon NPs, gold NPs, UCNPs and NPs doped with lanthanides/organic dyes, owing to their small size and large surface area, have shown significant progress in diagnostics as well as in therapeutic applications (Nune et al. 2009; Syamchand and Sony 2015; Wolfbeis 2015).

Amongst various nanoparticles, HAp NPs doped with lanthanides and organic dyes are being extensively studied as fluorescent probes due to their excellent biocompatibility, bioactivity and biodegradability. Their chemical and porous structure easily allows doping with organic dyes and many lanthanides; hence they have been used as fluorescent probes (Elliott 2013; Kay et al. 1964). Doping of HAp NPs with organic dye and lanthanide is discussed below:

### 1.6.1.1 Doping of HAp NPs with organic dye

Fluorescence intensity and quantum yield of dyes can be enhanced by doping of dyes on HAp NPs. This can also provide stability to the dye and reduce photobleaching. Moreover, biocompatible HAp NPs have the ability to pass through the cell membrane which could facilitate the use of dye-doped HAp NPs for *in vitro* and *in vivo* imaging. Optical properties of dye/fluorescent protein can be influenced by the environmental proteins/factors. Hence encapsulation of dye in HAp NPs can help to maintain their optical properties. Moreover, these NPs are easy to handle as compared to fluorescent dyes/proteins. Morgan et al reported successful encapsulation of various dyes such as cascade blue, 10-(3-sulfopropyl) acridinium betaine, fluorescein sodium salt, rhodamine and Cy3 amidite in HAp NPs (20-30nm) and exhibited four-fold increase in quantum efficiency after encapsulation as well as effective internalization in bovine aortic cells (Morgan et al. 2008). Calcium phosphate NPs encapsulated with indocyanine green (ICG), a NIR emitting dye, exhibited five-fold longer fluorescence half-life and two-fold higher quantum efficiency than ICG dye alone. They also showed accumulation in xenograft breast adenocarcinoma tumors within 24h of injection (Altinog˘lu et al. 2008). Ge et al. reported enhanced quantum yield as well as reduced photobleaching and quenching of methylene blue when methylene blue encapsulated silica layers were coated on HAp NPs by a modified Stöber method (Ge et al. 2013). Surface functionalization of HAp NPs with fluorescein isothiocyanate resulted in bright and stable fluorescent particles that were internalized by human cervical cancer cells-HeLa cells (Liu et al. 2011a). These studies suggest that encapsulation of organic dyes in HAp NPs could generate new attractive fluoroprobes for sensitive diagnostic imaging applications.

### 1.6.1.2 Lanthanides doped HAp NPs

Lanthanides (Ln) are rare earth metals with an electronic configuration of  $(Xe)4f^n$ , where n varies from 0 to 14. They are fifteen lanthanide elements from



lanthanum (La) through lutetium (Lu). All lanthanides are 'f' block elements (except La, which is 'd' block element) which form trivalent cations ( $\text{Ln}^{3+}$ ). They possess interesting optical properties such as prolonged luminescence as well as sharp excitation and emission spectra. These properties are the result of three types of electronic transitions involved in  $\text{Ln}^{3+}$  ions: (i) charge-transfer transitions: transfer of an electron from ligand to metal or from metal to ligand; (ii) 4f-5d transitions: the transfer of a 4f orbital electron into the 5d sub-shell; and (iii) sharp intra configurational 4f-4f transitions: the transition of an electron from 'f' orbital which is lower in energy to 'f' orbital which is higher in energy. Ln, due to their unique properties like large Stokes' shifts and long emission life times (from microseconds to milliseconds) are well suited for biological applications and have been doped in various inorganic matrices like silica, HAp etc. to enhance biocompatibility and reduce toxicity (Bünzli 2010; Bünzli and Eliseeva 2010; Hänninen and Härmä 2011).

Lanthanide doped HAp NPs has attracted significant interest for a variety of biomedical applications due to their favorable characteristics such as broad excitation spectra, long fluorescence life-time, sharply spiked emission spectra, large Stokes' shifts, high quantum yields (Doat et al. 2003; Lebugle et al. 2006) and excellent luminescent properties due to f-f electronic transitions (Binnemans 2009; Bünzli and Eliseeva 2010; Graeve et al. 2010). Moreover, the long lived fluorescence signals exhibited by Ln doped HAp NPs can be easily distinguished from the short lived background signals of most biological samples, thus, studies on synthesis and biological applications of Ln doped fluorescent HAp NPs, are being actively pursued (Ge and Selvin 2003; Marriott et al. 1994; Yuan et al. 2001). Fluorescence/luminescence intensities of Ln doped-HAp NPs have enhanced with increase in dopant concentrations (Syamchand and Sony 2015; Xie et al. 2016). Some studies showed that replacement of hydroxyl ( $\text{OH}^-$ ) group from HAp structure by fluorine ( $\text{F}^-$ ) ions enhanced the luminescence intensity of the rare earth doped HAp NPs which was attributed to the decrease in fluorescence quenching of Ln. Fluorine replaced HAp NPs exhibit low vibrational

energy as compared to HAp NPs, thus minimizing the quenching of the excited state of the  $\text{Ln}^{3+}$  (Hui and Wang 2011; Sun et al. 2013). Rare earth metals such as Europium ( $\text{Eu}^{3+}$ ), Terbium ( $\text{Tb}^{3+}$ ), ytterbium ( $\text{Yb}^{3+}$ ), gadolinium ( $\text{Gd}^{3+}$ ), neodymium ( $\text{Nd}^{3+}$ ),  $\text{La}^{3+}$  and praseodymium ( $\text{Pr}^{3+}$ ) doped HAp NPs have been studied for bioimaging and various biomedical applications (Syamchand and Sony 2015). Figure 1.5 describes the internalization of  $\text{Eu}^{3+}$  iron oxide doped HAp NPs by A549. Most strong emitting Ln such as  $\text{Eu}^{3+}$  and  $\text{Tb}^{3+}$ , have been doped with HAp and studied extensively by many researchers. Amongst all  $\text{Eu}^{3+}$  doping has received much interest due to several desirable properties such as long luminescent life times, biologically appropriate emission in the visible region, and lower sensitivity to quenching (Hanaoka et al. 2007).  $\text{Eu}^{3+}$  doped HAp NPs have been synthesized by various methods like co-precipitation, hydrothermal, microwave assisted hydrothermal, sol-gel, etc. The  $\text{Eu}^{3+}$  doped HAp fabricated using these methods resulted in different morphologies with various aspect ratios and particles in nanometric dimensions ( $\sim 100\text{nm}$ ) (André et al. 2012; Huang et al. 2012; Ternane et al. 1999). They exhibited excellent fluorescent properties and internalization by various cell lines such as breast cancer cell line- MCF7, human embryonic kidney cells- HEK293, HeLa and adenocarcinomic human alveolar basal epithelial cells- A549 cells, etc. Various studies reported on  $\text{Eu}^{3+}$  doped HAp NPs are represented in table 1.3.

Similarly, other rare earth metals such as  $\text{Tb}^{3+}$ ,  $\text{Yb}^{3+}$ ,  $\text{Gd}^{3+}$ ,  $\text{Nd}^{3+}$ ,  $\text{La}^{3+}$  and  $\text{Pr}^{3+}$  doped HAp NPs have also been studied for bioimaging and related applications (Ciobanu et al. 2014; Hui et al. 2012; Jadalannagari et al. 2014b; Li et al. 2008). Synthesis and biomedical applications of lanthanides other than Eu doped HAp NPs are described in table 1.4.

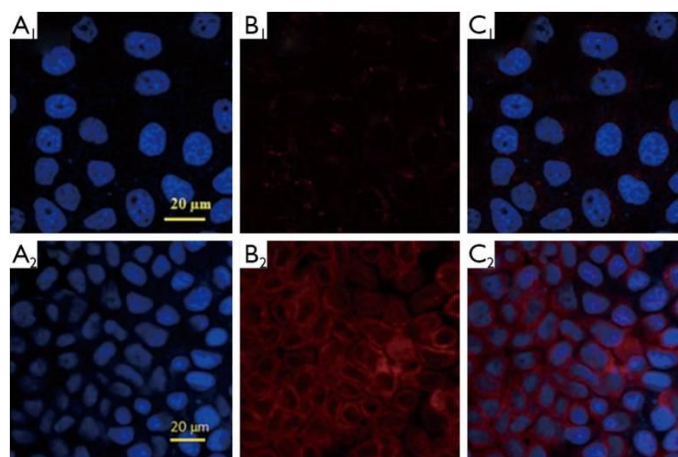


**Figure 1.5** Confocal laser scanning microscopy images of A549 cells incubated with fluoridated  $\text{Eu}^{3+}$ -HAP/iron oxide nanocomposites at 37 °C for 2 h without magnetic field (Row 1) and under a magnetic field of 1.3T (Row 2). (A) The blue channel with excitation at 340 nm. (B) The red channel with excitation at 405 nm. (C) The combined red and blue channels. (Pan et al. 2015).

Recently, doping of biocompatible HAp NPs with two or more lanthanides has gained much interest in multi-modal imaging techniques. Multi-modal imaging has emerged as a technology that utilizes strength of two or more imaging modalities/techniques (MRI, CT, optical imaging etc.) while overcoming their limitations to build a hybrid imaging platform. It thereby ensures better elucidation of physiological mechanisms at molecular and cellular level to improve diagnosis and therapeutics (Savita et al. 2010). Dual lanthanides doped HAp NPs of various shapes and imaging properties have been fabricated using methods such as hydrothermal, wet chemical, co-precipitation and sol-gel synthesis. These NPs are studied as multi-modal *in vivo* and *in vitro* imaging agents (Ashokan et al. 2010; Chen et al. 2011; Li et al. 2012b; Liu et al. 2014b; Pan et al. 2015).

Reported studies on lanthanides doped HAp NPs are summarized in Table 1.4. Based on all the above studies it can be summarized that HAp nanosystems present an efficient platform for doping with a variety of lanthanides/organic dyes as well as surface modification with myriad functional moieties (reporters,

proteins, etc.) for fabrication of novel nanoconjugates with desirable properties. These HAp nanoconjugates also possess excellent biocompatibility, exhibit stable luminescent properties and cellular internalization ability. HAp NPs modified in this manner could serve as a potential nanosystem for bioimaging and therapeutics.

**Table 1.4** Lanthanide doped HAp NPs for use in bioimaging and biolabeling

| Dopant                            | Properties  | Applications                                     | Ref                 |
|-----------------------------------|---|--|---------------------|
| Eu-doped HAp                      | Particle shaped changed from rod to sphere with increase in dopant concentration upto 7.5%  | Potential application in bio-imaging             | (Huang et al. 2012) |
| Arginine modified Eu-HAp          | Reduction in size of HAp NPs after functionalization with arginine and $\text{Eu}^{3+}$ , internalization into cytoplasm of human lung epithelial cells | Potential application in bio-imaging             | (Zhao et al. 2011)  |
| Eu-doped HAp                      | The luminescence enhanced with increase in $\text{Eu}^{3+}$ concentration and with thermal treatment  | Fluorescent probe for cell labeling              | (Han et al. 2013)   |
| Eu-doped HAp                      | particle size- 13nm; enhanced fluorescence intensity with increase in $\text{Eu}^{3+}$ concentration up to 12%  | Fluorescent probe for <i>in vivo</i> bio-imaging | (Hasna et al. 2013) |
| Luminescent and mesoporous Eu-HAp | Hexagonal mesostructure, rod like morphology, particle size 20-40nm diameter and 100-200nm length   | Theranostic agent                                | (Yang et al. 2008b) |
| Eu- doped apatite                 | Non toxic and photostable, internalized by human epithelial cells   | Luminescent probe                                | (Doat et al. 2003)  |

|  |  |   |                        |
|--|--|---|------------------------|
| Folate coated<br>Eu-doped<br>HAp   | low toxicity, good photostability, targeted towards cancer cells, specifically internalized by breast cancer -MCF-7 cells  | Promising tool for diagnosis of cancer at its early stage                               | (Pan et al. 2013)      |
| Eu-doped<br>fluorine<br>substituted<br>HAp                                   | nanorod-like shape and dropped aspect ratios with increase in pH from 3.0 to 11.0, increased luminescence intensity with increasing substitution of OH <sup>-</sup> with F <sup>-</sup> , low toxicity to HeLa cells | Fluorescent probe for labeling  | (Sun et al. 2013)      |
| Polyacrylic<br>acid<br>functionalized<br>Eu doped<br>HAp and<br>fluorapatite | Nanospindal shape, length-150-200nm, diameter-35-40nm, more fluorescence intensity for fluorapatite than hydroxyapatite, negligible toxicity for monkey kidney epithelial cells-Vero cell                            | Potential tool as a luminescent biolabels and tracking devices in drug delivery systems | (Escudero et al. 2013) |
| Eu- doped<br>HAp   | Mesoporous nanometric structure of diameter 15-20nm, pore size increase with increase in Eu concentration, internalization in HEK cell line  | Fluorescence imaging and drug delivery  | (Popa et al. 2014)     |
| Eu-doped<br>HAp<br>nanowhisker   | Nanowhisker with diameter ~80nm, crystalline, negligible cytotoxicity towards osteoblast cells   | Multimodal bioimaging   | (Wagner et al. 2013)   |

**Table 1.5:** Lanthanides doped HAp NPs for use in bioimaging and biolabeling

| <b>Dopant</b>  | <b>Properties</b>  | <b>Applications</b>                               | <b>Ref</b>                    |
|--|--|---|-------------------------------|
| Tb doped HAp   | 20nm, crystalline, non toxic and internalized by mesenchymal stem cells                    | Fluorescence bioimaging                           | (Li et al. 2008)              |
| Eu and Tb co-doped HAp   | Nanorods, size increased with increase in dopant concentration, crystalline, monodisperse, | Drug carrier and optical imaging                  | (Yang et al. 2008a)           |
| Eu and Tb co-doped HAp   | Nanorods, diameter- 20nm, internalized by A549   | Fluorescent probe for bioimaging                  | (Hui et al. 2012)             |
| Gd <sup>3+</sup> and Pr <sup>3+</sup> co-doping HAp                          | Nanosphere, crystalline  | Phototherapy lamps to treat skin diseases         | (Mokoen a et al. 2014)        |
| CePO <sub>4</sub> :Tb doped HAp  | Nanorods, length- 50-100nm, diameter-5-10nm  | Redox luminescence switch                         | (Chen et al. 2013)            |
| Nd <sup>3+</sup> doped HAp   | Needle shape, particle size decreased with increase in dopant concentration                | drug delivery and NIR fluorescence imaging system | (Victor et al. 2014)          |
| La <sup>3+</sup> doped HAp   | Nanorods, length- 80-100nm, diameter 20-25, internalized by MCF7 cells                     | Biolabeling and bioimaging                        | (Jadalan nagari et al. 2014b) |
| Yttrium orthovanadate:Yb <sup>3+</sup> , Er <sup>3+</sup> functionalized HAp | Nanorods, length 120-200nm, diameter-30-50nm, bright green up-conversion luminescence      | Bioimaging  | (Cheng et al. 2014)           |

**Table 1.6** Lanthanide doped HAp nanomaterials for multimodal imaging

| Dopant  | Properties   | Applications  | Ref                   |
|---|--|---|-----------------------|
| Eu <sup>3+</sup> and Gd <sup>3+</sup> doped HAp   | Nanorods, length-80-100nm, diameter-10-50nm, Eu <sup>3+</sup> and Gd <sup>3+</sup> luminescence and paramagnetism    | MRI, CT as well as fluorescence imaging, drug delivery    | (Chen et al. 2011)    |
| Folic acid functionalized Eu <sup>3+</sup> and Gd <sup>3+</sup> doped HAp                 | Nanosphere, diameter-30nm  | MRI, X-ray and NIR imaging, cancer targeted drug delivery | (Ashokan et al. 2010) |
| Aptamer capped Gd <sup>3+</sup> and strontium doped HAp                                   | Mesoporous nanorods, length-100-120nm, diameter-20nm   | Bioimaging and site specific controlled drug delivery     | (Li et al. 2012b)     |
| Tb <sup>3+</sup> and Gd <sup>3+</sup> dual doped HAp                                      | Nanosphere, diameter-40-100nm, crystallinity decreased with increase in Tb/Gd doping, luminescence and paramagnetism | Potential application in bimodal imaging                  | (Liu et al. 2014b)    |
| HAp functionalized with UcNPs Na(Y/Gd)F <sub>4</sub> :Yb <sup>3+</sup> , Er <sup>3+</sup> | Nanofibers, diameter-75-200, luminescent and magnetic ,internalization by osteoblast cells                           | MRI and fluorescence imaging                              | (Liu et al. 2014a)    |

### 1.6.1.3 Fluorescence property in HAp NPs caused due to defects

HAp is not a known fluorescent material, however fluorescence property can be generated either by doping it with organic dye/rare earth metal/ transition metal or by creating defects/impurities in crystal lattice. Very few researchers have described defect related synthesis of luminescence in HAp NPs. Zhang et al reported nano and microcrystal HAp with various morphologies (microsphere, microflowers, microsheets, nanowires and nanorods) fabricated using hydrothermal process. These micro and nano systems under UV light excitation exhibited bright blue emission which was attributed to the presence of  $\text{CO}^{2-}$  radical in the crystal lattice, introduced through the precursor material, trisodium citrate. These nanosystems are proposed for biolabeling applications (Zhang et al. 2009). Zhang et al have also worked on the synthesis of mesoporous self activated luminescent  $\text{Sr}^{2+}$  doped HAp NPs. Luminescence/fluorescence properties of these NPs were also attributed to the presence of  $\text{CO}^{2-}$  radical in the crystal lattice which was introduced through trisodium citrate. These nanosystems exhibited excellent fluorescence as well as drug loading and release capacity (Zhang et al. 2010). Kumar et al have fabricated flower-like HAp NPs from eggshell via microwave conversion process. These NPs showed carbonated impurities and fluorescence related to it (Kumar et al. 2012). Such self activated fluorescence HAp NPs could be promising agents for biolabelling and bioimaging.

### 1.6.2 HAp for gene delivery

Gene delivery is the process of artificially introducing genetic material into host cells and typically involves viral and non-viral vector systems. Gene delivery using viral vector is the oldest technique which was first studied in *Salmonella* (Zinder and Lederberg 1952). Although, it is the most efficient method for transfer of DNA into cells, the use of retroviruses, adenoviruses and other viruses can cause recombination, immunogenicity and carcinogenicity to cells. Hence, non-viral vectors are advantageous over viral vector even though they have low



transfection efficiency (Nayerossadat et al. 2012). Non-viral systems used for gene delivery include gene gun, electroporation, microinjection, cationic and anionic lipids, cationic polymers, peptides, nanoparticles and ceramic particles of calcium phosphate (Nayerossadat et al. 2012; Ramamoorth and Narvekar 2015).

Amongst all the non-viral systems, calcium phosphate method has been used over the past 30 years as an efficient method to introduce genetic material into cells (Graham and van der Eb 1973). The basic methodology of calcium phosphate mediated gene delivery process is described in Figure 1.6. This technique involves mixing DNA with calcium chloride in a buffered saline/phosphate solution to obtain a calcium-phosphate-DNA co-precipitate, which is then transferred onto the cultured cells (Graham and van der Eb 1973; Maitra 2005). The calcium-phosphate-DNA precipitate gains entry into cells through pores, and is dissolved in the acidic environment of the endosome that causes the release of the DNA from the precipitate and increases the  $\text{Ca}^{2+}$  concentration. This results in the rupture of the endosomal membrane due to osmotic imbalance caused by  $\text{Ca}^{2+}$ , thus, delivering the gene into the cytosol and preventing it from endosomal degradation. Further, it is transferred to the nucleus through nuclear pore complex (Maitra 2005; Seelos 1997; Tan et al. 2007; Tram Do et al. 2012). Calcium phosphate method is biocompatible, easy to handle and can also protect gene from endosomal and cytoplasmic degradation. However, transfection efficiency achieved using this method depends on many factors such as pH of the buffer, cell type, time of contact between precipitate and cells as well as salt (calcium/phosphate) concentrations. Variations in these factors may change the size of calcium-phosphate-DNA precipitate which could affect the uptake of the precipitate by cells and hence transfection efficiencies. Therefore, this method has low reproducibility and has to be optimized for every cell line and laboratory (Jordan and Wurm 2004; Maitra 2005; Seelos 1997; Urabe et al. 2000). Moreover, transfection solution is difficult to store due to the ability of calcium phosphate crystals to grow over time and this method is only applicable *in vitro*. Due to these shortcomings, active research is being carried out to

synthesize calcium phosphate nanoparticles of various sizes and shapes to improve reproducibility and transfection efficiencies. These nanoparticles have been successfully used for *in vitro* and *in vivo* transfection (Bisht et al. 2005; Liu et al. 2011b; Maitra 2005; Nouri et al. 2012).

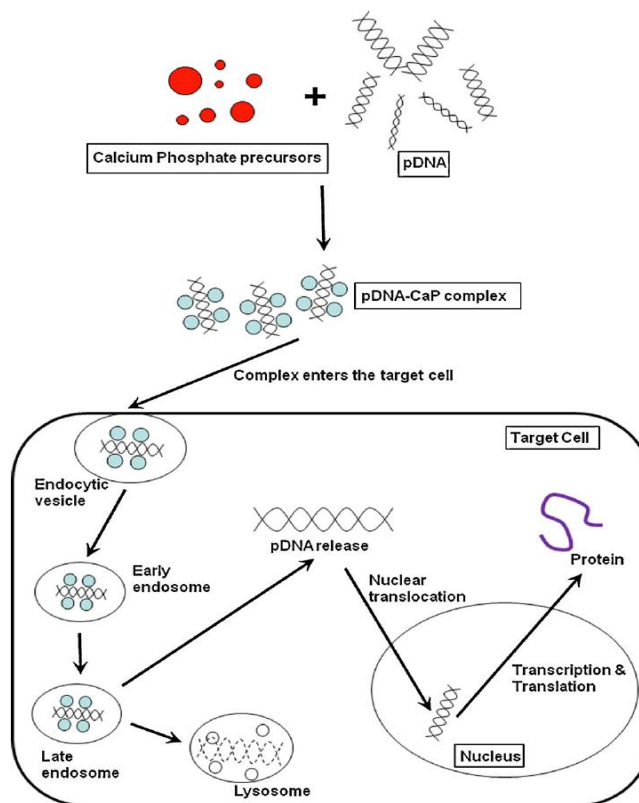


**Figure 1.6:** Schematics of pDNA-Calcium phosphate gene delivery. Once the pDNA-CaP complex is formed by the co-precipitation process, the complex enters the cell through endocytosis. Through the endocytic pathway, pDNA translocates into the nucleus, and subsequently become translated and transcribed, expressing therapeutic proteins of interest (Lee et al. 2012).

HAp is the most stable phase of calcium phosphate and potential candidate for transfection due to their biocompatibility, biological stability, easy synthesis and diffusion through cell membrane. HAp NPs have high binding affinity to nucleic acids due to the ionic interactions between  $\text{Ca}^{2+}$  and the negative charge of nucleic acid (Tram Do et al. 2012; Uskoković and Uskoković 2011; Xu et al. 2016). Binding of DNA to HAp improves the stability and transportability of DNA through cell membrane. The DNA from the calcium phosphate/HAp NPs-DNA complex is released at pH 5.0 (endosomal pH) thereby increasing the concentration of free  $\text{Ca}^{2+}$ . This increased  $\text{Ca}^{2+}$  concentration disrupts the endosomal membrane through osmotic imbalance facilitating the entry of DNA into the cytoplasm and subsequently into the nucleus through the nuclear pore complex (Maitra 2005; Tram Do et al. 2012).

Gene delivery using HAp NPs in animal and plant cells has been reported by many researchers. HAp nanorods fabricated by hydrothermal technique have been shown to absorb green fluorescent protein plasmid (EGFP) to form HAp NPs- EGFP complex that were successfully transfected into gastric cancer cell-SGC-790. Moreover, these complexes also exhibited *in vivo* gene expression in the cytoplasm and nuclei of the liver, kidney and brain tissue cells of mice when injected into mice through tail vein (Zhu et al. 2004). HAp NPs are being actively explored for the transfection of therapeutic genes into inner ear to cure intractable diseases, such as sudden hearing loss, presbycusis, etc. (Sun et al. 2008; Wu et al. 2012). Sun et al exhibited transfection of recombinant plasmids containing reporter green fluorescent protein (GFP) and therapeutic neurotrophin3 genes into HeLa cells, primary cultures of cochlear neurons from mice and the spiral ganglion neurons of the inner ears of guinea pigs using HAp nanorods (Sun et al. 2008). Wu et al modified HAp NPs with polyethylenimine, - an efficient carrier for gene and exhibited transfection of recombinant plasmids containing GFP and therapeutic neurotrophin3 genes into the inner ear. Thus, these nanosystems could be used as gene therapy for inner ear diseases (Wu et al. 2012).

HAp NPs may also be surface modified using positively charged molecules such as histidine, lysine, poly L-lysine, arginine, and protamine sulfate to increase binding affinity towards the negatively charged DNA and thus increase the transfection efficiencies. Wang et al and Zhong et al have reported increase DNA binding efficiency and hence enhanced transfection efficiency with arginine surface modification of HAp (Wang et al. 2015; Zhao et al. 2011). Wang et al have shown increased transfection efficiency to 45% in HeLa cells using arginine modified HAp nanorods prepared by hydrothermal method (Wang et al. 2015). Similarly, Tan et al reported that HAp NPs modified with protamine sulfate exhibited three-times higher transfection efficiency than unmodified HAp NPs in human liver cancer cell line-HepG2, human nasopharyngeal carcinoma-CNE2 and melanoma-B16 cell line (Tan et al. 2007). Xiong et al demonstrated that magnetic lamellar HAp NPs, synthesized using template-assisted self assembly process, also exhibited 47% higher transfection efficiency in mouse fibroblast-L929 cell line under the influence of magnetic field. These NPs by an external magnetic force can be attracted to precise location to increase transfection efficiency (Xiong et al. 2015). Thus, HAp could be modified to enhance transfection efficiency and could be used as a safe and effective gene vector.

### **1.6.3 Drug delivery using HAp**

Nanocarriers are emerging and potential carriers used for targeted and controlled drug delivery. Due to their size, shape and physicochemical properties they are easily taken up by cells as compared to large molecules. They can transport drugs to the site of action thereby reducing the systemic side effects of the drug. Nanocarriers can also protect drug from rapid degradation or clearance, which results in enhanced drug concentration at the target tissues, thereby lowering the dosage of drugs (Soppimath et al. 2001; Wilczewska et al. 2012). HAp, due to its excellent adsorption properties, biocompatibility, easily tunable physicochemical properties, and pH dependent dissolution, has potential for use as a nano-drug carrier (LeGeros 2002; Suchanek and Yoshimura 1998; Thomann et al. 1990). HAp degradation rate is pH dependent, which increases with the change in pH

from alkaline to acidic conditions. The pH dependent dissolution of HAp NPs is an interesting property for drug delivery applications, as they are stable in extracellular environment where pH is 7.4 and enables release of drug in endosome where pH is 4-5. It also helps preferential drug release in cancer tissues where environment is acidic (Li et al. 2012b; Yang et al. 2013). HAp NPs have been used as drug carriers for various antibiotics, anticancer, anti-inflammatory, and protein drugs (Yang et al. 2013; Ye et al. 2010; Yoon et al. 2015; Zhang et al. 2010). Drug loading-release capacity and therapeutic properties depend on morphology, porosity and surface structure of HAp NPs.

Hollow mesoporous HAp nanospheres synthesized by an opposite ion core/shell strategy exhibited five times higher drug loading and three-fold higher drug release capacity than HAp NPs. This nanopreparation exhibited a pH-responsive release of doxorubicin in breast cancer cell lines-BT20 (Yang et al. 2013). Folic acid and polyethylene glycol (PEG) functionalized HAp nanorods loaded with anticancer drug, paclitaxel showed targeted delivery with an initial burst release followed later by a sustained release (Venkatasubbu et al. 2013). Multifunctional drug delivery systems comprising of needle shaped luminescent doped HAp NPs complexed with cyclodextrin not only exhibited an increased adsorption of doxorubicin but, also an enhanced uptake of drug loaded HAp NPs in C6 glioma cells (Victor et al. 2014). HAp NPs loaded with antibiotics like cephalexin or norfloxacin, amoxicillin, ciprofloxacin, gentamycin, amphotericin B, imipenem, fosfomycin, etc., have been tested for the treatment of osteomyelitis (Chai et al. 2007; Krisanapiboon et al. 2006; Rauschmann et al. 2005; Son et al. 2011; Stigter et al. 2004; Thi et al. 2010). HAp functionalized with 1,2,3,4-butanetetracarboxylic acid crosslinked hydroxypropyl- $\beta$ -cyclodextrin polymer showed controlled and prolonged release of ciprofloxacin/vancomycin for the treatment of bone infection (Leprêtre et al. 2009). Iron ( $\text{Fe}^{3+}$ ) doped HAp nanospheres (75nm) impregnated with amoxicillin as well as the anticancer drug, 5-fluorouracil exhibited efficient antibacterial and anti-cancer activities against bacterial cells such as *Escherichia coli*, *Staphylococcus aureus*, and

*Staphylococcus epidermidis*, and the cancerous cells, osteocarcinoma cell line-MG63 (Sarath Chandra et al. 2012). Thus, modification of HAp NPs for targeted drug delivery could provide new opportunities in the field of controlled delivery using nanodevice.

#### **1.6.4 HAp NPs coating for orthopedic implants**

Medical implants are devices that replace a fraction or the whole biological structure inside or on the surface of the body. Currently, implants are routinely used for wide range of applications such as orthopedics, pacemakers, cardiovascular stents, defibrillators, neural prosthetics, etc. (Cowley and Woodward 2011). Orthopedic implants are the largest implantable device segment in market. Metallic materials such as stainless steel and alloys of titanium, cobalt and magnesium are commonly used as orthopedic implants to replenish bone defects, due to their high tensile strength and high fracture toughness (Chen and Thouas 2015). Surface modification of these metal implants with biocompatible ceramics has been reported to improve bioactivity and osteointegration properties of these materials (Moxon et al. 2004; Pilliar 1987; Sennerby et al. 2005; Webster et al. 2000). HAp, the major component of human hard tissues is widely used as coatings on implant surfaces which provides an optimal environment for growth of bone tissues and enhances biological activities of the implants (Gadow et al. 2010; Suchanek and Yoshimura 1998; Zhou and Lee 2011). HAp NPs have been coated on various metallic implants such as surgical grade stainless steel (Gopi et al. 2011; Liu et al. 2002a; Shibli and Jayalekshmi 2008; Thanh et al. 2013), cobalt-chromium alloys, and titanium metal and its alloy (Benea et al. 2015; Goudarzi et al. 2014; Parcharoen et al. 2014) using different techniques such as plasma spraying (Guo et al. 2004; Sun et al. 2001) magnetron sputtering (Nieh et al. 2001; Van Dijk et al. 1996), laser ablation (Ball et al. 2001; Fernandez-Pradas et al. 2001), sol-gel process (Kim et al. 2004; Liu et al. 2002a; Milella et al. 2001), electrochemical and electrodeposition (Benea et al. 2015; Gopi et al. 2012; Thanh et al. 2013) to enhance bonding strength to the metallic substrate. Amongst all the metal

implants, titanium is considered to be less susceptible to corrosion and hence is widely used as implant material. Wijesinghe et al have prepared HAp NP coated custom-made titanium metal implants and these implants were found very stable under the corrosive environment (Wijesinghe et al. 2016).

Success of these implants not only depends on osteointegration and biocompatibility but also on their ability to combat microbial infection. In order to reduce the incidence of implant-associated infections, several biomaterial surface treatments have been proposed. These include coating of implant surfaces with zinc (Zn), copper (Cu) or silver (Ag) ions (Ersek and Denton 1984; MacKeen et al. 1987; Wan et al. 2007), impregnating NPs with antimicrobial agents (Abdelghany et al. 2012; Vasilev et al. 2009), providing an anti-adhesive surface (Bruellhoff et al. 2010; Donelli and Francolini 2013), delivering antibacterial agents to disrupt cell-cell communication and preventing bacterial aggregation & biofilm formation. Loading of various antibiotics such as vancomycin, chlorhexidine, gentamicin, cephalothin, carbenicillin, amoxicillin, cefamandol, and tobramycin onto HAp coatings have been shown to reduce infections (Stigter et al. 2004). However, antibiotics loaded in the implant material cannot prevent long term post surgical infections due to their tendency of getting washed out by body fluids (Abdelghany et al. 2012). Besides, excessive use of antibiotics could lead to the development of drug resistance and toxicity to local tissues. HAp NPs doped with transition metal ions like Ag/Zn/Cu have strong antimicrobial/anti-biofilm properties (Kim et al. 1998). Silver ions exhibit broad spectrum antibacterial activity and are being actively studied for the control and prevention of growth of biofilms and planktonic cells (Wan et al. 2007). Several *in vitro* studies have reported that silver doped HAp coatings and films exhibit good antimicrobial and anti-biofilm properties against various microbial infections (Chen et al. 2008b; Ciobanu et al. 2012; Rameshbabu et al. 2007; Stanić et al. 2011). Therefore, silver doped HAp coatings on titanium metal or alloys could be used as potential medical implants which could enhance the success of medical implant.

## 1.7 Biocompatibility and non-toxicity

Biocompatibility and non-cytotoxicity are the prerequisites for biomedical applications of nano-materials. HAp NPs are considered to be biocompatible and non-cytotoxic due to their chemical similarity to the bone component. However, their toxicity depends on the size, shape, charge, particle concentration, methods of synthesis, time of exposure and cell types (Albrecht et al. 2009; Motskin et al. 2009). Motskin et al. demonstrated that HAp NPs synthesized using precipitation method exhibited lower toxicity than that of HAp obtained using colloidal-gel method, on human monocytes'-derived macrophages. This difference in toxicity was attributed to the physicochemical properties of HAp NPs which changed with the method of preparation (Motskin et al. 2009). Similarly, shape and cell type dependent cytotoxicity of HAp NPs on rat alveolar macrophage cells-NR8383 and primary alveolar macrophages has also been reported. They have described that HAp NPs of various shapes like nano needles, nano rods, nano plate, fine needle and HAp protein composite showed no cytotoxicity and reactive oxygen species generation(ROS) in primary alveolar macrophages while only fine needle HAp exhibited cytotoxicity and ROS generation in NR8383 cell line (Albrecht et al. 2009). HAp NPs exhibited enhanced proliferation in osteoblasts, and mesenchymal stem cells as compared to bulk HAp (Cai et al. 2007; Chesnutt et al. 2009; Lü et al. 2013).

Based on all the above studies it can be summarized that HAp NPs of various morphologies can be synthesized using different methods and also easily modified with functional moieties to develop novel nanoconjugates. These HAp NPs present a biocompatible system for various biological applications such as, bioimaging, targeted drugs/ genes/protein delivery.



## 1.8 Gaps in Existing Research

Based on the literature survey, following gaps were identified and the objectives were framed accordingly:

1) Methods that have been used for synthesis of HAp NPs include chemical precipitation, hydrothermal treatment, emulsion techniques, precipitation from complex solutions followed by microwave heating, wet chemical methods and mechanochemical synthesis. Most of these techniques require high temperature or complex procedure. Hence there is a requirement for the development of simple 'room temperature' based synthesis protocols for hydroxyapatite nanoparticles which could fabricate NPs of various morphologies.

2) Bioimaging using organic dyes, fluorescent proteins, and lanthanide based organic chelates suffer from inherent drawbacks such as short Stokes' shift, poor photochemical stability, susceptibility to photo-bleaching, decomposition under repeated excitation and cytotoxicity to biological systems. To overcome these problems, there is a need of a system that is more sensitive and non-cytotoxic. Synthesis of self fluorescent biocompatible hydroxyapatite nanoparticles may be a good alternative for bioimaging applications.

3) Most widely used methods for yeast and bacterial transformation are chemical transformation and electroporation. Both the methods require preparation of competent cells and their recovery. Most importantly it is still difficult to achieve high transformation efficiency in yeast and Gram-positive bacteria. Therefore, there is need for development of easy and efficient process for yeast and bacterial transformation. Development of simple and efficient nanoparticles based plasmid DNA could be advantageous for transformation.

### **1.9 Aims and objectives of the research work**

In view of the above perceived gaps in the literature, the following objectives have been proposed:

1. Room temperature synthesis of fluorescent hydroxyapatite nanoparticles and their characterization studies.
2. Study on potential applications of the synthesized fluorescent hydroxyapatite nanoparticles for bioimaging.
3. Development of one step process for DNA delivery in prokaryotic and eukaryotic systems using fluorescent hydroxyapatite nanoparticles.

## CHAPTER 2

### **Room Temperature Synthesis and Characterization of Self activated Fluorescent Hydroxyapatite by Modified Sol-gel Technique**

#### **2.1 Introduction**

Hydroxyapatite nanoparticles (HAp NPs) due to their large surface area are being used in wide variety of applications including drug delivery, bioimaging, hard tissue repairing, catalysis, water purification and protein chromatography. Size, morphology and chemical composition of HAp plays vital role to determine their applications and properties. Thus, much effort has been dedicated to develop nano or microcrystals of HAp with well defined morphologies and accurately tunable sizes (Padmanabhan et al. 2009; Wang et al. 2010b; Yang et al. 2014; Zhang et al. 2009).

In recent years, various techniques have been developed for the fabrication of HAp NPs of different morphologies. Commonly used techniques include wet chemical synthesis, co-precipitation, solid-state reaction, hydrothermal method and sol-gel method (Koutsopoulos 2002; Okada and Matsumoto 2015; Wang et al. 2010b; Zhang et al. 2009; Zhang and Vecchio 2007). Variation in the synthesis procedure leads to difference in crystallinity, morphology and stoichiometry. Wet chemical synthesis can control the morphology and crystallinity by altering temperature and time of reaction however, these NPs were irregular in sizes and shapes (Koutsopoulos 2002; Monmaturapoj 2008; Okada and Matsumoto 2015). Solid-state reactions usually produce a stoichiometric and well crystallized product however, they require relatively high temperatures and long heat treatment times (Koutsopoulos 2002; Okada 2015). The hydrothermal technique usually results in HAp powders with high degree of crystallinity and Ca:P ratios close to stoichiometric values. However, it is time consuming and requires special instrumentation (Koutsopoulos 2002; Okada and Matsumoto 2015; Yang et al. 2014). Sol-gel synthesis of HAp NPs has gained

much interest due its molecular mixing of calcium and phosphorous precursors which improves chemical homogeneity, ability to generate nanocrystalline powders, product purity and synthesis can be carried out at comparatively low temperatures (Jadalannagari et al. 2011; Kim and Kumta 2004; Okada and Matsumoto 2015). This method has also been proven to be an efficient and suitable process for preparation of controllable, uniform and reproducible morphologies (Koutsopoulos 2002; Okada 2015).

In last two decades, fluorescent materials have gained much interest for variety of applications ranging from optoelectronics to biomedicine which includes lighting (such as fluorescent lamps), information displays (such as television tubes, computer monitor tubes, and radar screens), scintillation and bioimaging/biolabeling. Thus significant efforts have been dedicated for the fabrication of luminescent materials with high photoluminescent efficiency and excellent optical properties (Kim et al. 2000; Liu et al. 2013; Museur et al. 2012; Podkościelna 2014). Nanomaterials due to their unique physical (structural, electronic, magnetic and optical) and chemical properties have been investigated as fluorescent materials (Wang et al. 2005). Various fluorescent nanomaterials such as QDs, UcNPs and lanthanide doped NPs have been extensively used for biological applications due to their exceptional properties such as high quantum yield, large Stokes' shift and low photobleaching (Nune et al. 2009; Syamchand and Sony 2015; Wolfbeis 2015). However, these NPs are cytotoxic in nature due to presence of transition metal or lanthanides which have limited their applications.

Recently, defect related fluorescence nanomaterials which do not contain any transition metal or rare earth activators are being studied for biomedical applications. In defect related nanomaterials, fluorescence is attributed to vacancies/ impurities present or created in the material (Bol and Meijerink 2000; Zeng et al. 2010; Zhang and Lin 2012). These luminescent materials include metal oxides, silica, phosphate and carbon-based materials. They are mostly

fabricated using methods such as hydrothermal process, sol–gel method and wet chemical precipitation (Baker and Baker 2010; Loh et al. 2010; Zhang and Lin 2012). Defect related fluorescent HAp NPs have also been fabricated using hydrothermal method where fluorescence has been attributed to  $\text{CO}^{2-}$  impurities in the crystal lattice. These novel nanomaterials have excellent optical properties, high chemical stability and less toxicity, however, they are less reproducible (Kumar et al. 2012; Zhang et al. 2010; Zhang et al. 2009). Therefore fabrication of biocompatible HAp NPs where fluorescence is attributed to asymmetry/variation in shape could be a promising agent for various biological applications.

In this chapter, we report the synthesis of rod shaped HAp with various aspect ratios (thin rods, short rods, rods and microrods) at room temperature by modified sol-gel method. Their characterization and photoluminescence properties are presented in this chapter.

## 2.2 Materials and methods

### 2.2.1 Synthesis of HAp NPs

**Materials:** Calcium chloride (SD-fine chemicals), orthophosphoric acid (Merck), triethylamine (Merck), acetyl acetone (Merck) ammonium hydroxide (Merck) and ethanol were used as precursor materials.

HAp was synthesized using modified sol gel method; various protocols described below were followed and also illustrated schematically (Figure 2.1a and b):

Method 1: 2M calcium chloride ( $\text{CaCl}_2$ ) was dissolved in 50mL dimethyl sulfoxide (DMSO) and stirred for 30mins using magnetic stirrer, followed by drop-wise addition of 1M orthophosphoric acid ( $\text{H}_3\text{PO}_4$ ). Ca:P atomic ratio was maintained at 1.67. Subsequently, 50mL triethyl amine (TEA), a stabilizing agent was added dropwise under continuous stirring, and the sol obtained was stirred for 1h. The pH was adjusted to 10 using liquid ammonia and stirring was continued till the

complete formation of gel. The gel obtained was centrifuged at  $4000\times g$  for 10min, washed thrice with ethanol and dialyzed (using dialysis bag, Bangalore genie 110) against de-ionized water(DI) for 12h with change of water after every 2h for active removal of adsorbed ions. The dialyzed samples were dried at room temperature for 12h and ground using a mortar and pestle.

Method 2: As described in method 1, 1M orthophosphoric acid was added dropwise into 2M calcium chloride solution and Ca:P atomic ratio was maintained at 1.67. The stabilizing agent used was acetyl acetone (ACA), 50mL of which was added dropwise under continuous stirring. The sol obtained was stirred for 1h, pH was adjusted to 10.0 using liquid ammonia and stirring was continued till gel formation. Further processing of the gel to obtain a powder was as described in Method 1.

Method 3: 2M solution of calcium chloride in 50mL DI and 1M solution of orthophosphoric acid in 50mL TEA were prepared. Orthophosphoric acid solution was added dropwise to the calcium chloride solution and obtained sol was stirred for 1h using a magnetic stirrer. The Ca:P molar ratio was maintained at 1.67. The pH of this sol was adjusted to 10.0 using ammonium hydroxide solution. Subsequently, the sol was dialyzed against DI for 12h with change of water once every 2h. The gel obtained after dialysis was dried at room temperature for 12h and ground using mortar and pestle to obtain a powder.

Method 4: 2M calcium chloride solution was dissolved in 50mL DI. In this method, orthophosphoric acid was dissolved in 50mL of ACA instead of TEA. As described in method 3, orthophosphoric acid solution was added dropwise to the calcium chloride solution to obtain gel. Gel was further dialyzed, dried and ground into fine powder as described in method3

Method 5: 2M calcium chloride was dissolved in 50mL DI and 1M orthophosphoric acid was added drop-wise to it. In this procedure no stabilizing agent was added. The mixture was heated at  $80^{\circ}\text{C}$  for 1h followed by dialysis of

sample against DW for 12h with change of water after every 2h. The sample obtained after dialysis was dried at room temperature for 12h and ground using a mortar and pestle.

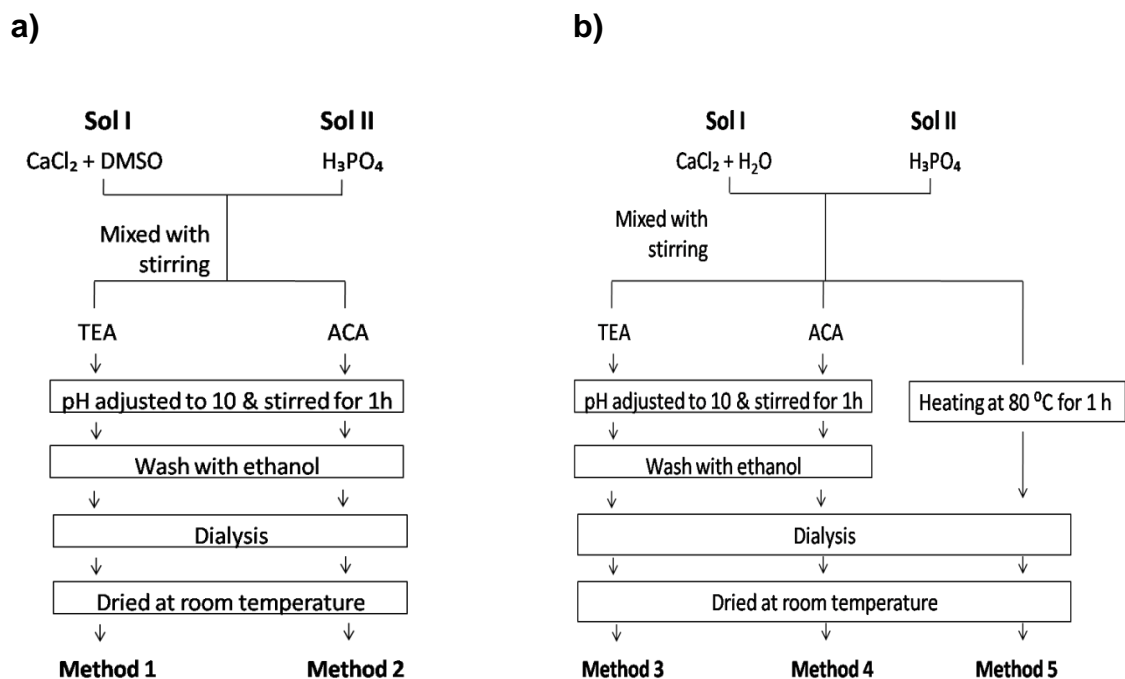


**Figure 2.1** Schematic illustration of synthesis of HAp NPs by using DMSO (a) and water (b) as solvent while TEA/ACA as reducing agents.

## 2.2.2 Characterization of the HAp NPs

Several techniques have been used to characterize HAp. Following is a brief description of these techniques.

### 2.2.2.1 X-ray diffraction

X-ray diffraction (XRD) is a non-destructive technique commonly used for the characterization of crystalline materials. It is mainly used for phase identification,

studying crystal structures and atomic spacing of samples. In this technique, monochromatic X-ray radiations produced through cathode tube are directed toward the samples. The interaction of the incident rays with the sample produces diffraction pattern which is used for the identification of size and shape of the unit cell. XRD studies were carried out by preparing a fine-grained sample by grinding it in the mortar and pestle. The sample was then put into the sample slide and pressed flat with a glass slide to obtain a uniform smear, assuring a flat upper surface. XRD studies of all the synthesized and commercially purchased (Sigma-Aldrich) powdered HAp samples were carried out using X-Ray Diffractometer (Miniflex II Rigaku) with monochromatic  $\text{CuK}\alpha$  radiation ( $\lambda = 1.5405\text{\AA}$ ) and a scan range of  $2\theta = 20^\circ$  to  $80^\circ$ . The crystallite sizes were determined using Scherrer's equation

$$X_D = \frac{k\lambda}{\beta \cos\theta} \quad (1)$$

where  $X_D$  is the crystallite size in  $\text{\AA}$ ,  $k$  is the shape constant (0.9),  $\lambda$  is the X-ray ( $\text{CuK}\alpha$ ) wavelength in  $\text{\AA}$ ,  $\theta$  is the diffraction angle in degrees and  $\beta$  (in radian) is the half width measured for the  $[h\ k\ l]$  value of  $[300]$  and  $[002]$  peak [Landi, E et al 2000].

The degree of crystallinity ( $X_c$ ), corresponding to  $[h\ k\ l]$  value of  $[002]$  was evaluated using the relation,

$$X_c = \left( \frac{k}{\beta_{002}} \right)^3 \quad (2)$$

where,  $k$  is a constant having a value of 0.24 for HAp (Landi et al. 2000). The lattice parameters ( $a=b, c$ ) of hexagonal crystal HAp were calculated using the formula:

$$\frac{1}{d^2} = \left( \frac{h^2 + hk + k^2}{a^2} \right) + \frac{l^2}{c^2} \quad (3)$$



Where (h k l) are Bragg's diffraction planes and d is inter planar spacing calculated using Braggs law

$$\lambda = 2d_{hkl} \sin \theta_{hkl}. \quad (4)$$

### 2.2.2.2 Fourier transform infrared spectroscopy

Fourier transform infrared (FTIR) is a sensitive technique used to obtain chemical composition of compounds. It is based on absorption spectra of compounds (solid/liquid/gas) that are a unique reflection of their molecular structure. The sample pellets for FTIR analysis were obtained by mixing 1mg of the powdered sample (all the HAp samples synthesized as described in Method 1 to 5 and commercially purchased HAp) with 100mg spectroscopic grade KBr (Merck). KBr (approximately 100 mg) was dried in oven at 100°C for 6h and ground into a fine powder using a clean mortar and pestle. The sample mix was then pressed into thin pellets at a pressure of 7 tonnes for 2min using a KBr mini press. Sample pellet was placed in the sample holder and FTIR spectra were obtained over the region 4000–450cm<sup>-1</sup> using the 8201 PC Shimadzu IR prestige-21.

### 2.2.2.3 Raman spectroscopy

Raman spectroscopy is used to detect the vibrational, rotational, and other low-frequency modes in compounds. It is based on inelastic scattering, or Raman scattering, of monochromatic light, usually emitted from a laser of visible/ near infrared/ ultraviolet range. This laser light interacts with the molecular vibrations, phonons or other excitations in the samples resulting in shift in the energy that provides information about the vibration modes in the samples. Finely powdered samples (all synthesized and commercially purchased HAp) were placed under Olympus microscope which is connected to Bruker Senterra Raman spectrometer and Raman spectra of all the samples were recorded in the 3700-400cm<sup>-1</sup> region using the 532nm wavelength.

#### **2.2.2.4 Transmission electron microscope**

The transmission electron microscope (TEM) operates on the same basic principles as the light microscope but instead of light uses electrons. In TEM, electrons are used as a source of illumination and their low wavelength gives thousand times higher resolution than light microscope. TEM has become valuable tool in biological and materials research due to its ability to produce high magnifications. Electrons travel through vacuum in the column of the microscope and interact with specimen to form an image. All the HAp samples (all synthesized and commercially purchased HAp) were prepared by dispersing 1mg sample in 5mL water and sonicating it for 15min at 3RPS (40 W) using Microson™ Sonicator. A drop of the colloidal solution thus obtained was placed onto a carbon-coated copper grid and dried in air. TEM analysis of all the samples were carried out using a JEOL JEM-2100F operating at 200 kV.

#### **2.2.2.5 Energy dispersive analysis of X-ray**

The energy dispersive analysis of X-ray (EDAX) is used to obtain elemental composition of the compound. The sample powders were deposited on a carbon tape, mounted on a sample holder and gold coated for EDAX analysis. The EDAX of all synthesized HAp samples were carried out using a JEOL, JSM-5800LV scanning electron microscope equipped with EDAX and operated at 20keV.

#### **2.2.2.6 Dynamic light scattering and zeta potential**

Dynamic light scattering (DLS) is a technique used to determine the mean particle size of small particles. All synthesized HAp samples for DLS and zeta potential analysis were prepared by dispersing 1mg sample in 5mL water and sonicating it for 15min at 3RPS (40W) using Microson™ Sonicator. Particle size of samples were analyzed using (DLS) particle size analyzer (Delsa Nano S, Beckman Coulter, USA).

Zeta potential analysis was used to determine surface charge of nanoparticles. Zeta potential of HAp NPs was studied using Zeta Plus, zeta potential analyzer (Delsa Nano S, Beckman Coulter, USA) at room-temperature.

### 2.2.2.7 Photoluminescence spectroscopy

Photoluminescence (PL) spectroscopy is a contactless, non-destructive method and used to obtain emission spectrum of samples when excited using specific wavelength. The sample pellets for PL analysis were obtained by taking 50mg of each sample and pressing into thin pellets at a pressure of 7 tonnes for 2min using a KBr mini press. Prepared pellets of all the synthesized and commercially purchased HAp samples were excited using monochromatic light from 325nm He-Cd laser and emission spectra were recorded. The fluorescence spectra of the samples were also recorded at various temperatures ranging from 300-15K. Fluorescence excitation spectra of the samples were determined using spectrofluorometer (Shimadzu RF 5301), at an emission wavelength of 502nm. The samples were suspended in water (1mg/mL) and sonicated for 15min before analysis.

The fluorescence of the sample was also observed under epi-fluorescence microscope (Olympus BX41) using fluorescein isothiocyanate (FITC) and tetramethylrhodamine (TRITC) filters.

Stokes' shift was estimated as follows:

$$\Delta\nu = \nu_{em} - \nu_{ex} \quad (5)$$

where,  $\Delta\nu$  is Stokes' shift in  $\text{cm}^{-1}$ ,  $\nu_{em}$  is the wavenumber of the emission maxima in  $\text{cm}^{-1}$  and  $\nu_{ex}$  is the wavenumber of the excitation maxima in  $\text{cm}^{-1}$ .

### 2.2.2.8 Electron Spin Resonance

Electron spin resonance (ESR) is a method for studying electronic structures of materials with unpaired electrons. ESR spectra of synthesized and commercially

purchased HAp were recorded using JEOL ESR spectrometer (JES-FA200). All the measurements were performed at room temperature.

## **2.3 Results and discussion**

### **2.3.1 Synthesis and characterization of HAp NPs**

In the current work, we have synthesized a new class of HAp at room temperature by modified sol-gel method using triethyl amine (TEA) or acetyl acetone (ACA) as stabilizing agents with either water or dimethyl sulfoxide (DMSO) as the solvent. Water and DMSO were selected as solvents based on the differences in their polarities, which would eventually influence the interactions among the calcium ions resulting in varied morphologies. DMSO being less polar of the two and aprotic in nature facilitates the formation of smaller particles (Khoza et al. 2012). To study the effect of basic and acidic stabilizing agents on the shape and size of HAp NPs, TEA (as basic) and ACA (as acidic) were used. Recently, HAp NPs with different morphologies are being synthesized using various methods such as precipitation, hydrothermal processing, emulsion, sol-gel synthesis, etc. (Ferraz et al. 2004; Koutsopoulos 2002; Liu et al. 2002b; Okada and Matsumoto 2015). Variations in particle size have been described through nucleation and growth of NPs. The process of nucleation and growth of the NPs primarily depends on the corresponding monomer concentration and their solubility (Thanh et al. 2013). The growth, and thereby the morphology of the NPs is further controlled by the addition of stabilizing/capping agents such as ethylenediamine tetraacetic acid (EDTA), hexadecyl trimethyl-ammonium bromide, sodium dodecyl sulfate (SDS), etc., (Morsy 2014; Ramimoghadam et al. 2012; Thanh et al. 2013).

#### **2.3.1.1 XRD analysis**

The phase purity and crystallinity of samples were determined using XRD analysis. The XRD spectra (Figure 2.2), of all the synthesized HAp and commercially purchased sigma control HAp corresponded well with the

hexagonal HAp crystal (ICDD 09-0432). All the HAp characteristic peaks at 25.8°, 31.34° and 33.97° corresponding to [hkl] lattice of [002], [211] and [300], respectively were observed in the spectra. Sample prepared without stabilizing agent as well as ACA as a stabilizing agent and water as a solvent showed  $\beta$ -TCP peaks along with HAp peaks (Figure 2.2 c and d). Relative intensities of characteristic HAp peaks ([002], [211] and [300]) are varying in each spectrum, indicating the possibility of variation in the orientation of growth under different synthesis conditions. Similar observations were noted by few researchers where changes in the intensities of peaks were attributed to variation in the synthesis conditions such as pH, reaction time and calcination temperatures and time (Cengiz et al. 2008; Liu et al. 2001; Liu et al. 2002b; Yang et al. 2014; Zhang et al. 2009; Zhang and Vecchio 2007). The crystallite size calculated for [002] and [300] lattice, crystallinity and unit cell parameters of commercially available HAp and synthesized HAp are presented in Table 2.1. HAp synthesized using ACA and DMSO showed lower while HAp synthesized using water and TEA showed higher crystallinity as well as crystallite size.

### 2.3.1.2 FTIR analysis

The FTIR studies were carried out to identify the various functional groups associated with HAp. All the HAp NPs exhibited the characteristic signature HAp bands in the FTIR spectra (Figure 2.3a). The signature HAp peaks recorded at  $\sim 565\text{cm}^{-1}$  are attributed to the bending modes of P-O bonds in phosphate groups, with contribution from the -OH of the apatite group at  $\sim 605\text{cm}^{-1}$ . The peaks noted  $\sim 1031\text{cm}^{-1}$  are attributed the stretching modes of the  $\text{PO}_4$ . The bands in the region  $3400\text{cm}^{-1}$  are attributed to -OH bonds and those observed near  $\sim 3571\text{cm}^{-1}$  are associated with -OH stretching vibration of HAp (Jadalannagari et al. 2014a; Jadalannagari et al. 2014b; Jadalannagari et al. 2011; Ramanan and Venkatesh 2004)

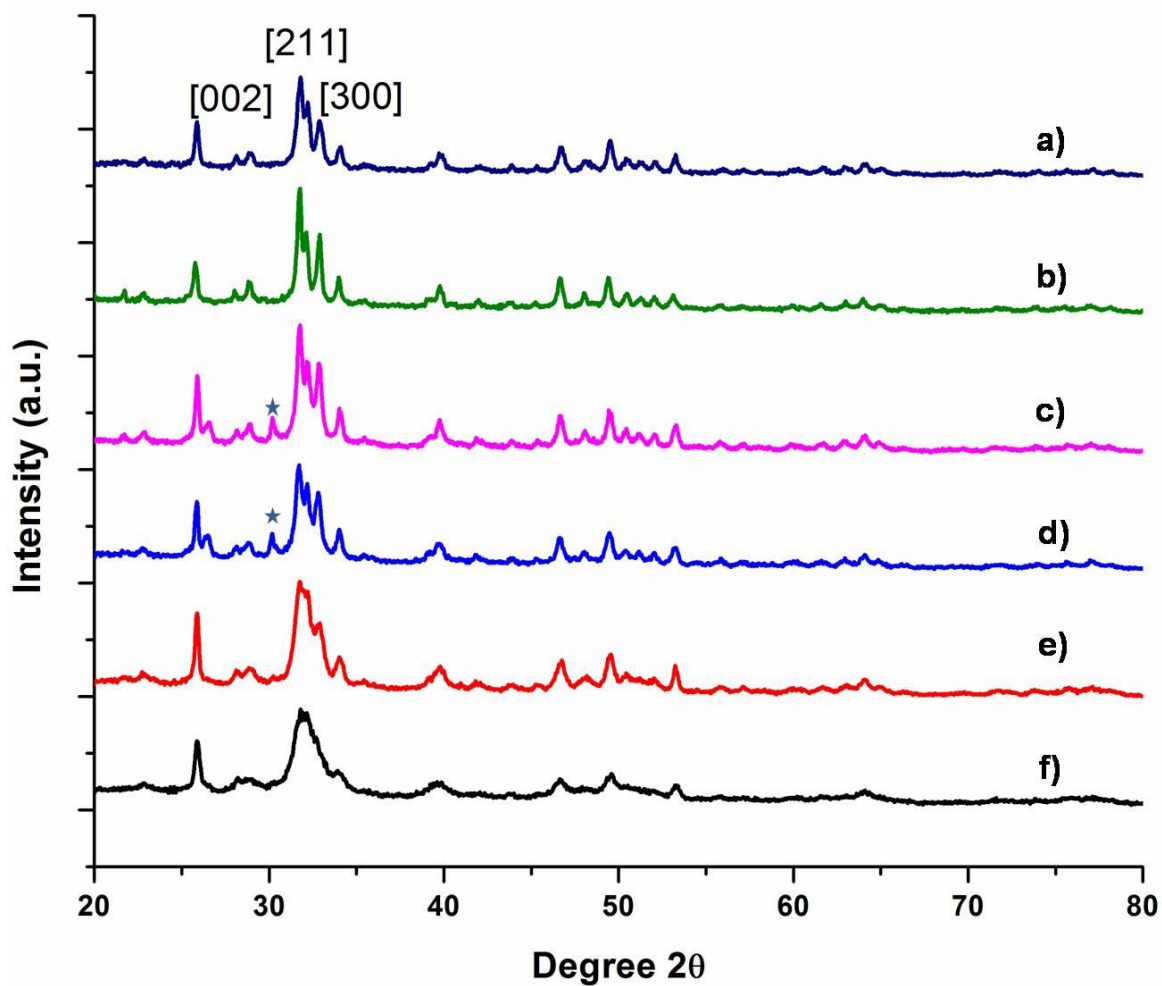


**Figure 2.2** XRD spectra of HAp samples obtained using various stabilizing agents (TEA and ACA) and solvents (water and DMSO) a) Sigma-control b) TEA and water c) no stabilizing agent and in water d) ACA and water e) ACA and DMSO f) TEA and DMSO.

**Table 2.1:** Crystallite size, crystallinity and unit cell parameters of fabricated cells

| HAp samples synthesized with various conditions |             | Crystallite size $X_D$ (nm) |       | Crystallinity $X_s$ | Unit cell parameters |      |
|---|-------------|-----------------------------|-------|---------------------|----------------------|------|
| Solvent   | Stabilizing | [002]                       | [300] |                     | a(Å)                 | c(Å) |
| Water   | TEA         | 32.9                        | 20.22 | 0.790               | 9.67                 | 6.93 |
| DMSO  | TEA         | 29.0                        | 14.70 | 0.653               | 9.47                 | 6.84 |
| DMSO  | ACA         | 25.8                        | 11.00 | 0.474               | 9.38                 | 6.80 |
| Water   | ACA         | 33.0                        | 22.00 | 0.715               | 9.72                 | 6.95 |
| Water   | NA          | 31.1                        | 17.60 | 0.832               | 9.63                 | 6.88 |
| Commercially available HAp                      |             | 30.3                        | 19.03 | 0.772               | 9.62                 | 6.90 |

### 2.3.1.3 Raman spectra analysis

Vibrational, rotational and low frequency modes in HAp samples were determined by Raman spectroscopy. Raman spectra (Figure 2.3b) show very intense band at  $\sim 961\text{cm}^{-1}$  which is the characteristic peak of HAp and attributed to symmetric stretching mode of  $\text{PO}_4^{3-}$ . The asymmetric stretching and triply symmetric bending modes of  $\text{PO}_4^{3-}$  are observed at  $\sim 1050$ ,  $\sim 450$  and  $592\text{cm}^{-1}$  respectively (Koutsopoulos 2002; Markovic et al. 2004; Walters et al. 1990; Yamini et al. 2014).

### 2.3.1.4 EDAX analysis

The energy dispersive analysis of X-ray of all synthesized HAp (thin rod, short rod, rod and microrods) shown in (Figure 2.4). EDAX analysis identifies the elemental composition of materials. EDAX systems are attached to SEM instrument. EDAX spectrum of all synthesized HAp (thin rod, short rod, rod and microrods) exhibited a peak corresponding to calcium (Ca), phosphorous (P) and oxygen (O).

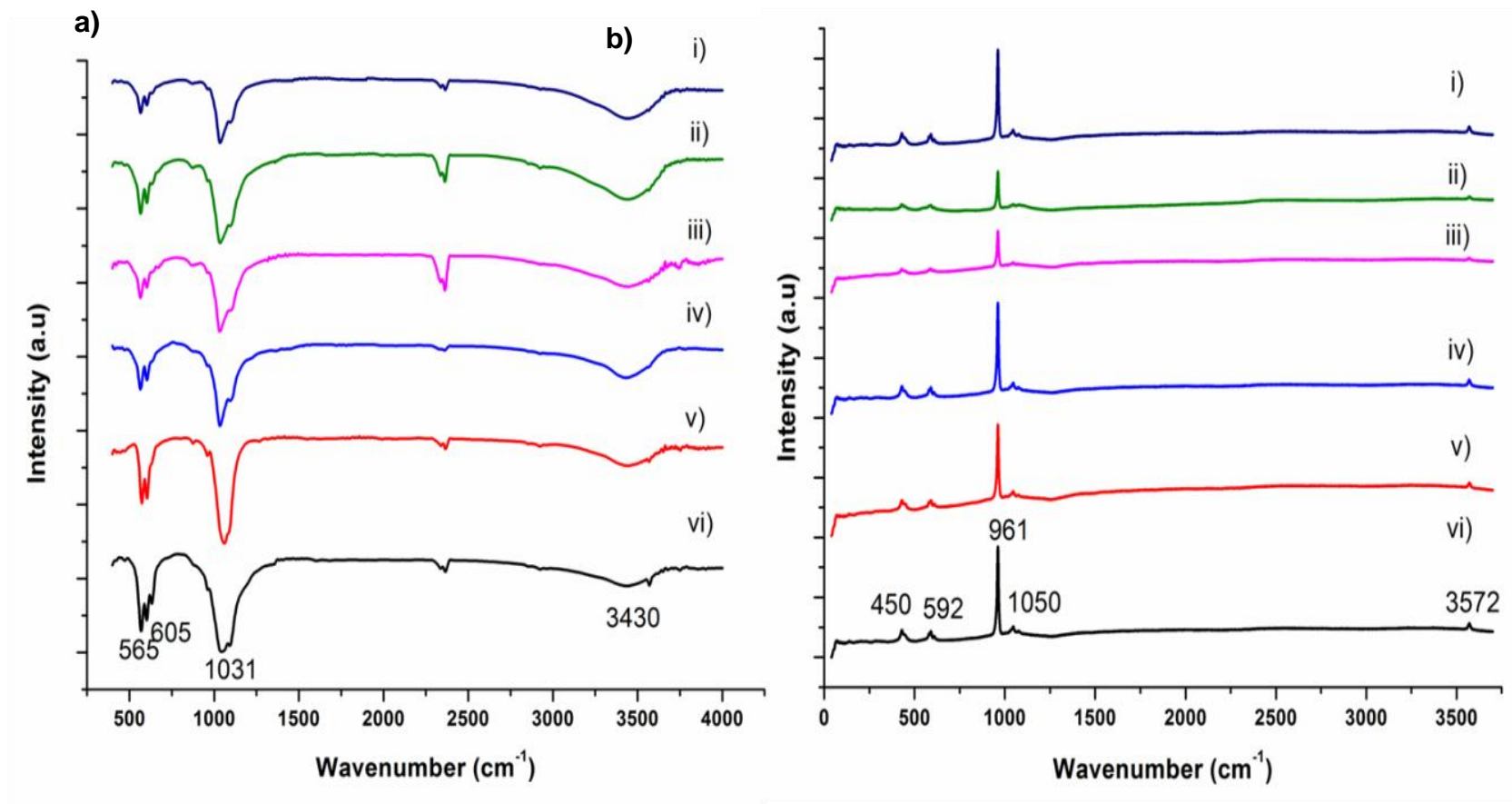


**Figure 2.3** a) FTIR b) Raman spectra of HAp samples obtained using various stabilizing agents (TEA and ACA) and solvents (water and DMSO) i) commercially purchased control from Sigma ii) ACA and water iii) no stabilizing agent and in water iv) TEA and water v) TEA and DMSO vi) ACA and DMSO



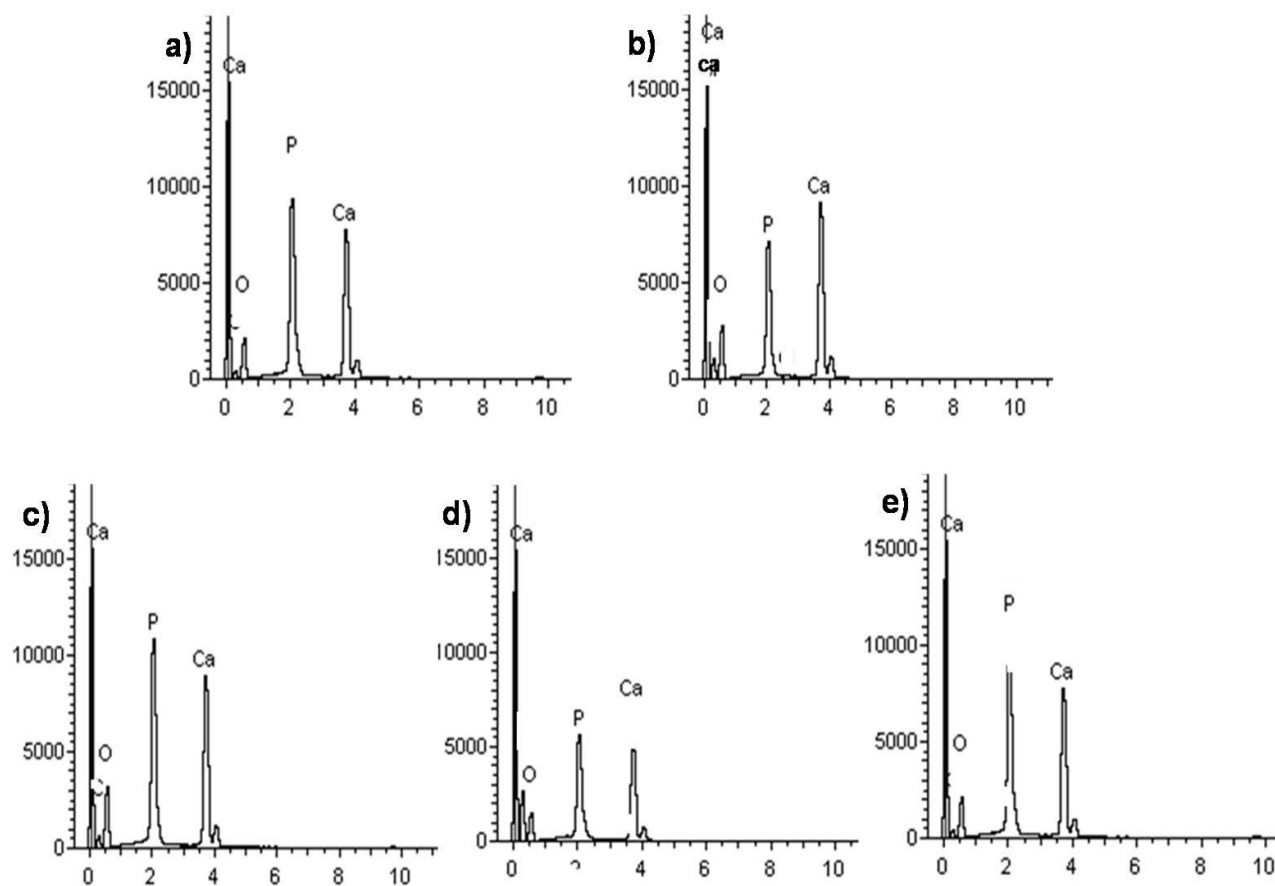


**Figure 2.4** EDAX spectra of HAp samples obtained using various stabilizing agents (TEA and ACA) and solvents (water and DMSO) a) ACA and water b) no stabilizing agent and in water c) TEA and water d) TEA and DMSO e) ACA and DMSO.

### 2.3.1.5 TEM analysis

Morphologies of samples were confirmed using TEM analysis. Depending on the conditions used in the reaction mixture (please refer to the materials and methods), the newly formed particles exhibited rod morphology with various aspect ratios (Table 2.2 and Figure 2.5). It was observed that NPs synthesized using water as a solvent and TEA as a stabilizing agent, were rod shaped with average length 92.8nm and average diameter 23.2nm (Figure 2.5a). The shape changed to short rods with an average length 35nm and an average diameter 7nm when DMSO was used as a solvent keeping TEA as the stabilizing agent (Figure 2.5b). Thin rods of average length 62.5nm and diameter 6.2nm were obtained when the stabilizing agent was changed to ACA while maintaining DMSO as the solvent (Figure 2.5c). When water was used as the solvent and ACA as the stabilizing agent, the particles obtained were irregular shaped with mixed morphologies (Figure 2.5d). In the absence of either of the stabilizing agents, HAp microparticles of rod shape with an average length 1.42 $\mu$ m and diameter 0.29 $\mu$ m were formed (Figure 2.5e). This demonstrated the role of stabilizing agent in controlling nucleation and growth, which resulted in different sizes of rods. The details of all the synthesized NPs are summarized in Table 2.2. To the best of our knowledge, this is the first study to report the effect of TEA and ACA as stabilizing agents with water and DMSO as solvents, on the morphology of HAp NPs. Particle /hydrodynamic sizes of HAp were also confirmed by dynamic light scattering (DLS) and are presented in table 2.2. Change in crystallinity and morphology of HAp has been reported with variation in reaction parameters such as pH (Kumar et al. 2004; Zhang et al. 2009), time of reaction (Yang et al. 2014), temperature of calcination (Kumar et al. 2004; Wang et al. 2010b), stabilizing agents (Wang et al. 2010b; Yang et al. 2014) and solvents (Wang et al. 2010b). Morphological variations were attributed to change in pH from 4 to 9 as at pH  $\geq$ 7 (neutral and basic) the adsorption probability of OH<sup>-</sup> ions onto the surface of the Ca<sub>5</sub>(PO<sub>4</sub>)<sub>3</sub>OH was high which resulted in isotropic or weak-anisotropic growth resulting in short and elongated rod structure. However,

at pH below 7 (acidic) the probability of the adsorption of  $\text{OH}^-$  ions was limited and preferentially resulted in anisotropic growth; resulting in two-dimensional microsheets, three-dimensional microflowers, and three dimensional microspheres (Zhang et al. 2009). Needle shaped HAp synthesized using coprecipitation method changed to spheroidal when calcination temperature increased from 40 -100°C which is attributed to increase in the growth rate and decrease in aspect ratio with the increase in temperature (Kumar et al. 2004). Variation in reaction time from 40 to 600min produced different morphologies of HAp such as microsphere and flower like structure (Yang et al. 2014). HAp with various morphologies, such as sphere, rod, needle, wire and bamboo leaf-like were obtained by controlling the solvent system (ethanol and water), pH (4-9) and reaction temperature (25-60°C). Diameter of NPs increases when solvent system changed from water to ethanol which is attributed to less solubility of calcium salt in ethanol hence increasing supersaturation (Wang et al. 2010b).

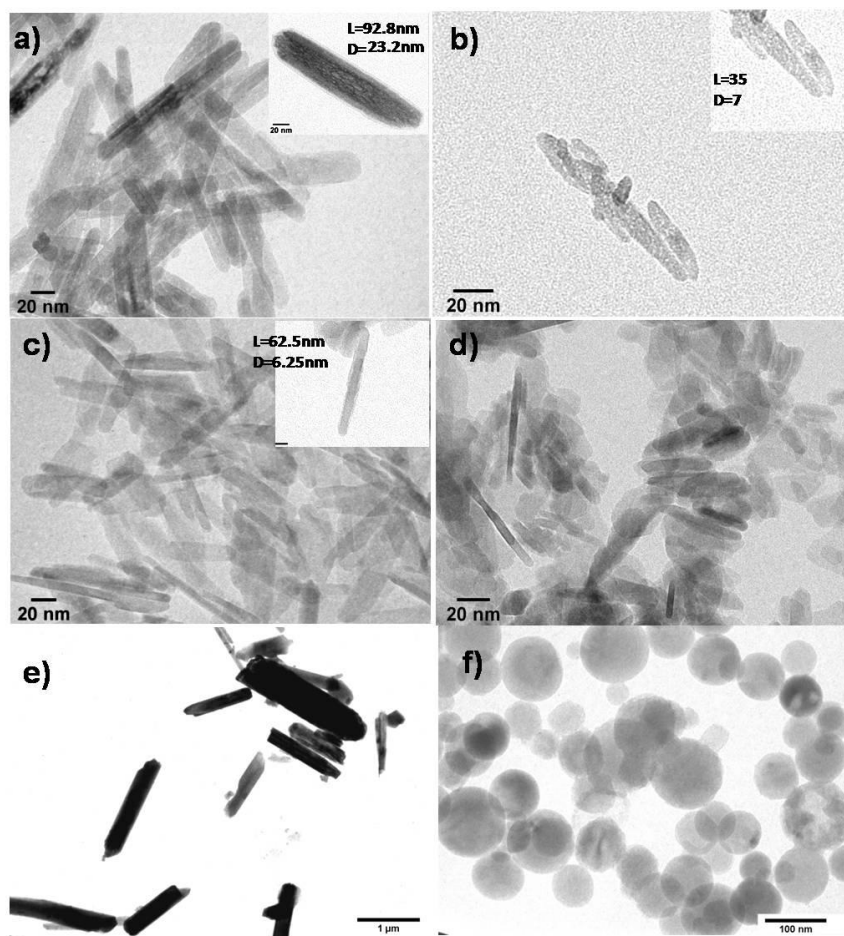


**Figure 2.5** TEM micrographs of HAp NPs with different morphologies obtained using varied stabilizing agents (TEA and ACA) and solvents (water and DMSO) a) rods with average length 92.8nm and average diameter 23.2nm were obtained when water was used as a solvent and TEA as a stabilizing agent b) short-rods with average length 35nm and average diameter 7nm were obtained when DMSO was used as a solvent and TEA as a stabilizing agent c) thin-rods with average length 62.5nm and average diameter 6.2nm were obtained when DMSO was used as a solvent and ACA as a stabilizing agent d) mixed morphology nanostructures were obtained when water was used as a solvent and ACA as a stabilizing agent e) microrods with average length of 1.42 $\mu$ m and average diameter of 0.29 $\mu$ m without using any stabilizing agent while maintaining Ca/P ratio 1.67 f) spherical sigma-cont

**Table 2.2:** Different morphologies of HAp NPs synthesized using various solvent/stabilizing agent combinations.

| Solvent | Stabilizing Agent | Morphology          | Size and shape using TEM |                       | Aspect ratio <sup>a</sup> (A/B) | Particle size using DLS (nm) |
|---------|-------------------|---------------------|--------------------------|-----------------------|---------------------------------|------------------------------|
|         |                   |                     | Avg length (A) (nm)      | Avg diameter (B) (nm) |                                 | size (nm)                    |
| DMSO    | Tri-ethyl amine   | Short-rod           | 35                       | 7                     | 1:5                             | 28±10                        |
| DMSO    | Acetyl acetone    | Thin-rod            | 62.5                     | 6.2                   | 1:10                            | 57±10                        |
| Water   | Tri-ethyl amine   | Rod                 | 92.8                     | 23.2                  | 1:4                             | 85±10                        |
| Water   | Acetyl acetone    | Mixed and irregular | 30-90                    | 6-25                  | NA <sup>b</sup>                 | NA <sup>b</sup>              |
| Water   | NA                | Microrods           | 1420                     | 290                   | 1:5                             | 1523±10                      |

**Aspect ratio<sup>a</sup>**=ratio of average length and average diameter

**NA<sup>b</sup>** = Not applicable due to its mixed morphology

### 2.3.1.6 Zeta potential measurement

Zeta potential analysis of all the synthesized HAp NPs was performed to determine surface charge. Zeta potential values for thin rod, short rod, rod, mixed and irregular morphology and microrod shaped HAp NPs were 13.25, 3.85, 2.12, 6.92 and 4.37 mV respectively. Zeta potential value of HAp NPs showed higher positive value when ACA was used as a stabilizing agent and this could be attributed to the acidic nature of ACA contributing positive surface charge. Similar observations were reported by Berg et al where they have studied the effect of pH on zeta potential using TiO<sub>2</sub>, Fe<sub>2</sub>O<sub>3</sub>, Al<sub>2</sub>O<sub>3</sub>, ZnO, and CeO<sub>2</sub> NPs, and observed that with a decrease in pH the positive zeta potential increased (Berg et

al. 2009). Similarly, zeta potential value of poly lactide and poly (D,L-lactide-coglycolide) polymeric NPs at  $\text{pH} \geq 7$  was negative, whilst at  $\text{pH} < 7$  resulted in NPs with positive zeta potential (Sahoo et al. 2002). Since the particles synthesized using water as a solvent and ACA as a stabilizing agent showed irregular morphology, these NPs were excluded for further studies.

### 2.3.1.7 Self-activated fluorescent properties of HAp NPs

HAp is not known to be a fluorescent material; however, in this study all the HAp NPs synthesized using TEA/ACA as stabilizing agents and water/DMSO as solvents at room temperature by modified sol-gel method exhibited green and red fluorescence under epi-fluorescence microscope using FITC and TRITC filters (Figure 2.6). Mechanism of the fluorescence of the newly synthesized HAp NPs is not very clear at this stage, because, neither  $\text{Ca}^{2+}$  nor  $\text{PO}_4^{3-}$  are known to show any fluorescing property; hence this behavior could most probably be attributed to self-activated fluorescence of these particles and have been designated as “fluorescent HAp NPs” (fHAp)s. A few reports have mentioned the observation of luminescence in HAp NPs wherein fluorescence has been attributed to the presence of  $\text{CO}^{2-}$  radical in the crystal lattice, introduced through the precursor material (Kumar et al. 2012; Zhang et al. 2010; Zhang et al. 2009; Zhanglei et al. 2012). All these studies have shown blue emission with maxima between 400-460nm. In the present work, all the fHAp)s prepared by the room temperature sol-gel method exhibited excitation at 325nm ( $\lambda_{\text{ex}}$ ) (shown as inset in Figure 2.7), and has resulted in a broad emission spectrum ranging from 350-750nm with maximum at 502nm ( $\lambda_{\text{em}}$ ) and additional peaks at 528nm, 567nm and 609nm (Figure 2.7). The peak at  $\sim 442\text{nm}$  is characteristic peak of He-Cd laser. The emission spectra of all fHAp)s synthesized were similar, but with significant changes in the intensity of fluorescence signal, which was in the order thin rod > short rod > rod > microrods. Amongst all fHAp)s, thin rods exhibited highest fluorescence intensity and intensity was decreased with decreasing aspect ratio. All fHAp)s exhibited large Stokes' shift of 177nm, which is desirable

property to minimize overlap between absorption and emission spectra (Peng et al. 2005).

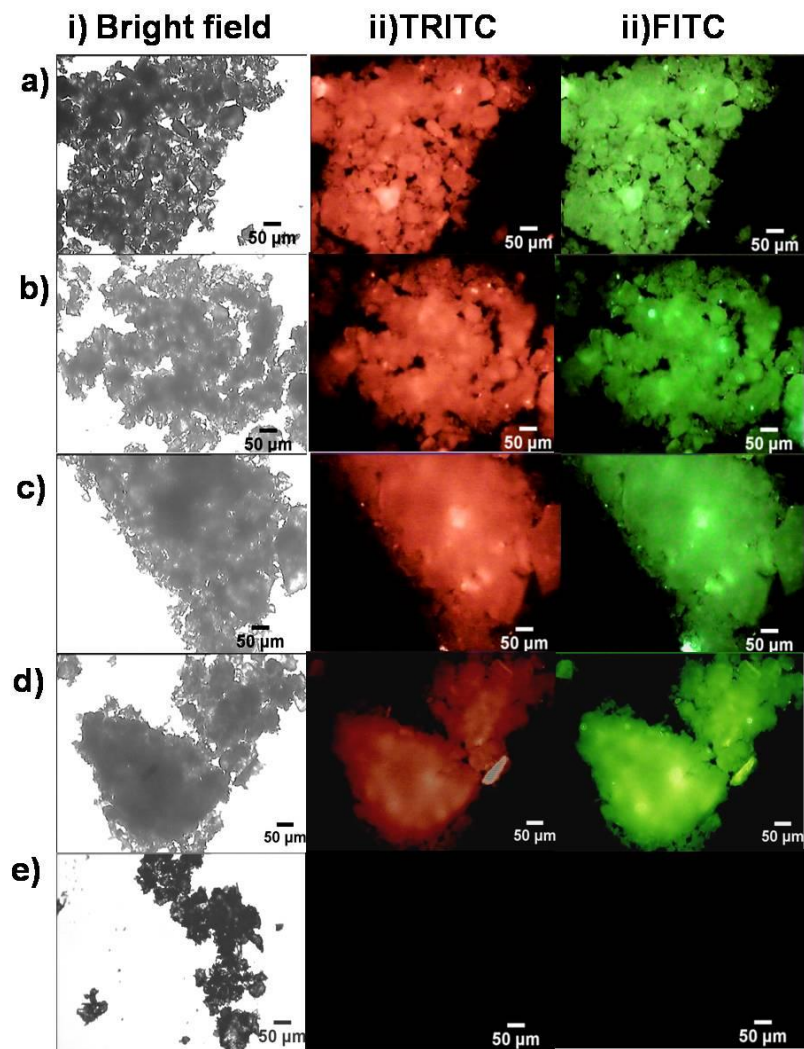


**Figure 2.6** Epi-fluorescence microscope images of fHAp NPs using FITC (green) and TRITC (red) filters a) thin-rods b) short-rods c) rods, synthesized at room temperature by modified sol-gel method. d) microrods synthesized without stabilizing agents. All the fHAp exhibit both green and red fluorescence. Commercially obtained spherical HAp NPs (symmetric in shape) that do not show any fluorescence are shown for comparison in (e).



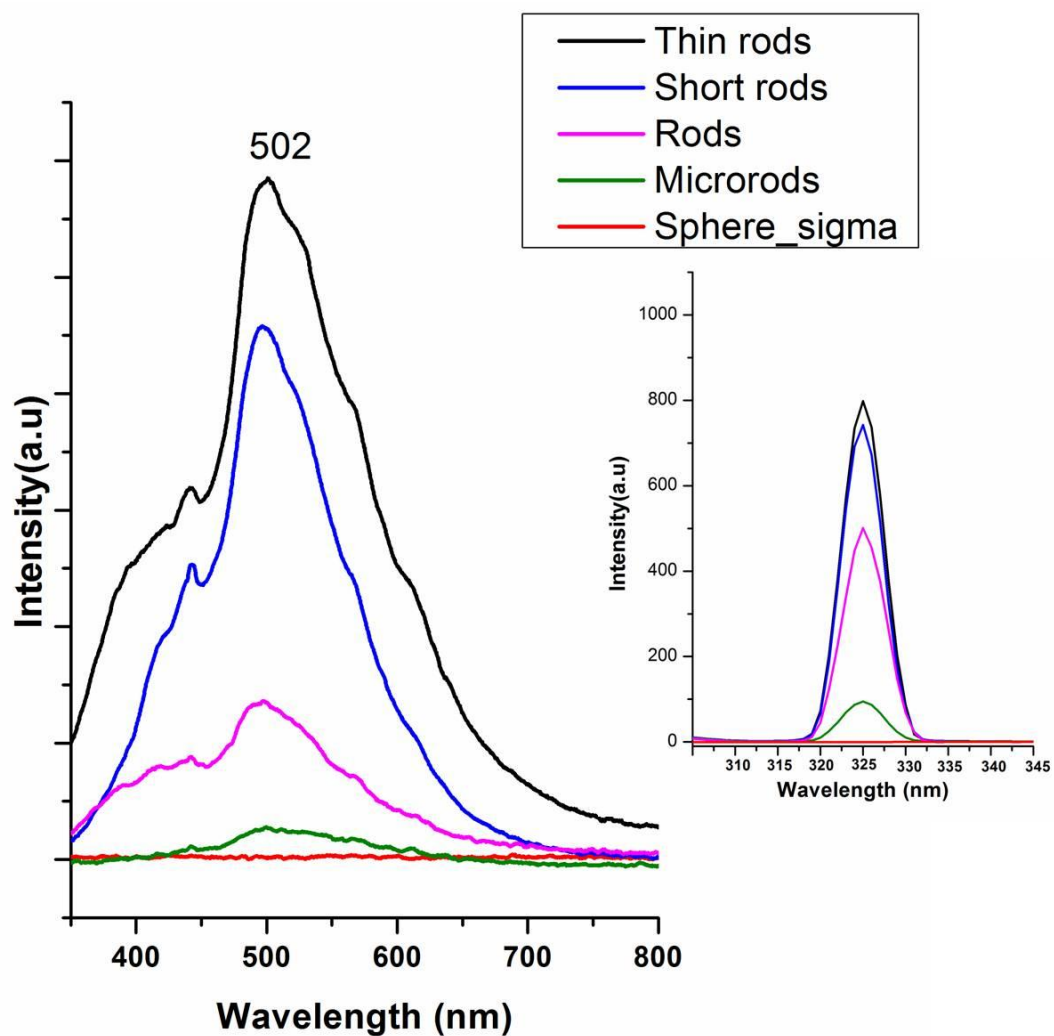


**Figure 2.7** Fluorescence spectra of fHAPs at an excitation of 325nm. fHAPs exhibit a broad emission spectrum ranging from 350-750nm with maximum at 502nm and additional peaks at 528nm, 567nm and 609nm. The fluorescence spectrum of commercially obtained spherical HAp NPs (red) is shown for comparison. Although, the emission spectra of fHAPs were similar, significant changes in the intensity of fluorescence signal of the order of thin-rods (black line) > short-rods (blue) > rods (magenta) > microrods (green) were observed.



Further to elucidate the mechanism of fluorescence property of all three fHAPs which having rod like morphology with different aspect ratios, their fluorescence spectra were carried out at different temperatures ranging from 300K to 15K. Presence of defects in the fHAPs, can be traced by observing changes in the fluorescence signals as a function of temperature. Peaks due to shallow defects, obscured at room temperature and are recorded at low temperatures due to their sharpening of the fluorescence peaks. Additionally at low temperature, increase in the emitted signal intensity is observed due to the suppression of phonon assisted non-radiative transitions (Gerigk et al. 2015; Wang et al. 2011a; Ye et al. 2007). In the current study, only an increase in the intensity of the emitted fluorescence signal, without any additional peaks, was observed at low temperatures along with a shift of  $\lambda_{em}$  maximum from 502nm to 528nm (Figure 2.8). This clearly indicates that there are no shallow defects present in the fHAPs and the observed fluorescence could be attributed to their asymmetry in morphology as all of the characterized fHAPs were of rod like shape. To confirm this assumption, similar experiments were further carried out on commercially available symmetric spherical shaped HAP NPs (Figure 2.5f). As expected, these spherical HAP NPs did not show any fluorescence (Figure 2.6e and 2.7), confirming the presence of fluorescence due to asymmetry in morphology of fHAPs. ESR spectra of fHAPs confirmed the presence of free electrons in NPs having been confined in the asymmetric morphology. These fHAPs exhibited ESR signals with three hyperfine splittings and “g” values indicative of presence of free electrons (Figure 2.9). These free electrons, due to their confinement in an asymmetric potential created by the elongated structure of the fHAPs, have discrete energy levels which are optically active, leading to fluorescence phenomena. On the other hand, the commercially obtained symmetric spherical HAPs did not show any ESR signal (Figure 2.9e). This observation further underlines the importance of asymmetry for observations of fluorescence.

All the above studies show that HAP NPs with various rod morphologies synthesized using different solvents and stabilizing agents (Figure 2.5), exhibit

excellent self activated fluorescence (Figure 2.6 and 2.7). Presence of self activated fluorescence was attributed to the electronic transition in the asymmetric structure of HAp NPs as confirmed by ESR spectroscopy and absence of fluorescence in symmetric HAp NPs.

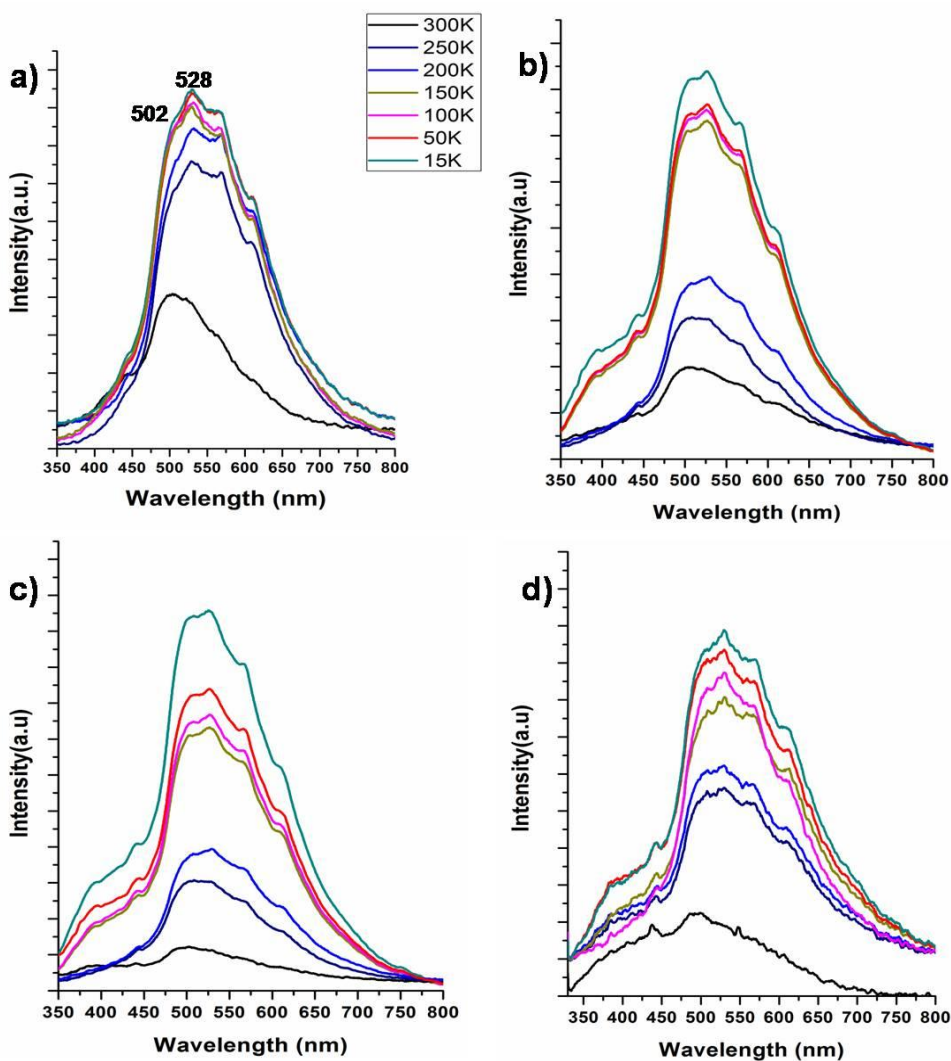


**Figure 2.8** Fluorescence spectra of a) thin rod b) short rods c) rods d) microrods fHAPs at different temperatures ranging from 300 to 15K. The emission signals across the spectra are shown with a connected line for clarity. Only an increase in the intensity of the emitted fluorescence signal, without any additional peaks was observed at low temperatures.

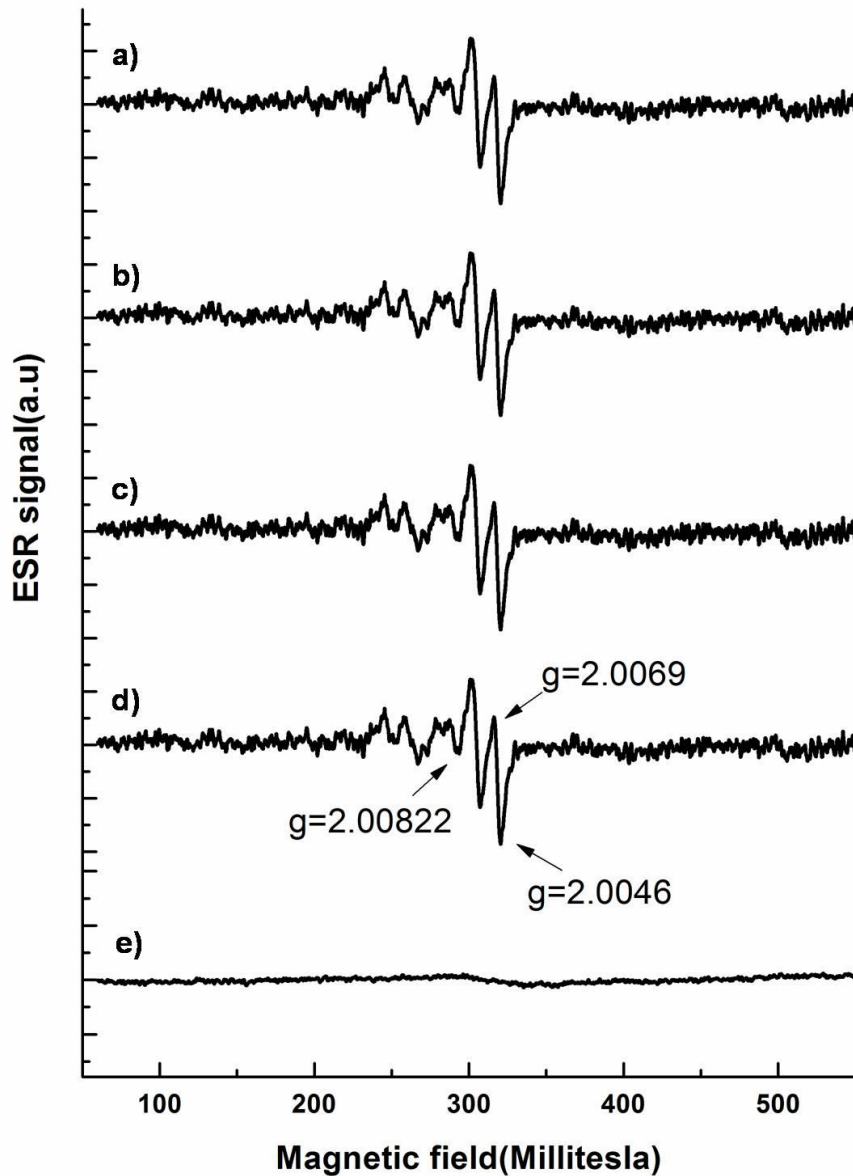


**Figure 2.9** ESR spectra of a) thin-rods b) short rods c) rods d) microrods fHAp with three hyperfine splittings and “g” values (2.0082, 2.0069 and 2.0046) indicating the presence of free electrons owing to the asymmetric nature of these NPs. For comparison, the ESR spectrum of the commercially obtained spherical HAp NPs, which are symmetric, is shown in (e). Notice the absence of hyperfine splitting in the case of spherical HAp NPs.

## **2.4 Conclusion**

A new class of self activated fluorescence HAp NPs (fHAPs) with varied aspect ratios was synthesized at room temperature by sol-gel method. Solvents and stabilizing agents played an important role in obtaining HAp NPs with different morphologies (rods, thin-rods, short-rods). The intense fluorescence observed is most probably associated with the electronic transitions arising due to asymmetric structure of the NPs as all of them have elongated morphology. These biocompatible fHAPs provides exciting opportunities in the field of biomedicine for theranostic purposes .

## CHAPTER 3

### **Self Activated Fluorescent Hydroxyapatite Nanoparticles: A Promising Alternative for Bioimaging and Biolabeling**

#### **3.1 Introduction**

Since the time of Galileo, imaging technique has become the "eyes of science" rendering an exquisite sense of vision to medical science and research. This technique facilitates the study of biological processes, including the observable changes in receptor kinetics, cellular signaling and the movement of molecules through membranes (Kherlopian et al. 2008; Prasad 2003; Vonesch et al. 2006). Imaging techniques such as magnetic resonance imaging, computed tomography, fluorescence imaging, radio imaging, etc., enable visualization of multi-dimensional and multi-parameter data (Kherlopian et al. 2008). Compared to other techniques, fluorescence imaging is advantageous as it is highly sensitive, minimally-invasive and safe (Ntziachristos 2006). Fluorescent labeling using usual organic dyes, fluorescent proteins and lanthanide chelates are the preferred methods to observe biological events and processes in both living and non-viable systems (Wang et al. 2005). However, they possess inherent drawbacks such as short Stokes' shift, poor photochemical stability, susceptibility to photo-bleaching and decomposition under repeated excitation (Wolfbeis 2015). In view of the existing limitations, more efficient fluorescent nanomaterials have been developed as alternative bio-imaging agents.

Fluorescent nanomaterials including quantum dots, nanoparticles (NPs) doped with lanthanides, UCNPs, metal NPs etc., have shown significant progress in diagnostics and therapeutic applications, owing to their small size and large surface area (Nune et al. 2009; Syamchand and Sony 2015; Wolfbeis 2015). Among these, hydroxyapatite (HAp) NPs doped with lanthanides and organic dyes are being extensively studied as fluorescent probes. Fluorescent lanthanide ( $\text{Eu}^{3+}$ ,  $\text{Tb}^{3+}$ ,  $\text{Yb}^{3+}$ ,  $\text{Er}^{3+}$ , etc.) doped HAp NPs have been reported to possess

narrow emission bandwidths, high photo-chemical stability and long fluorescence lifetimes. (Altinog˘lu et al. 2008; Bastakoti et al. 2013; Lebugle et al. 2006; Li et al. 2008; Mondéjar et al. 2007; Morgan et al. 2008). HAp NPs have been successfully used for applications in the field of biomedical science ranging from bone regeneration to drug delivery (Zhou and Lee 2011). HAp is composed of ions commonly found in physiological environments, which makes it highly biocompatible (Tabaković et al. 2012). However, HAp NPs doped with lanthanides are toxic; resulting in their limited *in-vivo* applications (Mondéjar et al. 2007). Therefore, there is clear need for developing alternative fluorescent nanomaterials for bio-imaging, with biocompatible and tunable photo-luminescent properties.

In chapter 2, synthesis and characterization of self-activated fluorescent HAp NPs (fHAp) have been described. These fHAp of rod shape with different aspect ratios (thin rods, short rods, rods and microrods) exhibited excellent fluorescent property. The aim of the current work was to explore the possible applications of thin rod, short rod and rod fHAp for bioimaging and biolabelling.

## 3.2 Materials and methods

### 3.2.1 Biocompatibility studies

Several assays were carried out to test the cytotoxicity and biocompatibility of all the synthesized fHAp. Following is the brief description of these assays.

#### 3.2.1.1 3-(4,5-dimethylthiazol-2-yl)-2,5-diphenyltetrazolium bromide (MTT) assay

Cytotoxicity of thin rod, short rod and rod shaped self activated fluorescent NPs (fHAp) was measured by MTT (3-(4,5-dimethylthiazol-2-yl)-2,5-diphenyltetrazolium bromide) method (Kherlopian et al. 2008). Exponentially growing human cervical cancer cells (HeLa) were inoculated with  $5 \times 10^4$  cells/well supplemented with Dulbecco's modified Eagle's medium (DMEM) with 5% Fetal

bovine serum (FBS) (complete media). The cells were exposed to various concentrations (10, 30, 50, 100, 500 and 1000 $\mu$ g/mL) of the fHAPs dispersed in DMEM, and incubated for 24h. MTT (20 $\mu$ L of 5mg/mL) was added to the test samples, and the plates were incubated at 37°C for 4h. The media was pipetted out carefully without disturbing the cells after 4h. For dissolving the formazan crystals, 150 $\mu$ L of DMSO was added, and the absorbance was measured at 570nm using UV-visible spectrophotometer (UV-2450). All measurements were done in triplicates. The relative cell viability (%) was calculated as:

$$([A_t] / [A_c]) \times 100, \quad (6)$$

Where,  $[A_t]$  is the absorbance of the test sample and  $[A_c]$  is the absorbance of the cells without treatment.

### 3.2.1.2 Lactate dehydrogenase assay

Cytotoxicity was also measured using lactate dehydrogenase assay (LDH). LDH activity in the cell medium was determined using a commercial LDH kit (Coral Clinical Systems, India). LDH assay was carried out using HeLa cell lines. Growth medium obtained from HeLa cells incubated in complete media with varying concentrations (10, 30, 50, 100, 500 and 1000 $\mu$ g/mL) of fHAPs (thin rods, short rods and rods) for 24h was used for LDH analysis. The protocol followed was as specified by the manufacturer (Coral Clinical Systems) for the LDH kit. Absorbance was measured at 340nm (Thermofisher scientific Multiskan™ GO Microplate Spectrophotometer).

### 3.2.1.3 Reactive oxygen species generation assay

Intracellular reactive oxygen species (ROS) generation was determined using 2', 7'- dichlorofluorescein diacetate (DCFH-DA), a fluorescent probe that readily diffuses through the cell membrane into the cellular cytoplasm, where it is enzymatically hydrolyzed to non-fluorescent DCFH. The oxidation of DCFH to highly fluorescent 2', 7'- dichlorofluorescein provides a quantitative estimate of

ROS formation (Meena et al. 2012; Xu et al. 2012). The ROS studies were carried out using HeLa cell line. Exponentially growing cells ( $5 \times 10^4$  cells/ well), were seeded in 24-well plates supplemented with complete media. After 24h of growth the cells were exposed to varying concentrations of fHAp (10, 30, 50, 100, 500 and 1000 $\mu$ g/mL) dispersed in DMEM, and incubated for 24h. Following exposure, DCFH-DA (20 $\mu$ M) was added to all the wells, and the plate was incubated in the dark at 37°C for 30mins. The fluorescence was measured using a spectrofluorometer (JASCO FP-6300), with an excitation wavelength of 485nm, and an emission wavelength of 530nm. Hydrogen peroxide (H<sub>2</sub>O<sub>2</sub>) of 1 $\mu$ M concentration was used as positive control. All the experiments were performed in triplicates.

Similar MTT, LDH and ROS experiments were performed on transformed aneuploid immortal keratinocyte cell line (HaCaT).

#### 3.2.1.4 Hemolytic assay

The hemolytic activity of all the fHAp was investigated according to the method described by Dobrovolskaia et al (Dobrovolskaia et al. 2008). 4mL blood was collected from a healthy human and diluted with 5mL of sterile saline solution. 20 $\mu$ L of the diluted blood was then added to the 10, 30, 50, 100, 500 and 1000 $\mu$ g/mL of fHAp and equilibrated at 37°C for 30min. Subsequently, the tubes were incubated for 60min in water bath shaker at 37°C and centrifuged at 700 $\times$  g for 10min. The amount of free hemoglobin was determined by measuring the absorbance of the supernatant at 540nm (UV Spectrophotometer Shimadzu UV 2450). Sterile saline solution and distilled water were used as the negative and positive controls, respectively. The percent hemolysis rate (%HR) was calculated using (Jadalannagari et al. 2014a)

$$\%HR = \frac{D_t - D_{nc}}{D_{pc} - D_{nc}} \times 100 \quad (7)$$



Where  $D_t$ ,  $D_{nc}$  and  $D_{pc}$  are the absorbance of the sample, the negative control and the positive control, respectively. All the experiments were run in triplicates.

### 3.2.2 Fluorescence stability

The fluorescence spectra of all three fHAp (thin rod, short rod and rods) in liquid media were recorded using spectrofluorometer (JascoFP-6300) by dispersing in DMEM, Luria Bertani (LB), Sabouraud dextrose media (SB) and phosphate buffer saline (PBS) at pH 7. Fluorescence of fHAp in respective media was recorded at various time intervals (0, 2, 4, 6, 8, 10 and 12h).

### 3.2.3 Uptake of HAp NPs by eukaryotic and prokaryotic cells

HeLa, HaCat and MG63 cells were maintained in DMEM supplemented with 10% fetal bovine serum with antibiotics. Cells were maintained at 37°C in a humidified atmosphere with 5% CO<sub>2</sub> and sub-cultivated according to standard cell culture protocols (Freshney 2005). Exponentially growing cells were inoculated at a concentration of  $5 \times 10^4$  cells/well onto 2 × 2cm glass slide in a 6 well plate supplemented with 1mL complete media and were grown for 12h. The cells were incubated with various concentrations of thin rod, short rod and rod fHAp [10, 30, 50, 70, 100 and 500µg/mL] for 4h and the glass slides were washed twice with PBS (pH 7), to remove un-internalized particles and debris. These slides were observed using epi-fluorescence microscope under TRITC and FITC filters.

*Candida albicans* (MTCC 183) as a representative of yeast culture was used to study the internalization of fHAp. Culture was grown in Sabouraud dextrose media (SB) at 37°C in an incubator. Exponentially growing cells were inoculated at a concentration of  $10^6$  cells/well onto 2 × 2cm glass slide in a 6 well plate supplemented with 2mL SB media for 48h. The cells were then incubated with various concentrations of all three fHAp [10, 30, 50, 70, 100 and 500µg/mL] for 4h and the glass slides were washed twice with PBS (pH 7) to remove un-

internalized particles and debris. These slides were observed using epi-fluorescence microscope under TRITC and FITC filters.

Similar studies were done with bacterial cultures, using *Escherichia coli* (NCIM 2345) and *Staphylococcus aureus* (MTCC 737) as the Gram-negative and Gram-positive culture, respectively. Both the cultures were grown in Luria Bertani (LB) medium at 37°C in a shaker incubator. Exponentially growing cells were inoculated at a concentration of  $10^6$  cells/well onto 2 × 2cm glass slide in a 6 well plate supplemented with 2mL LB media for 6h. The cells were then incubated with all the three fHAp [10, 30, 50, 70, 100 and 500µg/mL] for 4h after which the glass slides were washed twice with PBS (pH 7) to remove un-internalized particles and debris. These slides were observed using epi-fluorescence microscope under TRITC and FITC filters. All the studies were carried out in triplicates

Quantitative fluorescence image analysis and average fluorescence intensity was carried out on ImageJ software, for all the cultures tested for internalization experiments, using the following formula:

$$\text{CTCF} = \text{ID} - (\text{A} - \text{B}) \quad (8)$$

where, CTCF is the corrected total cell fluorescence, ID is integrated density, A is area of selected cell, and B is the mean fluorescence of background readings.

### 3.2.4 Time dependent uptake studies of thin rods

Based on previous results thin rods fHAp were selected for time dependent studies using HeLa, *C. albicans*, *E. coli* and *S. aureus* cells as representatives of eukaryotic and prokaryotic cells. Exponentially growing HeLa cells ( $5 \times 10^4$  cells/well) were grown as described in Section 3.2.1. These cells were then incubated with optimized concentration of thin rod fHAp (30µg/mL) for various time intervals (0, 2, 4, 6, 8, 10, 12, 14, and 15h), the glass slides were removed after respective time intervals and washed twice with PBS (pH 7), to remove

uninternalized particles and debris. These slides were observed using epi-fluorescence microscope under TRITC and FITC filters.

*C. albicans* cells ( $10^6$  cells/well) were cultured in 24 well plate with 1mL SB media for 48h and then incubated with thin rod fHAp (70 $\mu$ g/mL) for various time periods (0, 2, 4, 6, 8, 10, 12, and 15h). After respective time interval culture was heat fixed on glass slide and observed using epi-fluorescence microscope under TRITC and FITC filters.

Similar studies were carried out with *E. coli* and *S. aureus*,  $10^6$  cells/well were inoculated in a 24 well plate supplemented with 1mL LB media for 6h and then incubated with thin rod fHAp (50 $\mu$ g/mL) for various time interval (0, 2, 4, 6, 8, 10, 12 and 15h) after respective time period cells were heat fixed as described earlier and observed under epi-fluorescence microscope.

### **3.2.5 Statistical analysis**

All the experiments were carried out in triplicates on different days. The results are expressed as mean  $\pm$  standard error. Microsoft<sup>TM</sup> Excel 2007 software was used for statistical analysis. The differences between the untreated controls and treated groups for multiple comparisons were determined by One-way Analysis of Variance (ANOVA) test. Two tailed Student's t-test was used to analyze any significant differences between the control and the individual experimental groups. 'p' values of less than 0.05 ( $p < 0.05$ ) were considered significant.

### **3.3 Results and discussion**

In this chapter, bioimaging studies on self-activated fluorescence hydroxyapatite nanoparticles (fHAp) of rod shape with different aspect ratios (thin rods, rods and short rods) are reported.

### 3.3.1 Biocompatibility

Biolabelling and bioimaging are important techniques for detection and diagnosis of diseases. To use any material for such purposes, its cytotoxicity and biocompatibility needs to be studied. Thus MTT, LDH and ROS generation assays were carried out to determine effect of all three fHAp (thin rods, short rods and rods) on the cell viability of tumorigenic (HeLa) and nontumorigenic (HaCaT) cell lines. HeLa cell line is derived from cervical cancer cells and tumorigenic. However, HaCaT cell line is a spontaneously transformed aneuploid immortal keratinocyte cells from adult human skin and nontumorigenic. Although HaCaT cells are immortalized, they are similar to normal keratinocytes and exhibits normal differentiation (Boukamp et al. 1988).

#### 3.3.1.1 MTT assay

MTT assay is a colorimetric assay that measures the reduction of MTT by mitochondrial enzyme succinate dehydrogenase. The MTT enters into the mitochondria where it is reduced to an insoluble, purple coloured formazan product. Since reduction of MTT can only occur in metabolically active cells the level of formation of formazan is directly related to viability of the cells. Formazon is then dissolved in isopropanol/DMSO and quantified using spectrometry (Gerlier and Thomasset 1986). Figure 3.1a and 3.2a shows result of cell viability measured using MTT assay on HeLa and HaCaT cells respectively. There was no significant differences ( $p > 0.05$ ) between the cell viability of all three fHAp treated and untreated HeLa as well as HaCaT cells (Figure 3.1a and 3.2a). At very high concentration of 1000 $\mu$ g/mL, HeLa cell viability was ~95.5, 94.5 and 93.78 % while for HaCaT cells it was ~97, 96 and 95% for thin rods, short rods and rods fHAp, respectively.

### 3.3.1.2 LDH assay

Further to confirm the non toxic nature of fHAPs, LDH assay was carried out by incubating various concentrations (10-1000 $\mu$ g/mL) of fHAPs with HeLa cells. LDH is also a colorimetric assay and is based on the release of lactose dehydrogenase enzyme after damage of cell membrane or cell lysis. LDH is a soluble enzyme located in the cytosol. The enzyme is released into the surrounding culture medium upon cell damage or cell lysis, processes that occur during both apoptosis and necrosis. LDH activity, therefore, can be used as an indicator of cell membrane integrity, and thus a measurement of cytotoxicity (Chan et al. 2013). We examined effect of fHAPs on LDH leakage into the medium. In order to determine the effect of fHAPs (thin rod, rods and short rods) on LDH leakage, the HeLa cells were incubated with various concentrations (10-1000 $\mu$ g/mL) of fHAPs and LDH leakage was measured after 24h. There was no significant difference ( $p>0.05$ ) between the cell viability of cells treated with all three types of fHAPs as compared to untreated HeLa cells and HaCaT cells (Figure 3.1b and 3.2b). Even at 1000 $\mu$ g/mL, cell viability for HeLa cells was 97, 95.5 and 94.5% while for HaCaT cells it was 98.5, 97 and 95.5% for thin rods, short rods and rods shaped fHAPs respectively.

### 3.3.1.3 ROS generation assay

It has been described that NPs can be toxic, not only by directly affecting cells but also indirectly by the induction of cell stress. Changes in the level of reactive oxygen species (ROS) is marker of cell stress (Manke et al. 2013). Although ROS generation is essential mechanism in metabolism, excess production of ROS can damage cells by protein denaturation, DNA damage and altering macromolecules like polyunsaturated fatty acids in membrane lipids (Mohanty et al. 2000). Therefore, we have carried out ROS assay to determine ROS generation in HeLa and HaCaT cells exposed to all three types of fHAPs. ROS generation for HeLa was ~1.17, ~1.4 and ~1.6 % and for HaCaT it was ~0.89, ~0.98 and 1.1 % at high concentrations of 1000 $\mu$ g/mL for thin rods, short rods

and rod shaped fHAPs, respectively (Figure 3.1c and 3.2c). This indicates that fHAPs do not generate any stress on cells proving it to be non toxic. A significant difference ( $P < 0.05$ ) in ROS generation was found between the control group (cell exposed with  $H_2O_2$ ) and the experimental groups (all three fHAPs). All the above results signify that fHAPs do not show any cytotoxic effect and ROS generation, even at a very high concentration of  $1000\mu\text{g/mL}$ , implying that these fHAPs are biocompatible and could be used as safe bioimaging agents. Although there was no significant difference between cell viability of all three fHAPs, it was in the order of thin rods > short rods > rods. Thin rods showed more cell viability and less ROS generation in both HaCaT and HeLa cell lines. It is also observed that all three fHAPs showed more cell viability and less ROS generation in HaCaT cells (Figure 3.2) than in HeLa cells (Figure 3.1). This could be attributed to cell types and size of NPs. Shape and cell dependent toxicity of HAP NPs have been already reported (Akbarzadeh et al. 2013; Motskin et al. 2009). HAP NPs showed more toxicity towards cancerous cells than to normal cells (Chen et al. 2007; Han et al. 2014). In recent years, use of lanthanide doped HAP NPs due to their favorable characteristics such as broad excitation spectra, long fluorescence life-time, sharply spiked emission spectra, large Stokes' shifts, high quantum yields has successfully resulted in a series of multifunctional fluorescent materials for bio-imaging and bio-labeling (Mondéjar et al. 2007; Resch-Genger et al. 2008). However, rare-earth elements are toxic and have adverse effects due to their accumulation in the body (Ge et al. 2015; Mondéjar et al. 2007). Since these fHAPs do not contain any toxic dopants, they may be used as safe alternatives for bioimaging/biolabeling.

#### **3.3.1.4 Hemolytic assay**

NPs for theranostic applications are mostly administrated intravenously or orally therefore their effect on human blood components are of extreme importance. Red blood cell lysis with nanomaterials could be limiting factor for their *in vivo* applications. Therefore, hemolytic assay was performed to examine the

interaction of various concentrations (10-1000 $\mu$ g/mL) of all three fHAPs (thin rod, short rods and rods) with red blood cell membranes by measuring the release of hemoglobin. Figure 3.1d shows the % hemolytic rate. No hemolysis was observed after exposure of fHAPs to human red blood cells and the hemolytic rate was ~0.98, 0.99 and 1.2% up to concentrations of 1000 $\mu$ g/mL for thin rods, short rod and rod shaped morphologies respectively (Figure 3.1d). There was a significant difference ( $P>0.05$ ) observed between the positive control group (human red blood cells exposed to tap water) and experimental group (human red blood cells exposed to all three fHAPs). According to ASTM F 756-00, samples with hemolysis rate less than 2% can be considered non-hemolytic, indicating that all three fHAPs are non-hemolytic (Dobrovolskaia et al. 2008). This indicates that all three fHAPs are hemocompatible and could be used for therapeutic and diagnostic applications. Hemocompatibility of HAp NPs has been demonstrated earlier by many research groups. HAp NPs of various sizes ranging from 20-150nm synthesized using methods such as co-precipitation, sol-gel and emulsion technique were found to be compatible to human red blood cells even at very high concentrations (Jadalannagari et al. 2014a; Tank et al. 2013; Victor and Sharma 2011; Wang et al. 2011b).



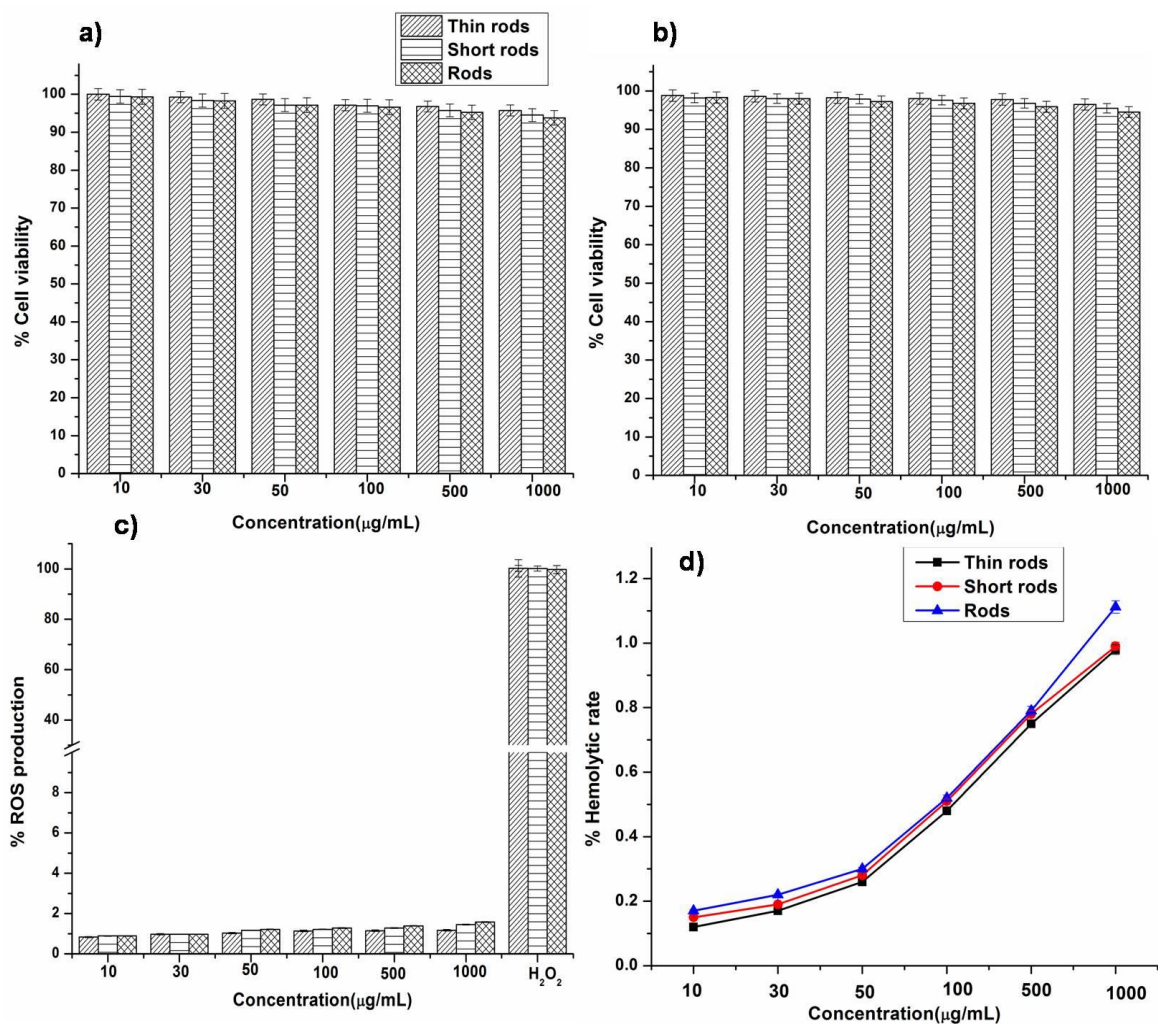


**Figure 3.1** a) MTT and b) LDH c) ROS generation data showing non-toxicity, no oxidative stress on HeLa cell lines after 24h d) hemolytic rate of thin rods, short rods and rods fHAPs NPs various concentrations ranging from 10-1000  $\mu\text{g/mL}$ .



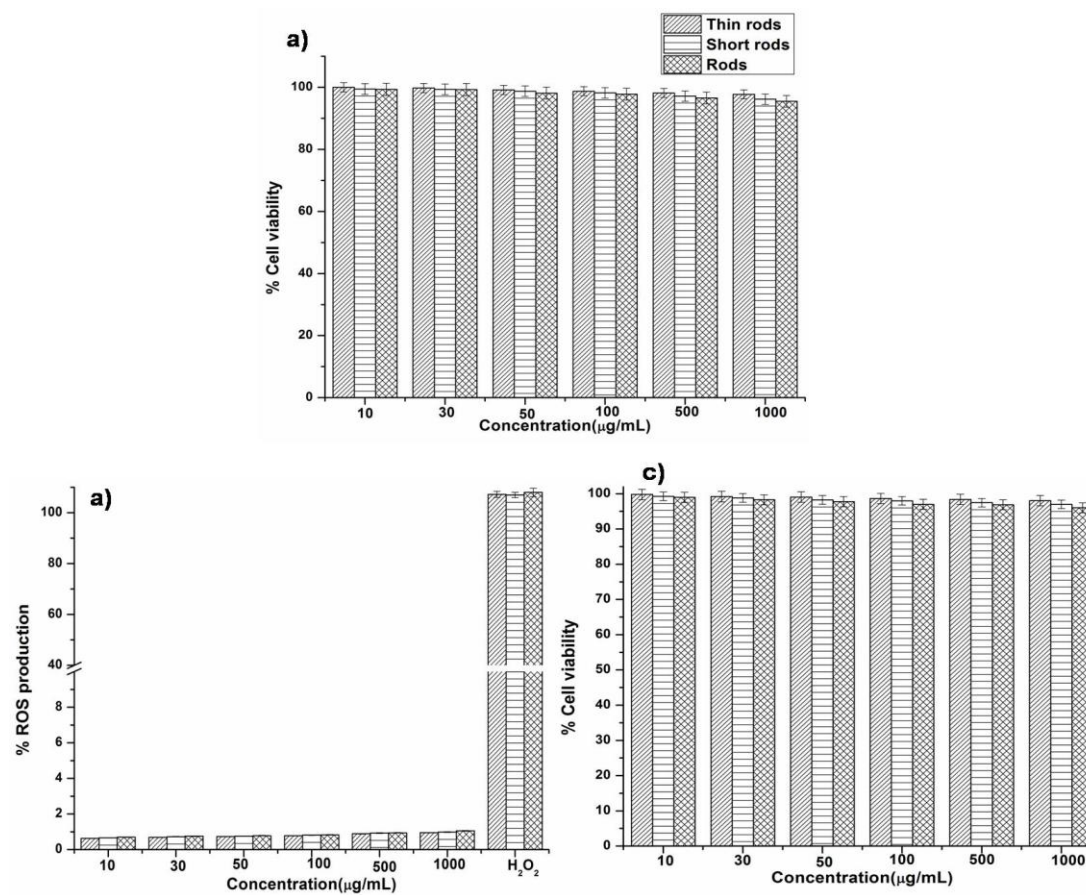


**Figure 3.2** a) MTT and b) LDH c) ROS generation data showing non-toxicity, no oxidative stress on HaCaT cell lines after 24h.

### 3.3.2 Fluorescence stability

In order to be a good bioimaging/labeling agent, the fHAPs need to retain their fluorescing nature in biological environment. To check this, all the three fHAPs were placed in phosphate buffered saline (PBS, pH 7) to mimic the extracellular environment, and in Dulbecco's modified Eagle's medium (DMEM), to mimic *in-vitro* conditions. No change in the pattern of fluorescence spectra of thin rod (Figure 3.3a), short rod (Figure 3.3b) and rods (Figure 3.3c) was observed under all these conditions indicating that fluorescence of fHAPs is not dependent on the environment, and is rather an intrinsic property of the nanoparticles (Figure 3.3).

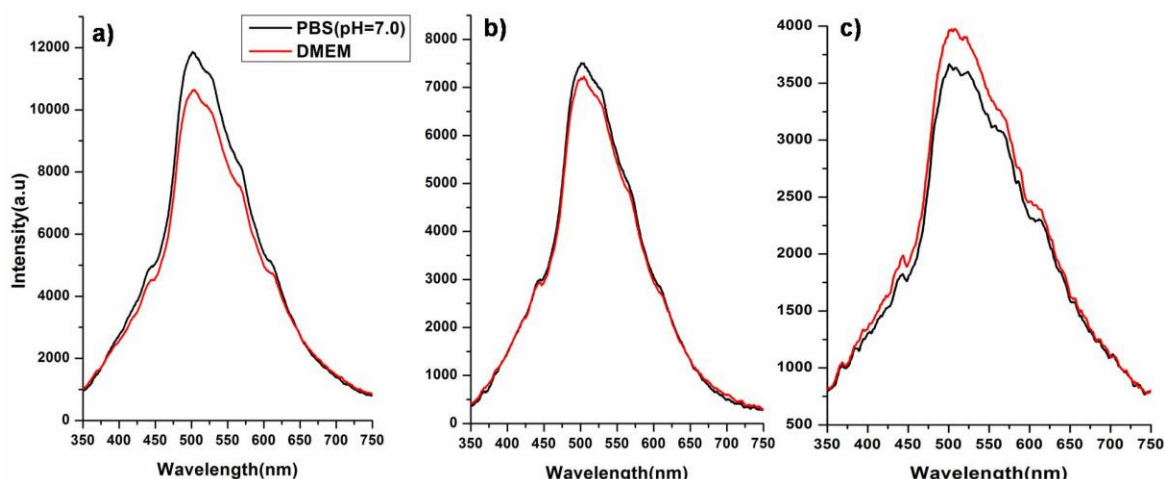


**Figure 3.3** Fluorescence spectra of a) thin rod b) short rod c) rod fHAPs in biological media DMEM (red) and PBS (pH 7) (black). No change in fluorescence spectra in both the conditions indicating that fluorescence of fHAPs is not dependent on the surrounding environment, and is rather an intrinsic property of the nanoparticles.

Fluorescence stability of all three fHAPs was further carried out in complex media (LB, SB, DMEM) used for growth of eukaryotic and prokaryotic cells, and PBS by suspending them in these media and recording their fluorescence spectra at

specific time intervals (0,2,4,6,8,10 and 12h). Relative fluorescence intensity of all three fHAPs dispersed in LB, SB, DMEM with FBS, and DMEM without FBS was highest at 0<sup>th</sup> h and then there was slow decrease in intensity till 4h, and a sudden drop in relative intensity between 4-6h was observed. However, these fHAPs dispersed in PBS exhibited slow decrease in intensity till 6h and then a drop between 6-12h (Figure 3.4). The decrease in fluorescence intensity could be due to adsorption of bio-micromolecules (electrolytes, proteins, lipids, etc) present in complex media (LB, SB, DMEM) on to the NPs enhancing the inter-particle interaction and resulting in aggregation (Moore et al. 2015; Rausch et al. 2010). Fluorescence stability of fHAPs in various media was in the order of PBS> DMEM without FBS> LB> SB>DMEM with FBS>PBS. Thin rod (Figure 3.4a), short rod (Figure 3.4b) and rod (Figure 3.4c) shaped fHAPs exhibited similar pattern of decrease in fluorescence intensities. Interestingly, sonication of the fHAPs with decreased fluorescence resulted in reappearance of the lost fluorescence. This can be attributed to the dispersion of the aggregates on sonication, and supports the assumption that decrease in fluorescence intensity was due to aggregation. Similar reduction in fluorescence intensity due to aggregation was observed in conjugated polymer NPs and attributed to intrinsic quenching of fluorescence in aggregates (Jakubiak et al. 1999; Jiang et al. 2007).

### 3.3.3 Uptake of fHAPs by eukaryotic and prokaryotic cells

Cellular internalization of fluorescent NPs is essential to study cellular/molecular events *in-situ*. The applications of all fHAPs (thin rods, rods and short rods) as *in-situ* fluorescent probes were explored by examining their potential of cellular internalization in both prokaryotic and eukaryotic systems. HeLa, MG63, HaCaT, *C. albicans*, *S. aureus* and *E. coli* were used as the representatives of eukaryotic and prokaryotic cells.

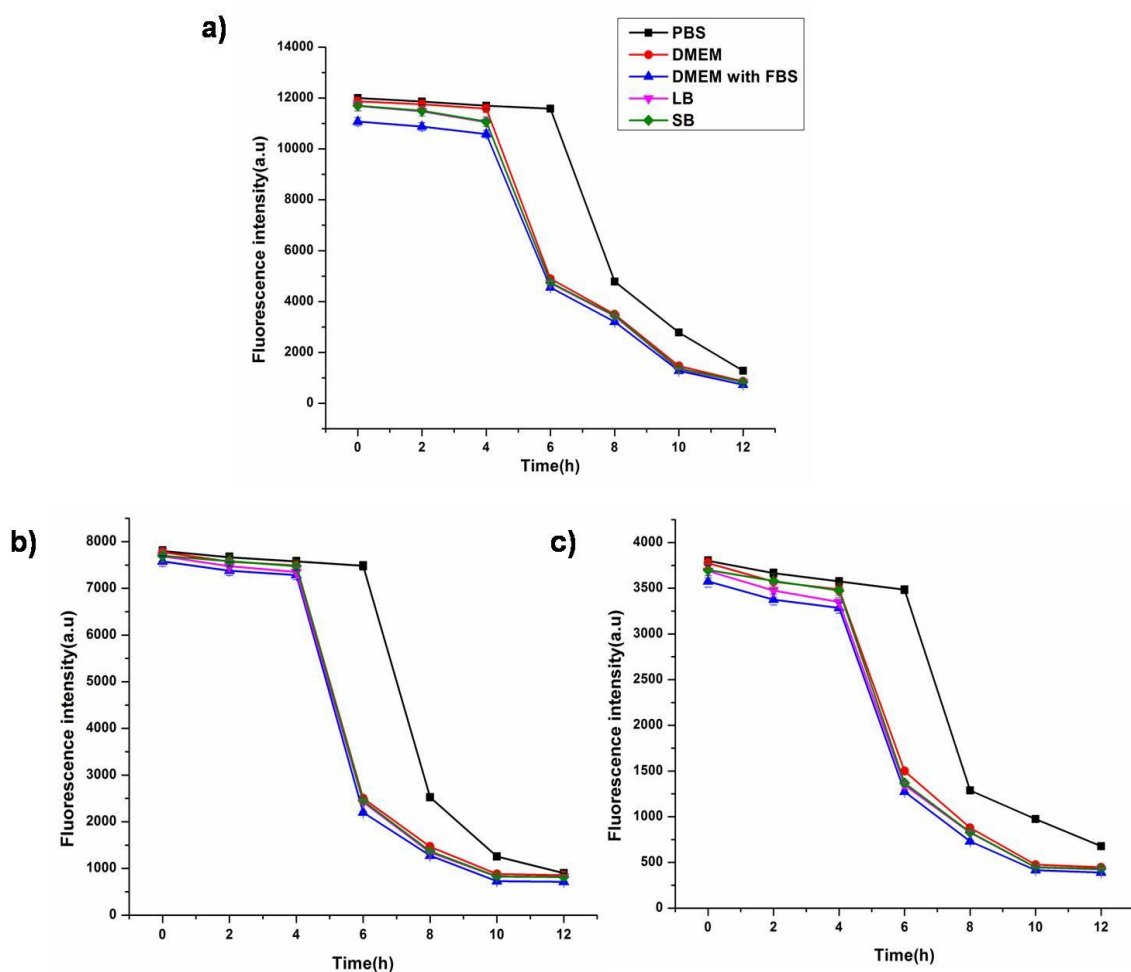


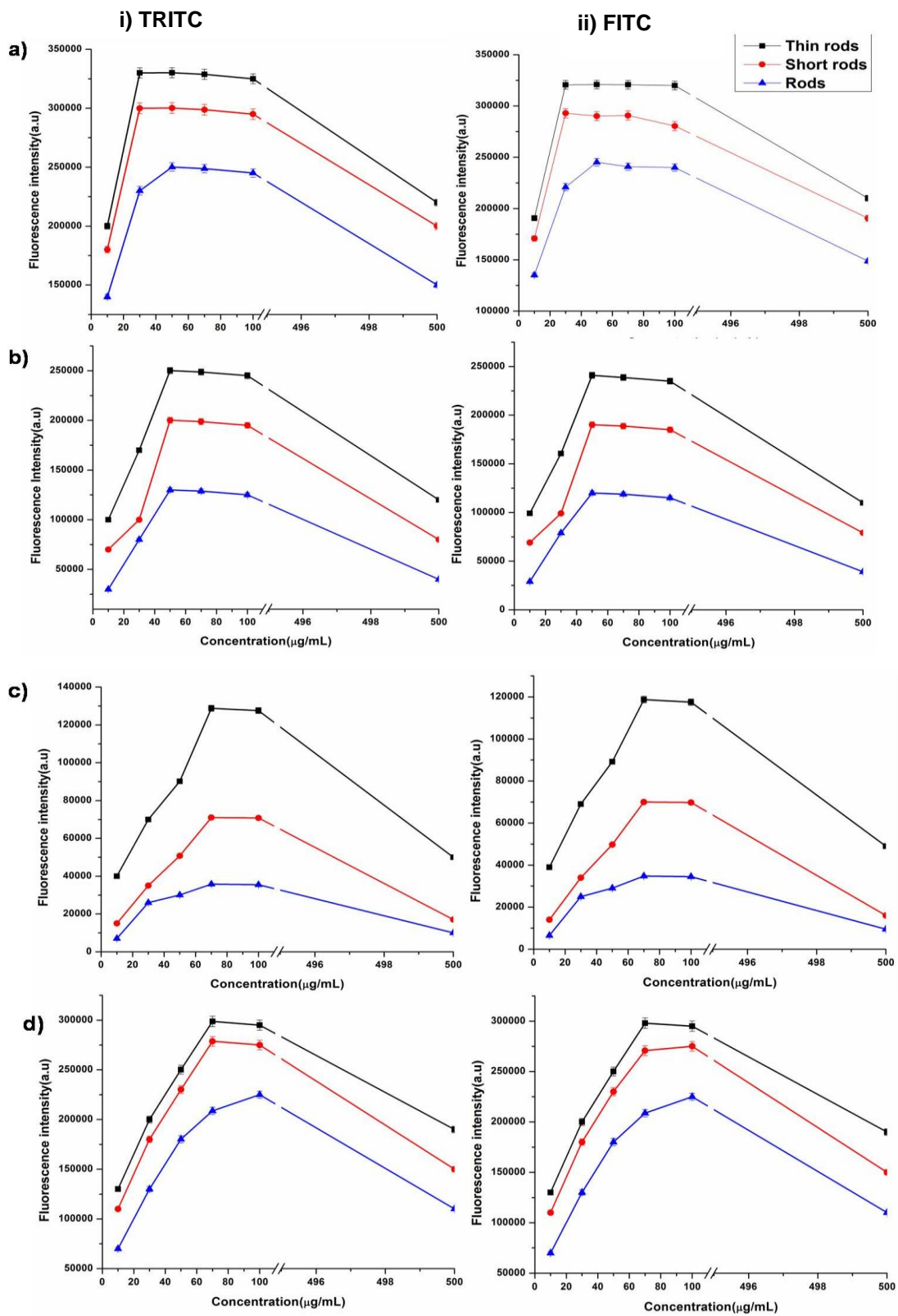
**Figure 3.4** Relative fluorescence intensities of a) thin rods b) short rods c) rods, obtained in PBS, DMEM, DMEM plus FBS, LB and SB media for different time intervals (0-12h).

Each cell type was inoculated with various concentrations (10, 30, 50, 70, 100 and 500 $\mu$ g/mL) of fHAPs for 4h to obtain optimized concentrations and observed under the microscope using FITC and TRITC filters. The average fluorescence intensities of the cells imaged under microscope were calculated by “imagej” software Figure 3.5 shows average relative fluorescence intensities of all cell types internalized with fHAPs, observed under both TRITC (Figure 3.5i) and FITC filters (Figure 3.5ii). There was no significant difference ( $P < 0.05$ ) between the average relative fluorescence intensities observed under FITC and TRITC filters for all cell types internalized with all fHAPs. The optimized concentrations of thin

rod, short rod and rods for which highest cell fluorescence intensities were achieved for HeLa (Figure 3.5a), MG63 (Figure 3.5b), HaCaT (Figure 3.5c), *C. albicans* (Figure 3.5d), *E. coli* (Figure 3.5e) and *S. aureus* (Figure 3.5f) cells are presented in Table 3.1. It was also observed that there was a reduction in cell fluorescence intensity at high concentrations of 500µg/mL for all these cell types with all three fHAPs, this could be due to aggregation of NPs at very high concentration which affected internalization resulting in reduced cell fluorescence intensity (Figure 3.5). Internalization of fHAPs was observed with all cell types; however, the magnitude of internalization varied, and was a property of cell type and aspect ratio of the fHAPs. Among all three fHAPs, thin rod fHAPs has shown maximum relative fluorescence intensity for all the cell types this could be due to their relatively high fluorescence intensities compared to short rods and rod shaped fHAPs (as described in chapter 2). Relative fluorescence intensities exhibited by the different cell types after internalization of fHAPs were in the order of HeLa> MG63> *C. albicans*>*E. coli*>*S. aureus*> HaCaT cells. It was noted that among cell lines (HeLa, MG63 and HaCaT), HeLa (Figure 3.6) showed maximum internalization while HaCaT (Figure 3.8) showed minimum internalization which could be attributed to specific cell properties of tumor cell line such as enhanced differentiation, proliferation and surface receptor expression than that of immortalized normal cell line. Similar results were reported showing that gold and silicon dioxide NPs were internalized less efficiently in immortalized normal cell line than the tumor cell lines (Coulter et al. 2012; Hsiao et al. 2014).

**Table3.1** : Optimized concentrations of all three fHAPs for which highest cell fluorescence intensities were achieved for HeLa, MG63, *C. albicans*, *S. aureus* and *E. coli* cells.

| Samples<br>(µg/mL) | HeLa | MG63 | HaCaT | <i>E. coli</i> | <i>S. aureus</i> | <i>C. albicans</i> |
|--------------------|------|------|-------|----------------|------------------|--------------------|
| Thin rods          | 30   | 50   | 100   | 50             | 50               | 70                 |
| Short rods         | 30   | 50   | NA    | 50             | 50               | 70                 |
| Rods               | 50   | 100  | NA    | 70             | 70               | 100                |





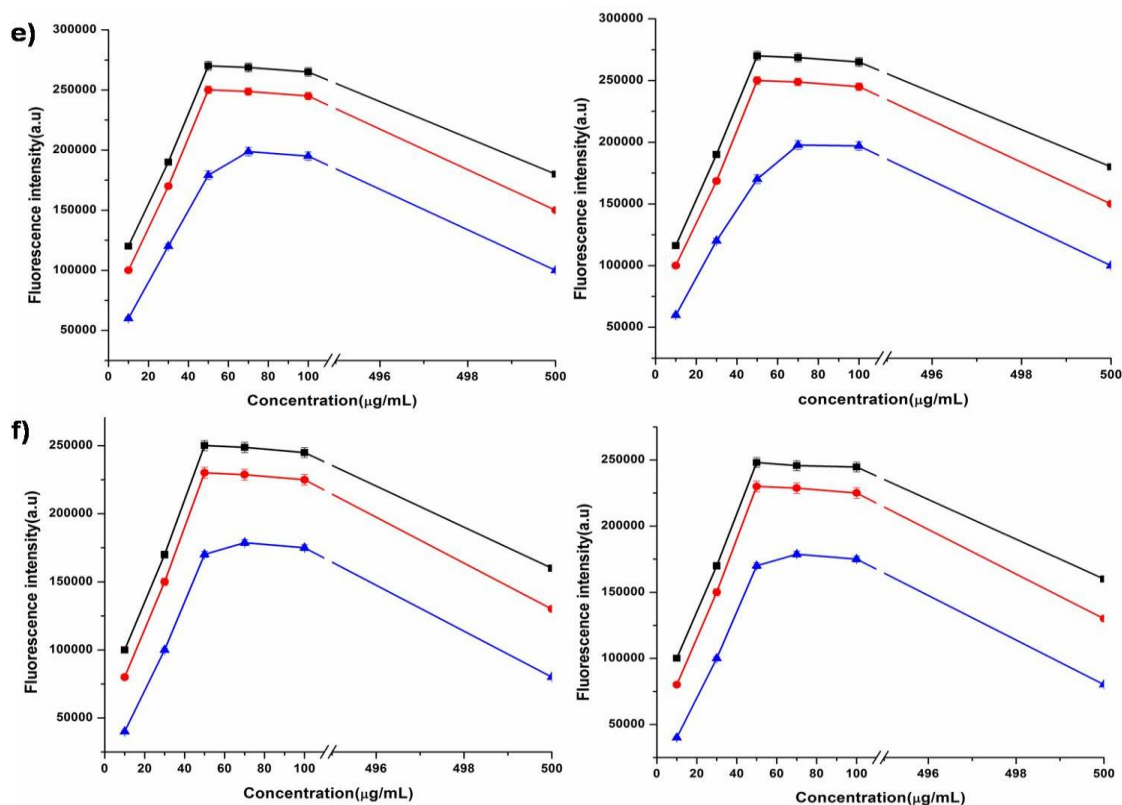


**Figure 3.5** Average relative fluorescence intensities of a) HeLa b) MG63 c) HaCaT d) *C. albicans* e) *E. coli* f) *S. aureus* under i) TRITC and ii) FTIC filters using thin rods (black line), short rods (red) and rods (blue).

Internalization of all three fHAPs at concentrations exhibiting highest cell fluorescence intensities with HeLa, MG63, HaCaT *C. albicans*, *E. coli* and *S. aureus* are shown in Figure 3.6, 3.7, 3.8, 3.9, 3.10 and 3.11. These are indicative images showing internalization with bright intracellular green and red fluorescence in all cell types, under epi-fluorescence microscope. As can be seen from these figures and described earlier, among all fHAPs, thin rods showed maximum fluorescence intensity in all cell types. Internalization of HAP and lanthanide doped HAP NPs by cells such as fibroblasts, epithelial cells, monocytes, macrophages, human hepatoma etc., (Chen et al. 2012; Doat et al. 2003; Motskin et al. 2011; Motskin et al. 2009; Tabaković et al. 2012) have been extensively studied by many groups. NPs such as quantum dots, carbon dots,

lanthanide-based fluorophores, UcNPs, etc. are being studied as multimodal, multifunctional fluorescent probes for *in vitro* and *in vivo* bio-imaging. However, cytotoxicity of these particles is of great concern, limiting their *in vivo* applications (Lewinski et al. 2008; Mondéjar et al. 2007). This limitation can easily be overcome by using non-toxic and self-activated fluorescence of HAp.

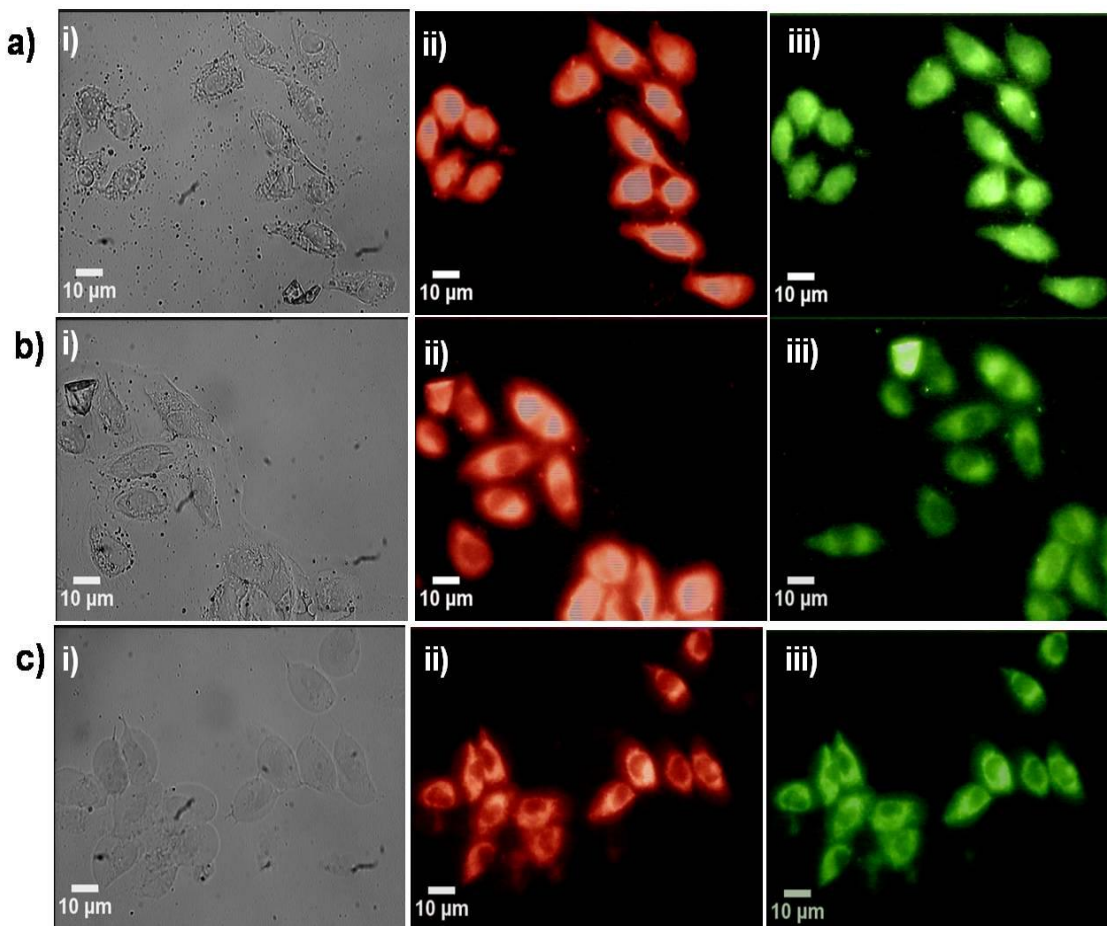


**Figure 3.6** Bright intracellular fluorescence with green and red emissions was observed inside the cells under epi-fluorescence microscope, using (i) bright field (ii)TRITC and (iii) FITC filter indicating that a) thin rods b) short rods c) rod HAp NPs were internalized by HeLa cells.



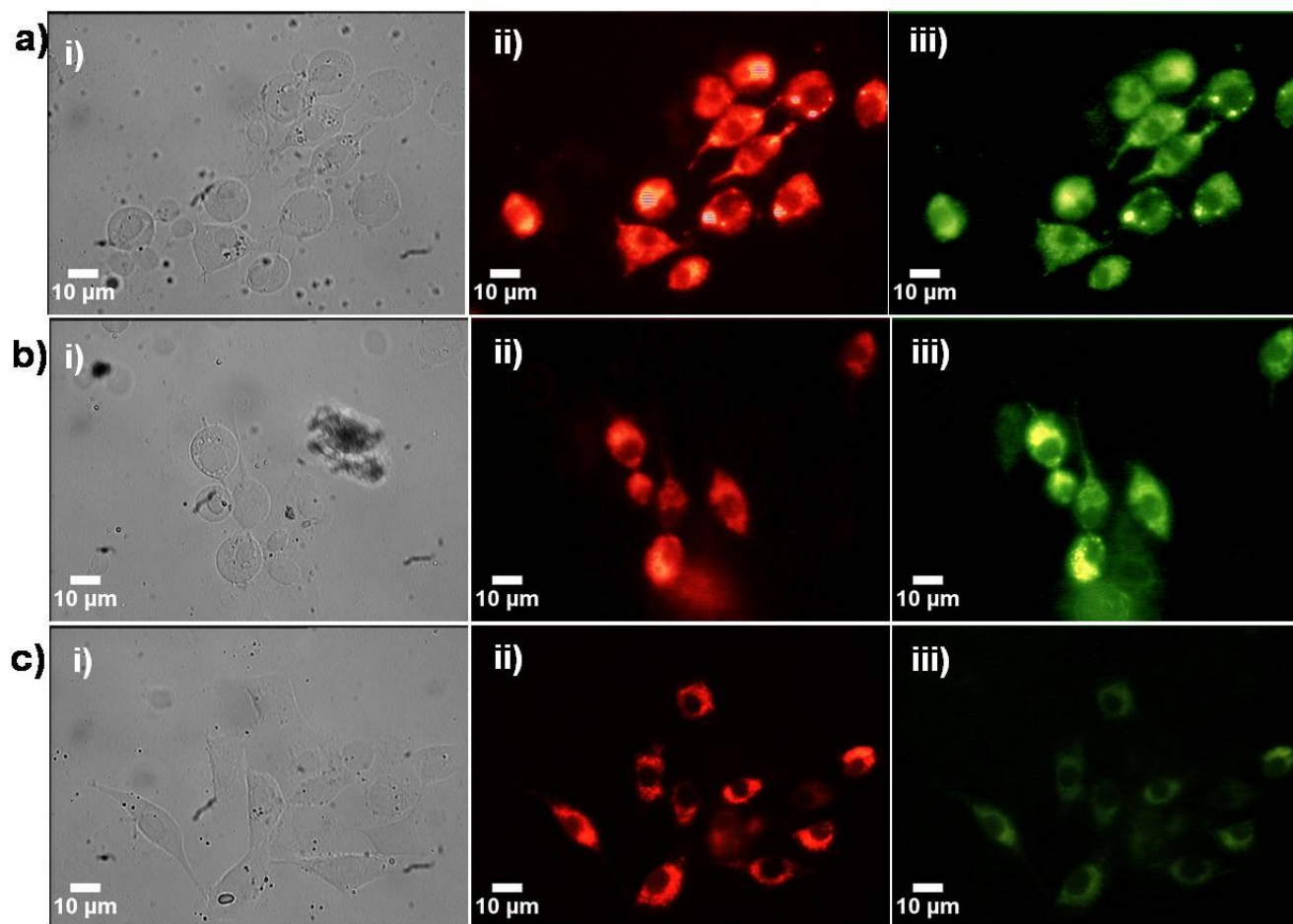


**Figure 3.7** Bright intracellular fluorescence with green and red emissions was observed inside the cells under epifluorescence microscope, using (i) bright field (ii) TRITC and (iii) FITC filter indicating that a) thin rods b) short rods c) rod HAp NPs were internalized by MG63 cells.

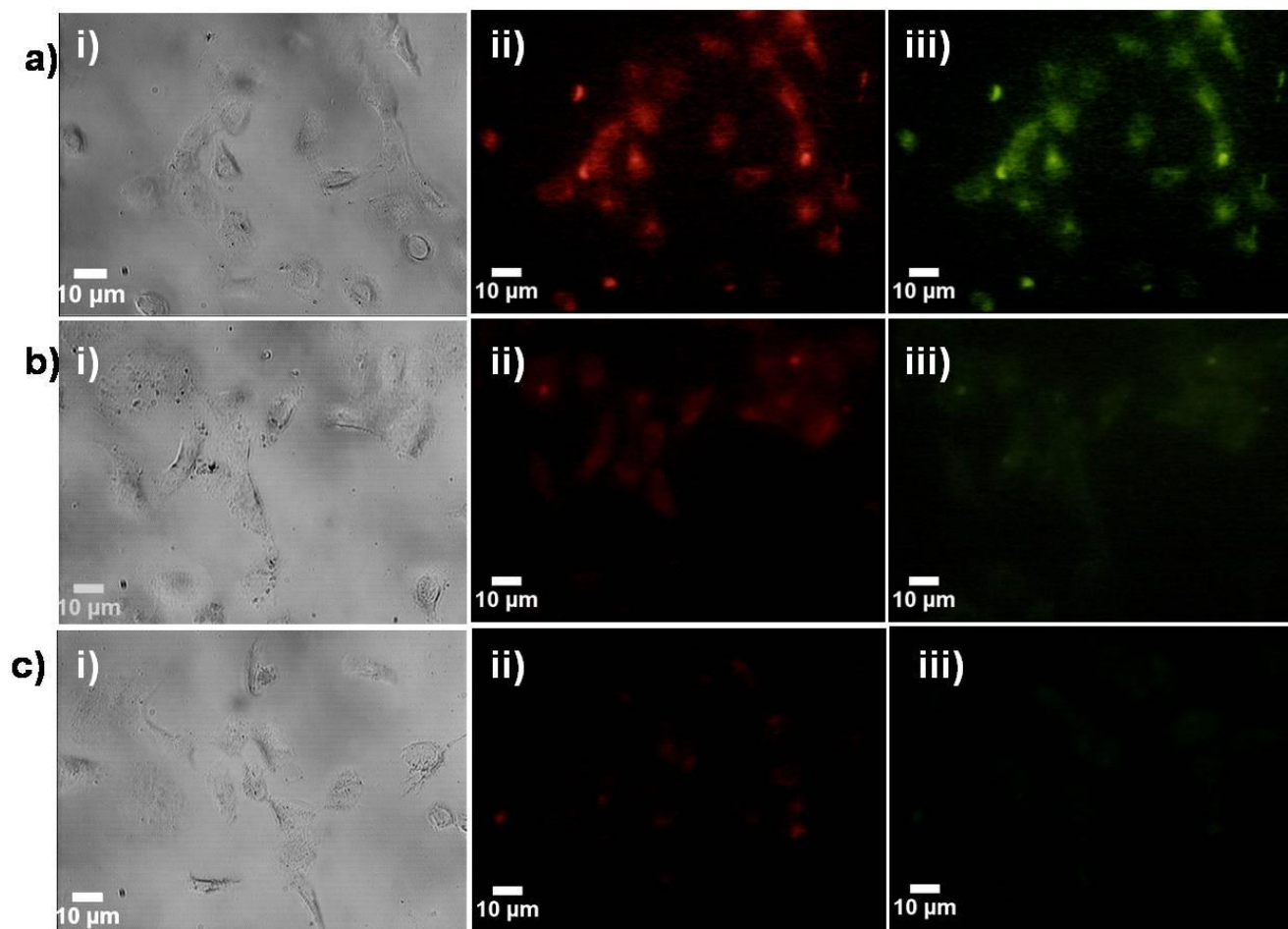


**Figure 3.8** Bright intracellular fluorescence with green and red emissions was observed inside the cells under epifluorescence microscope, using (i) bright field (ii) TRITC and (iii) FITC filter indicating that a) thin rods b) short rods c) rod HAp NPs were internalized by HaCaT cells.

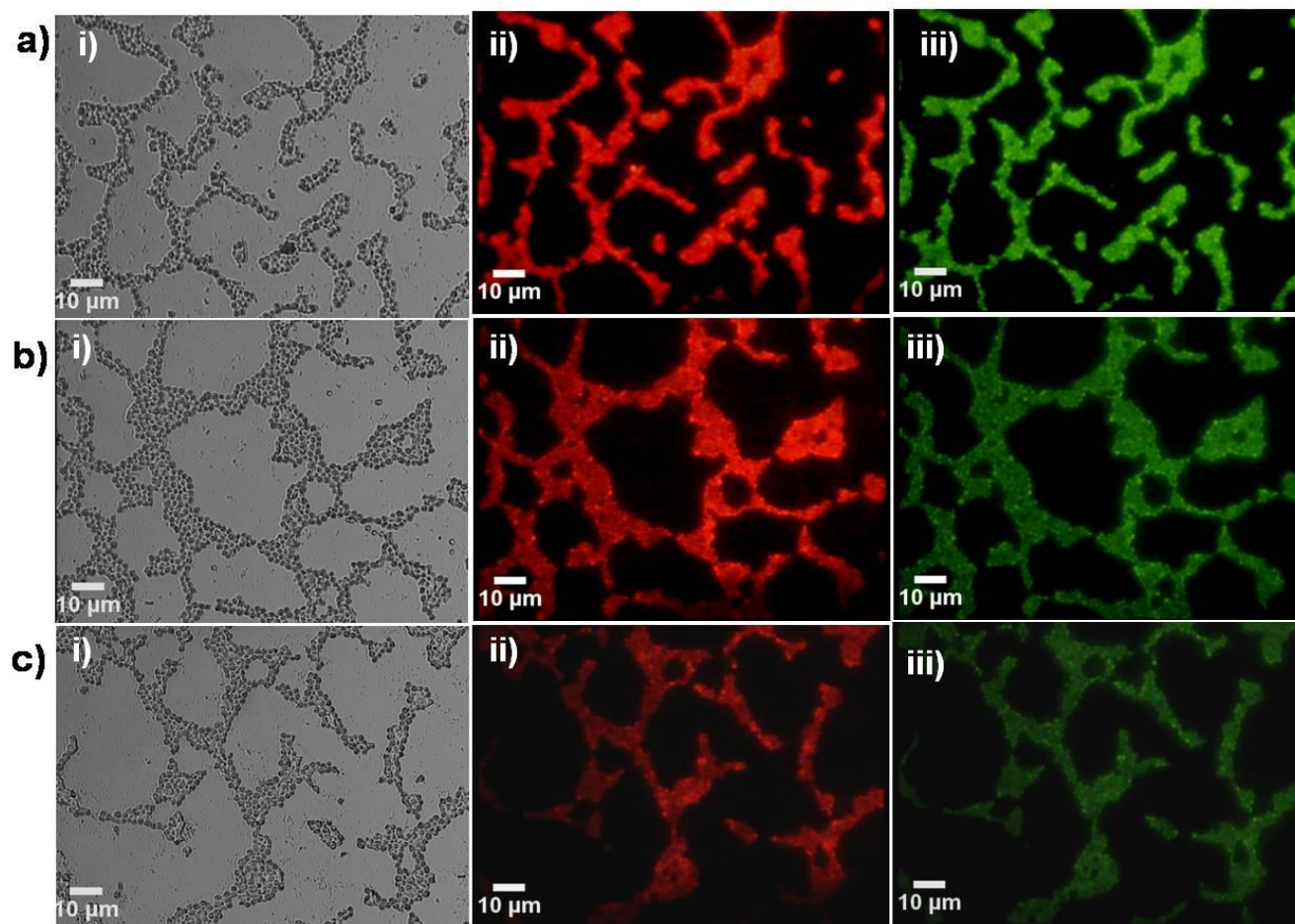


**Figure 3.9** Bright intracellular fluorescence with green and red emissions was observed inside the cells under epifluorescence microscope, using (i) bright field, (ii) TRITC and (iii) FITC filter indicating that a) thin rods b) short rods c) rod HAp NPs were internalized by *C. albicans* cells.



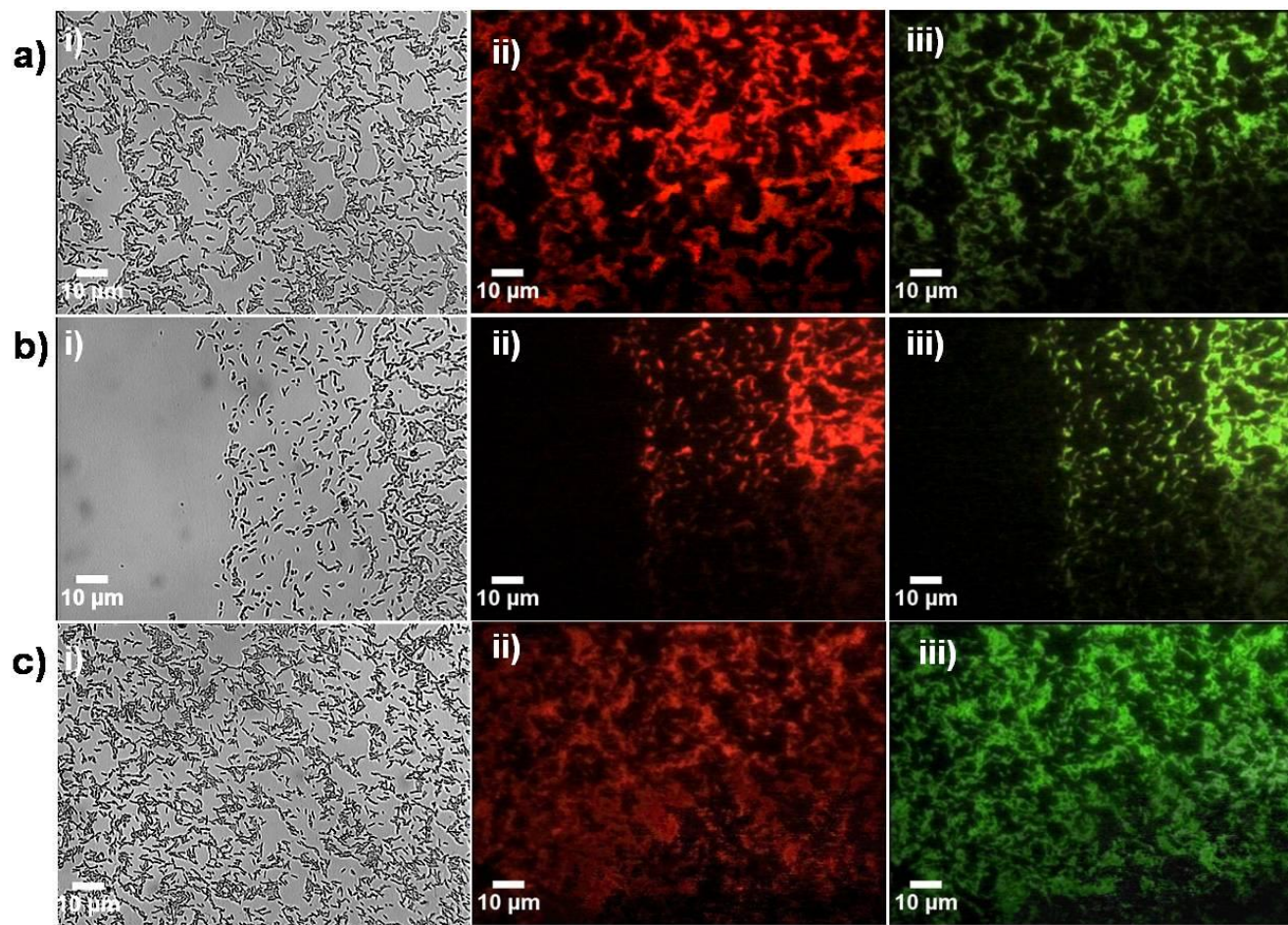


**Figure 3.10** Bright intracellular fluorescence with green and red emissions was observed inside the cells under epifluorescence microscope, using (i) bright field, (ii) TRITC and (iii) FITC filter indicating that a) thin rods b) short rods c) rod HAp NPs were internalized by *E. coli* cells.

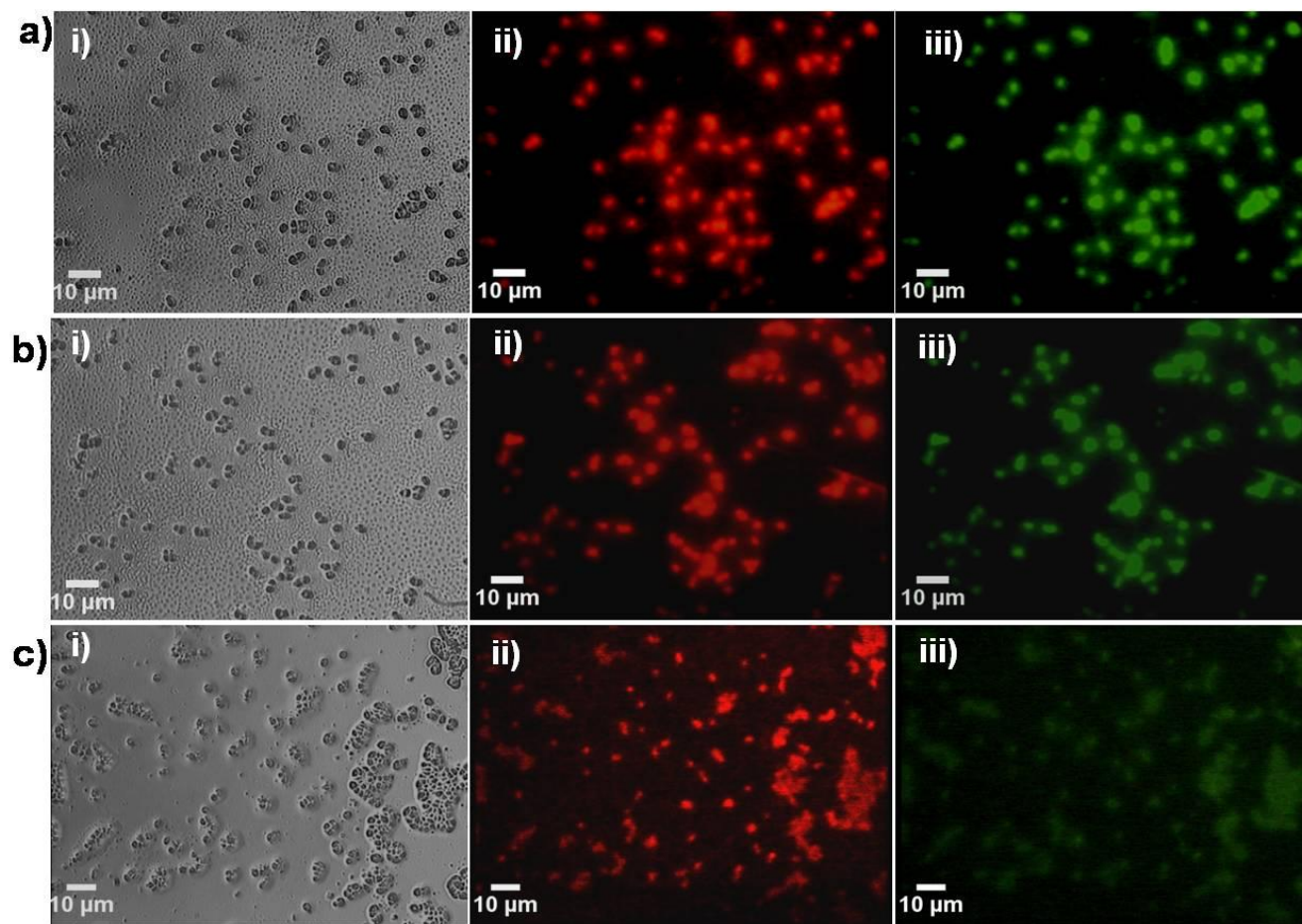


**Figure 3.11** Bright intracellular fluorescence with green and red emissions was observed inside the cells under epifluorescence microscope, using (i) bright field (ii) TRITC and (iii) FITC filter indicating that a) thin rods b) short rods c) rod HAp NPs were internalized by *S. aureus* cells

### 3.3.4 Time dependent uptake studies of thin rods

Thin rods fHAPs were further selected for studies on time dependent internalization as it exhibited the highest fluorescence intensity in all cell types. This experiment was performed by estimating the fluorescence intensity at regular time intervals (0, 2, 4, 6, 8, 10, 12 and 15h) after internalization of thin rod fHAPs inside eukaryotic and prokaryotic cells. It was observed that the HeLa, *E. coli*, *S. aureus* and *C. albicans* cells started exhibiting fluorescence within 2h of exposure to fHAPs, and the highest fluorescence intensity was noted at 4h (Figure 3.12). In HeLa and *C. albicans* cells, there was sudden drop in fluorescence intensity after 4h while in *E. coli* and *S. aureus* there was steady decrease in fluorescence between 4 and 6h and sudden drop after 8h. Decrease in fluorescence intensity after 4h in all cell types could be due to gradual aggregation of NPs with increase in time (Figure 3.12).

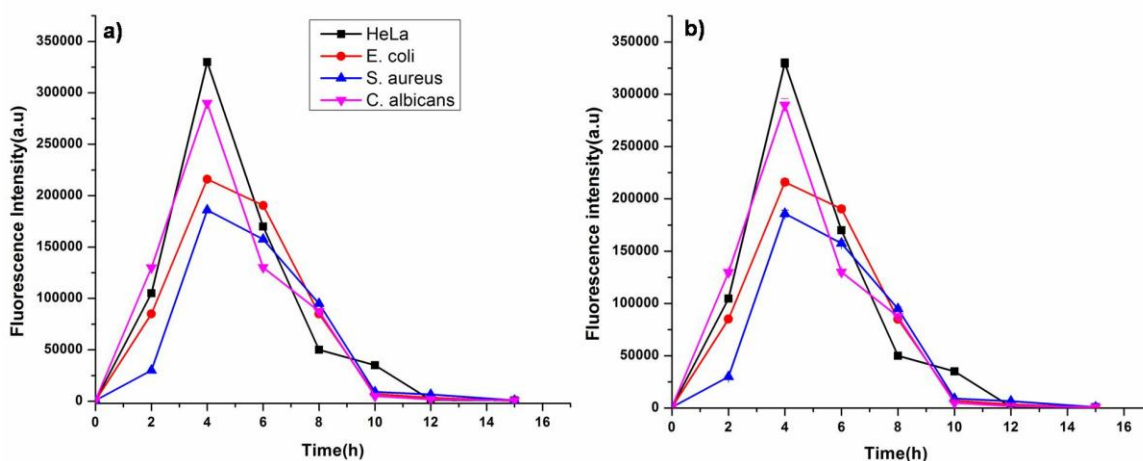


**Figure 3.12** Time dependent internalization of thin rods in HeLa (black colour line), *E. coli* (red colour line), *S. aureus* (blue colour line) and *C. albicans* (magenta colour line) observed under a) TRITC and b) FITC filter.



All the above studies show that these self activated fluorescence HAp NPs are non-toxic to HeLa and HaCaT cells and are also hemocompatible (Figure 3.1 and 3.2). All fHAp were also easily internalized by HeLa, HaCaT, MG63, *E. coli*, *S. aureus* and *C. albicans* (Figure 3.6, 3.7, 3.8, 3.9, 3.10 and 3.11) and could be used as *in-vitro* bioimaging agent.

### 3.4 Conclusion

Self activated fluorescent HAp NPs (fHAp) of rod shaped with three different aspect ratios (thin rods, short rods and rods) exhibited excellent internalization by both prokaryotic and eukaryotic systems without causing any cytotoxicity. To the best of our knowledge, this is the first report on uptake and fluorescence of undoped HAp NPs in yeast, bacterial and animal cells. We believe that these fHAp provide a safe and equally dependable alternative for the current fluorescent materials. By tagging these fHAp with specific antibodies, RNA, aptamers or proteins; they can further be modified to specifically recognize certain types of pathogens in blood or environmental samples making on-site diagnosis a possibility.

## CHAPTER 4

### **Novel One Step Transformation Method for *Escherichia coli* and *Staphylococcus aureus* Using Arginine-glucose Functionalized Fluorescent Hydroxyapatite Nanoparticles**

#### **4.1 Introduction**

A revolution in microbiology was sparked by the discovery of the recombinant DNA technology; wherein traditional microbiology was combined with molecular biology to produce desirable products such as primary/secondary metabolites, proteins, biopharmaceuticals, industrial enzymes, etc. (Adrio and Demain 2010; Demain and Vaishnav 2009). Recombination in bacteria occurs through three processes, conjugation: transfer of DNA through cell to cell contact; transduction of DNA from host to recipient cell via bacteriophages; and transformation: uptake of DNA by competent cells (Griffith 1928). Competence can be natural or induced artificially through chemical method, electroporation, protoplasting, etc. Artificial transformation of plasmid into *E. coli* using chemical method signaled the birth of genetic engineering (Cohen et al. 1972; Mandel and Higa 1970; Benzinger et al. 1978; Hopwood and Wright 1978). However, low frequency of recombinants obtained through these methods prevented the widespread use of recombinant DNA technology by industries. Improvement in various transformation techniques, significantly enhanced the transformation efficiency and brought a remarkable change (Tu et al. 2005; Yasui et al. 2009). There was increased interest in the application of genetic recombination for the production of important microbial products like antibiotics, enzymes etc. (Adrio and Demain 2010). Transformation techniques such as chemical, electroporation techniques etc. were further modified by many researchers to get desired process efficiency and products (Aune and Aachmann 2010; Hanahan et al. 1991; Tu et al. 2005). Although these well established methods are being routinely used for plasmid DNA (pDNA) transformation in both Gram-positive and Gram-negative bacteria,



transformation in Gram-positive bacterial strains is still a challenge (Arnaud et al. 2004; Dunny et al. 1991; Löfblom et al. 2007).

Recently, nanomaterial mediated transformation using sepiolite nanofibers (Yoshida et al. 2001), carbon nanotubes (Tan et al. 2010), gold (Chatterjee and Sarkar 2014) and chitosan (Bozkir and Saka 2004) NPs have been reported. These methods exhibit increased transformation efficiency and do not require the preparation of competent cells thereby reducing time of transformation process. However, only transformation in *E. coli*, a Gram-negative bacterial strain was established using these nanomaterials and transformation in Gram-positive bacteria is still a difficult process. In view of this, development of efficient NPs based method for transformation in both Gram-positive and Gram-negative bacterial strains is needed.

HAp NPs due to presence of  $\text{Ca}^{2+}$  ions have high binding affinity to nucleic acids and can be transported across the cell membrane. They have successfully been used as carriers for gene transformation in animal and plant cells (Tram Do et al. 2012; Uskoković and Uskoković 2011; Xu et al. 2016). However, the potential of HAp NPs has not been explored for pDNA transformation in prokaryotic cells. In this context, we have studied fHaps as a vehicle for transformation in Gram-positive and Gram-negative bacteria.

## 4.2 Materials and methods

**Bacterial strains:** For transformation studies *E. coli* DH5 $\alpha$  and *S. aureus* MTCC 737 were procured from Microbial Type Culture Collection and Gene Bank Chandigarh.

### 4.2.1 Synthesis of hydroxyapatite nanoparticles

fHaps of rod morphology with various aspect ratios (rod, short and thin rods) were synthesized using modified sol-gel method as discussed in chapter 2.

Based on pDNA binding efficiency, thin-rod fHApS were selected and functionalized with positively charged amino acids and glucose.

#### 4.2.2 Functionalization of thin-rod fHApS with amino acids and glucose

2M calcium chloride was dissolved in DMSO, stirred for 30min and orthophosphoric acid was added drop-wise. Ca:P atomic ratio was maintained at 1.67. Subsequently, acetyl acetone as a stabilizing agent was added to the above solution and stirred for 1h. The pH was adjusted to 10 using liquid ammonia and stirring was continued until the complete formation of gel. Subsequently, 0.1wt% respective amino acids namely arginine (R-fHApS), lysine (K-fHApS) and histidine (H-fHApS) were added to the gel, followed by stirring for 30min. The obtained gel was washed thoroughly with ethanol and dialyzed (using dialysis bag, Bangalore genie 110) against de-ionized (DI) water for 12h with frequent change of water for active removal of adsorbed ions. The dialyzed samples were dried at room temperature.

Based on preliminary results obtained, arginine functionalized fHApS (R-fHApS) were further modified with glucose (R-G-fHApS). 0.3wt% glucose was added in addition to 0.1wt% arginine during the synthesis process and rests of the steps were similar as mentioned above.

#### 4.2.3 Characterization

X-ray diffraction (XRD) studies of fHApS and functionalized fHApS(H-fHApS, K-fHApS, R-fHApS and R-G-fHApS) were carried out for phase identification using X-Ray diffractometer (Miniflex II Rigaku, Japan) with monochromatic  $\text{CuK}\alpha$  radiation ( $\lambda = 1.5405 \text{ \AA}$ ) and a scan range of  $2\theta = 20^\circ$  to  $80^\circ$ . The functional groups present in the synthesized compounds were ascertained by Fourier transform infrared spectroscopy (FTIR) (8201 PC Shimadzu, Japan), over the  $4000\text{--}450\text{cm}^{-1}$  region. The pellets for FTIR analysis were obtained by mixing 1mg of the powdered sample with spectroscopic grade KBr (Merck). The transmission

electron microscopy studies of fHAp and all functionalized fHAp were carried out using transmission electron microscope (TEM) (Phillips CM 200). The NPs were suspended in DI water and sonicated for 15-20min. A drop of the suspension was placed on copper coated TEM grids and air dried in vacuum desiccators for imaging. Zeta potential of fHAp, H-fHAp, K-fHAp, R-fHAp and R-G-fHAp were determined with zeta potential analyzer (Delsa Nano S, Beckman Coulter, USA) at room-temperature. The samples were prepared by diluting the NPs suspension with DI water.

#### 4.2.4 Aggregation studies of R-G-fHAp using dynamic light scattering

DLS studies of R-G-fHAp were carried out in minimal media (M.M), phosphate buffer saline of pH 7 (PBS), Luria broth (LB) and Dulbecco's modified Eagle's media (DMEM). R-G-fHAp (0.1mg/3mL) were dispersed in respective medium and sonicated using probe sonicator for 15mins. The samples were analyzed immediately after sonication using DLS analyzer (Nano plus Micromeritics).

#### 4.2.5 Plasmid isolation

Plasmid was isolated using Qiagen plasmid isolation midi prep kit The protocol followed was as specified by the manufacturer (Qiagen plasmid midi kit) Plasmid used for further experiments is shuttle vector with Ori sites (origin of replication) for *E. coli* and *S. aureus*. It contained kanamycin resistance genes and was 10Kb in size. It is represented as pDNA in following text.

#### 4.2.6 Plasmid DNA binding efficiency to NPs

Short-rods, rods and thin-rod shaped fHAp (0, 10, 30, 50, 70, 100, 130 and 150 $\mu$ g/mL) were suspended in DI water, sonicated for 10min and mixed with 100ng of pDNA at various fHAp:pDNA ratios (0:1, 10:1, 30:1, 50:1, 70:1, 100:1, 130:1 and 150:1). The suspensions were incubated at room temperature for 5min, centrifuged at 22000 $\times$  g for 3min and the pellet obtained was suspended in 50 $\mu$ L of Tris- ethylenediaminetetraacetic acid (EDTA) buffer. Unbound pDNA was

quantified by measuring the optical density (OD) of the supernatant at 260nm using UV spectrometer (UV2450, Shimadzu, Japan), using supernatant of the NPs without pDNA as a blank. The DNA binding efficiencies (B.E) were determined using the equation:

$$\%B.E = \frac{[(pDNA)_i - (pDNA)_f]}{[(pDNA)_i]} \times 100, \quad (9)$$

where %B.E = percent binding efficiency,

$[(pDNA)_i]$  = the optical density of the initial amount of pDNA added to the reaction mixture and

$[(pDNA)_f]$  = the optical density of the unbound pDNA remaining in the sample (Olton et al. 2007).

Similar protocol was followed to determine the B.E for functionalized fHAp (H-fHAp, K-fHAp, R-fHAp and R-G-fHAp)-pDNA complexes and NP:pDNA concentrations used were 0:1, 10:1, 30:1, 50:1, 70:1 and 100:1.

Each of the dissolved pellets (20 $\mu$ L) was loaded on 0.8% agarose gel and the gel was run using electrophoresis apparatus at 80mV for 1h using tris borate EDTA buffer. It was stained with ethidium bromide for 10min and the results were recorded using a gel imager (Life technologies, India).

#### 4.2.7 Stability of R-G-fHAp-pDNA complex

R-G-fHAp-pDNA complex (100 $\mu$ L) of 50:1 ratio of R-G-fHAp:pDNA, was incubated at 37, 60, 80 and 90°C for 1h and at room temperature for 30 days. Subsequently complexes were centrifuged at 22000 $\times$  g for 3min and the pellet obtained was suspended in 100 $\mu$ L of Tris-EDTA buffer. Each of the dissolved pellets was loaded on to agarose gel and the gel was run using electrophoresis apparatus at 80mV for 1h. It was stained with ethidium bromide for 10min and the results were recorded using a gel imager (Life technologies, India). Similar experiments were performed to test the attachment of pDNA to NPs under

various pH conditions by incubating the R-G-fHAp-pDNA complexes in citrate buffer of pH 4, phosphate buffer of pH 6 and 7, Tris HCl buffer of pH 9 and Triethylamine HCl buffer of pH 11 for 1h. Adherence of the plasmid DNA to NP-pDNA complex was determined by running agarose gel as mentioned above.

#### **4.2.8 Effect of physical shear force R-G-fHAp-pDNA complex**

Complex (100 $\mu$ L) was placed in sonication bath (Microson<sup>TM</sup> Sonicator) for 0, 2, 5, 10 and 30s. Subsequently, the samples were centrifuged at 22000 $\times$  g for 3min and the pellet obtained was suspended in 100 $\mu$ L of Tris-EDTA buffer. Attachment of the plasmid DNA was determined as mentioned above.

#### **4.2.9 Transformation of non-competent *E. coli* and *S. aureus***

For the transformation studies, *E. coli DH5 $\alpha$*  and *S. aureus* MTCC 737 strains were used as the model Gram-negative and Gram-positive bacteria. Both the bacterial strains were kanamycin-sensitive, whereas the selected plasmid of size 10Kb had the genes for kanamycin resistance. Both bacterial strains from glycerol stock were streaked on Luria-Bertani (LB) plates and incubated at 37 $^{\circ}$ C for 20h. Single colony from each streaked plate is inoculated into separate 10mL LB at 37 $^{\circ}$ C for 12h. Subsequently, 1% of respective culture was added to 10mL LB media and incubated at 37 $^{\circ}$ C for 4h (optical density at 600nm=0.4). Culture was then centrifuged in two tubes, containing 1mL respective bacterial culture, at 15000 $\times$  g for 5mins at room temperature. Subsequently, to dissolve obtained pellets, 200 $\mu$ L Tris-minimal media was added in one set and in another set 200 $\mu$ L of LB media was added. 20 $\mu$ L of NPs-pDNA complex of ratio 50:1 was added to each bacterial suspension, vortexed for 5min and incubated at 37 $^{\circ}$ C for 1h on rotary shaker. Subsequently, 100 $\mu$ L cell suspension was transferred on LB plates with kanamycin (50 $\mu$ g/mL) and incubated at 37 $^{\circ}$ C for 24h. The colonies were counted and transformation efficiencies (T.E) were calculated using the formula:

T.E = number of colonies on plate/ concentration of pDNA present in 100 $\mu$ L cell suspension (in  $\mu$ g). (10)

Similar protocol was followed to measure the T.E for R-fHAp and R-G-fHAp mediated transformation. All the experiments were carried out in triplicates

#### **4.2.10 Transformation using chemical and electroporation methods**

##### **4.2.10.1 Chemical method**

###### **Preparation of competent cells using chemical method**

Overnight (18h) grown (1mL) *E. coli* bacterial culture was inoculated in 100mL LB media at 37°C on shaker incubator for 4h (OD=0.4). Subsequently, the culture was placed on ice for 10mins and centrifuged at 2700x g for 10min at 4°C. The cell pellet obtained was dissolved in ice cold 100mM CaCl<sub>2</sub> and incubated on ice for 30min. After prescribed time period, solution was again centrifuged at 2700x g for 10min at 4°C and the pellet was dissolved in 100mM MgCl<sub>2</sub>. It was again incubated on ice for 20min and centrifuged at 2700x g for 10min at 4°C. Obtained pellet was suspended in 20% glycerol and stored at -80°C.

###### **Chemical transformation**

Plasmid DNA of 100ng was added into competent cells and heat shock was given by incubating on ice for 30mins, followed by 42°C for 60sec and again on ice for 5min. After heat shock treatment, 900 $\mu$ L of LB/M.M was added and incubated for 2h at 37°C on a shaker at 125 rpm. Subsequently, 100 $\mu$ L cell suspension was transferred on LB plates with kanamycin and incubated at 37°C for 24h.

#### 4.2.10.2 Electroporation method

##### Preparation of electrocompetent cells

Overnight (18h) grown (1mL) *E. coli* or *S. aureus* bacterial culture was inoculated in 100mL LB media and incubated at 37°C on shaker incubator for 4h (OD=0.4). Subsequently, culture was placed on ice for 10mins and centrifuged at 2700x g for 10min at 4°C. The obtained pellet was suspended in 250µL of 10% ice cold glycerol and this cell suspension was stored at -80°C, and used for electroporation.

##### Electroporation

pDNA of 100ng was added into electrocompetent cells and mixed properly. pDNA-cell mix was transferred into ice cold 1 mm-electroporation cuvette. The electroporation cuvette was placed in the electroporator which was set to 1.8Kv for *E. coli* and 2.0Kv for *S. aureus*, 150ohms and 22µF module and press pulse. Immediately 1mL of LB media was added into it and incubated at 37°C on shaker incubator for 1h. Subsequently, 100µL cell suspension was transferred on LB plates with kanamycin and incubated at 37°C for 24h.

#### 4.2.11 Cell toxicity and growth kinetics studies

Cell viability studies using R-G-fHAPs were carried out by MTT (Riss et al. 2015) as well as Resazurin assay (Riss et al. 2015; Sarker et al. 2007) in 24 well plates. Exponentially growing *E. coli* and *S. aureus* cells were inoculated with  $5 \times 10^5$  cells/well in M.M. Both the bacterial cultures were exposed to various concentrations (10, 50, 100, 500 and 1000µg/mL) of the respective NPs dispersed in PBS, and incubated for 6, 12 and 18h. MTT (20µL of 5mg/mL) was added to the test samples, and the plates were incubated at 37°C for 4h. The media was aspirated out carefully without disturbing the cells after 4h. For dissolving the formazan crystals, 150µL of DMSO was added, and the absorbance was measured at 570nm using UV-visible spectrophotometer. All

measurements were carried out in triplicates. The relative cell viability (%) was calculated as described in section 3.2.1.1 using equation (6).

Similar protocol was followed for Resazurin assay, where resazurin dye (10 $\mu$ L of 5mg/mL) was added to the test samples after respective time intervals mentioned above, the plates were further incubated at 37°C for 4h, and absorbance was measured at 560nm using UV-visible spectrophotometer (UV-2450, Shimadzu, Japan). The relative cell viability (%) was calculated as mentioned above.

For growth kinetic studies, bacteria (*E. coli* and *S. aureus*) were grown in presence of fHAp (10, 50, 100, 500, 1000 $\mu$ g/mL). An aliquot of 1mL was withdrawn every 2h, till 18<sup>th</sup> hour, and the optical density was recorded at 600nm on a UV-visible spectrophotometer (UV-2450, Shimadzu, Japan). The growth kinetics parameters such as maximum specific growth rate ( $\mu_{max}$ ; h<sup>-1</sup>) and doubling time ( $t_d$ ; min) were determined according to Berney *et al.*, and Breidt *et al* (Berney et al. 2006; Breidt et al. 1994). Bacterial culture (*E. coli* and *S. aureus*) grown in the absence of R-G-fHAp served as positive control.

#### 4.2.12 Statistical analysis

The statistical analysis was carried out as described in section 3.2.5

### 4.3 Results and discussion

The aim of this study is to transform plasmid DNA (pDNA) in Gram-positive and Gram-negative bacteria using fHAp as vehicle. To achieve transformation, binding of pDNA to fHAp is necessary, therefore first, we determined the binding affinity of pDNA to thin rod, short rod and rod shaped fHAp (as described in chapter 2) by suspending the NPs with pDNA in TE buffer and estimating the amount of unbound pDNA by measuring the absorbance at 260nm (as described in materials and methods). The binding efficiencies (B.E) of rods, short rods and thin rod shaped fHAp were calculated at various NPs:pDNA ratios (10:1,30:1,50:1,70:1,100:1, 130:1and 150:1). B.E of all three fHAp was in the



order of thin rod>short rods>rods. In case of thin rods, the B.E increased with increasing NPs:pDNA ratio up to 100:1 with B.E of 50%, beyond which it was constant (Figure 4.1a). Short rods and rods showed similar trend of increase in BE with NPs:pDNA ratio, and maximum B.E was obtained at the ratio of 130:1 and 150:1 which was 27% and 15% for short rods and rod shaped fHAp, respectively (Figure 4.1a). Agarose gel electrophoresis was carried out to confirm the binding of pDNA to NPs and formation of fHAp-pDNA complex at NPs:pDNA ratio of 150:1. Figure 4.1b, lane i-iii shows rod, short rod and thin rods fHAp-pDNA complex respectively at NPs:pDNA ratio of 150:1, demonstrating that pDNA has bound with all three fHAp. Lane iv is the control (naked pDNA without NPs). Agarose gel image also showed similar trend of increase in pDNA binding affinity with change in aspect ratio from rod to thin rods (Figure 4.1b). Among all the fHAp, thin rods exhibited highest B.E. (Figure 4.1a and b) and hence were selected for further surface modification. Highest binding affinity of thin rods could be attributed to increased aspect ratio and positive charge on the surface of thin rods (+13.25mv) as compared to short rods (+3.85mv) and rod shaped (+2.12mv) morphologies (as described in chapter2).

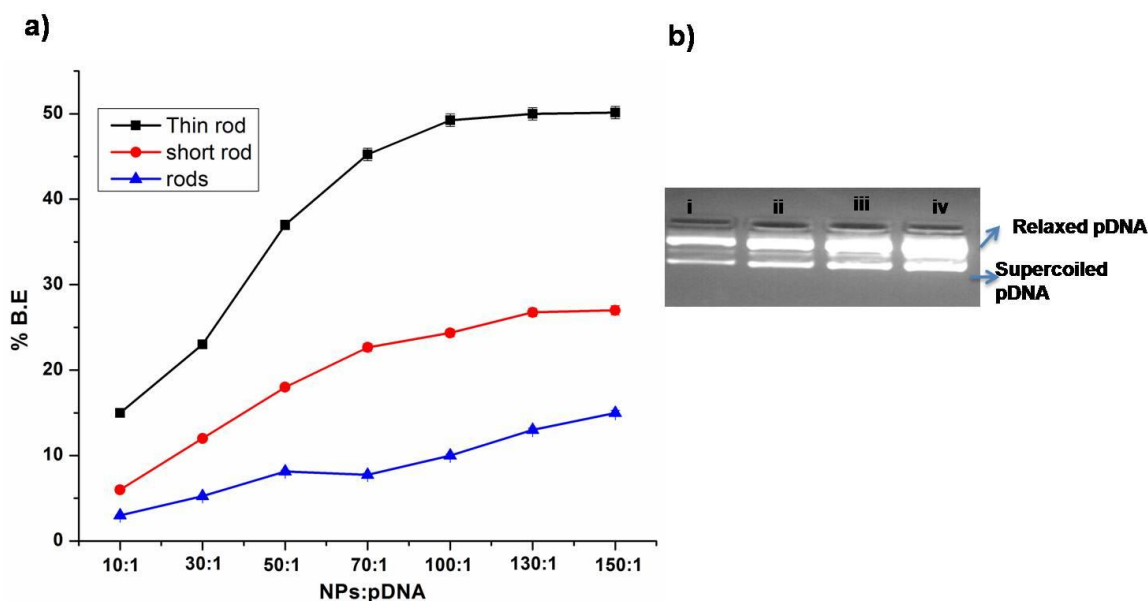


**Figure 4.1** Binding efficiencies of NPs:pDNA with various ratios a) Thin rod (black line), short rod (red line) and rod (blue line) shaped fHAp. The order of B.E. is thin rod > short rod > rod shaped fHAp b) Image of agarose gel electrophoresis confirming binding of pDNA to rod fHAp (lane i), short rod fHAp (lane ii) and rod fHAp (lane iii) at NPs:pDNA ratio of 150:1, lane iv is control.

#### 4.3.1 Functionalization of fHAp

In this study, we have functionalized thin rod shaped fHAp with histidine (H-fHAp), lysine (K-fHAp) and arginine (R-fHAp), using modified sol-gel method at room temperature (Jadalannagari et al. 2011). The idea behind functionalization of fHAp, with positively charged amino acids like histidine/lysine/arginine, was to enhance the positive surface charge and hence the formation of NPs-pDNA complex through electrostatic interactions which could help to increase transformation efficiency (T.E). Synthesis of fHAp using methods like wet chemical and precipitation techniques and subsequent functionalization with various amino acids such as arginine, lysine, valine, etc., have been reported earlier (Gonzalez-McQuire et al. 2004; Li et al. 2012a; Matsumoto et al. 2002; Ueno 2010; Ueno and Shimabayashi 2009; Wang et al. 2015; Yan-Zhong et al. 2011). These NPs were studied for the effects of

functionalization on their crystallinity, solubility, and possible application for gene therapy (Gonzalez-McQuire et al. 2004; Li et al. 2012a; Liuyun et al. 2015; Matsumoto et al. 2002; Wang et al. 2015; Yan-Zhong et al. 2011).

### 4.3.2 Characterization of fHApS

The formation of the fHApS and functionalized fHApS was confirmed by carrying out XRD and FTIR analysis. The XRD spectra (Figure 4.2a) of these NPs corresponded well with the hexagonal HAp structure, indicating that the obtained compounds were well crystallized HAp (ICDD 09-0432). The XRD patterns of the functionalized fHApS were similar to that of fHApS, showing characteristic peaks at  $25.8^\circ$ ,  $31.34^\circ$ ,  $31.95^\circ$  and  $33.97^\circ$  corresponding to [hkl] lattice of [002], [211], [112] and [300], respectively. The FTIR studies were carried out to identify the various functional groups associated with HAp and the amino acids (Figure 4.2b). The signature HAp peaks recorded at  $\sim 600\text{cm}^{-1}$  are attributed to the bending modes of P-O bonds in phosphate groups, with contribution from the -OH of the apatite group at  $\sim 605\text{cm}^{-1}$ . The bands in the region of  $3400\text{cm}^{-1}$  are attributed to -OH bonds and those observed near  $\sim 3571\text{cm}^{-1}$  are associated with -OH stretching vibration of HAp (Jadalannagari et al. 2014a; Jadalannagari et al. 2014b; Ramanan and Venkatesh 2004). In case of H-fHApS, amide I and amide II bands were recorded at  $\sim 1649$  and  $\sim 1527\text{cm}^{-1}$ , while in K-fHApS they were noted at  $\sim 1655$  and  $\sim 1511\text{cm}^{-1}$  respectively.  $\text{NH}_2^+$  stretching and amide I bands were observed in the spectrum of R-fHApS at  $\sim 1448$  and  $\sim 1644\text{cm}^{-1}$ , respectively. Amide I bands between  $1600$  and  $1700\text{cm}^{-1}$  are mainly associated with the C=O stretching vibrations; amide II bands between  $1510$  and  $1580\text{cm}^{-1}$  are associated with N-H bending and C-N stretching vibrations. Presence of amide I group at  $\sim 1650\text{cm}^{-1}$  and amide II at  $\sim 1537\text{cm}^{-1}$  for lysine functionalized HAp NPs and amino group in arginine functionalized fHApS in the region of  $1400$  to  $1420\text{cm}^{-1}$  has been reported (Ueno 2010; Ueno and Shimabayashi 2009; Wang et al. 2015; Yan-Zhong et al. 2011).

Morphology of HAp and functionalized HAp NPs was studied using TEM. fHAp, H-fHAp, K-fHAp and R-fHAp exhibited similar thin rod morphology with average length of 62.5nm and diameter of 6.2nm (Figure 4.2c). Similar results with no change in particle size, when functionalized with basic amino acids such as arginine/lysine were reported for fHAp synthesized by wet chemical method and were attributed to the nature of the side chain (Gonzalez-McQuire et al. 2004; Matsumoto et al. 2002). On the contrary, a reduction in particle size was reported when fHAp synthesized by hydrothermal method were functionalized with arginine, and attributed to static effect between the positive  $\text{NH}_2$  group of amino acids with negative hydroxyl group of HAp (Wang et al. 2015; Yan-Zhong et al. 2011). Decrease in particle size was noted after functionalization with acidic amino acids and has also been attributed to the nature of the side chains (Gonzalez-McQuire et al. 2004; Matsumoto et al. 2002). Thus, the interactions between the functional groups of the surface radicals and HAp, as well as the methods of synthesis are responsible for the variations observed in particle size.

Zeta potential measurements of all the fHAp were carried out to measure the surface charge. An increase in the zeta value from  $\sim+13.25\text{mv}$  to  $\sim+64$ ,  $\sim+29$  and  $\sim+47\text{mv}$ , was noted when fHAp was functionalized with arginine, histidine and lysine, respectively. Increase in zeta potential values further confirmed functionalization of fHAp with positively charged amino acids. This could be attributed to binding of  $\alpha$  carboxylate group of amino acid to fHAp such that the positively charged amino groups are exposed at the NP/solvent interface thereby increasing the positive charge at the surface (Dong et al. 2013; Liuyun et al. 2015; Wang et al. 2015; Yan-Zhong et al. 2011). The order of increase in zeta potential values was R-fHAp > K-fHAp > H-fHAp which corroborated with the increase in basic nature of the amino acids. Similar observations were noted for arginine/lysine functionalized HAp synthesized by hydrothermal and wet chemical methods, wherein, increase in zeta potential from  $-10\pm 5$  to  $30\pm 5\text{mv}$  and  $-50$  to  $10\text{mv}$ , was reported after functionalization with arginine and lysine, respectively (Dong et al. 2013; Liuyun et al. 2015; Wang et al. 2015; Yan-Zhong

et al. 2011) Since aggregation of NPs limits their biological applications, aggregation studies of R-G-fHApS using DLS were carried out after dispersion in various media. Sizes of R-G-fHApS in PBS, MM and LB were 107, 110 and 340nm respectively. R-G-fHApS dispersed in LB media showed almost 3 times larger size than in M.M and PBS medium. This could be attributed to the presence of bio-micromolecules (electrolytes, proteins, lipids, etc) in media which are easily adsorbed on to the NPs enhancing the inter-particle interaction, resulting in aggregation (Moore et al. 2015; Rausch et al. 2010).

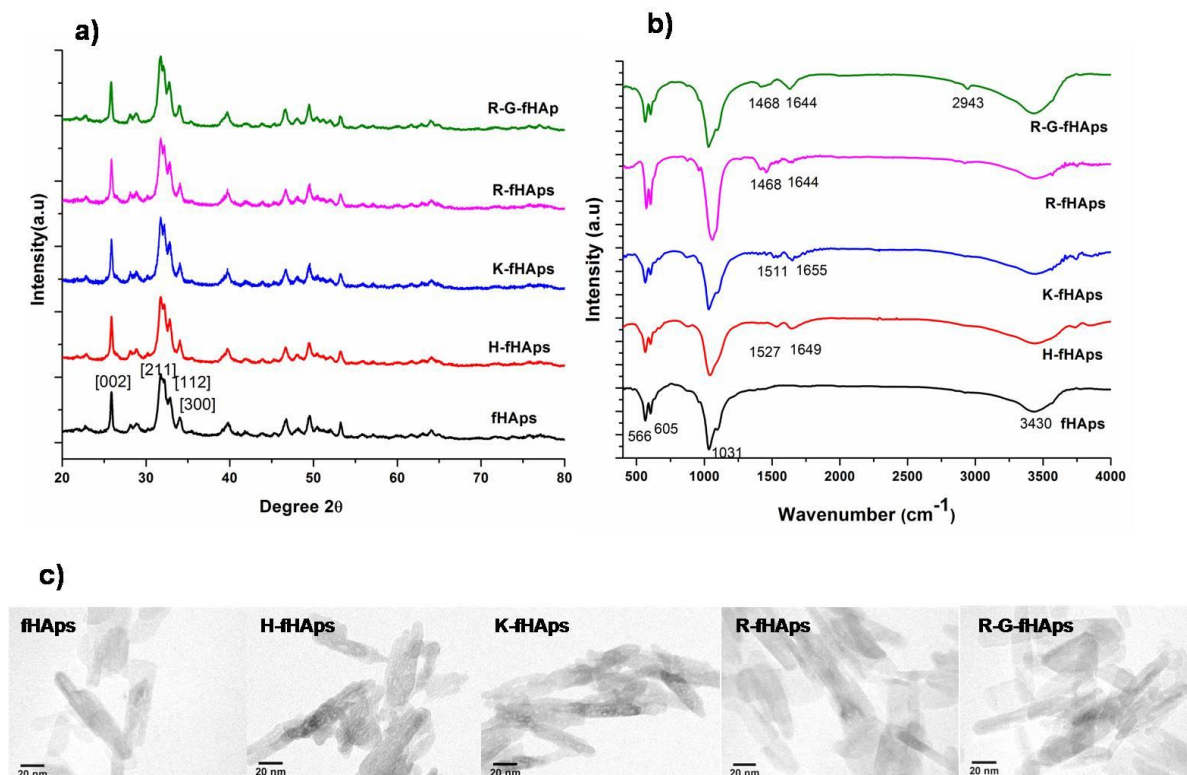


**Figure 4.2** a) XRD pattern b) FTIR spectra and c) TEM micrographs of fHApS, H-fHApS, K-fHApS, R-fHApS and R-G-fHApS. Characteristic XRD peaks of HAp were observed in all the samples. FTIR spectra showed characteristic bands of HAp, amide I, amide II, NH<sub>2</sub> and glucose. TEM morphology observed was similar for all the samples.

### 4.3.3 Binding of pDNA to functionalized fHApS

Binding of pDNA to NPs with high affinity is desirable for their proposed application of bacterial transformation. Therefore, we studied the B.E of pDNA with all functionalized fHApS at various NPs:pDNA ratios to obtain optimized ratio where B.E is maximum. Figure 4.3a shows B.E (calculated as mentioned in materials and methods) of pDNA with thin rod fHApS and amino acid functionalized thin rod fHApS (H-fHApS, K-fHApS and R-fHApS) at various NPs:pDNA ratio (0:1, 10:1, 30:1, 50:1, 70:1 and 100:1). B.E of functionalized fHApS increased with increase in NPs:pDNA ratio. H-fHApS:pDNA and K-fHApS:pDNA ratio of 70:1 and above showed maximum B.E of ~70 and ~80%, respectively while R-fHApS:pDNA exhibited maximum B.E of ~90% at ratio of 50:1 and above (Figure 4.3a). As NPs:pDNA ratio of 70:1 shows highest B.E for all the three amino acid functionalized fHApS, we have selected this ratio to demonstrate the formation of H-fHApS-pDNA (lane ii), K-fHApS-pDNA (lane iii) and R-fHApS-pDNA (lane iv) complex using agarose gel electrophoresis (Figure 4.3b). Lane i is the control (naked pDNA without NPs). There was significant ( $p < 0.05$ ) difference between B.E of fHApS and amino acid functionalized fHApS (H-fHApS, K-fHApS and R-fHApS) which was in the order of R-fHApS > K-fHApS > H-fHApS > fHApS (Figure 4.3a). R-fHApS showed highest B.E which could be attributed to higher positive charge on the surface allowing maximum binding of negatively charged pDNA (Figure 4.3a and b). Calcium phosphate/HAp NPs exhibit binding affinity for DNA to form complexes and have been explored for transfection (Neumann et al. 2009; Olton et al. 2007; Tram Do et al. 2012; Uskoković and Uskoković 2011). B.E and transfection efficiency was further improved with histidine/lysine/arginine/ protamine sulfate functionalization (Li et al. 2012a; Liuyun et al. 2015; Tan et al. 2007; Wang et al. 2015; Yan-Zhong et al. 2011). In this study, since the R-fHApS exhibited significantly higher B.E ( $p < 0.05$ ) and higher zeta potential value (Figure 4.3a), it was further functionalized with glucose (R-G-fHApS) with the idea of increasing the cellular uptake as glucose is a preferred carbon source for growth.

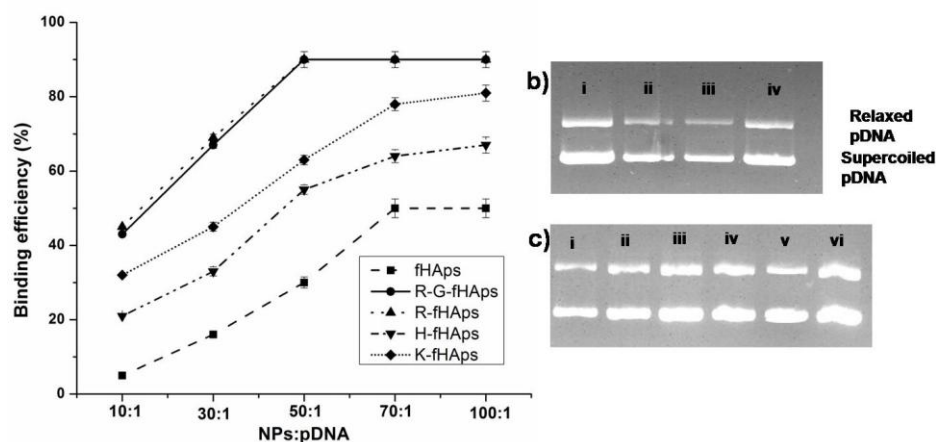


**Figure 4.3** Binding efficiencies of NPs:pDNA with various ratios a) fHAp-pDNA(dash), H-fHAp-pDNA(dash dot dot), K-fHAp-pDNA (short dots), R-fHAp-pDNA(dots) and R-G-fHAp-pDNA (straight line). b) Image of agarose gel electrophoresis, H-fHAp (lane ii), K-fHAp (lane iii) and R-fHAp (lane iv)-pDNA complex at NPs:pDNA ratio of 70:1, lane i is control. c) Image of agarose gel electrophoresis, Lane i-v shows R-G-fHAp-pDNA complex when weight ratios of R-G-fHAp:pDNA were 10:1, 30:1, 50:1, 70:1 and 100:1 respectively. Lane vi is control (0:1).

Surface modification of R-fHAp with glucose did not affect the XRD spectra and morphology (Figure 4.2 a and c). Presence of glucose on R-fHAp, was confirmed by FTIR studies, wherein an additional band at  $\sim 2943\text{cm}^{-1}$  representing  $-\text{CH}$  bonds from glucose was noted (Figure 4.2b). CH bands in D-glucose have been reported around  $2900\text{-}2980\text{cm}^{-1}$  (Ibrahim et al. 2006). The zeta potential value of R-G-fHAp was  $+62.3\text{mV}$  which was similar to R-fHAp ( $+64\text{mV}$ ), the difference being insignificant ( $p > 0.05$ ). Correspondingly there was no significant change ( $p > 0.05$ ) in the B.E between R-fHAp and R-G-fHAp, with  $\sim 90\%$  B.E for NP:pDNA ratios  $\geq 50:1$  (Figure 2a). Agarose gel electrophoresis confirmed the binding of pDNA to R-G-fHAp (Figure 2b). Since, ratios  $\geq 50:1$  exhibited  $90\%$  B.E and high band intensities, they were chosen for transformation experiments.



#### 4.3.4 Stability of R-G-fHApS-pDNA complex

Stability of R-G-fHApS-pDNA complex is essential for the transformation process. Therefore, we studied stability of complexes at various temperatures, pH and towards sonication-induced stress. It was observed that R-G-fHApS-pDNA complexes were stable in the temperature of range 37 to 90°C. As can be seen from gel image (Figure 4.4a), lane i-v shows R-G-fHApS-pDNA complex after incubating it at different temperatures of 37, 60, 80, 90°C and room temperature respectively. pDNA remained intact and stable at room temperature even after 30 days (Figure 4.4b, lane i). Complexes are also stable in buffer of pH 6, 7, 9 and 11 (Figure 4.4c, lane i-iv respectively). The complex dissolved in buffer of pH 4 and below, and no band for R-G-fHApS-pDNA complex was observed (Lane v; Figure 4.4c). This was attributed to dissolution of fHApS in acidic pH of ~4-5 (Lee et al. 2012; Suchanek and Yoshimura 1998; Thomann et al. 1990). Sonication-induced stress also did not exhibit any effect on R-G-fHApS-pDNA complex (Figure 4.4d). Lane i-v of Figure 4.4d shows R-G-fHApS-pDNA complexes after placing them in Sonication bath for 0, 2, 5, 10 and 30s respectively.

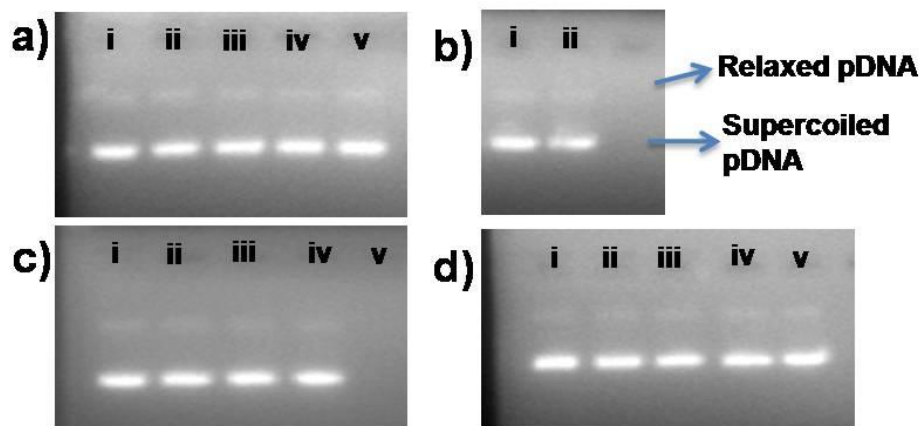


**Figure 4.4** Image of agarose gel electrophoresis, demonstrating stability of R-G-fHApS-pDNA complex a) in the temperature of 37(lane i), 60 (lane ii), 80 (lane iii), 90°C (lane iv) and room temperature(lane v) b) at room temperature for 30 days (lane i- control R-G-fHApS-pDNA complex, ii- complex after 30 days) c) in buffer (lane i- control R-G-fHApS-pDNA complex, ii- complex after 30 days) c) in buffer



of pH 4 (lane v), 6 (lane i), 7 (lane ii), 9 (lane iii) and 11 (lane iv) d) in sonication-induced stress for 0 (lane i), 2 (lane ii), 5 (lane iii), 10 (lane iv) and 30s (lane v).

#### 4.3.5 Transformation of non-competent bacteria cells

Bacterial transformation is one of the most important and routinely used techniques in genetic research; however conventional methods used for transforming pDNA into bacteria needs preparation of competent cells and also provide variable transformation efficiencies. In addition, it is difficult to transform pDNA into Gram-positive bacterial cells due to presence of thick peptidoglycan layer. There are few reports on bacterial transformation using nanoparticles like chitosan, carbon, sepiolite and gold which do not require preparation of competent cells (Bozkir and Saka 2004; Chatterjee and Sarkar 2014; Tan et al. 2010; Yoshida et al. 2001). However, these nanoparticles are studied only for *E. coli* (Gram-negative bacteria) and not for Gram-positive bacteria. Achieving high transformation efficiency in Gram positive bacteria is still a challenge. In the present work, we have studied HAp NPs as a vehicle for delivering pDNA into both Gram-positive (*S. aureus*) and Gram-negative (*E. coli*) bacteria. Bacteria in log phase are exponentially growing hence could take up more NP-pDNA complex and were selected for transformation process. Transformation in *E. coli* and *S. aureus* was carried out using fHAp, R-fHAp, R-G-fHAp as the vehicle for transporting pDNA using LB and M.M (Figure 4.5) and transformation efficiencies (T.E) were compared with commonly used methods such as chemical ( $\text{CaCl}_2$ ) and electroporation. Transformation efficiencies (T.E) obtained using all the above methods are presented in Table 4.1. T.E obtained using fHAp, R-fHAp and R-G-fHAp as vehicle in M.M was significantly ( $p < 0.05$ ) higher than with LB media for both *E. coli* and *S. aureus*. This could be attributed to abundance of bio-micromolecules (electrolytes, proteins, lipids, etc) in complex media in comparison to minimal media, which are easily adsorbed on to the NPs enhancing the inter-particle interaction, resulting in aggregation (Moore et al. 2015; Rausch et al. 2010) and reduction in transformation of NP-pDNA complex. Functionalization with arginine had a positive effect on T.E of both *E. coli* and *S.*

*aureus*. T.E of *E. coli* and *S. aureus* was significantly higher ( $p < 0.05$ ) for R-G-fHAp as compared to fHAp, R-fHAp,  $\text{CaCl}_2$  and electroporation methods. There was a 100 times increase in T.E of *E. coli* and *S. aureus* in M.M and L.B media after arginine functionalization (R-fHAp) as compared to control (fHAp) (Table 4.1). This could be attributed to higher binding affinity of pDNA to R-fHAp than fHAp. Wang et al have also reported 4.5 times increase in transfection efficiency in HeLa cells after functionalization of HAp with arginine (Wang et al. 2015). Similar results of 4.5 times increase in transfection efficiency in HeLa cells using arginine functionalized HAp NPs has been reported (Wang et al. 2015). Further, surface modification with glucose resulted in  $10^3$  and  $10^5$  times increase in T.E as compared to the R-fHAp and fHAp, respectively in both *E. coli* and *S. aureus* using M.M media (Table1). Similarly using L.B media there was  $10^2$  and  $10^4$  times increase in T.E as compared to the R-fHAp and fHAp, respectively. T.E in *E. coli* by R-G-fHAp using M.M was 100 and 1000 times higher than  $\text{CaCl}_2$  and electroporation methods, respectively (carried out in LB media). To the best of our knowledge this is the first report of surface modification of fHAp with glucose for increasing cellular uptake, resulting in a highly significant increase in T.E (Table1). However, the concept of glucosylation of NPs to increase cellular uptake has been explored in drug delivery for the treatment of cancer wherein NPs like 2-deoxy-D-glucose modified poly(ethylene glycol)-co-poly(trimethylene carbonate), glucose-functionalized multidrug terpolymer and glucose modified poly lactic-co-glycolic acid showed higher uptake than non-glucosylated NPs in C6 (glioma), HepG2, and L929 cells (Jiang et al. 2014; Wang et al. 2013).

HAp NPs have been extensively studied as non-viral vectors for plant and animal cells. It has long been used to transfect many cell lines such as gastric cancer SGC-7901, HeLa, HepG2, bone cells, spleen cells (Tram Do et al. 2012; Uskoković and Uskoković 2011; Xu et al. 2016) and also to transform gene in tobacco plant (Naqvi et al. 2012). However, its potential to transform pDNA into bacteria has not yet been explored. fHAp are most stable phase of calcium phosphate and potential candidate for gene transformation due to its

biocompatibility, nucleic acid binding efficiency, biological stability, easy synthesis and easy diffusion through cell membrane (Tram Do et al. 2012; Uskoković and Uskoković 2011; Xu et al. 2016).

**Table 4.1:** Transformation efficiencies of *E. coli* and *S. aureus* obtained using nanoparticles mediated (fHAp, R-fHAp, R-G-fHAp), calcium chloride and electroporation methods.

|                   | <i>E. coli</i>   |        | <i>S. aureus</i> |        |
|-------------------|------------------|--------|------------------|--------|
|                   | cfu/ $\mu$ g DNA |        | cfu/ $\mu$ g DNA |        |
|                   | LB               | M.M    | L.B              | M.M    |
| fHAp              | $10^3$           | $10^4$ | $7 \times 10^1$  | $10^2$ |
| R-fHAp            | $10^5$           | $10^6$ | $10^3$           | $10^4$ |
| R-G-fHAp          | $10^7$           | $10^9$ | $10^5$           | $10^7$ |
| CaCl <sub>2</sub> | $10^7$           | $10^6$ | NA               | NA     |
| Electroporation   | $10^6$           | $10^4$ | $10^5$           | $10^4$ |

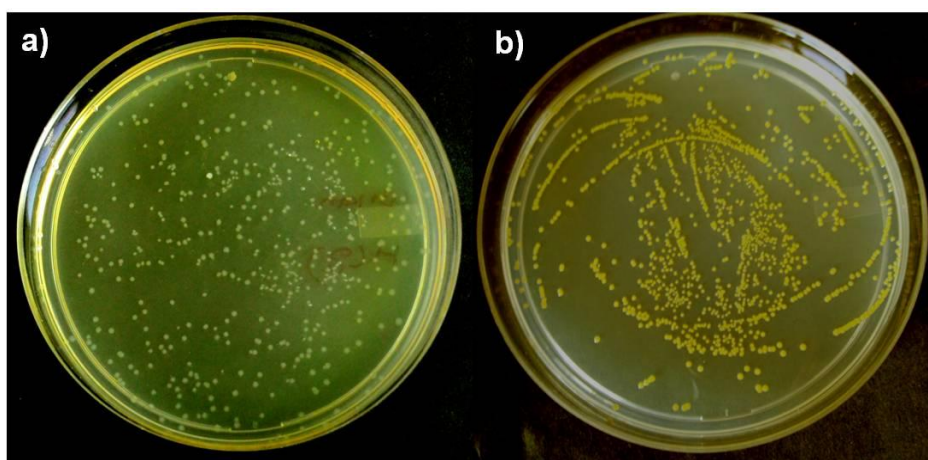


**Figure 4.5** Transformed bacterial colonies of a) *E. coli* (b) *S. aureus* on kanamycin containing LB agar plates. Both the strains were transformed using R-G-fHAp without preparation of competent cells.

#### 4.3.6 Plasmid isolation from transformed *E. coli* and *S. aureus*

Plasmid DNA was isolated from transformed *E. coli* and *S. aureus* colonies cultured on LB plates containing kanamycin to confirm the transformation using R-G-fHAPs. Figure 4.6 shows the agarose gel image of pDNA isolated from transformed *E.coli* (lane i) and *S. aureus* (lane ii). There was no difference between pDNA isolated from transformed *E. coli*, *S. aureus* and control pDNA confirming the transformation.

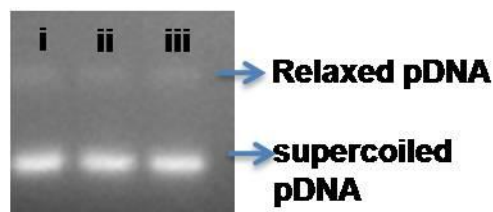


**Figure 4.6** Agarose gel image of pDNA i) isolated from *E.coli* ii) *S. aureus* transformed using R-G-fHAPs iii) control pDNA.

#### 4.3.7 Cell viability and growth kinetics

An important condition for successful transformation is non toxicity of the NPs towards bacterial cells. To test the effect of R-G-fHAPs on viability of *E. coli* and *S. aureus*, time and dose dependent studies of R-G-fHAPs were carried out using MTT and Resazurin assays (Figure 4.7). There was no significant difference ( $p > 0.05$ ) between the cell viability of cells treated with functionalized NPs as compared to untreated control at various concentrations (10, 50, 100, 500 and 1000  $\mu\text{g}/\text{mL}$ ) for both the bacterial strains, indicating non-toxicity of NPs (Figure 4.7ai and bi). Similar results were obtained with Resazurin assay further confirming the non-toxic nature of NPs (Figure 4.7b).

*E. coli* and *S. aureus* was treated with different concentrations of R-G-fHAPs (10, 50, 100, 500 and 1000  $\mu\text{g}/\text{mL}$ ) for various time intervals to study the effect of these NPs on the growth profile. Growth profile of *E. coli* and *S. aureus* treated with R-G-fHAPs at all the concentrations (10-1000  $\mu\text{g}/\text{mL}$ ) was found to be similar

to that of the control (without NPs) (Figure 4.7aii and bii). Growth kinetics parameters like specific growth rates and doubling times were also calculated. Maximum specific growth rate and doubling time of *E. coli* and *S. aureus* in presence R-G-fHAPs are presented in Table 4.2. There was no significant difference ( $p>0.05$ ) between growth parameters of bacterial cells grown in presence of R-G-fHAPs and control (without NPs). Maximum specific growth rate and doubling time for *E. coli* in presence of 1000 $\mu\text{g/mL}$  R-G-fHAPs were 1.54 $\text{h}^{-1}$  and 27min, while in the control (without NPs) it was 1.66 $\text{h}^{-1}$  and 25 min respectively. Correspondingly for *S. aureus* the values were 0.831 $\text{h}^{-1}$ , 50min and 0.86 $\text{h}^{-1}$ , 48min, respectively (Table 4.2).

**Table 4.2** Growth kinetics parameters of *E. coli* and *S. aureus* at different concentrations of R-G-fHAPs.

| Concentrations | <i>E.coli</i>                                    |                              | <i>S.aureus</i>                                 |                              |
|----------------|--|------------------------------|---|------------------------------|
|                | Specific growth rate ( $\mu$ : $\text{h}^{-1}$ ) | Doubling time ( $t_d$ : min) | Specific growth rate( $\mu$ : $\text{h}^{-1}$ ) | Doubling time ( $t_d$ : min) |
| Control        | 1.66   | 25.00                        | 0.860   | 48.00                        |
| 10             | 1.63   | 25.50                        | 0.849   | 48.97                        |
| 50             | 1.61   | 25.82                        | 0.841   | 49.44                        |
| 100            | 1.59   | 26.15                        | 0.838   | 49.61                        |
| 500            | 1.56   | 26.66                        | 0.831   | 50.09                        |
| 1000           | 1.54   | 27.00                        | 0.831   | 50.09                        |

All the above studies show that R-G-fHAPs have high binding affinity to pDNA (Figure 4.3) and also contributes towards achievement of high T.E for both *E. coli* and *S. aureus* without preparation of competent cells (Table 4.1). These NPs are non-toxic and could be used as a safe plasmid DNA delivery vehicle for both Gram-positive and Gram-negative bacterial cells.



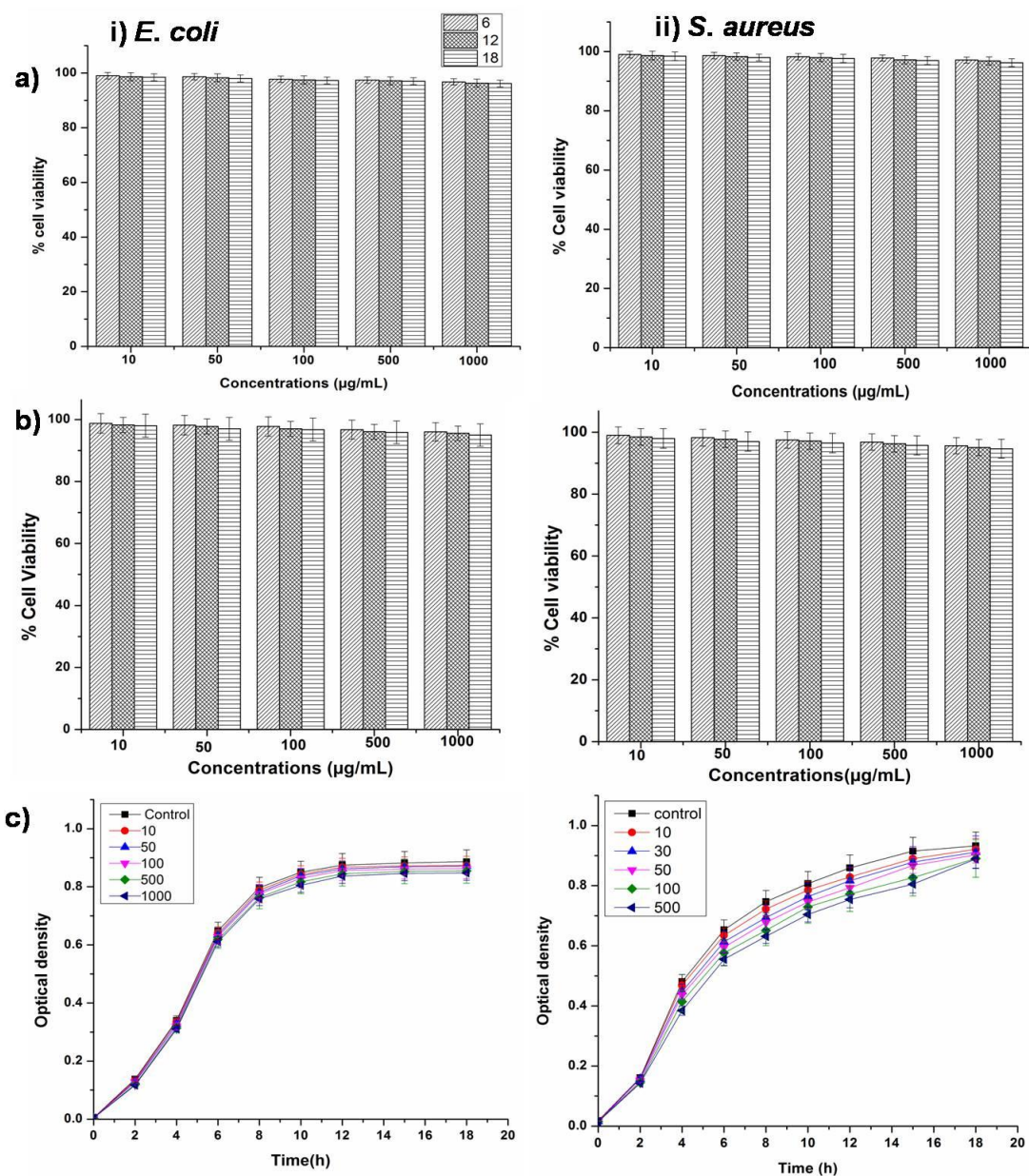


**Figure 4.7** a) MTT and b) Resazurin data showing non-toxic nature of R-G-fHAPs on i) *E. coli* and ii) *S. aureus* after 6, 12 and 18h of growth in presence of various concentrations ranging from 10-1000  $\mu\text{g/mL}$ . c) Growth curve showing no change of growth pattern in presence of R-G-fHAPs at various concentrations.

#### 4.4 Conclusion

This study, demonstrated that fHAp can serve as a vehicle for plasmid transformation of both Gram-positive and Gram-negative bacteria. Functionalization of fHAp with positively charged amino acids (arginine/lysine/histidine) enhanced the zeta potential as well as binding efficiency to pDNA. Arginine functionalization resulted in highest binding efficiency (90%) and successful transformation with an efficiency of  $10^6$  cfu/ $\mu$ g of pDNA. Glucose functionalization of R-fHAp in M.M led to a 1000 times increase in T.E in both *E. coli* and *S. aureus*. The advantages of the nanovehicle delivery system reported in the current study are: i) it does not require preparation of competent cells; ii) can be carried out at room temperature; iii) high transformation efficiency in both Gram-positive and Gram-negative bacteria; iv) non toxic nature of the NPs. This novel bacterial transformation method can provide exciting opportunities in the field of recombinant DNA technology.

## CHAPTER 5

### **One Step Transformation Method for *C. albicans* Using Modified-Fluorescent Hydroxyapatite Nanoparticles**

#### **5.1 Introduction**

Yeast has been associated with humans for preparation of bread, wine, beer, sake, etc, since 8000 years and these ancient processes are the basis of modern biotechnology (Legras et al. 2007; Sicard and Legras 2011). Recently, yeast species have been used as experimental models to study signal processes and also to characterize some molecular events associated with human mitochondrial and neurodegenerative diseases (Botstein and Fink 2011; Khurana and Lindquist 2010; Tenreiro et al. 2013). To advance use of yeast in industries and research, development of modified yeast strain by delivering nucleic acid into the cell is the most important step (Demain and Vaishnav 2009; Meyer 2008). Several types of yeast species such as *Saccharomyces*, *Aspergillus*, *Rhizopus*, etc. are genetically engineered for efficient production of various drugs, industrial enzymes, vaccines, chemicals etc (Ino et al. 2009; Pompon et al. 1995). In spite of many advantages of modified yeast; it is difficult to deliver DNA into yeast due to the presence of tough cell wall which is composed of mannose-containing proteins and glycans.

Various approaches such as lithium acetate (LiAc)-based methodologies, electroporation, gene gun transformation, protoplast transformation, etc, have been developed to deliver nucleic acid into yeast cells (Becker and Guarente 1991; Butow et al. 1996; Gietz and Schiestl 2007a; Gietz and Schiestl 2007b; Gietz and Woods 2006; Klebe et al. 1983; Klein and Jones 1999). However, these methods have limitations such as low transformation efficiency, high toxicity, need for costly reagents and equipments. Hence there is need for development of transformation methods which are more efficient, less toxic and reproducible.



Recently, nanotechnology based approaches have received more attention in the field of gene delivery. Nanomaterials exhibit higher DNA binding capacity and cellular uptake than bulk materials due to their high surface area to volume ratio. Filyak et al used comb-like nanoscale oligoelectrolyte polymer as delivery vehicle to achieve high transformation efficiency in *Saccharomyces cerevisiae*, *Hansenula polymorpha* and *Pichia pastoris*. They were able to achieve 15 and 79 times more transformants in *Hansenula polymorpha* and *Pichia pastoris*, respectively as compared to LiAc method (Filyak et al. 2013). Xue et al studied that coating of DNA with polyethylenimine-dextran sulfate NPs increased the efficiency of electroporation process by four times as compared to naked DNA (Xue et al. 2013). Although, work on nanotechnology based approaches for easy delivery of DNA in yeast cells have been initiated, there is still need to advance the technique for more efficient gene delivery in yeast.

In this chapter, we report the synthesis of arginine(R), glucose (G) and polyethylene glycol (PEG) functionalized thin-rod fHAp (modified-fHAp) and studied it as a vehicle for DNA delivery in *Candida albicans*.

## 5.2 Materials and Methods

**Yeast strains:** For transformation studies *Candida albicans* 183 were purchased from NCIM, National Chemical Laboratory, Pune. Genticin were purchased from Himedia

### 5.2.1 Synthesis of functionalized modified-fHAp NPs

Thin-rod fHAp were prepared as described in 2.2.1. After the completion of gel formation, 0.1 wt% arginine (R), 0.3 wt% glucose (G) and 0.05 wt% polyethylene glycol (PEG) were added to the solution to functionalize the fHAp surface and stirred for 2h. The gel obtained was washed thoroughly with ethanol and the dialyzed (using dialysis bag, Bangalore genie 110) against de-ionized water for 12h with frequent change of water for active removal of adsorbed ions. The

dialyzed samples were dried at room temperature and referred as modified-fHAPs in the following text.

### 5.2.2 Characterization

X-ray diffraction (XRD) studies of fHAPs and modified fHAPs were carried out for phase confirmation using X-Ray diffractometer (Miniflex II Rigaku, Japan) with monochromatic  $\text{CuK}_\alpha$  radiation ( $\lambda = 1.5405 \text{ \AA}$ ) and a scan range of  $2\theta = 20^\circ$  to  $80^\circ$ . The functional groups present in the synthesized compounds were ascertained by Fourier transform infrared spectroscopy (FTIR) (8201 PC Shimadzu, Japan), over the  $4000\text{--}450\text{cm}^{-1}$  region. The pellets for FTIR analysis were obtained by mixing 1mg of the powdered sample with spectroscopic grade KBr (Merck). The transmission electron microscopy studies of fHAPs and modified-fHAPs were carried out using transmission electron microscope (TEM) (Phillips CM 200). The NPs were suspended in DI water and sonicated for 15-20min. A drop of the suspension was placed on copper coated TEM grids and air dried in vacuum desiccators for imaging. Zeta potential of modified HAP NPs was determined with zeta potential analyzer (Delsa Nano S, Beckman Coulter, USA) at room-temperature. The samples were prepared by diluting the NPs suspension with DI water.

### 5.2.3 Modified fHAPs-pDNA complex

Complexes between modified fHAPs and plasmid DNA were prepared using similar method as described in section 4.2.6. Plasmid DNA containing kanamycin and gentamicin resistance gene were used for all the experiments and referred as a pDNA in further text. In brief, pDNA-modified fHAPs complexes were formed by mixing pDNA ( $0.5\mu\text{g/mL}$ ) with the solution of modified fHAPs ( $10\text{--}100\mu\text{g/mL}$ ) suspension at various fHAPs/pDNA mass ratios (0:1, 10:1, 30:1, 50:1, 70:1, and 100:1) and incubated at room temperature for 5min before loading onto the agarose gel. The solution was centrifuged at  $22000\times g$  for 3min and the pellet was suspended in TE buffer.  $20\mu\text{L}$  of each of the modified fHAPs-pDNA

complexes were loaded on 0.8% of agarose gel and stained with ethidium bromide for 10min. The staining results were investigated under UV trans-illuminator. To calculate DNA binding efficiency, the amount of unbound, non-precipitated DNA remaining in the supernatant after centrifugation of each suspension was quantified by measuring the absorbance at 260nm using UV spectrometer (UV2450, Shimadzu, Japan). The supernatant of the modified fHApS without addition of pDNA were used as the blank. The binding efficiencies were determined as described in section 4.2.6 (Olton et al. 2007).

Each of the dissolved pellets (20 $\mu$ L) was loaded on 0.8% agarose gel and the gel was run using electrophoresis apparatus at 80mV for 1h using tris borate EDTA buffer. It was stained with ethidium bromide for 10min and the results were recorded using a gel imager (Life technologies, India).

#### **5.2.4 Stability of modified-fHApS-pDNA complex**

Modified-fHApS-pDNA complex (100 $\mu$ L), of 50:1 ratio of modified-fHApS:pDNA, was incubated at 37, 60, 80 and 90°C for 1h and at room temperature for 30 days. Subsequently complexes were centrifuged at 22000 $\times$  g for 3min and the pellet obtained was suspended in 100 $\mu$ L of Tris-EDTA buffer. Each of the dissolved pellets was loaded on to agarose gel and the gel was run using electrophoresis apparatus at 80mV for 1h. It was stained with ethidium bromide for 10min and the results were recorded using a gel imager (Life technologies, India). Similar experiments were performed to test the attachment of the pDNA to the NPs under various pH conditions by incubating the modified-fHApS-pDNA complexes in citrate buffer of pH 4, phosphate buffer of pH 6 and 7, Tris HCl buffer of pH 9 and Triethylamine HCl buffer of pH 11 for 1h. Adherence/attachment of the plasmid DNA to NPs was determined by running agarose gel as mentioned above.

### 5.2.5 Effect of physical shear force modified-fHAp-pDNA complex

Complex (100 $\mu$ L) was placed in Sonication bath (Microson<sup>TM</sup> Sonicator) for 0, 2, 5, 10 and 30s. Subsequently, the samples were centrifuged at 22000 $\times$  g for 3min and the pellet obtained was suspended in 100 $\mu$ L of Tris-EDTA buffer. Adherence/attachment of the plasmid DNA to NPs was determined as mentioned above.

### 5.2.6 Transformation of non-competent *C. albicans* cells

*C. albicans* is chosen as a model yeast organism for transformation studies. This strain was kanamycin and geneticin sensitive, whereas selected plasmid of size 10Kb contains genes for kanamycin and geneticin resistance. A loopfull of *C. albicans* culture was taken from the glycerol stock and streaked on Sabouraud dextrose agar (SBA) plates (1.8% agarose, pH 7) and incubated at 37 $^{\circ}$ C for 48h. Single colony from the streaked plate was inoculated into 10mL of Sabouraud broth (SB) and incubated at 37 $^{\circ}$ C overnight. After 18-24h,  $2 \times 10^8$  cells were added to 20mL SB and incubated at 37 $^{\circ}$ C in shaking incubator at 120rpm for 6-8 h. Subsequently, the culture broth was divided into two sets (each set contains 6 tubes with 1mL culture per tube), and centrifuged at 15000 $\times$  g for 5mins at room temperature. The pellets obtained were dissolved in 200 $\mu$ L of Tris-minimal media for the first set and 200 $\mu$ L of SB media for the second set. 20 $\mu$ L of modified HAp NPs-pDNA complex of various ratios (0:1, 10:1, 30:1, 50:1, 70:1 and 100:1) was added to the cell suspensions and mixed gently. Heat shock treatment was given by incubating the cell suspensions on ice for 15min, followed by 47 $^{\circ}$ C for 30–60s and again on ice for 2min. Subsequently, the cells were incubated at 37 $^{\circ}$ C for 1h on a rotary shaker at 120rpm, and 100 $\mu$ L of the cell suspension was spread plated on SB plates containing kanamycin (200 $\mu$ g/mL) and geneticin (100 $\mu$ g/mL) and incubated at 37 $^{\circ}$ C for 24h. The colonies were counted and transformation efficiencies (T.E) were calculated as described in section 4.2.9. Similar protocol was followed to measure the T.E for HAp NPs, R-HAp NPs and R-G-HAp NPs mediated transformation.

## 5.2.7 Electroporation method

### Preparation of electrocompetent cells

1mL of overnight (18h) grown *C. albicans* culture was inoculated in 100mL SB media and incubated at 37°C at 120rpm on shaker incubator for 6-8h (OD=0.6) and centrifuged at 2700x g for 10min at 4°C. Subsequently, the cells pellet was washed twice with 20mL of cold water, and once with 20mL electroporation buffer (1M sorbitol/1mM CaCl<sub>2</sub>). The cell pellet was suspended in 20mL of 0.1M lithium acetate/10mM dithiothreitol and incubated at 37°C at 120rpm on shaker incubator for 30min. Next, the cell suspension was centrifuged at 2700x g for 10min at 4°C; given a wash with 50mL of electroporation buffer and suspended in 1mL of the same buffer. The cell suspension was stored at -80°C, and used for electroporation.

### Electroporation

Plasmid DNA of 500ng concentration was added into 200µL electrocompetent cells and mixed properly. pDNA-cell mix was transferred into ice cold 1mm-electroporation cuvette. The electroporation cuvette was placed in the electroporator which was set to 2.5kV; 150ohms; 22µF module and press pulse. Immediately 1mL of SB media was added into it and incubated at 37°C on shaker incubator for 1h. Subsequently, 100µL of cell suspension was plated on SB plates with kanamycin and gentamicin, and incubated at 37°C for 36h.

## 5.2.8 Plasmid isolation from *C. albicans*

Plasmid was isolated using Qiagen plasmid isolation midi prep kit. Plasmid was isolated using Qiagen plasmid isolation midi prep kit The protocol followed was as specified by the manufacturer (Qiagen plasmid midi kit) Plasmid used for further contained kanamycin and gentamicin resistance genes and was 10Kb in size.

### 5.2.9 Cell viability and growth kinetics

Cell viability studies were carried out on modified-fHAPs using MTT (Riss et al. 2015) and Resazurin assay (Riss et al. 2015; Sarker et al. 2007) in 24 well plates. Exponentially growing *C. albicans* cells were inoculated with  $5 \times 10^5$  cells/well in SB Cells were exposed to various concentrations (10, 100, 500 and 1000  $\mu\text{g/mL}$ ) of the NPs dispersed in PBS, and incubated for 12, 24 and 36h. MTT (20  $\mu\text{L}$  of 5mg/mL) was added to the test samples, and the plates were incubated at 37°C for 4h. The media was aspirated out carefully without disturbing the cells after 4h. For dissolving the formazan crystals, 150  $\mu\text{L}$  of DMSO was added, and the absorbance was measured at 570nm using UV-visible spectrophotometer. All measurements were carried out in triplicates. The relative cell viability (%) was calculated as described in section 3.2.1.1 using equation (6).

Similar protocol was followed for Resazurin assay, where resazurin dye (10  $\mu\text{L}$  of 5mg/mL) was added to the test samples after respective time intervals mentioned above, the plates were further incubated at 37°C for 4h, and absorbance was measured at 560nm using UV-visible spectrophotometer (UV-2450, Shimadzu, Japan). The relative cell viability (%) was calculated as mentioned above.

For growth kinetic studies, *C. albicans* cells were grown in presence of various concentrations of modified fHAPs (10, 50, 100, 500, 1000  $\mu\text{g/mL}$ ). An aliquot of 1mL was withdrawn every 5h, till 45<sup>th</sup>h, and the optical density was recorded at 600nm on a UV-visible spectrophotometer (UV-2450, Shimadzu, Japan). The growth kinetics parameters such as maximum specific growth rate ( $\mu_{\text{max}}$ ;  $\text{h}^{-1}$ ) and doubling time ( $t_d$ ; min) were determined according to Berney et al., and Breidt et al (Berney et al. 2006; Breidt et al. 1994). *C. albicans* cells grown in the absence of modified HAP NPs served as the positive control.

### 5.2.10 Statistical analysis

Statistical analysis was carried out as described in 3.2.5.

## 5.3 Results and discussion

### 5.3.1 Synthesis and characterization

Currently, hydroxyapatite nanoparticles (HAp NPs) are being extensively studied as a gene vector due to its favorable characteristics such as biocompatibility, gene binding efficiency, biological stability and ease of synthesis (Zhu et al. 2004). Synthesis of functionalized HAp NPs with various amino acids (arginine, lysine, valine, etc.) or PEG for gene, drug delivery and other biomedical applications has been reported earlier (Gonzalez-McQuire et al. 2004; Matsumoto et al. 2002; Venkatasubbu et al. 2013; Zhang et al. 2013). In chapter 4, we have synthesized arginine glucose functionalized fHAp to use it as a vehicle for pDNA delivery in Gram-positive and Gram-negative bacteria. Herein, we have synthesized fHAp functionalized with arginine (R), glucose (G) and polyethylene glycol (PEG) molecules at room temperature using modified sol gel method for pDNA transformation into yeast cells. fHAp were functionalized with arginine a positively charged amino acid, glucose and PEG with the idea that arginine could enhance positive charge and hence binding of pDNA, glucose an essential carbon source for growth will enhance the uptake of NPs-pDNA complex, and PEG could help pDNA to bind on the surface of yeast cells and enhance the transformation efficiency (Chen et al. 2008a; Gietz and Schiestl 2007a). The concept of PEGylation of NPs to increase cellular uptake has been explored for variety of applications such drug delivery, gene delivery and bioimaging (Andreani et al. 2014; Jokerst et al. 2011; Xiao et al. 2011). R-G-PEG-fHAp are referred as a “modified-fHAp” in the following text. The XRD spectra (Figure 5.1a) of these NPs corresponded well with the hexagonal HAp structure, indicating that the obtained compounds were well crystallized HAp (ICDD 09-0432). The XRD patterns of the modified fHAp were similar to that of

fHAp, showing characteristic HAp peaks. The XRD peaks of the unfunctionalized and functionalized fHAp were similar showing characteristic peaks at 25.8, 31.34, 31.95 and 33.972 corresponding to [002], [211], [112] and [300], respectively. The FTIR studies were carried out to identify the various functional groups associated with fHAp and the amino acids (Figure 5.1b). The signature HAp peaks were recorded in both fHAp and modified fHAp, band at  $\sim 600\text{cm}^{-1}$  are attributed to the bending modes of P-O bonds in phosphate groups, with contribution from the -OH of the apatite group at  $\sim 605\text{cm}^{-1}$ . The bands in the region  $3400\text{cm}^{-1}$  are attributed to -OH bonds and those observed near  $\sim 3571\text{cm}^{-1}$  are associated with -OH stretching vibration of HAp (Ramanan and Venkatesh 2004). In modified-fHAp,  $\text{NH}_2$ , amide I, -CH and C-O-C stretching bands corresponding to arginine, glucose and PEG were also observed near  $\sim 1448$ ,  $\sim 1644$ ,  $\sim 2943$  and  $\sim 1100$  respectively (Gonzalez-McQuire et al. 2004; Matsumoto et al. 2002; Venkatasubbu et al. 2013; Zhang et al. 2013). Morphology of fHAp and modified-fHAp was studied using TEM. fHAp, and modified-fHAp exhibited similar thin rod morphology with average length of 62.5nm and diameter of 6.2nm (Figure 5.1c). Similar observations were noted by few researchers wherein there was no change in particle size and morphology upon functionalization of fHAp with arginine/PEG. There was no change in particle size and shape of arginine functionalized fHAp which is attributed to the side chain of amino acid (Dong et al. 2013; Liuyun et al. 2015; Wang et al. 2015; Yan-Zhong et al. 2011).

Modification with PEG changed particle size; average length was increased from 62.5 to 72.7nm and diameter from 6.2 to 8.3nm. Increase in particle size as a result of PEGylation is dependent on the molecular weight of PEG molecule. PEGylation with high molecular weight PEG contributes towards a larger increase in size as compared to low molecular weight PEG, and is attributed to the length of the PEG chain (Anbarasu et al. 2015; Andreani et al. 2014; Manson et al. 2011; Pelaz et al. 2015). In this study, PEGylation was carried out using



PEG of low molecular weight of 6000kDa hence increase in size was negligible (Figure 5.1c).

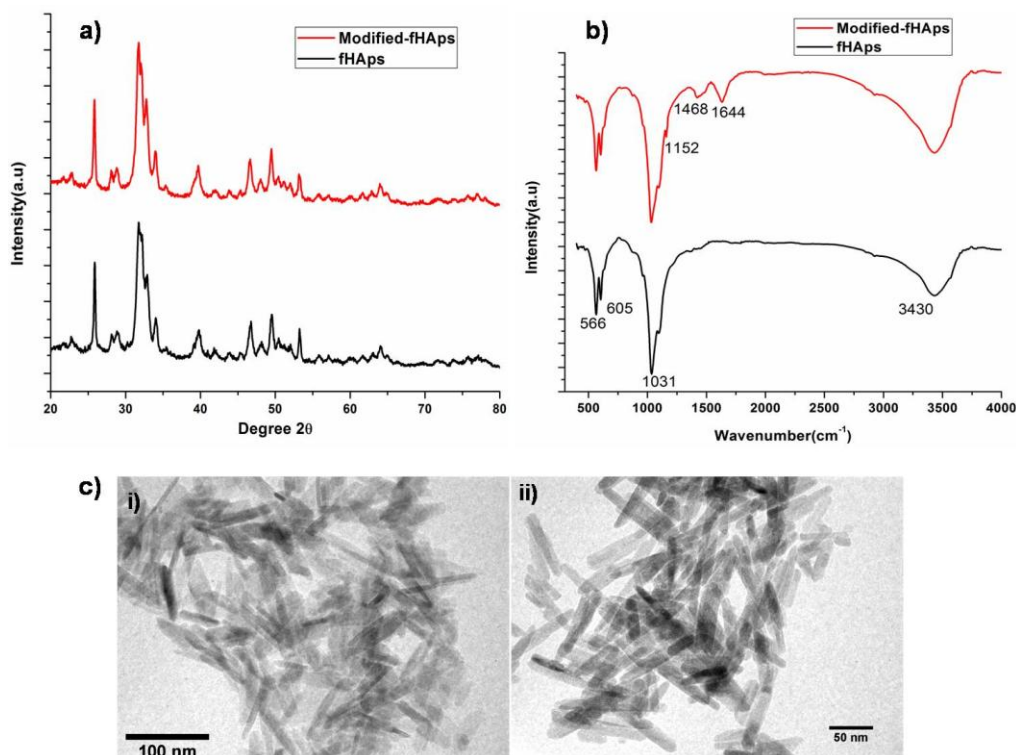


**Figure 5.1** a) XRD pattern b) FTIR spectra and c) TEM micrographs of fHAp and modified-fHAp. Characteristic XRD peaks of fHAp were observed in all the samples. FTIR spectra showed characteristic bands of HAp, amide I, amide II, NH<sub>2</sub> glucose and PEG. TEM morphology observed was same for modified-fHAp with average length and diameter of 72.7nm and 8.3nm.

Zeta potential measurements of all the fHAp were carried out to measure the surface charge. An increase in the zeta value from  $\sim +13.25$ mv to  $\sim +72$ mv, was noted after functionalization. Increase in zeta potential after functionalization of HAp with arginine from  $\sim +13.25$ mv to  $\sim +64$  is demonstrated in 4.3.2. PEG functionalization has increased positive zeta potential from  $\sim +64$  to  $\sim +72$ , this could be attributed to binding of OH<sup>-</sup> ions of PEG to fHAp such that the positively charged H<sup>+</sup> ions are exposed at the NP/solvent interface thereby increasing the positive charge at the surface. Decrease in negative surface

charge after functionalization with PEG has been observed in many NPs such as gold, silica and  $\text{Fe}_3\text{O}_4$  NPs (Anbarasu et al. 2015; Andreani et al. 2014; Manson et al. 2011).

### 5.3.2 Binding efficiency of pDNA binding to modified-fHAp

Binding of pDNA to NPs is essential to use modified-fHAp as pDNA vehicle for yeast transformation. Hence, we studied the binding efficiency (B.E) of pDNA with modified-fHAp (as described in materials and methods). B.E of modified-fHAp was significantly higher ( $p < 0.05$ ) than fHAp and attributed to more positive charge on the surface due to arginine and PEG functionalization which enhanced the pDNA binding. B.E of pDNA to modified-fHAp was  $< 70\%$  when NPs:pDNA was 10:1 and 30:1, it increased to  $\sim 93.6\%$  when NP:pDNA was 50:1, 70:1 and 100:1 (Figure 5.2a). This clearly indicates that the loading capacity of pDNA onto the NPs is dependent on NPs concentration and is critical in controlling transformation efficiency. Binding of pDNA to modified-fHAp was confirmed by running these complexes on agarose electrophoresis gel. As shown in Figure 5.2b, lane i-v shows pDNA–modified-fHAp complex when mass ratios of modified-HAp to pDNA were 10:1, 30:1 50:1, 70:1, and 100:1 respectively demonstrating pDNA have bound with modified-fHAp.

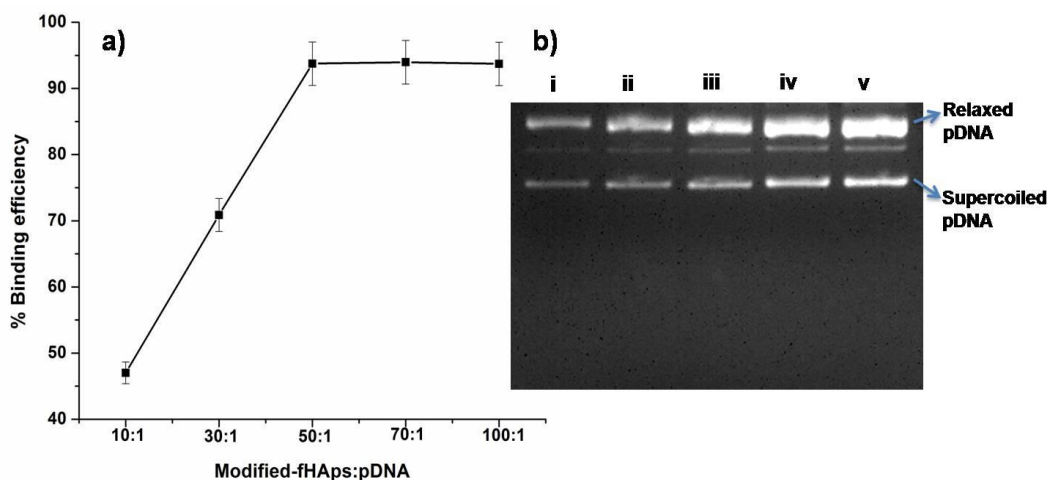


**Figure 5.2** a) Binding efficiencies of modified-fHAp:pDNA of various ratios b) Image of agarose gel electrophoresis confirming binding of pDNA to modified-fHAp. Lane i-v shows modified-fHAp-pDNA complex when weight ratios of modified-fHAp:pDNA were 10:1, 30:1, 50:1, 70:1 and 100:1 respectively.

### 5.3.3 Stability of modified-fHAp-pDNA complex

Modified-fHAp-pDNA complex needs to be stable for the transformation process. Therefore, we determined stability of complexes at various temperatures, pH and towards sonication-induced stress. It was noted that modified-fHAp-pDNA complexes were stable in the temperature of range 37 to 90°C. As can be seen from gel image (Figure 5.3a), lane i-v shows modified-HAp NPs-pDNA complex after incubating it at different temperatures of 37, 60, 80, 90°C and room temperature respectively. It was observed that modified-HAp-pDNA complexes were stable and pDNA remained intact even after 30 days at room temperature (Figure 5.3b, lane i). Complexes were also stable in buffer of pH 6, 7, 9 and 11 (Figure 5.3c, lane i-iv respectively). The complex dissolved in buffer of pH 4 and below, and no band for modified-fHAp-pDNA complex was observed (Lane v; Figure 5.3c). This was due to dissolution property of HAp in acidic pH of ~4-5 (Thomann 1990, Suchanek 1998; LeGeros2002). There was no effect of sonication-induced stress on modified-fHAp-pDNA complex (Figure

5.3d). Lane i-v of Figure 5.3d shows modified-fHAp-pDNA complexes after placing them in Sonication bath for 0, 2, 5, 10 and 30s respectively.

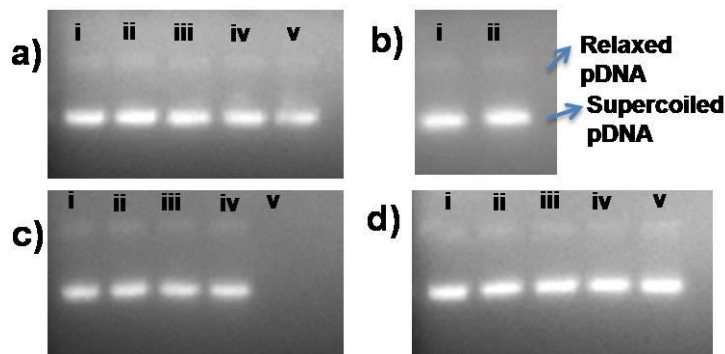


**Figure 5.3** Image of agarose gel electrophoresis, demonstrating stability of modified-fHAp-pDNA complex a) in the temperature of 37(lane i), 60 (lane ii), 80 (lane iii), 90°C (lane iv) and room temperature(lane v) b) at room temperature for 30 days (lane i- control modified-fHAp-pDNA complex, ii- complex after 30 days) c) in buffer of pH 4 (lane v), 6 (lane i), 7 (lane ii), 9 (lane iii) and 11 (lane iv) d) in sonication-induced stress for 0 (lane i), 2 (lane ii), 5 (lane iii), 10 (lane iv) and 30s (lane v).

### 5.3.4 Yeast Transformation

Presently, delivery of nucleic acid in yeast cells is vital process to produce modified yeast species for the production of many industrial and biopharmaceutical products such as vaccines, certain enzymes like insulin, human serum albumin, etc. Herein, arginine, glucose and PEG functionalized (modified-fHAp) were used to transform pDNA using *C. albicans* as the model organism. In this work, we have chosen *C. albicans* as model yeast organism to develop efficient process of transformation without preparation of competent cells using modified-fHAp as pDNA delivery vehicle. Transformation method was carried out at various ratios of modified-fHAp:pDNA (0:1, 10:1, 30:1, 50:1, 70:1 and 100:1), using SB and M.M media, to obtain the optimum ratio where T.E is maximum. T.E obtained using all the above ratios are presented in Table 5.1.

In M.M media, the T.E. at NPs:pDNA ratio of 10:1, was  $10^3$  cfu/ $\mu$ g, which increased with increase in NPs:pDNA ratio up to 70:1 at which the T.E. was  $10^6$  cfu/ $\mu$ g, and remained constant at 100:1. Similarly in SB media obtained T.E at a ratio of 10:1 was 37 cfu/ $\mu$ g which increased to  $10^4$  cfu/ $\mu$ g at 70:1 and remained constant thereafter. Higher T.E in MM as compared to SB could be attributed to aggregation of modified fHAp-pDNA complex in SB media due to abundance of micromolecules which absorb onto NPs-pDNA complex resulting in increased inter-particle interaction (Moore et al. 2015; Rausch et al. 2010).

Further, we carried out transformation in *C. albicans* by fHAp, R-G-fHAp as the vehicle at NP:pDNA ratio of 70:1 using SB and M.M, and commonly used electroporation method to compare T.E with modified-fHAp. Transformation efficiencies (T.E) obtained using all the above methods are presented in Table 5.2. T.E obtained using fHAp, R-G-fHAp and modified fHAp as vehicle in M.M was significantly ( $p < 0.05$ ) higher than with LB media. T.E. using NPs as vehicle were in the order of modified-fHAp > R-G-fHAp > fHAp. Arginine and glucose functionalization of HAp NPs exhibited 10 times increase in T.E compared to HAp NPs. Similar observation was noted during transformation of Gram-positive and Gram-negative bacteria using R-G-fHAp (4.3.5). The functionalization of R-G-fHAp with PEG had a positive effect on T.E of *C. albicans*, which resulted in 10 and 1000 times increase in T.E as compared to the R-G-fHAp and fHAp, respectively both with M.M/SB media (Table 5.2). The T.E of *C. albicans* using modified-fHAp in M.M was 1000 times higher than electroporation method (carried out in SB media). To the best of our knowledge, this is the first report on surface modification of fHAp with glucose, arginine and PEG as a nanovehicle for transformation of pDNA in *C. albicans* (Figure 5.4 and Table 5.2). It has been reported that functionalization of NPs with PEG prevents agglomeration and surface oxidation rendering them more biocompatible (Manson et al. 2011; Venkatasubbu et al. 2013). PEG has also been used with LiAc method to achieve high transformation efficiency in *Saccharomyces cerevisiae* (Gietz and Schiestl 2007a; Gietz et al. 1995; Gietz and Woods 2006). Fluorescence

microscopy studies of pDNA transformation using LiAc method have shown that pDNA was able to bind to yeast cell surface only in the presence of PEG. No transformants were obtained in the absence of PEG (Chen et al. 2008a). In the present study, modified-fHAPs transformed pDNA into *C. albicans* without the requirement for preparation of competent cells; this helps yeast cells to remain intact and is beneficial for the easy recovery of transformed cells.



**Figure 5.4** Transformed *C. albicans* on kanamycin and gentamicin containing SB agar plates. It was transformed using modified-fHAPs without preparation of competent cells.

**Table 5.1:** Transformation efficiencies of *C. albicans* obtained using modified-fHAPs of various NP:pDNA ratio.

| Modified-fHAPs:pDNA | T.E of <i>C. albicans</i> (cfu/ $\mu$ g) |                 |
|---------------------|--|-----------------|
|                     | M.M                                      | SB              |
| 0:1                 | 0  | 0               |
| 10:1                | $10^3$                                   | 37              |
| 30:1                | $6 \times 10^4$                          | $7 \times 10^2$ |
| 50:1                | $2 \times 10^5$                          | $10^3$          |
| 70:1                | $3 \times 10^6$                          | $10^4$          |
| 100:1               | $5 \times 10^6$                          | $3 \times 10^4$ |

**Table 5.2:** Transformation efficiencies of *C. albicans* obtained using nanoparticles mediated (fHAp, R-G-fHAp, modified-fHAp), and electroporation method.

|                 | T.E of <i>C. albicans</i> (cfu/ $\mu$ g) |        |
|-----------------|--|--------|
|                 | M.M                                      | SB     |
| Modified-fHAp   | $3 \times 10^6$                          | $10^4$ |
| R-G-fHAp        | $10^5$                                   | $10^3$ |
| fHAp            | $6 \times 10^3$                          | 70     |
| Electroporation | $5 \times 10^2$                          | $10^3$ |

### 5.3.5 Plasmid isolation from transformed *C. albicans*

Plasmid DNA was isolated from transformed *C. albicans* colonies cultured on SB plates containing kanamycin and gentamicin to confirm the transformation using modified-HAp NPs. Figure 5.5 shows the agarose gel image of pDNA isolated from *C. albicans* transformed using modified-fHAp. There was no difference between pDNA isolated from transformed *C. albicans* and control pDNA confirming the transformation.

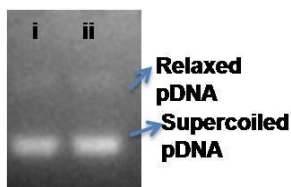


**Figure 5.5** Agarose gel image of pDNA i) isolated from *C. albicans* transformed using modified-fHAp ii) control pDNA.

### 5.3.6 Cell toxicity and Growth kinetics

Non-toxicity of nanomaterial towards yeast cells is an essential requisite to use it as a successful vehicle for transformation. To determine the effect of modified-

fHAPs on viability of *C. albicans*, time and dose dependent studies were carried out using MTT and Resazurin assays (Figure 5.6a and b). There was no significant difference ( $p>0.05$ ) between the cell viability of cells treated with modified-fHAPs as compared to untreated control at various concentrations (10, 50, 100, 500 and 1000 $\mu\text{g}/\text{mL}$ ) for *C. albicans*, indicating non-toxicity of NPs (Figure 5.6a). Similar results were obtained with Resazurin assay further confirming the non-toxic nature of NPs (Figure 5.6b).

*C. albicans* was treated with different concentrations of modified-fHAPs (10, 50, 100, 500 and 1000 $\mu\text{g}/\text{mL}$ ) for various time intervals to study the effect of NPs on the growth profile. The growth profile of *C. albicans* treated with modified-fHAPs at all the concentrations (10-1000 $\mu\text{g}/\text{mL}$ ) was similar to that of the control (without NPs) (Figure 5.6c). Growth kinetics parameters like maximum specific growth rates and doubling times were also calculated (Table 5.2). There was no significant difference ( $p>0.05$ ) between growth parameters of yeast cells grown in presence of modified-fHAPs and control (without NPs). Maximum specific growth rate and doubling time for *C. albicans* in presence of 1000 $\mu\text{g}/\text{mL}$  modified-fHAPs were 0.513 $\text{h}^{-1}$  and 81min, while in the control (without NPs) it was 0.524 $\text{h}^{-1}$  and 79.35min, respectively (Table 5.2). All these studies show that modified-fHAPs are non toxic and could be used as a potential plasmid DNA delivery vehicle for yeast cells.

**Table 5.3:** Growth kinetics parameters of *C. albicans* at different concentrations of modified-fHAPs.

| Concentrations | <i>C. albicans</i>                               |                              |
|----------------|--|------------------------------|
|                | Specific growth rate ( $\mu$ : $\text{h}^{-1}$ ) | Doubling time ( $t_d$ : min) |
| Control        | 0.524  | 79.35                        |
| 10             | 0.520  | 79.96                        |
| 50             | 0.516  | 80.581                       |
| 100            | 0.515  | 80.737                       |
| 500            | 0.515  | 80.737                       |
| 1000           | 0.513  | 81                           |



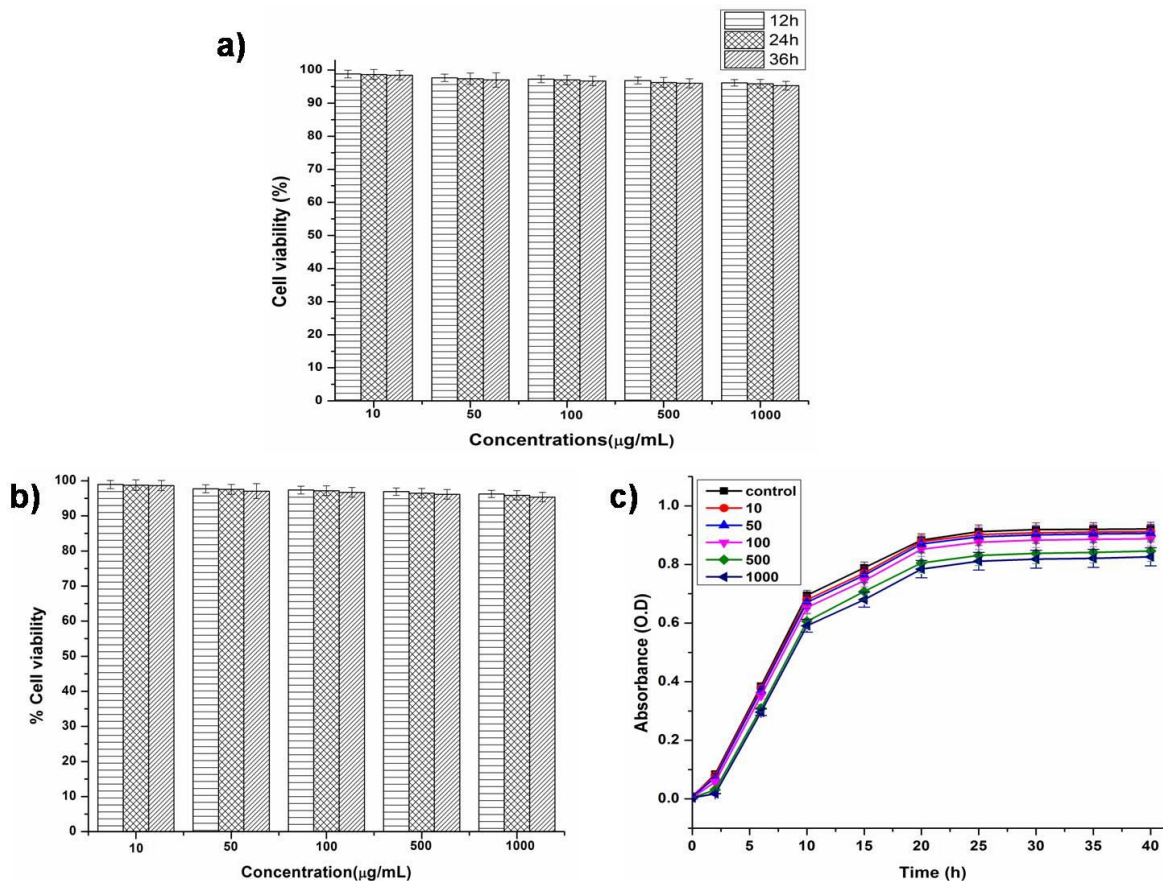


**Figure 5.6** a) MTT and b) Resazurin data showing non-toxic nature of modified-HAp NPs on *C. albicans* after 12, 24 and 36h of growth. c) Growth curve showing no effect on growth profile in presence of 10 to 1000µg/mL modified-fHApS

#### 5.4 Conclusion

This study, demonstrated that modified-fHApS can serve as a vehicle for plasmid transformation in *C. albicans*. Functionalization of fHApS with the positively charged amino acid, arginine, and PEG increased the zeta potential as well as binding efficiency of the nanovehicle to pDNA. Modified-fHApS resulted in high binding efficiency (93%) and successful transformation in *C. albicans* with a T.E. of  $10^6$ cfu/µg. This nanovehicle delivery system does not require preparation of competent cells and is also non-toxic to yeast cells. This new method could provide exciting opportunities to advance the applications of yeast in the field of biotechnology.

## **Summary of Results and Conclusion**

The present work was carried out with the aim of synthesizing hydroxyapatite nanoparticles (NPs) with self activating fluorescence property for bioimaging, and gene delivery applications. A new class of HAp NPs with varied aspect ratios was synthesized at room temperature by a modified sol-gel method. Solvents and stabilizing agents played an important role in obtaining HAp with different morphologies such as rods, thin rods, short rods and microrods. Triethyl amine (TEA) or acetyl acetone (ACA) were used as stabilizing agents with either water or dimethyl sulfoxide (DMSO) as the solvent. Water and DMSO were selected as solvents based on the differences in their polarities, which would eventually influence the interactions among the calcium ions resulting in varied morphologies. TEA (as basic) and ACA (as acidic) were used to study the effect of basic and acidic stabilizing agents on the shape and size of HAp NPs.

Synthesized HAp NPs were characterized using X-ray diffraction (XRD), Fourier transform infrared (FTIR), Raman spectroscopy, transmission electron microscopy (TEM), energy dispersive analysis of X-ray (EDAX), zeta potential measurement, photoluminescence spectroscopy and electron spin resonance (ESR) were used to characterize these NPs. The phase purity and crystallinity of samples were determined using XRD analysis. Although, the XRD spectra, of all the synthesized HAp corresponded well with the hexagonal HAp crystal (ICDD 09-0432), relative intensities of characteristic HAp peaks varied between samples. This could be due to the possible variation in the orientation of growth under different synthesis conditions. In FITR spectra, characteristic functional groups associated with HAp were exhibited in all the HAp samples. Vibrational, rotational and low frequency modes in HAp samples were determined by Raman spectroscopy. Elemental composition of all synthesized HAp as determined by EDAX confirmed the presence of calcium (Ca), phosphorous (P) and oxygen (O). Morphologies of samples were confirmed using TEM analysis and exhibited rod morphology with various aspect ratios. It was observed that NPs synthesized

using water as a solvent and TEA as a stabilizing agent, were rod shaped with average length of 92.8nm and average diameter of 23.2nm. The shapes changed to short rods with an average length 35nm and an average diameter 7nm when DMSO was used as a solvent keeping TEA as the stabilizing agent. Thin rods of average length 62.5nm and diameter 6.2nm were obtained when the stabilizing agent was changed to ACA while maintaining DMSO as the solvent. When water was used as the solvent and ACA as the stabilizing agent, the particles obtained were irregular shaped with mixed morphologies. In the absence of either of the stabilizing agents, HAp microparticles of rod shape with an average length 1.42 $\mu$ m and diameter 0.29 $\mu$ m were formed. This demonstrated the role of stabilizing agent in controlling nucleation and growth, which resulted in different sizes of rods. Zeta potential value of HAp NPs showed higher positive value when ACA was used as a stabilizing agent and this could be attributed to the acidic nature of ACA contributing a positive surface charge.

HAp is not known to be a fluorescent material; however, in this study all the HAp NPs synthesized using TEA/ACA as stabilizing agents and water/DMSO as solvents at room temperature by modified sol-gel method exhibited broad emission spectrum ranging from 350-750nm with maximum at 502nm and additional peaks at 528nm, 567nm and 609nm on excitation at 325nm. The emission spectra of all self activated fluorescent HAp NPs(fHAPs) synthesized were similar, but with significant changes in the intensity of fluorescence signal, which was in the order thin rod > short rod > rod > microrods. Amongst all fHAPs, thin rods exhibited highest fluorescence intensity and the intensity decreased with decreasing aspect ratio. All fHAPs exhibited large Stokes' shift of 177nm, which is a desirable property to minimize overlap between absorption and emission spectra. Self activated fluorescence property of HAp NPs is most probably associated with the electronic transitions arising due to asymmetric structure of the NPs as all of them have elongated morphology. Microrods were in micrometer size therefore were omitted for further studies.

The thin rod, short rod and rod shaped fHApS did not exhibit any cytotoxic effect and reactive oxygen species (ROS) generation as was confirmed by 3-(4,5-dimethylthiazol-2-yl)-2,5-diphenyltetrazolium bromide (MTT), lactate dehydrogenase (LDH) and ROS assays in human cervical cancer (HeLa) and keratinocyte (HaCaT) cells. These NPs were also hemocompatible and able to retain fluorescence properties in biological media such as Dulbecco's modified Eagle's Medium and phosphate buffer saline. This indicated that fluorescence of fHApS is not dependent on the environment, and is rather an intrinsic property of the NPs. Moreover, these NPs exhibited excellent internalization by both eukaryotic and prokaryotic cells such as HeLa, bone osteosarcoma cells (MG63), HaCaT, *Escherichia coli* (*E. coli*), *Staphylococcus aureus* (*S. aureus*) and *Candida albicans* (*C. albicans*) without causing any cytotoxicity. These multifunctional NPs provide exciting opportunities in the field of bio-medical sciences, making it possible to carry out both imaging and treatment in conjunction.

Another aim of this study was to develop one step plasmid transformation process for eukaryotic and prokaryotic systems. To achieve transformation binding of plasmid DNA (pDNA) to NPs is necessary. Therefore, binding efficiency of pDNA to thin rod, short rod and rod shaped fHApS was estimated. Thin rod fHApS exhibited maximum binding efficiency to pDNA compared to short rod and rod shaped fHApS. Therefore, thin rod fHApS were selected for functionalization with positively charged amino acids (arginine(R)/lysine(K)/histidine(H)) which enhanced the zeta potential as well as binding efficiency to pDNA. Arginine functionalization resulted in highest binding efficiency (B.E = 90%) and successful transformation in *E. coli* and *S. aureus*-prokaryotic cells. Arginine functionalized fHApS (R-fHApS) were further functionalized with glucose to increase transformation efficiency (T.E) as glucose is major carbon source for bacteria. These functionalized fHApS exhibited all characteristic peaks of HAp in XRD and size observed using TEM was similar to unfunctionalized control fHApS. FTIR spectra exhibited additional glucose and

amino acid peaks with HAp characteristic peaks. Glucose functionalization of R-fHAp exhibited similar B.E as compared to that of R-fHAp; however T.E obtained increased 1000 fold in both *E. coli* and *S. aureus*. To study the effect of media on T.E, transformation was carried out using two different media i.e., minimal medium (M.M) and complex Luria-Bertani (LB) medium. T.E of *E. coli* in M.M and LB were  $10^9$ cfu/ $\mu$ g and  $10^7$ cfu/ $\mu$ g, respectively, using R-G-fHAp as pDNA vehicle. Similarly, for *S. aureus*, T.E in M.M and LB were  $10^7$ cfu/ $\mu$ g and  $10^5$  cfu/ $\mu$ g, respectively.

R-G-fHAp were further functionalized with polyethylene glycol (modified-fHAp) to use it as a pDNA vehicle for *C. albicans* transformation. PEG functionalization helped pDNA to bind on the surface of yeast cells and enhanced the T.E of *C. albicans*. Modified-fHAp exhibited characteristic HAp peaks in XRD and FTIR spectra. The FTIR spectra additionally exhibited glucose, arginine and PEG peaks. The average particle length of modified-fHAp was increased from 62.5 to 72.7nm and diameter from 6.2 to 8.3nm as compared to that of R-G-HAp NPs which may be attributed to the PEG functionalization. These NPs also exhibited an enhanced pDNA binding efficiency of 93.5% as compared to R-G-fHAp. T.E in *C. albicans* using modified-fHAp was carried out using M.M and Sabouraud broth (SB). T.E achieved in M.M and SB was  $10^6$  cfu/ $\mu$ g and  $10^4$  cfu/ $\mu$ g, respectively.

The advantages of the HAp NPs based nanovehicle delivery system reported in the study are: i) it does not require preparation of competent cells; ii) can be carried out at room temperature; iii) high transformation efficiency in Gram-positive and Gram-negative bacteria, and yeast cells ; iv) non toxic nature of the NPs. This novel method can provide exciting opportunities in the field of recombinant DNA technology.

Thus, some of the important conclusions that may be drawn from present work are as follows:

1. This is the first study to demonstrate synthesis of new class of non-toxic, self-activated fluorescent HAp NPs with different aspect ratios (thin rods, short rods, rods) by changing the stabilizing agents and solvents.
2. The presence of fluorescence was due to the electronic transition in the asymmetric structure (rod morphology) of HAp NPs.
3. The self activated fluorescent HAp NPs exhibited an emission maximum in the visible range with large stroke shift and excellent internalization by prokaryotic and eukaryotic cells, which make these particles excellent candidates for bioimaging applications.
4. This is first report on development of a one step method of plasmid DNA transformation for Gram-positive, Gram-negative bacterial cells and yeast cells using functionalized HAp NPs.

It is evident from the above information, that the present work reports several new findings and highlights the fact that HAp NPs synthesized at room temperature may find application either as efficient bioimaging agent or gene delivery vehicle in prokaryotic and eukaryotic cells.

### Future scope of work

1. This study demonstrates the room temperature synthesis of hydroxyapatite nanoparticles (HAp NPs) with rod shape morphology of different aspect ratios. In future, use of different stabilizing/capping agents and/or solvents would enable synthesis of uniformly distributed, stable, non-aggregating HAp NPs with varied morphologies.
2. The HAp NPs obtained during course of this work exhibited excellent self-activated fluorescence and *in-vitro* internalization by prokaryotic and eukaryotic cells. These non-toxic NPs could be modified with various tagging ligands/antibodies and used as a site directed bioimaging agent for *in-vitro/in-vivo* applications.
3. The functionalized HAp NPs synthesized in this work is used as a vehicle for delivery of plasmid DNA for transformation of yeast, Gram-positive and Gram-negative bacterial cells. These NPs may be further explored for transformation in plant systems or for *in-vivo* gene delivery applications.

## References

- Abdelghany SM, Quinn DJ, Ingram RJ, Gilmore BF, Donnelly RF, Taggart CC, Scott CJ (2012) Gentamicin-loaded nanoparticles show improved antimicrobial effects towards *Pseudomonas aeruginosa* infection. *Int J Nanomedicine* 7:4053-63 doi:10.2147/IJN.S34341
- Adrio J-L, Demain AL (2010) Recombinant organisms for production of industrial products. *Bioengineered bugs* 1:116-131
- Akbarzadeh A, Rezaei-Sadabady R, Davaran S, Joo SW, Zarghami N, Hanifehpour Y, Samiei M, Kouhi M, Nejati-Koshki K (2013) Liposome: classification, preparation, and applications. *Nanoscale research letters* 8:1-9
- Albrecht C, Scherbart AM, van Berlo D, Braunbarth CM, Schins RP, Scheel J (2009) Evaluation of cytotoxic effects and oxidative stress with hydroxyapatite dispersions of different physicochemical properties in rat NR8383 cells and primary macrophages. *Toxicology in vitro* 23:520-530
- Alivisatos AP (1996) Semiconductor clusters, nanocrystals, and quantum dots. *Science* 271:933
- Altinog˘lu EI, Russin TJ, Kaiser JM, Barth BM, Eklund PC, Kester M, Adair JH (2008) Near-infrared emitting fluorophore-doped calcium phosphate nanoparticles for in vivo imaging of human breast cancer. *ACS Nano* 2:2075-2084
- Anbarasu M, Anandan M, Chinnasamy E, Gopinath V, Balamurugan K (2015) Synthesis and characterization of polyethylene glycol (PEG) coated Fe<sub>3</sub>O<sub>4</sub> nanoparticles by chemical co-precipitation method for biomedical applications. *Spectrochimica Acta Part A: Molecular and Biomolecular Spectroscopy* 135:536-539



- André R, Paris E, Gurgel M, Rosa I, Paiva-Santos C, Li M, Varela JA, Longo E (2012) Structural evolution of Eu-doped hydroxyapatite nanorods monitored by photoluminescence emission. *Journal of Alloys and Compounds* 531:50-54
- Andreani T, de Souza ALR, Kiill CP, Lorenzón EN, Fangueiro JF, Calpena AC, Chaud MV, Garcia ML, Gremião MPD, Silva AM (2014) Preparation and characterization of PEG-coated silica nanoparticles for oral insulin delivery. *International journal of pharmaceutics* 473:627-635
- Arnaud M, Chastanet A, Débarbouillé M (2004) New vector for efficient allelic replacement in naturally nontransformable, low-GC-content, gram-positive bacteria. *Applied and environmental microbiology* 70:6887-6891
- Ashokan A, Menon D, Nair S, Koyakutty M (2010) A molecular receptor targeted, hydroxyapatite nanocrystal based multi-modal contrast agent. *Biomaterials* 31:2606-2616
- Aune TEV, Aachmann FL (2010) Methodologies to increase the transformation efficiencies and the range of bacteria that can be transformed. *Applied microbiology and biotechnology* 85:1301-1313
- Baddiel C, Berry E (1966) Spectra structure correlations in hydroxy and fluorapatite. *Spectrochimica Acta* 22:1407-1416
- Baker SN, Baker GA (2010) Luminescent carbon nanodots: emergent nanolights. *Angewandte Chemie International Edition* 49:6726-6744
- Ball M, Downes S, Scotchford C, Antonov E, Bagratashvili V, Popov V, Lo W-J, Grant D, Howdle S (2001) Osteoblast growth on titanium foils coated with hydroxyapatite by pulsed laser ablation. *Biomaterials* 22:337-347
- Bangham A (1993) Liposomes: the Babraham connection. *Chemistry and physics of lipids* 64:275-285

- Bastakoti BP, Hsu YC, Liao SH, Wu KCW, Inoue M, Yusa Si, Nakashima K, Yamauchi Y (2013) Inorganic–organic hybrid nanoparticles with biocompatible calcium phosphate thin shells for fluorescence enhancement. *Chemistry–An Asian Journal* 8:1301-1305
- Baughman RH, Zakhidov AA, de Heer WA (2002) Carbon nanotubes--the route toward applications. *science* 297:787-792
- Becker DM, Guarente L (1991) [12] High-efficiency transformation of yeast by electroporation. *Methods in enzymology* 194:182-187
- Benea L, Danaila E, Ponthiaux P (2015) Effect of titania anodic formation and hydroxyapatite electrodeposition on electrochemical behaviour of Ti–6Al–4V alloy under fretting conditions for biomedical applications. *Corrosion Science* 91:262-271
- Benzinger R, Kleber I, Huskey R (1978) Transfection of *Escherichia coli* Spheroplasts: Infectious Lambda Prophage DNA. *Journal of General Virology* 39:531-535
- Berg JM, Romoser A, Banerjee N, Zebda R, Sayes CM (2009) The relationship between pH and zeta potential of ~ 30 nm metal oxide nanoparticle suspensions relevant to in vitro toxicological evaluations. *Nanotoxicology* 3:276-283
- Berney M, Weilenmann H-U, Ihssen J, Bassin C, Egli T (2006) Specific growth rate determines the sensitivity of *Escherichia coli* to thermal, UVA, and solar disinfection. *Applied and environmental microbiology* 72:2586-2593
- Binnemans K (2009) Lanthanide-based luminescent hybrid materials. *Chemical reviews* 109:4283-4374

- Bisht S, Bhakta G, Mitra S, Maitra A (2005) pDNA loaded calcium phosphate nanoparticles: highly efficient non-viral vector for gene delivery. *International journal of pharmaceutics* 288:157-168
- Bol A, Meijerink A (2000) Doped semiconductor nanoparticles—a new class of luminescent materials? *Journal of Luminescence* 87:315-318
- Botstein D, Fink GR (2011) Yeast: an experimental organism for 21st Century biology. *Genetics* 189:695-704
- Boukamp P, Petrussevska RT, Breitkreutz D, Hornung J, Markham A, Fusenig NE (1988) Normal keratinization in a spontaneously immortalized aneuploid human keratinocyte cell line. *The Journal of cell biology* 106:761-771
- Bozkir A, Saka OM (2004) Chitosan-DNA nanoparticles: effect on DNA integrity, bacterial transformation and transfection efficiency. *Journal of drug targeting* 12:281-288
- Breidt F, Romick T, Fleming H (1994) A Rapid method for the determination of bacterial growth kinetics 1. *Journal of Rapid Methods & Automation in Microbiology* 3:59-68
- Briak-BenAbdeslam HE, Mochales C, Ginebra MP, Nurit J, Planell JA, Boudeville P (2003) Dry mechanochemical synthesis of hydroxyapatites from dicalcium phosphate dihydrate and calcium oxide: A kinetic study. *Journal of Biomedical Materials Research Part A* 67:927-937
- Bruellhoff K, Fiedler J, Möller M, Groll J, Brenner RE (2010) Surface coating strategies to prevent biofilm formation on implant surfaces. *Int J Artif Organs* 33:646-653
- Bünzli J-CG (2010) Lanthanide luminescence for biomedical analyses and imaging. *Chemical reviews* 110:2729-2755

- Bünzli J-CG, Eliseeva SV (2010) Basics of lanthanide photophysics Lanthanide Luminescence. Springer series of fluorescence 7:1-45
- Burda C, Chen X, Narayanan R, El-Sayed MA (2005) Chemistry and properties of nanocrystals of different shapes. Chemical reviews 105:1025-1102
- Butow RA, Henke RM, Moran JV, Belcher SM, Perlman PS (1996) [24] Transformation of *Saccharomyces cerevisiae* mitochondria using the biolistic gun. Methods in enzymology 264:265-278
- Cai Y, Liu Y, Yan W, Hu Q, Tao J, Zhang M, Shi Z, Tang R (2007) Role of hydroxyapatite nanoparticle size in bone cell proliferation. Journal of Materials Chemistry 17:3780-3787
- Cengiz B, Gokce Y, Yildiz N, Aktas Z, Calimli A (2008) Synthesis and characterization of hydroxyapatite nanoparticles. Colloids and Surfaces A: Physicochemical and Engineering Aspects 322:29-33
- Chai F, Hornez J-C, Blanchemain N, Neut C, Descamps M, Hildebrand H (2007) Antibacterial activation of hydroxyapatite (HA) with controlled porosity by different antibiotics. Biomolecular engineering 24:510-514
- Chan FK-M, Moriwaki K, De Rosa MJ (2013) Detection of necrosis by release of lactate dehydrogenase activity. Immune Homeostasis: Methods and Protocols 979:65-70
- Chatterjee S, Sarkar K (2014) Surface-functionalized gold nanoparticles mediate bacterial transformation: a nanobiotechnological approach. Biotechnology letters 36:265-271
- Chen F, Huang P, Zhu Y-J, Wu J, Cui D-X (2012) Multifunctional Eu<sup>3+</sup>/Gd<sup>3+</sup> dual-doped calcium phosphate vesicle-like nanospheres for sustained drug release and imaging. Biomaterials 33:6447-6455

- Chen F, Huang P, Zhu Y-J, Wu J, Zhang C-L, Cui D-X (2011) The photoluminescence, drug delivery and imaging properties of multifunctional Eu<sup>3+</sup>/Gd<sup>3+</sup> dual-doped hydroxyapatite nanorods. *Biomaterials* 32:9031-9039
- Chen G, Qiu H, Prasad PN, Chen X (2014) Upconversion nanoparticles: design, nanochemistry, and applications in theranostics. *Chemical reviews* 114:5161-5214
- Chen G, Zhao H, Rosei F, Ma D (2013) Effect of redox reaction products on the luminescence switching behavior in CePO<sub>4</sub>: Tb nanorods. *The Journal of Physical Chemistry C* 117:10031-10038
- Chen J-F, Wang Y-H, Guo F, Wang X-M, Zheng C (2000) Synthesis of nanoparticles with novel technology: high-gravity reactive precipitation. *Industrial & Engineering Chemistry Research* 39:948-954
- Chen P, Liu H-H, Cui R, Zhang Z-L, Pang D-W, Xie Z-X, Zheng H-Z, Lu Z-X, Tong H (2008a) Visualized investigation of yeast transformation induced with Li<sup>+</sup> and polyethylene glycol. *Talanta* 77:262-268
- Chen Q, Thouas GA (2015) Metallic implant biomaterials. *Materials Science and Engineering: R: Reports* 87:1-57
- Chen X, Deng C, Tang S, Zhang M (2007) Mitochondria-dependent apoptosis induced by nanoscale hydroxyapatite in human gastric cancer SGC-7901 cells. *Biological and Pharmaceutical Bulletin* 30:128-132
- Chen Y, Zheng X, Xie Y, Ding C, Ruan H, Fan C (2008b) Anti-bacterial and cytotoxic properties of plasma sprayed silver-containing HA coatings. *Journal of Materials Science: Materials in Medicine* 19:3603-3609

- Cheng F, Sun K, Zhao Y, Liang Y, Xin Q, Sun X (2014) Synthesis and characterization of HA/YVO 4: Yb 3+, Er 3+ up-conversion luminescent nano-rods. *Ceramics International* 40:11329-11334
- Chesnutt BM, Yuan Y, Buddington K, Haggard WO, Bumgardner JD (2009) Composite chitosan/nano-hydroxyapatite scaffolds induce osteocalcin production by osteoblasts in vitro and support bone formation in vivo. *Tissue Engineering Part A* 15:2571-2579
- Ciobanu CS, Iconaru SL, Chifiriuc MC, Costescu A, Le Coustumer P, Predoi D (2012) Synthesis and antimicrobial activity of silver-doped hydroxyapatite nanoparticles. *BioMed Research International* 2013:1-10
- Ciobanu CS, Popa CL, Predoi D (2014) Sm: HAp nanopowders present antibacterial activity against *Enterococcus faecalis*. *Journal of Nanomaterials* 2014:1-9
- Cohen SN, Chang AC, Hsu L (1972) Nonchromosomal antibiotic resistance in bacteria: genetic transformation of *Escherichia coli* by R-factor DNA. *Proceedings of the National Academy of Sciences* 69:2110-2114
- Coulter JA, Jain S, Butterworth KT, Taggart LE, Dickson GR, McMahon SJ, Hyland WB, Muir MF, Trainor C, Hounsell AR (2012) Cell type-dependent uptake, localization, and cytotoxicity of 1.9 nm gold nanoparticles. *Int J Nanomedicine* 7: 2673–2685
- Cowley A, Woodward B (2011) A healthy future: platinum in medical applications. *Platinum Metals Review* 55:98-107
- Daniel M-C, Astruc D (2004) Gold nanoparticles: assembly, supramolecular chemistry, quantum-size-related properties, and applications toward biology, catalysis, and nanotechnology. *Chemical reviews* 104(1):293-346

- Demain AL, Vaishnav P (2009) Production of recombinant proteins by microbes and higher organisms. *Biotechnology advances* 27(3):297-306
- Doat A, Fanjul M, Pelle F, Hollande E, Lebugle A (2003) Europium-doped bioapatite: a new photostable biological probe, internalizable by human cells. *Biomaterials* 24:3365-3371
- Dobrovolskaia MA, Clogston JD, Neun BW, Hall JB, Patri AK, McNeil SE (2008) Method for analysis of nanoparticle hemolytic properties in vitro. *Nano letters* 8:2180-2187
- Donelli G, Francolini I (2013) Efficacy of antiadhesive, antibiotic and antiseptic coatings in preventing catheter-related infections: review. *Journal of chemotherapy* 13: 595-606
- Dong S, Roman M (2007) Fluorescently labeled cellulose nanocrystals for bioimaging applications. *Journal of the American Chemical Society* 129:13810-13811
- Dong S, Tang Q, Long M, Guan J, Ye L, Li G (2013) The cooperative effect of p53 and Rb in local nanotherapy in a rabbit VX2 model of hepatocellular carcinoma. *International journal of nanomedicine* 8:3757-3768
- Dorozhkin SV (2007) Calcium orthophosphates. *Journal of materials science* 42:1061-1095
- Dunny GM, Lee LN, LeBlanc DJ (1991) Improved electroporation and cloning vector system for gram-positive bacteria. *Applied and environmental microbiology* 57:1194-1201
- Dykman L, Khlebtsov N (2011) Gold nanoparticles in biology and medicine: recent advances and prospects. *Acta Naturae* 3:34-55

- Elliott JC (2013) Structure and chemistry of the apatites and other calcium orthophosphates Elsevier 18: 1-186
- Ersek RA, Denton DR (1984) Silver-impregnated porcine xenografts for treatment of meshed autografts. *Annals of plastic surgery* 13:482-487
- Escudero A, Calvo ME, Rivera-Fernández S, De la Fuente JM, Ocaña M (2013) Microwave-assisted synthesis of biocompatible europium-doped calcium hydroxyapatite and fluoroapatite luminescent nanospindles functionalized with poly (acrylic acid). *Langmuir* 29:1985-1994
- Ettinger A, Wittmann T (2014) Fluorescence live cell imaging. *Methods in cell biology* 123:77-94
- Fathi M, Hanifi A (2007) Evaluation and characterization of nanostructure hydroxyapatite powder prepared by simple sol-gel method. *Materials letters* 61:3978-3983
- Felgner PL, Gadek TR, Holm M, Roman R, Chan HW, Wenz M, Northrop JP, Ringold GM, Danielsen M (1987) Lipofection: a highly efficient, lipid-mediated DNA-transfection procedure. *Proceedings of the National Academy of Sciences* 84:7413-7417
- Felgner PL, Ringold G (1989) Cationic liposome-mediated transfection. *Nature* 337:387-388
- Fernandez-Pradas J, Cleries L, Martinez E, Sardin G, Esteve J, Morenza J (2001) Influence of thickness on the properties of hydroxyapatite coatings deposited by KrF laser ablation. *Biomaterials* 22:2171-2175
- Ferraz M, Monteiro F, Manuel C (2004) Hydroxyapatite nanoparticles: a review of preparation methodologies. *Journal of Applied Biomaterials and Biomechanics* 2:74-80



- Feynman RP (1960) There's plenty of room at the bottom. *Engineering and science* 23:22-36
- Filyak Y, Finiuk N, Mitina N, Bilyk O, Titorenko V, Hrydzhuk O, Zaichenko A, Stoika R (2013) A novel method for genetic transformation of yeast cells using oligoelectrolyte polymeric nanoscale carriers. *Biotechniques* 54:35-43 doi:10.2144/000113980
- Fowler B (1974) Infrared studies of apatites. II. Preparation of normal and isotopically substituted calcium, strontium, and barium hydroxyapatites and spectra-structure-composition correlations. *Inorganic Chemistry* 13:207-214
- Freshney, R. I. (2005). *Culture of specific cell types*. John Wiley & Sons, Inc.
- Furuzono T, Walsh D, Sato K, Sonoda K, Tanaka J (2001) Effect of reaction temperature on the morphology and size of hydroxyapatite nanoparticles in an emulsion system. *Journal of materials science letters* 20:111-114
- Gadow R, Killinger A, Stiegler N (2010) Hydroxyapatite coatings for biomedical applications deposited by different thermal spray techniques. *Surface and Coatings Technology* 205:1157-1164
- Ge K, Zhang C, Jia G, Ren H, Wang J, Tan A, Liang X-J, Zang A, Zhang J (2015) Defect-Related Luminescent Mesoporous Silica Nanoparticles Employed for Novel Detectable Nanocarrier. *ACS applied materials & interfaces* 7:10905-10914
- Ge P, Selvin PR (2003) Thiol-reactive luminescent lanthanide chelates: part 2. *Bioconjugate chemistry* 14:870-876
- Ge X, Li C, Fan C, Feng X, Cao B (2013) Enhanced photoluminescence properties of methylene blue dye encapsulated in nanosized

- hydroxyapatite/silica particles with core-shell structure. *Applied Physics A* 113:583-589
- Gerigk M, Ehrenreich P, Wagner MR, Wimmer I, Reparaz JS, Torres CMS, Schmidt-Mende L, Polarz S (2015) Nanoparticle shape anisotropy and photoluminescence properties: Europium containing ZnO as a Model Case. *Nanoscale* 7:16969-16982
- Gerlier D, Thomasset N (1986) Use of MTT colorimetric assay to measure cell activation. *Journal of immunological methods* 94:57-63
- Gietz RD, Schiestl RH (2007a) High-efficiency yeast transformation using the LiAc/SS carrier DNA/PEG method. *Nature protocols* 2:31-34
- Gietz RD, Schiestl RH (2007b) Large-scale high-efficiency yeast transformation using the LiAc/SS carrier DNA/PEG method. *Nature protocols* 2:38-41
- Gietz RD, Schiestl RH, Willems AR, Woods RA (1995) Studies on the transformation of intact yeast cells by the LiAc/ss-DNA/PEG procedure. *Yeast* 11:355-360
- Gietz RD, Woods RA (2006) Yeast transformation by the LiAc/SS Carrier DNA/PEG method. *Yeast Protocol* 313:107-120
- Gleiter H (2000) Nanostructured materials: basic concepts and microstructure. *Acta materialia* 48:1-29
- Gonzalez-McQuire R, Chane-Ching J-Y, Vignaud E, Lebugle A, Mann S (2004) Synthesis and characterization of amino acid-functionalized hydroxyapatite nanorods. *Journal of Materials Chemistry* 14:2277-2281
- Gopi D, Indira J, Kavitha L (2012) A comparative study on the direct and pulsed current electrodeposition of hydroxyapatite coatings on surgical grade stainless steel. *Surface and Coatings Technology* 206:2859-2869

- Gopi D, Prakash VCA, Kavitha L, Kannan S, Bhalaji P, Shinyjoy E, Ferreira J (2011) A facile electrodeposition of hydroxyapatite onto borate passivated surgical grade stainless steel. *Corrosion Science* 53:2328-2334
- Goudarzi M, Batmanghelich F, Afshar A, Dolati A, Mortazavi G (2014) Development of electrophoretically deposited hydroxyapatite coatings on anodized nanotubular TiO<sub>2</sub> structures: corrosion and sintering temperature. *Applied Surface Science* 301:250-257
- Graeve OA, Kanakala R, Madadi A, Williams BC, Glass KC (2010) Luminescence variations in hydroxyapatites doped with Eu 2+ and Eu 3+ ions. *Biomaterials* 31:4259-4267
- Graham FL, van der Eb AJ (1973) A new technique for the assay of infectivity of human adenovirus 5 DNA. *Virology* 52:456-467
- Griffith F (1928) The significance of pneumococcal types. *Journal of Hygiene* 27:113-159
- Guo H, Miao X, Chen Y, Cheang P, Khor KA (2004) Characterization of hydroxyapatite–and bioglass–316L fibre composites prepared by spark plasma sintering. *Materials Letters* 58:304-307
- Han Y, Li S, Cao X, Yuan L, Wang Y, Yin Y, Qiu T, Dai H, Wang X (2014) Different inhibitory effect and mechanism of hydroxyapatite nanoparticles on normal cells and cancer cells in vitro and in vivo. *Scientific reports* 4:7131- 7140
- Han Y, Wang X, Dai H, Li S (2013) Synthesis and luminescence of Eu 3+ doped hydroxyapatite nanocrystallines: effects of calcinations and Eu 3+ content. *Journal of luminescence* 135:281-287
- Hanahan D, Jessee J, Bloom FR (1991) [4] Plasmid transformation of *Escherichia coli* and other bacteria. *Methods in enzymology* 204:63-113

- Hanaoka K, Kikuchi K, Kobayashi S, Nagano T (2007) Time-resolved long-lived luminescence imaging method employing luminescent lanthanide probes with a new microscopy system. *Journal of the American Chemical Society* 129:13502-13509
- Hänninen P, Härmä H (2011) Lanthanide luminescence: photophysical, analytical and biological aspects. *Springer Science & Business Media* 7:1-46
- Hardman R (2006) A toxicologic review of quantum dots: toxicity depends on physicochemical and environmental factors. *Environmental health perspectives* 114:165-172
- Hasna K, Kumar SS, Komath M, Varma MR, Jayaraj M, Kumar KR (2013) Synthesis of chemically pure, luminescent Eu<sup>3+</sup> doped Hap nanoparticles: a promising fluorescent probe for in vivo imaging applications. *Physical Chemistry Chemical Physics* 15:8106-8111
- He H, Pham-Huy LA, Dramou P, Xiao D, Zuo P, Pham-Huy C (2013) Carbon nanotubes: applications in pharmacy and medicine. *BioMed research international* 2013:1-12
- Hopwood DA, Wright HM (1978) Bacterial protoplast fusion: recombination in fused protoplasts of *Streptomyces coelicolor*. *Molecular and General Genetics* MGG 162:307-317
- Hsiao I-L, Gramatke AM, Joksimovic R, Sokolowski M, Gradzielski M, Haase A (2014) Size and cell type dependent uptake of silica nanoparticles. *Journal of Nanomedicine & Nanotechnology* 2014:1-10
- Huang SP, Zhu J, Zhou KC (2012) Influence of pH on the Morphology and Luminescence Properties of Europium-doped Hydroxyapatite Nanoparticles. In: *Advanced Materials Research Trans Tech Publ* 391: 1132-1137

- Hui J, Wang X (2011) Luminescent, Colloidal, F-Substituted, Hydroxyapatite Nanocrystals. *Chemistry–A European Journal* 17:6926-6930
- Hui J, Zhang X, Zhang Z, Wang S, Tao L, Wei Y, Wang X (2012) Fluoridated HAp: Ln<sup>3+</sup>(Ln= Eu or Tb) nanoparticles for cell-imaging. *Nanoscale* 4:6967-6970
- Ibrahim M, Alaam M, El-Haes H, Jalbout AF, Leon Ad (2006) Analysis of the structure and vibrational spectra of glucose and fructose. *Ecletica quimica* 31:15-21
- Ino K, Kitagawa Y, Watanabe T, Shiku H, Koide M, Itayama T, Yasukawa T, Matsue T (2009) Detection of hormone active chemicals using genetically engineered yeast cells and microfluidic devices with interdigitated array electrodes. *Electrophoresis* 30:3406-3412
- Jadalannagari S, Deshmukh K, Ramanan SR, Kowshik M (2014a) Antimicrobial activity of hemocompatible silver doped hydroxyapatite nanoparticles synthesized by modified sol–gel technique. *Applied Nanoscience* 4:133-141
- Jadalannagari S, Deshmukh K, Verma AK, Kowshik RV, Ramanan M, Roy S (2014b) Lanthanum-doped hydroxyapatite nanoparticles as biocompatible fluorescent probes for cellular internalization and biolabeling. *Science of Advanced Materials* 6:312-319
- Jadalannagari S, More S, Kowshik M, Ramanan SR (2011) Low temperature synthesis of hydroxyapatite nano-rods by a modified sol–gel technique. *Materials Science and Engineering: C* 31:1534-1538
- Jakubiak R, Collison CJ, Wan WC, Rothberg LJ, Hsieh BR (1999) Aggregation quenching of luminescence in electroluminescent conjugated polymers. *The Journal of Physical Chemistry A* 103:2394-2398

- Jarcho M (1981) Calcium phosphate ceramics as hard tissue prosthetics. *Clinical orthopaedics and related research* 157:259-278
- Jiang H, Zhao X, Schanze KS (2007) Effects of polymer aggregation and quencher size on amplified fluorescence quenching of conjugated polyelectrolytes. *Langmuir* 23:9481-9486
- Jiang X, Xin H, Ren Q, Gu J, Zhu L, Du F, Feng C, Xie Y, Sha X, Fang X (2014) Nanoparticles of 2-deoxy-D-glucose functionalized poly (ethylene glycol)-co-poly (trimethylene carbonate) for dual-targeted drug delivery in glioma treatment. *Biomaterials* 35:518-529
- Jokerst JV, Lobovkina T, Zare RN, Gambhir SS (2011) Nanoparticle PEGylation for imaging and therapy. *Nanomedicine* 6:715-728
- Jordan M, Wurm F (2004) Transfection of adherent and suspended cells by calcium phosphate. *Methods* 33:136-143
- Katsuki H, Furuta S, Komarneni S (1999) Microwave-versus Conventional-Hydrothermal Synthesis of Hydroxyapatite Crystals from Gypsum. *Journal of the American Ceramic Society* 82:2257-2259
- Kay MI, Young R, Posner A (1964) Crystal structure of hydroxyapatite. *Nature* 204:1050-1052
- Kherlopian AR, Song T, Duan Q, Neimark MA, Po MJ, Gohagan JK, Laine AF (2008) A review of imaging techniques for systems biology. *BMC systems biology* 2:1-18
- Khoza PB, Moloto MJ, Sikhwivhilu LM (2012) The effect of solvents, acetone, water, and ethanol, on the morphological and optical properties of ZnO nanoparticles prepared by microwave. *Journal of Nanotechnology* 2012:1-6

- Khurana V, Lindquist S (2010) Modelling neurodegeneration in *Saccharomyces cerevisiae*: why cook with baker's yeast? *Nature Reviews Neuroscience* 11:436-449
- Kim D, Cho H, Kim C (2000) Blue light emitting polymers. *Progress in Polymer Science* 25:1089-1139
- Kim H-W, Koh Y-H, Li L-H, Lee S, Kim H-E (2004) Hydroxyapatite coating on titanium substrate with titania buffer layer processed by sol-gel method. *Biomaterials* 25:2533-2538
- Kim I-S, Kumta PN (2004) Sol-gel synthesis and characterization of nanostructured hydroxyapatite powder. *Materials Science and Engineering: B* 111:232-236
- Kim T, Feng Q, Kim J, Wu J, Wang H, Chen G, Cui F (1998) Antimicrobial effects of metal ions (Ag<sup>+</sup>, Cu<sup>2+</sup>, Zn<sup>2+</sup>) in hydroxyapatite. *Journal of materials science: Materials in Medicine* 9:129-134
- Klebe RJ, Harriss JV, Sharp ZD, Douglas MG (1983) A general method for polyethylene-glycol-induced genetic transformation of bacteria and yeast. *Gene* 25:333-341
- Klein TM, Jones TJ (1999) Methods of genetic transformation: The gene gun. *Molecular improvement of cereal crops*. Springer 5: 21-42
- Koutsopoulos S (2002) Synthesis and characterization of hydroxyapatite crystals: a review study on the analytical methods. *Journal of biomedical materials research* 62:600-612
- Krisanapiboon A, Buranapanitkit B, Oungbho K (2006) Biocompatibility of hydroxyapatite composite as a local drug delivery system. *Journal of Orthopaedic Surgery* 14:315-318

- Kumar GS, Thamizhavel A, Girija E (2012b) Microwave conversion of eggshells into flower-like hydroxyapatite nanostructure for biomedical applications. *Materials Letters* 76:198-200
- Kumar R, Prakash K, Cheang P, Khor K (2004) Temperature driven morphological changes of chemically precipitated hydroxyapatite nanoparticles. *Langmuir* 20:5196-5200
- Landi E, Tampieri A, Celotti G, Sprio S (2000) Densification behaviour and mechanisms of synthetic hydroxyapatites. *Journal of the European Ceramic Society* 20:2377-2387
- Lebugle A, Pelle F, Charvillat C, Rousselot I, Chane-Ching J-Y (2006) Colloidal and monocrystalline Ln<sup>3+</sup> doped apatite calcium phosphate as biocompatible fluorescent probes. *Chemical communications*(6):606-608
- Lee D, Upadhye K, Kumta PN (2012) Nano-sized calcium phosphate (CaP) carriers for non-viral gene delivery. *Materials Science and Engineering: B* 177:289-302
- LeGeros R, Lin S, Rohanizadeh R, Mijares D, LeGeros J (2003) Biphasic calcium phosphate bioceramics: preparation, properties and applications. *Journal of materials science: Materials in Medicine* 14:201-209
- LeGeros RZ (2002) Properties of osteoconductive biomaterials: calcium phosphates. *Clinical orthopaedics and related research* 395:81-98
- Legras J-L, Merdinoglu D, Cornuet J, Karst F (2007) Bread, beer and wine: *Saccharomyces cerevisiae* diversity reflects human history. *Molecular ecology* 16:2091-2102
- Leprêtre S, Chai F, Hornez J-C, Vermet G, Neut C, Descamps M, Hildebrand HF, Martel B (2009) Prolonged local antibiotics delivery from hydroxyapatite functionalised with cyclodextrin polymers. *Biomaterials* 30:6086-6093



- Lewinski N, Colvin V, Drezek R (2008) Cytotoxicity of nanoparticles. *small* 4:26-49
- Li G, Ye L, Pan J, Long M, Zhao Z, Yang H, Tian J, Wen Y, Dong S, Guan J (2012a) Antitumoural hydroxyapatite nanoparticles-mediated hepatoma-targeted trans-arterial embolization gene therapy: in vitro and in vivo studies. *Liver International* 32:998-1007
- Li L, Liu Y, Tao J, Zhang M, Pan H, Xu X, Tang R (2008) Surface modification of hydroxyapatite nanocrystallite by a small amount of terbium provides a biocompatible fluorescent probe. *The Journal of Physical Chemistry C* 112:12219-12224
- Li Z, Liu Z, Yin M, Yang X, Yuan Q, Ren J, Qu X (2012b) Aptamer-capped multifunctional mesoporous strontium hydroxyapatite nanovehicle for cancer-cell-responsive drug delivery and imaging. *Biomacromolecules* 13:4257-4263
- Lim G, Wang J, Ng S, Gan L (1996) Processing of fine hydroxyapatite powders via an inverse microemulsion route. *Materials letters* 28:431-436
- Liu D-M, Troczynski T, Tseng WJ (2001) Water-based sol-gel synthesis of hydroxyapatite: process development. *Biomaterials* 22:1721-1730
- Liu D-M, Yang Q, Troczynski T (2002a) Sol-gel hydroxyapatite coatings on stainless steel substrates. *Biomaterials* 23:691-698
- Liu D-M, Yang Q, Troczynski T, Tseng WJ (2002b) Structural evolution of sol-gel-derived hydroxyapatite. *Biomaterials* 23:1679-1687
- Liu H, Xi P, Xie G, Chen F, Li Z, Bai D, Zeng Z (2011a) Biocompatible hydroxyapatite nanoparticles as a redox luminescence switch. *JBIC Journal of Biological Inorganic Chemistry* 16:1135-1140

- Liu M, Liu H, Sun S, Li X, Zhou Y, Hou Z, Lin J (2014a) Multifunctional hydroxyapatite/Na (Y/Gd) F4: Yb<sup>3+</sup>, Er<sup>3+</sup> composite fibers for drug delivery and dual modal imaging. *Langmuir* 30:1176-1182
- Liu X, Dai Q, Austin L, Coutts J, Knowles G, Zou J, Chen H, Huo Q (2008) A one-step homogeneous immunoassay for cancer biomarker detection using gold nanoparticle probes coupled with dynamic light scattering. *Journal of the American Chemical Society* 130:2780-2782
- Liu Y, Tu D, Zhu H, Chen X (2013) Lanthanide-doped luminescent nanoprobe: controlled synthesis, optical spectroscopy, and bioapplications. *Chemical Society Reviews* 42:6924-6958
- Liu Y, Wang T, He F, Liu Q, Zhang D, Xiang S, Su S, Zhang J (2011b) An efficient calcium phosphate nanoparticle-based nonviral vector for gene delivery. *Int J Nanomed* 6:721-727
- Liu Z, Wang Q, Yao S, Yang L, Yu S, Feng X, Li F (2014b) Synthesis and characterization of Tb<sup>3+</sup>/Gd<sup>3+</sup> dual-doped multifunctional hydroxyapatite nanoparticles. *Ceramics International* 40:2613-2617
- Liuyun J, Lixin J, Chengdong X, Lijuan X, Ye L (2015) Effect of L-lysine-assisted surface grafting for nano-hydroxyapatite on mechanical properties and in vitro bioactivity of poly (lactic acid-co-glycolic acid). *Journal of biomaterials applications* 30:750-758
- Löfblom J, Kronqvist N, Uhlén M, Ståhl S, Wernérus H (2007) Optimization of electroporation-mediated transformation: *Staphylococcus carnosus* as model organism. *Journal of applied microbiology* 102:736-747
- Loh KP, Bao Q, Eda G, Chhowalla M (2010) Graphene oxide as a chemically tunable platform for optical applications. *Nature chemistry* 2:1015-1024

- Loo SCJ, Siew YE, Ho S, Boey FYC, Ma J (2008) Synthesis and hydrothermal treatment of nanostructured hydroxyapatite of controllable sizes. *Journal of Materials Science: Materials in Medicine* 19:1389-1397
- Lü L-X, Zhang X-F, Wang Y-Y, Ortiz L, Mao X, Jiang Z-L, Xiao Z-D, Huang N-P (2013) Effects of hydroxyapatite-containing composite nanofibers on osteogenesis of mesenchymal stem cells in vitro and bone regeneration in vivo. *ACS applied materials & interfaces* 5:319-330
- MacKeen PC, Person S, Warner SC, Snipes W, Stevens S (1987) Silver-coated nylon fiber as an antibacterial agent. *Antimicrobial agents and chemotherapy* 31:93-99
- Maitra A (2005) Calcium phosphate nanoparticles: second-generation nonviral vectors in gene therapy. *Expert review of molecular diagnostics* 5:893-905
- Mandel M, Higa A (1970) Calcium-dependent bacteriophage DNA infection. *Journal of molecular biology* 53:159-162
- Manke A, Wang L, Rojanasakul Y (2013) Mechanisms of nanoparticle-induced oxidative stress and toxicity. *BioMed research international* 2013:1-15
- Manson J, Kumar D, Meenan BJ, Dixon D (2011) Polyethylene glycol functionalized gold nanoparticles: the influence of capping density on stability in various media. *Gold Bulletin* 44:99-105
- Markovic M, Fowler BO, Tung MS (2004) Preparation and comprehensive characterization of a calcium hydroxyapatite reference material. *Journal of research of the National Institute of Standards and Technology* 109:553-568
- Marriott G, Heidecker M, Diamandis EP, Yan-Marriott Y (1994) Time-resolved delayed luminescence image microscopy using an europium ion chelate complex. *Biophysical journal* 67:957-965

- Matsumoto T, Okazaki M, Inoue M, Hamada Y, Taira M, Takahashi J (2002) Crystallinity and solubility characteristics of hydroxyapatite adsorbed amino acid. *Biomaterials* 23:2241-2247
- Meena R, Kesari KK, Rani M, Paulraj R (2012) Effects of hydroxyapatite nanoparticles on proliferation and apoptosis of human breast cancer cells (MCF-7). *Journal of Nanoparticle Research* 14:1-11
- Meyer V (2008) Genetic engineering of filamentous fungi—progress, obstacles and future trends. *Biotechnology advances* 26:177-185
- Milella E, Cosentino F, Licciulli A, Massaro C (2001) Preparation and characterisation of titania/hydroxyapatite composite coatings obtained by sol-gel process. *Biomaterials* 22:1425-1431
- Mohanty P, Hamouda W, Garg R, Aljada A, Ghanim H, Dandona P (2000) Glucose challenge stimulates reactive oxygen species (ROS) generation by leucocytes. *The journal of clinical endocrinology & metabolism* 85:2970-2973
- Mokoena P, Nagpure I, Kumar V, Kroon R, Olivier E, Neethling J, Swart H, Ntwaeaborwa O (2014) Enhanced UVB emission and analysis of chemical states of Ca 5 (PO 4) 3 OH: Gd 3+, Pr 3+ phosphor prepared by co-precipitation. *Journal of Physics and Chemistry of Solids* 75:998-1003
- Mondéjar SP, Kovtun A, Epple M (2007) Lanthanide-doped calcium phosphate nanoparticles with high internal crystallinity and with a shell of DNA as fluorescent probes in cell experiments. *Journal of Materials Chemistry* 17:4153-4159
- Monmaturapoj N (2008) Nano-size hydroxyapatite powders preparation by wet-chemical precipitation route. *Journal of Metals, Materials and Minerals* 18:15-20

- Monroe E, Votava W, Bass D, Mc Mullen J (1971) New calcium phosphate ceramic material for bone and tooth implants. *Journal of dental research* 50:860-861
- Moore TL, Rodriguez-Lorenzo L, Hirsch V, Balog S, Urban D, Jud C, Rothen-Rutishauser B, Lattuada M, Petri-Fink A (2015) Nanoparticle colloidal stability in cell culture media and impact on cellular interactions. *Chemical Society Reviews* 44:6287-6305
- Morgan TT, Muddana HS, Altinoglu EI, Rouse SM, Tabakovic A, Tabouillot T, Russin TJ, Shanmugavelandy SS, Butler PJ, Eklund PC (2008) Encapsulation of organic molecules in calcium phosphate nanocomposite particles for intracellular imaging and drug delivery. *Nano letters* 8:4108-4115
- Morsy SM (2014) Role of surfactants in nanotechnology and their applications. *Int J Curr Microbiol App Sci* 3:237-260
- Motskin M, Müller KH, Genoud C, Monteith AG, Skepper JN (2011) The sequestration of hydroxyapatite nanoparticles by human monocyte-macrophages in a compartment that allows free diffusion with the extracellular environment. *Biomaterials* 32:9470-9482
- Motskin M, Wright D, Muller K, Kyle N, Gard T, Porter A, Skepper J (2009) Hydroxyapatite nano and microparticles: correlation of particle properties with cytotoxicity and biostability. *Biomaterials* 30:3307-3317
- Moxon KA, Kalkhoran NM, Markert M, Sambito MA, McKenzie J, Webster JT (2004) Nanostructured surface modification of ceramic-based microelectrodes to enhance biocompatibility for a direct brain-machine interface. *IEEE Transactions on Biomedical Engineering* 51:881-889

- Museur L, Gorbovyi P, Traore M, Kanaev A, Rozes L, Sanchez C (2012) Luminescence properties of pHEMA-TiO<sub>2</sub> gels based hybrids materials. *Journal of Luminescence* 132:1192-1199
- Naqvi S, Maitra A, Abdin M, Akmal M, Arora I, Samim M (2012) Calcium phosphate nanoparticle mediated genetic transformation in plants. *Journal of Materials Chemistry* 22:3500-3507
- Nayerossadat N, Maedeh T, Ali PA (2012) Viral and nonviral delivery systems for gene delivery. *Advanced biomedical research* 1(1):27-37
- Neumann S, Kovtun A, Dietzel ID, Epple M, Heumann R (2009) The use of size-defined DNA-functionalized calcium phosphate nanoparticles to minimise intracellular calcium disturbance during transfection. *Biomaterials* 30:6794-6802
- Nieh T, Jankowski A, Koike J (2001) Processing and characterization of hydroxyapatite coatings on titanium produced by magnetron sputtering. *Journal of Materials Research* 16:3238-3245
- Nouri A, Castro R, Santos JL, Fernandes C, Rodrigues J, Tomás H (2012) Calcium phosphate-mediated gene delivery using simulated body fluid (SBF). *International journal of pharmaceutics* 434:199-208
- Ntziachristos V (2006) Fluorescence molecular imaging. *Annu Rev Biomed Eng* 8:1-33
- Nune SK, Gunda P, Thallapally PK, Lin Y-Y, Laird Forrest M, Berkland CJ (2009) Nanoparticles for biomedical imaging. *Expert opinion on drug delivery* 6:1175-1194
- Okada M, Matsumoto T (2015) Synthesis and modification of apatite nanoparticles for use in dental and medical applications. *Japanese Dental Science Review* 51:85-95

- Olton D, Li J, Wilson ME, Rogers T, Close J, Huang L, Kumta PN, Sfeir C (2007) Nanostructured calcium phosphates (NanoCaPs) for non-viral gene delivery: influence of the synthesis parameters on transfection efficiency. *Biomaterials* 28:1267-1279
- Padmanabhan SK, Balakrishnan A, Chu M-C, Lee YJ, Kim TN, Cho S-J (2009) Sol-gel synthesis and characterization of hydroxyapatite nanorods. *Particuology* 7:466-470
- Pan J, Liu W-J, Hua C, Wang L-L, Wan D, Gong J-B (2015) Polymeric nanocomposites loaded with fluoridated hydroxyapatite Ln<sup>3+</sup> (Ln= Eu or Tb)/iron oxide for magnetic targeted cellular imaging. *Cancer biology & medicine* 12:175-183
- Pan J, Wan D, Bian Y, Sun H, Zhang C, Jin F, Huang Z, Gong J (2013) Fluorescent hydroxyapatite-loaded biodegradable polymer nanoparticles with folate decoration for targeted imaging. *AIChE Journal* 59:4494-4501
- Parak WJ, Pellegrino T, Plank C (2005) Labelling of cells with quantum dots. *Nanotechnology* 16:R9-R25
- Parcharoen Y, Kajitvichyanukul P, Sirivisoot S, Termsuksawad P (2014) Hydroxyapatite electrodeposition on anodized titanium nanotubes for orthopedic applications. *Applied Surface Science* 311:54-61
- Pelaz B, del Pino P, Maffre P, Hartmann R, Gallego M, Rivera-Fernandez S, de la Fuente JM, Nienhaus GU, Parak WJ (2015) Surface functionalization of nanoparticles with polyethylene glycol: effects on protein adsorption and cellular uptake. *ACS nano* 9:6996-7008
- Penel G, Delfosse C, Descamps M, Leroy G (2005) Composition of bone and apatitic biomaterials as revealed by intravital Raman microspectroscopy. *Bone* 36:893-901

- Peng G, Tisch U, Adams O, Hakim M, Shehada N, Broza YY, Billan S, Abdah-Bortnyak R, Kuten A, Haick H (2009) Diagnosing lung cancer in exhaled breath using gold nanoparticles. *Nature nanotechnology* 4:669-673
- Peng X, Song F, Lu E, Wang Y, Zhou W, Fan J, Gao Y (2005) Heptamethine cyanine dyes with a large stokes shift and strong fluorescence: a paradigm for excited-state intramolecular charge transfer. *Journal of the American Chemical Society* 127:4170-4171
- Pilliar RM (1987) Porous-surfaced metallic implants for orthopedic applications. *Journal of biomedical materials research* 21:1-33
- Podkościelna B (2014) New photoluminescent copolymers of naphthalene-2, 7-diol dimethacrylate and N-vinyl-2-pyrrolidone. *Journal of Thermal Analysis and Calorimetry* 116:785-793
- Pompon D, Perret A, Bellamine A, Laine R, Gautier J-C, Urban P (1995) Genetically engineered yeast cells and their applications. *Toxicology letters* 82:815-822
- Popa CL, Ciobanu CS, Iconaru SL, Stan M, Dinischiotu A, Negriela CC, Motelica-Heino M, Guegan R, Predoi D (2014) Systematic investigation and in vitro biocompatibility studies on mesoporous europium doped hydroxyapatite. *Central European Journal of Chemistry* 12:1032-1046
- Prasad PN (2003) Bioimaging: principles and techniques. *Introduction to Biophotonics* 7:203-254
- Prener J (1967) The Growth and Crystallographic Properties of Calcium Fluor-and Chlorapatite Crystals. *Journal of the Electrochemical Society* 114:77-83
- Ramamoorth M, Narvekar A (2015) Non viral vectors in gene therapy-an overview. *J Clin Diagn Res* 9:GE01-GE06



- Ramanan SR, Venkatesh R (2004) A study of hydroxyapatite fibers prepared via sol-gel route. *Materials Letters* 58:3320-3323
- Rameshbabu N, Sampath Kumar T, Prabhakar T, Sastry V, Murty K, Prasad Rao K (2007) Antibacterial nanosized silver substituted hydroxyapatite: synthesis and characterization. *Journal of Biomedical Materials Research Part A* 80:581-591
- Ramimoghadam D, Hussein MZB, Taufiq-Yap YH (2012) The effect of sodium dodecyl sulfate (SDS) and cetyltrimethylammonium bromide (CTAB) on the properties of ZnO synthesized by hydrothermal method. *International journal of molecular sciences* 13:13275-13293
- Rao RR, Roopa H, Kannan T (1997) Solid state synthesis and thermal stability of HAP and HAP- $\beta$ -TCP composite ceramic powders. *Journal of Materials Science: Materials in Medicine* 8:511-518
- Rausch K, Reuter A, Fischer K, Schmidt M (2010) Evaluation of nanoparticle aggregation in human blood serum. *Biomacromolecules* 11:2836-2839
- Rauschmann MA, Wichelhaus TA, Stirnal V, Dingeldein E, Zichner L, Schnettler R, Alt V (2005) Nanocrystalline hydroxyapatite and calcium sulphate as biodegradable composite carrier material for local delivery of antibiotics in bone infections. *Biomaterials* 26:2677-2684
- Resch-Genger U, Grabolle M, Cavaliere-Jaricot S, Nitschke R, Nann T (2008) Quantum dots versus organic dyes as fluorescent labels. *Nature methods* 5:763-775
- Riss TL, Moravec RA, Niles AL, Benink HA, Worzella TJ, Minor L (2015) Cell viability assays.
- Sahoo SK, Panyam J, Prabha S, Labhasetwar V (2002) Residual polyvinyl alcohol associated with poly (D, L-lactide-co-glycolide) nanoparticles

- affects their physical properties and cellular uptake. *Journal of controlled release* 82:105-114
- Salata OV (2004) Applications of nanoparticles in biology and medicine. *Journal of nanobiotechnology* 2:1-6.
- Sanvicens N, Marco MP (2008) Multifunctional nanoparticles—properties and prospects for their use in human medicine. *Trends in biotechnology* 26:425-433
- Sarath Chandra V, Baskar G, Suganthi R, Elayaraja K, Ahymah Joshy M, Sofi Beaula W, Mythili R, Venkatraman G, Narayana Kalkura S (2012) Blood compatibility of iron-doped nanosize hydroxyapatite and its drug release. *ACS applied materials & interfaces* 4:1200-1210
- Sarker SD, Nahar L, Kumarasamy Y (2007) Microtitre plate-based antibacterial assay incorporating resazurin as an indicator of cell growth, and its application in the in vitro antibacterial screening of phytochemicals. *Methods* 42:321-324
- Savita N, Maitra S, Ravishankar U (2010) Multimodality molecular imaging—an overview with special focus on PET/CT. *Apollo Medicine* 7:190-199
- Schaming D, Remita H (2015) Nanotechnology: from the ancient time to nowadays. *Foundations of Chemistry* 17:187-205
- Seelos C (1997) A critical parameter determining the aging of DNA—calcium-phosphate precipitates. *Analytical biochemistry* 245:109-111
- Selvig KA (1972) The crystal structure of hydroxyapatite in dental enamel as seen with the electron microscope. *Journal of ultrastructure research* 41:369-375

- Sennerby L, Dasmah A, Larsson B, Iverhed M (2005) Bone Tissue Responses to Surface-Modified Zirconia Implants: A Histomorphometric and Removal Torque Study in the Rabbit. *Clinical Implant Dentistry and Related Research* 7:s13-s20
- Shiao Nh (2008) Cytotoxic effect of CdSe quantum dots on mouse embryonic development. *Acta Pharmacologica Sinica* 29:259-266
- Shibli S, Jayalekshmi A (2008) Development of phosphate inter layered hydroxyapatite coating for stainless steel implants. *Applied Surface Science* 254:4103-4110
- Sicard D, Legras J-L (2011) Bread, beer and wine: yeast domestication in the *Saccharomyces sensu stricto* complex. *Comptes rendus biologies* 334:229-236
- Son JS, Appleford M, Ong JL, Wenke JC, Kim JM, Choi SH, Oh DS (2011) Porous hydroxyapatite scaffold with three-dimensional localized drug delivery system using biodegradable microspheres. *Journal of controlled release* 153:133-140
- Soppimath KS, Aminabhavi TM, Kulkarni AR, Rudzinski WE (2001) Biodegradable polymeric nanoparticles as drug delivery devices. *Journal of controlled release* 70:1-20
- Stanić V, Janačković D, Dimitrijević S, Tanasković SB, Mitrić M, Pavlović MS, Krstić A, Jovanović D, Raičević S (2011) Synthesis of antimicrobial monophasic silver-doped hydroxyapatite nanopowders for bone tissue engineering. *Applied Surface Science* 257:4510-4518
- Stigter M, Bezemer J, De Groot K, Layrolle P (2004) Incorporation of different antibiotics into carbonated hydroxyapatite coatings on titanium implants, release and antibiotic efficacy. *Journal of controlled release* 99:127-137

- Suchanek W, Yoshimura M (1998) Processing and properties of hydroxyapatite-based biomaterials for use as hard tissue replacement implants. *Journal of Materials Research* 13:94-117
- Sun H, Jiang M, Zhu S (2008) In vitro and in vivo studies on hydroxyapatite nanoparticles as a novel vector for inner ear gene therapy. *Zhonghua er bi yan hou tou jing wai ke za zhi= Chinese journal of otorhinolaryngology head and neck surgery* 43:51-57
- Sun L, Berndt CC, Gross KA, Kucuk A (2001) Material fundamentals and clinical performance of plasma-sprayed hydroxyapatite coatings: a review. *Journal of biomedical materials research* 58:570-592
- Sun R, Chen K, Wu X, Zhao D, Sun Z (2013) Controlled synthesis and enhanced luminescence of europium-doped fluorine-substituted hydroxyapatite nanoparticles. *CrystEngComm* 15:3442-3447
- Sun Y, Xia Y (2002) Shape-controlled synthesis of gold and silver nanoparticles. *Science* 298:2176-2179
- Syamchand SS, Sony G (2015) Multifunctional hydroxyapatite nanoparticles for drug delivery and multimodal molecular imaging. *Microchimica Acta* 182:1567-1589
- Tabaković A, Kester M, Adair JH (2012) Calcium phosphate-based composite nanoparticles in bioimaging and therapeutic delivery applications. *Wiley Interdisciplinary Reviews: Nanomedicine and Nanobiotechnology* 4:96-112
- Tan H, Fu L, Seno M (2010) Optimization of bacterial plasmid transformation using nanomaterials based on the Yoshida effect. *International journal of molecular sciences* 11:4962-4972

- Tan K, Cheang P, Ho I, Lam P, Hui K (2007) Nanosized bioceramic particles could function as efficient gene delivery vehicles with target specificity for the spleen. *Gene therapy* 14:828-835
- Tank KP, Chudasama KS, Thaker VS, Joshi MJ (2013) Cobalt-doped nanohydroxyapatite: synthesis, characterization, antimicrobial and hemolytic studies. *Journal of Nanoparticle Research* 15:1-11
- Tenreiro S, Munder MC, Alberti S, Outeiro TF (2013) Harnessing the power of yeast to unravel the molecular basis of neurodegeneration. *Journal of neurochemistry* 127:438-452
- Ternane R, Trabelsi-Ayedi M, Kbir-Arigoib N, Piriou B (1999) Luminescent properties of Eu 3+ in calcium hydroxyapatite. *Journal of Luminescence* 81:165-170
- Thanh DTM, Nam PT, Phuong NT, Que LX, Van Anh N, Hoang T, Dai Lam T (2013) Controlling the electrodeposition, morphology and structure of hydroxyapatite coating on 316L stainless steel. *Materials Science and Engineering: C* 33:2037-2045
- Thanh NT, Green LA (2010) Functionalisation of nanoparticles for biomedical applications. *Nano Today* 5:213-230
- Thi TH, Chai F, Leprêtre S, Blanchemain N, Martel B, Siepmann F, Hildebrand H, Siepmann J, Flament M (2010) Bone implants modified with cyclodextrin: Study of drug release in bulk fluid and into agarose gel. *International journal of pharmaceutics* 400:74-85
- Thomann J, Voegel J, Gramain P (1990) Kinetics of dissolution of calcium hydroxyapatite powder. III: pH and sample conditioning effects. *Calcified tissue international* 46:121-129

- Torchilin VP (2005) Recent advances with liposomes as pharmaceutical carriers. *Nature reviews Drug discovery* 4:145-160
- Tram Do TN, Lee W-H, Loo C-Y, Zavgorodniy AV, Rohanizadeh R (2012) Hydroxyapatite nanoparticles as vectors for gene delivery. *Therapeutic delivery* 3:623-632
- True LD, Gao X (2007) Quantum dots for molecular pathology: their time has arrived. *The Journal of Molecular Diagnostics* 9:7-11
- Tu Z, He G, Li KX, Chen MJ, Chang J, Chen L, Yao Q, Liu DP, Ye H, Shi J (2005) An improved system for competent cell preparation and high efficiency plasmid transformation using different *Escherichia coli* strains. *Electronic Journal of Biotechnology* 8:113-120
- Ueno S (2010) Formation of poly-L-lysine-hydroxyapatite nanoparticles complexes and interactions between these complexes and lipid bilayer membrane. *Phosphorus Research Bulletin* 24:32-37
- Ueno S, Shimabayashi S (2009) Formation of poly-L-lysine-hydroxyapatite nanoparticles complexes and interactions between these complexes and lipid bilayer membrane. *Phosphorus Research Bulletin* 23:57-62
- Urabe M, Kume A, Tobita K, Ozawa K (2000) DNA/calcium phosphate precipitates mixed with medium are stable and maintain high transfection efficiency. *Analytical biochemistry* 278:91-92
- Uskoković V, Uskoković DP (2011) Nanosized hydroxyapatite and other calcium phosphates: chemistry of formation and application as drug and gene delivery agents. *Journal of Biomedical Materials Research Part B: Applied Biomaterials* 96:152-191

- Van Dijk K, Schaeken H, Wolke J, Jansen J (1996) Influence of annealing temperature on RF magnetron sputtered calcium phosphate coatings. *Biomaterials* 17:405-410
- Vasilev K, Cook J, Griesser HJ (2009) Antibacterial surfaces for biomedical devices. *Expert Review of Medical Devices* 6:553-567
- Venkatasubbu GD, Ramasamy S, Avadhani G, Ramakrishnan V, Kumar J (2013) Surface modification and paclitaxel drug delivery of folic acid modified polyethylene glycol functionalized hydroxyapatite nanoparticles. *Powder technology* 235:437-442
- Victor SP, Paul W, Jayabalan M, Sharma CP (2014) Supramolecular hydroxyapatite complexes as theranostic near-infrared luminescent drug carriers. *CrystEngComm* 16:9033-9042
- Victor SP, Sharma CP (2011) Development and evaluation of cyclodextrin complexed hydroxyapatite nanoparticles for preferential albumin adsorption. *Colloids and Surfaces B: Biointerfaces* 85:221-228
- Vonesch C, Aguet F, Vonesch J-L, Unser M (2006) The colored revolution of bioimaging. *IEEE signal processing magazine* 23:20-31
- Wagner DE, Eisenmann KM, Nestor-Kalinowski AL, Bhaduri SB (2013) A microwave-assisted solution combustion synthesis to produce europium-doped calcium phosphate nanowhiskers for bioimaging applications. *Acta biomaterialia* 9:8422-8432
- Wagner S, Gondikas A, Neubauer E, Hofmann T, von der Kammer F (2014) Spot the difference: engineered and natural nanoparticles in the environment—release, behavior, and fate. *Angewandte Chemie International Edition* 53:12398-12419

- Walters M, Leung Y, Blumenthal N, Konsker K, LeGeros R (1990) A Raman and infrared spectroscopic investigation of biological hydroxyapatite. *Journal of inorganic biochemistry* 39:193-200
- Wan Y, Raman S, He F, Huang Y (2007) Surface modification of medical metals by ion implantation of silver and copper. *Vacuum* 81:1114-1118
- Wang D, Xing G, Gao M, Yang L, Yang J, Wu T (2011a) Defects-mediated energy transfer in red-light-emitting Eu-doped ZnO nanowire arrays. *The Journal of Physical Chemistry C* 115:22729-22735
- Wang EC, Wang AZ (2014) Nanoparticles and their applications in cell and molecular biology. *Integrative Biology* 6:9-26
- Wang F, Banerjee D, Liu Y, Chen X, Liu X (2010a) Upconversion nanoparticles in biological labeling, imaging, and therapy. *Analyst* 135:1839-1854
- Wang F, Tan WB, Zhang Y, Fan X, Wang M (2005) Luminescent nanomaterials for biological labelling. *Nanotechnology* 17(1):R1-R13
- Wang G-h, Zhao Y-z, Juan T, Zhu S-h, Zhou K-c (2015) Arginine functionalized hydroxyapatite nanoparticles and its bioactivity for gene delivery. *Transactions of Nonferrous Metals Society of China* 25:490-496
- Wang J, Yin C, Tang G, Lin X, Wu Q (2013) Glucose-functionalized multidrug-conjugating nanoparticles based on amphiphilic terpolymer with enhanced anti-tumorous cell cytotoxicity. *International journal of pharmaceutics* 441:291-298
- Wang P, Li C, Gong H, Jiang X, Wang H, Li K (2010b) Effects of synthesis conditions on the morphology of hydroxyapatite nanoparticles produced by wet chemical process. *Powder Technology* 203:315-321



- Wang S, Wen S, Shen M, Guo R, Cao X, Wang J, Shi X (2011b) Aminopropyltriethoxysilane-mediated surface functionalization of hydroxyapatite nanoparticles: synthesis, characterization, and in vitro toxicity assay. *Int J Nanomedicine* 6:3449-3459
- Waychunas GA (2009) Natural nanoparticle structure, properties and reactivity from X-ray studies. *Powder Diffraction* 24:89-93
- Webster TJ, Ergun C, Doremus RH, Siegel RW, Bizios R (2000) Enhanced functions of osteoblasts on nanophase ceramics. *Biomaterials* 21:1803-1810
- Wijesinghe W, Mantilaka M, Senarathna KC, Herath H, Premachandra T, Ranasinghe C, Rajapakse R, Rajapakse R, Edirisinghe M, Mahalingam S (2016) Preparation of bone-implants by coating hydroxyapatite nanoparticles on self-formed titanium dioxide thin-layers on titanium metal surfaces. *Materials Science and Engineering: C* 63:172-184
- Wilczewska AZ, Niemirowicz K, Markiewicz KH, Car H (2012) Nanoparticles as drug delivery systems. *Pharmacological reports* 64:1020-1037
- Wolfbeis OS (2015) An overview of nanoparticles commonly used in fluorescent bioimaging. *Chemical Society Reviews* 44:4743-4768
- Woodard JR, Hilldore AJ, Lan SK, Park C, Morgan AW, Eurell JAC, Clark SG, Wheeler MB, Jamison RD, Johnson AJW (2007) The mechanical properties and osteoconductivity of hydroxyapatite bone scaffolds with multi-scale porosity. *Biomaterials* 28:45-54
- Wu X, Ding D, Jiang H, Xing X, Huang S, Liu H, Chen Z, Sun H (2012) Transfection using hydroxyapatite nanoparticles in the inner ear via an intact round window membrane in chinchilla. *Journal of Nanoparticle Research* 14:1-13

- Xiao K, Li Y, Luo J, Lee JS, Xiao W, Gonik AM, Agarwal RG, Lam KS (2011) The effect of surface charge on in vivo biodistribution of PEG-oligocholic acid based micellar nanoparticles. *Biomaterials* 32:3435-3446
- Xie Y, He W, Li F, Perera TSH, Gan L, Han Y, Wang X, Li S, Dai H (2016) Luminescence Enhanced Eu<sup>3+</sup>/Gd<sup>3+</sup> Co-Doped Hydroxyapatite Nanocrystals as Imaging Agents In Vitro and In Vivo. *ACS applied materials & interfaces* 8:10212-10219
- Xiong G, Wan Y, Zuo G, Ren K, Luo H (2015) Self-assembled magnetic lamellar hydroxyapatite as an efficient nano-vector for gene delivery. *Current Applied Physics* 15:811-818
- Xu H, Wei D, Gai X, Jiang Y (2016) Amine functionalised hydroxyapatite nanoparticles for anti-angiogenesis gene therapy of breast cancer. *Micro & Nano Letters* 11:416-419
- Xu J, Xu P, Li Z, Huang J, Yang Z (2012) Oxidative stress and apoptosis induced by hydroxyapatite nanoparticles in C6 cells. *Journal of Biomedical Materials Research Part A* 100:738-745
- Xue W, Wang H, Pei Z, Zhao W, Tian Y-S, Peng R-H, Yao Q-H (2013) An improved integrative transformation system for *Pichia pastoris* with DNA-polyethylenimine-dextran sulfate nanoparticles. *Biotechnology and bioprocess engineering* 18:581-586
- Yamini D, Venkatasubbu GD, Kumar J, Ramakrishnan V (2014) Raman scattering studies on PEG functionalized hydroxyapatite nanoparticles. *Spectrochimica Acta Part A: Molecular and Biomolecular Spectroscopy* 117:299-303

- Yan-Zhong Z, Yan-Yan H, Jun Z, Shai-Hong Z, Zhi-You L, Ke-Chao Z (2011) Characteristics of functionalized nano-hydroxyapatite and internalization by human epithelial cell. *Nanoscale research letters* 6:1-8
- Yang C, Yang P, Wang W, Wang J, Zhang M, Lin J (2008a) Solvothermal synthesis and characterization of Ln (Eu 3+, Tb 3+) doped hydroxyapatite. *Journal of colloid and interface science* 328:203-210
- Yang P, Quan Z, Li C, Kang X, Lian H, Lin J (2008b) Bioactive, luminescent and mesoporous europium-doped hydroxyapatite as a drug carrier. *Biomaterials* 29:4341-4347
- Yang Y-H, Liu C-H, Liang Y-H, Lin F-H, Wu KC-W (2013) Hollow mesoporous hydroxyapatite nanoparticles (hmHANPs) with enhanced drug loading and pH-responsive release properties for intracellular drug delivery. *Journal of Materials Chemistry B* 1:2447-2450
- Yang Y, Wu Q, Wang M, Long J, Mao Z, Chen X (2014) Hydrothermal synthesis of hydroxyapatite with different morphologies: influence of supersaturation of the reaction system. *Crystal Growth & Design* 14:4864-4871
- Yasui K, Kano Y, Tanaka K, Watanabe K, Shimizu-Kadota M, Yoshikawa H, Suzuki T (2009) Improvement of bacterial transformation efficiency using plasmid artificial modification. *Nucleic acids research* 37(1):e3-e3
- Ye F, Guo H, Zhang H, He X (2010) Polymeric micelle-templated synthesis of hydroxyapatite hollow nanoparticles for a drug delivery system. *Acta Biomaterialia* 6:2212-2218
- Ye H, Kong J, Shen W, Zhao J, Li X (2007) Temperature-dependent photoluminescence of undoped, N-doped and N-In codoped ZnO thin films. *Journal of Physics D: Applied Physics* 40:5588-5591

- Yoon J, Kim D, Siregar A, Lee BY, Kwon KY, Byun JH, Woo DK (2015) 5-Fluorouracil-coated Hydroxyapatite Nanoparticles as Anticancer Drug Delivery Carriers. *Bulletin of the Korean Chemical Society* 36:445-446
- Yoshida N, Ikeda T, Yoshida T, Sengoku T, Ogawa K (2001) Chrysotile asbestos fibers mediate transformation of *Escherichia coli* by exogenous plasmid DNA. *FEMS microbiology letters* 195:133-137
- Yuan J, Wang G, Majima K, Matsumoto K (2001) Synthesis of a terbium fluorescent chelate and its application to time-resolved fluoroimmunoassay. *Analytical chemistry* 73:1869-1876
- Zeng H, Duan G, Li Y, Yang S, Xu X, Cai W (2010) Blue luminescence of ZnO nanoparticles based on non-equilibrium processes: defect origins and emission controls. *Advanced Functional Materials* 20:561-572
- Zhang C, Li C, Huang S, Hou Z, Cheng Z, Yang P, Peng C, Lin J (2010) Self-activated luminescent and mesoporous strontium hydroxyapatite nanorods for drug delivery. *Biomaterials* 31:3374-3383
- Zhang C, Lin J (2012) Defect-related luminescent materials: synthesis, emission properties and applications. *Chemical Society Reviews* 41:7938-7961
- Zhang C, Yang J, Quan Z, Yang P, Li C, Hou Z, Lin J (2009) Hydroxyapatite nano- and microcrystals with multiform morphologies: controllable synthesis and luminescence properties. *Crystal Growth and Design* 9:2725-2733
- Zhang X, Hui J, Yang B, Yang Y, Fan D, Liu M, Tao L, Wei Y (2013) PEGylation of fluoridated hydroxyapatite (FAp): Ln<sup>3+</sup> nanorods for cell imaging. *Polymer Chemistry* 4:4120-4125
- Zhang X, Vecchio KS (2007) Hydrothermal synthesis of hydroxyapatite rods. *Journal of Crystal Growth* 308:133-140

- Zhanglei N, Chang Z, Wenjun L, Changyan S, Zhang J, Yang L (2012) Solvothermal synthesis and optical performance of one-dimensional strontium hydroxyapatite nanorod. *Chinese Journal of Chemical Engineering* 20:89-94
- Zhao Y-Z, Jun Z, Zhu S-H, Huang Y-Y, Li Z-Y, Zhou K-C (2011) Synthesis and characterization of arginine-modified and europium-doped hydroxyapatite nanoparticle and its cell viability. *Transactions of Nonferrous Metals Society of China* 21:1773-1778
- Zhou H, Lee J (2011) Nanoscale hydroxyapatite particles for bone tissue engineering. *Acta biomaterialia* 7:2769-2781
- Zhu S, Huang B, Zhou K, Huang S, Liu F, Li Y, Xue Z, Long Z (2004) Hydroxyapatite nanoparticles as a novel gene carrier. *Journal of Nanoparticle Research* 6:307-311
- Zinder ND, Lederberg J (1952) Genetic exchange in *Salmonella*. *Journal of bacteriology* 64:679-699

**Media and buffer composition**

**Minimal media**

|   |          |
|---|----------|
| Na <sub>2</sub> HPO <sub>4</sub> ( <u>anhydrous</u> ) | 6g/L     |
| KH <sub>2</sub> PO <sub>4</sub>                       | 3g/L     |
| NaCl  | 0.5g/L   |
| NH <sub>4</sub> Cl                                    | 1g/L     |
| MgSO <sub>4</sub> •7H <sub>2</sub> O                  | 0.260g/L |
| CaCl <sub>2</sub>                                     | 0.147g/L |
| Glucose   | 1g/L     |

**Tris-EDTA buffer**

|         |         |
|---------|---------|
| Tris-Cl | 1.21g/L |
| EDTA    | 0.29g/L |

**TAE (Tris-acetate-EDTA)**

|             |           |
|-------------|-----------|
| Trs-Cl      | 4.84g/L   |
| Acetic acid | 1.142mL/L |
| EDTA        | 0.292g/L  |

**Phosphate buffer saline**

|                                  |         |
|----------------------------------|---------|
| NaCl                             | 8g/L    |
| KCl                              | 0.2g/L  |
| Na <sub>2</sub> HPO <sub>4</sub> | 1.44g/L |
| KH <sub>2</sub> PO <sub>4</sub>  | 0.24g/L |

## List of publications and patent

### Publications and patents related to this thesis

#### Publications

- **Ketaki Deshmukh**, M. Monsoor Shaik, Sutapa Roy Ramanan, and Meenal Kowshik. "Self-Activated Fluorescent Hydroxyapatite Nanoparticles: A Promising Agent for Bioimaging and Biolabeling." *ACS Biomaterials Science & Engineering* 2, no. 8 (2016): 1257-1264.
- **Ketaki R Deshmukh**, Sutapa Roy Ramanan, and Meenal Kowshik. "Low-temperature-processed biocompatible Ag-HAp nanoparticles with anti-biofilm efficacy for tissue engineering applications." *Journal of Sol-Gel Science and Technology* 80, no. 3 (2016): 738-747.

#### Patent

- Nanomaterial based DNA delivery vehicle for bacterial transformation.  
(Application number: 1529/Mum/2013)

#### Other publications

- Naik, Kshipra, Pallavee Srivastava, **Ketaki Deshmukh**, S. Monsoor, and Meenal Kowshik. "Nanomaterial-Based Approaches for Prevention of Biofilm-Associated Infections on Medical Devices and Implants." *Journal of nanoscience and nanotechnology* 15, no. 12 (2015): 10108-10119.
- Jadalannagari, Sushma\*, **Ketaki Deshmukh\***, Anita KamraVerma, Richa Vohra Kowshik, MeenalRamanan, and Sutapa Roy. "Lanthanum-Doped Hydroxyapatite Nanoparticles as Biocompatible Fluorescent Probes for Cellular Internalization and Biolabeling." *Science of Advanced Materials* 6, no. 2 (2014): 312-319.
- Jadalannagari, Sushma\*, **Ketaki Deshmukh\***, Sutapa Roy Ramanan, and Meenal Kowshik. "Antimicrobial activity of hemocompatible silver doped hydroxyapatite nanoparticles synthesized by modified sol-gel technique." *Applied Nanoscience* 4, no. 2 (2014): 133-141. (\* -both authors contributed equally)

## **LIST OF WORKSHOPS AND CONFERENCES ATTENDED**

1. Ketaki Deshmukh, Sutapa Roy Ramanan and Meenal Kowshik (2012) Biocompatible AgCl-hydroxyapatite nanoparticles with excellent anti-biofilm efficacy: potential candidates for bone tissue engineering. (**Poster presentation** at International Conference on Supramolecules and Nanomaterials-Research and Applications ICSNA- 2013, Ahmedabad, Gujarat 6<sup>th</sup>- 8<sup>th</sup> Feb).
2. Ketaki Deshmukh, Sutapa Roy Ramanan and Meenal Kowshik (2012) Biocompatible AgCl-hydroxyapatite nanoparticles with excellent anti-biofilm efficacy: potential candidates for bone tissue engineering. (**Oral presentation** at UGC sponsored National seminar, Nanomaterials: Synthesis, characterization and applications during 2<sup>nd</sup> and 3<sup>rd</sup> February 2012) organized by Department of Chemistry, Smt.Parvatibai Chowgule College of Arts and Science, Margoa-Goa.
3. Ketaki Deshmukh, Sutapa Roy Ramanan and Meenal Kowshik (2014) Lanthanum Doped Hydroxyapatite Nanoparticles as Biocompatible Fluorescent Probe for Cellular Internalization and Biolabeling. (**Poster presentation** at International conference held at IISc Bangalore, 12-15<sup>th</sup> Feb 2014).



### **Brief Biography of the Candidate**

**Name:** Ketaki Deshmukh

**Education:** M.E (Biotechnology), BITS Pilani University (2012)

**Email:** ketaki03@gmail.com

#### **Work experience**

Ketaki Deshmukh has completed her Master of engineering in Biotechnology, BITS Pilani University, 2012. Subsequently she joined as a Research Scholar in the Department of Biological Sciences, at Birla Institute of Technology and Science, Pilani K. K. Birla Goa Campus for pursuing Ph.D. in Nanobiotechnology. Her research interest involves synthesis and applications of hydroxyapatite nanoparticles in Bioimaging and molecular biology.

She has published four research papers and one review article in International Journals and filed Indian patent.

**Brief Biography of the Supervisor**

Meenal Kowshik received her M.Sc. in Microbiology from Goa University in 1997. She worked on the biological synthesis of metallic and metal sulfide nanoparticles using yeasts at Agarkar Research Institute, and obtained her Ph.D. degree from Pune University (1999–2003). Subsequently, she joined Birla Institute of Technology and Science, Pilani-K. K. Birla Goa Campus, and is currently working as an Associate Professor in the Department of Biological Sciences. Her research interests include studies on biofunctionalization of silver based nanocomposites for antimicrobial applications, synthesis of biocompatible nanomaterials for tissue engineering and application of nanomaterials in molecular biology research. She is also working in the area of interactions of nanomaterials and microorganisms with respect to nanomaterial synthesis and toxicity, with special emphasis on halophilic archaeobacteria. She has received research grants from Department of Science and Technology and Ministry of Earth Sciences, and published about 30 papers in International and National journals.

## LICENSES

1. **Figure 1.4 b)** License no. 3997521394723
2. **Figure 1.5** Under creative common license
3. **Figure 1.6** License no. 3971210082183
4. **Figure 1.7** License no. 3997550989491